

THESIS FOR THE DEGREE OF DOCTOR OF PHILOSOPHY

Analyses of Resilient Behavior of Unbound Materials
for the Purpose of Predicting Permanent Deformation
Behavior

JAN ENGLUND

Department of Civil and Environmental Engineering
Division of GeoEngineering
CHALMERS UNIVERSITY OF TECHNOLOGY
Gothenburg, Sweden 2011

Analyses of Resilient Behavior of Unbound Materials for
the Purpose of Predicting Permanent Deformation Behavior
JAN ENGLUND
ISBN 978-91-7385-524-2

© JAN ENGLUND, 2011

Doktorsavhandlingar vid Chalmers tekniska högskola
Ny serie Nr 3205
ISSN 0346-718X

Department of Civil and Environmental Engineering
Division of GeoEngineering
Chalmers University of Technology
SE-412 96 Gothenburg
Sweden
Telephone + 46 (0)31 772 10 00
www.chalmers.se

Chalmers Reproservice
Gothenburg, Sweden 2011

Analyses of Resilient Behavior of Unbound Materials for the Purpose of Predicting Permanent Deformation Behavior

JAN ENGLUND

Department of Civil and Environmental Engineering

Division of GeoEngineering

Chalmers University of Technology

ABSTRACT

Post compaction is the unintended compaction of the unbound material that commences immediately after a road is brought into service and caused by densification of the material. Analogies to this post compaction can also be seen in laboratory and field tests.

The objective of the thesis is to identify the conditions for post compaction and separate it from permanent deformation caused by shearing/dilatation to facilitate process understanding. The relationship between permanent and resilient deformation is analyzed. The resilient performance is then described through the stress hardening behavior of the unbound materials using the so called k - θ model.

Input for the analysis of stress hardening behavior and permanent deformation comes from small scale laboratory tests and full scale field tests performed by VTI. The laboratory tests used are repeated load triaxial tests and the field tests are accelerated pavement tests using Heavy Vehicle Simulator and Falling Weight Deflectometer readings. A conceptual model of unbound material was set up to facilitate the analysis of the continuous stress hardening behavior from peak value observations in both the laboratory and the field tests.

The analysis shows that it is possible to describe the permanent deformation behavior of unbound road material by examining resilient behavior. However, it is not sufficient to use only resilient deformation or resilient modulus. For an adequate description it is necessary to evaluate the stress hardening behavior. This can be evaluated by using the k - θ model and a graphic presentation of its stress hardening parameters k_1 and k_2 . In such an analysis the stress hardening caused by post compaction can be separated from stress hardening caused by resting. The analysis also shows that there is a specific bulk stress level that separates compaction behavior and shearing behavior as a result of repeated loading.

Keywords: Falling Weight Deflectometer (FWD), Heavy Vehicle Simulator (HVS), Modulus, Permanent Deformation, Post Compaction, Resilient Deformation, Triaxial Testing, Unbound Material

PREFACE

The work on this doctoral thesis was carried out at the Division of GeoEngineering, Chalmers University of Technology, Gothenburg and Skanska Sverige AB. Supervisors were Professor Claes Alén and adjunct Professor Anders Lenngren. The examiner was Professor Gunnar Gustafson. Financial support for the project was provided by the Swedish Road Administration (SRA), SBUF, the VBT-Consortium, Skanska and Chalmers. The laboratory and field tests in Uddevalla and Linköping were carried out by VTI under the management of SRA.

The thesis is part of a PhD-project. In that project I also presented a licentiate thesis 2002 (Hansson J., 2002: Fatigue of unbound material in a road structure. Licentiate thesis, department of Geology (A 102), Chalmers University of Technology, Gothenburg, Sweden. (In Swedish)).

I am very grateful to Claes Alén, Anders Lenngren and Gunnar Gustafson for their interest and valuable discussions and comments. Anders Kullingsjö at the Division of GeoEngineering has helped me to describe the failure surfaces of Drucker-Prager and Mohr-Coulomb. I am also very grateful to Joakim Jeppsson at Skanska for helping with encouragement and financial support for starting the project again.

I am also grateful to Anders Huvstig, SRA, for initiating the project to Chalmers and to the reference group linked to the project: Carl-Gösta Enocksson, Håkan Thorén, Bo Johansson, Klas Hermelin, Fredrick Lekarp, Ulf Ekdahl, Kenneth Olsson and Johanna Thorsenius. I would also like to thank Håkan Carlsson at VTI for all his help with testing.

To my dear present and former colleagues at the Division of GeoEngineering, I thank you for your support and friendship during my years at Chalmers. To my dear colleagues at Skanska VTC Väst, I thank you for the support, friendship and cheerful moments. Finally, my special thanks to my parents and family for your support and encouragement, to my friends for their friendship and especially to my wife Jennie and my daughters Moa and Ebba for your patience and love.

Gothenburg, April, 2011

Jan Englund

TABLE OF CONTENTS

ABSTRACT	III
PREFACE	V
TABLE OF CONTENTS.....	VII
LIST OF NOTATIONS.....	IX
1 INTRODUCTION.....	1
1.1 Background.....	1
1.2 Objective.....	3
1.3 Hypothesis	3
1.4 Scope of work	5
1.5 Limitations.....	5
2 LITERATURE REVIEW.....	6
2.1 Introduction.....	6
2.2 Mechanisms of deformation in unbound granular material	6
2.3 Deformation behavior modeling.....	14
2.4 Measuring deformation behavior.....	28
2.5 Conclusions from the literature review.....	35
3 CONCEPTUAL MODEL AND EVALUATION METHOD	38
3.1 Evaluation of the condition of post compaction.....	38
3.2 Conceptual model of the triaxial laboratory test.....	39
3.3 Conceptual model of the FWD test.....	42
3.4 Conceptual model for describing the relationship between stress hardening, post compaction and shearing.....	43
4 IDENTIFICATION OF THE CONDITIONS FOR POST COMPACTION USING SMALL SCALE TESTS	59
4.1 Introduction.....	59
4.2 Description of the triaxial laboratory test.....	60
4.3 Description of the tested unbound material.....	61
4.4 Results.....	63
5 IDENTIFICATION OF POST COMPACTION USING FULL SCALE TESTS.....	73
5.1 Introduction.....	73
5.2 HVS Test Design and Evaluation	75

5.3	FWD test design and evaluation.....	78
5.4	Results.....	79
5.5	Results of the FWD test and the stress hardening evaluation.....	88
6	ANALYSIS	99
6.1	Introduction.....	99
6.2	Relationship between permanent and elastic deformation and comparison with permanent strain models.....	100
6.3	State of stress.....	107
6.4	Stress hardening behavior.....	122
6.5	Summary of the analysis	132
7	DISCUSSION.....	136
7.1	Discussion of the results.....	136
7.2	Use of the result	138
7.3	Hypotheses and objective	139
8	CONCLUSIONS	142
9	RECOMMENDATION OF FUTURE WORK.....	144
	REFERENCES	145
	APPENDICES	153
	Appendix A: Classification of the tested materials	
	Appendix B: Results from the laboratory test	
	Appendix C: Evaluation of deformation behavior	
	Appendix D: Evaluation of material models	
	Appendix E: Derivation of strength parameters	
	Appendix F: Evaluation of the empirical expression of internal friction angle	
	Appendix G: Derivation of the relationship between k_1 , k_2 , θ and M_r	
	Appendix H: Graphic presentation of the $k_1 - k_2$ relationship for each test cell separately	

LIST OF NOTATIONS

The following notations are used in the main text of the thesis:

Greek letters

α	Material parameter in Equation 2.15 connected to stress hardening [-]
γ	Material parameter in Equation 2.15 connected to the slope of the failure envelope of Drucker-Prager [-]
$\sqrt{\gamma}$	Slope of the failure envelope of Drucker-Prager [-]
θ	Bulk stress [kPa]
θ_0	Reference bulk stress = 1 [kPa]
ε_{ar}	Resilient axial strain [μ -strain]
ε_{el}	Elastic strain [μ -strain]
ε_p	Accumulated permanent strain [μ -strain]
$\varepsilon_{p,field}$	Accumulated permanent strain in field [μ -strain]
$\varepsilon_{p,lab}$	Accumulated permanent strain in laboratory [μ -strain]
ε_r	Resilient strain [μ -strain]
ν	Poisson's ratio [-]
σ_c	Confining stress [kPa]
σ_d	Deviatoric stress [kPa]
σ_h	Horizontal stress [kPa]
σ_v	Vertical stress [kPa]
σ_x	Compressive stress in x-direction [kPa]
σ_y	Compressive stress in y-direction [kPa]
σ_z	Compressive stress in z-direction [kPa]
σ_1	Largest principal stress [kPa]
$\sigma_{1,f}$	Largest principal stress at failure [kPa]
σ_2	Second largest principal stress [kPa]
σ_3	Third largest principal stress [kPa]
$\sigma_{3,0}$	Reference confining pressure = 1 [kPa]
τ	Shear stress [kPa]

Latin letters

a	Regression parameter in permanent deformation models [μ -strain]
A	Regression parameter of Equation 2.29 [-]
b	Regression parameter in permanent deformation models [-]
B	Regression parameter of Equation 2.29 [-]
d_{10}	Sieve size where 10% of the particles pass [mm]
d_{60}	Sieve size where 60% of the particles pass [mm]
D	Regression parameter of Equation 2.28 [-]
E	Elastic modulus [MPa]
G	Shear stiffness [MPa]
H	Regression parameter describing the permanent strain rate [-]
K_0	Lateral earth pressure coefficient at rest [-]
I_1	First stress invariant [kPa]
J	Final permanent strain in a permanent deformation model [μ -strain]
J_2	Second deviatoric stress tensor [kPa ²]
k	Cohesion intercept in Drucker-Prager [kPa]
K	Volumetric stiffness [MPa]
k_1	Regression parameter describing stress dependent resilient modulus [MPa]
k_1^*	Dimensionless regression parameter describing stress dependent resilient modulus [-]
k_1^{**}	Dimensionless regression parameter describing stress dependent resilient modulus [-]
k_2	Regression parameter describing stress dependent resilient modulus [-]
k_3	Regression parameter of Equation 2.25 [-]
k_4	Regression parameter of Equation 2.25 [-]
M	Slope of the failure envelope in the $q - p$ stress space [-]
M_r	Resilient modulus [MPa]
M_{r1}	Resilient modulus evaluated during the first load step at the 100 th load repetition [MPa]
M_{r2}	Resilient modulus evaluated during the first load step at the last load repetition [MPa]
M_{r3}	Resilient modulus evaluated during the second load step at the 100 th load repetition [MPa]
M_{r4}	Resilient modulus evaluated during the second load step at the last load repetition [MPa]

n	Material parameter in Equation 2.15 related to volume change behavior
N	Number of load repetitions
p	Mean stress [kPa]
p_a	Atmospheric pressure [kPa]
p_{max}	Maximum mean stress [kPa]
q	Deviatoric stress [kPa]
q_{max}	Maximum deviatoric stress [kPa]
Q	Regression parameter of Equation 2.28 [-]
Q_1	Regression parameter of Equation 2.28 [-]
Q_2	Regression parameter of Equation 2.28 [-]
S	Cohesion intercept in the $q - p$ stress space [kPa]

Acronyms

APT	Accelerated Pavement Test
CCP	Constant Confining Pressure triaxial test
DEM	Distinct Element Method
FWD	Falling Weight Deflectometer
HVS	Heavy Vehicle Simulator
LTPP	Long Term Pavement Performance
LVDT	Linear Voltage Differential Transformers
RMS	Root Mean Square
SRA	Swedish Road Administration
VCP	Variable Confining Pressure triaxial test
VTI	Transport Research Institute

1 INTRODUCTION

For the prediction of permanent deformation in road structures, use of analytical or mechanistic design methods is not very common in Sweden. Most design codes stipulate a maximum strain criterion derived from regression analyses. It has been found that there is a fair correlation between the “top of the subgrade” vertical elastic strain induced by a standard ten-ton axle and the permanent deformation observed on the surface. Thus, as the deformation rate can be related to the strain, any number of standard axles passing can be decided for a certain permissible deformation, e.g. a rut depth of 20 mm. As a single parameter criterion, research has yet to prove a better relationship. However, there are quite a few uncertainties for the pavement engineer to deal with.

Calculating the strain is not easy. The mechanical properties of each layer and the subgrade must be known. These properties also vary throughout the year. Non-linearity is handled by using a standard load and any deviation from that must thus be dealt with appropriately. Furthermore, a problem with regression relationships is that, no new materials can be introduced without a substantial testing and validation process. The possibility to consider permanent deformation in each layer of the road structure is also of interest as well as the development of permanent deformation over time. It would then be easier to compare different structures and see the influence of improvement in a single layer. The present thesis deals with the unbound layers of the road structure and their permanent deformation.

1.1 Background

Unbound granular material consists of single particles of different sizes. The source can be natural, such as gravel, or produced, such as crushed rock. Waste products are not very common. Stresses in the unbound material will be distributed through the contacts between the single grains. Deformation in the unbound material takes place in the contacts between the grains by crushing or sliding which will in turn move and rotate the single grains. Permanent deformation in the unbound material can be caused by compaction (volumetric) or shearing and the compaction can be intended or unintended.

Compaction of unbound material in a road structure has the purpose of increasing the bearing capacity of the material in order to avoid harmful deformation within the unbound layer but also within the whole road structure.

1. Introduction

There are different views on what exactly post compaction is. It is often referred to as the initial permanent deformation that has occurred in a road structure. In the present thesis, the definition of post compaction in unbound materials is the unintended compaction caused by wheel loads from heavy traffic after a road structure has been brought into service. Using this definition, post compaction is separated from permanent deformation caused by shearing.

Consequently, post compaction does not strictly occur in laboratory or field tests although the analogical behavior can be studied using these kinds of tests. Hence, the volumetric permanent strain that occurs in laboratory and field tests after the preparation of the sample or test surface will also be referred to as post compaction.

Post compaction is related to the stress level within the unbound material and the stress history. The response at higher stress levels is affected by loadings at lower stress levels. At higher vertical stress compared to horizontal stress, the risk of shearing and dilatation is increased. Shearing in the unbound materials occurs in road structures with a poor design regardless of whether the compaction is good or bad. Post compaction occurs in well designed road structures with insufficient compaction.

Excessive post compaction by traffic that cause permanent deformation reduces the serviceability and the service life of the road by several years and should therefore be minimized to an acceptable level, both with regard to serviceability and economy. To achieve this, a field test method used during the construction phase for quantification of the permanent deformation caused by post compaction is definitely needed. The test method must be reliable and provide a quick response at a low cost.

Permanent deformation tests where it is possible to see if the permanent deformation is caused by shearing or compaction is of course preferable. Then it is possible to quantify directly the effect of post compaction. However, it is difficult to separate compaction from shearing using field tests. It is also difficult to control all the parameters in a field test, such as the stress level. Permanent deformation tests are also time consuming and a quick response is important if the test is to be used as performance control during construction of the road structure. The measurement and evaluation of elastic properties can be used as a very quick method for evaluating compaction.

Well performed compaction by a roller will reduce the post compaction although the nature of compaction differs from real post compaction resulting from wheel loads of heavy traffic. The compaction control equipment of the rollers or the bearing capacity measurements using static plate bearing tests may therefore not be sufficient for quantifying post compaction. Instead a relationship between elastic response and post compaction in the field might be found. Hence, the first step for quantifying post compaction is to identify the conditions for it.

1.2 Objective

The objective of the present thesis is to identify the conditions for post compaction and separate it from permanent deformation caused by shearing/dilatation to facilitate process understanding.

1.3 Hypothesis

In order to identify the conditions for post compaction the relationships between permanent deformation caused by post compaction and shearing and their effect on the elastic response must be studied. The easiest way to find a relationship between elastic response and post compaction would be to compare the constant elastic properties before and after post compaction. However, the elastic properties of an unbound material are not constant but stress dependent and are also affected by pore volume, water content, grain size, time and so on. The effect of shearing on the elastic properties must also be clarified.

In the present thesis shearing/dilatation and post compaction are assumed not to occur at the same time as they are two conflicting processes. Compaction and post compaction reduce the pore volume and increase the density whilst shearing and dilatation cause the opposite. The volume reduction can be seen as increased density and permanent deformation.

During post compaction the permanent deformation rate (permanent deformation/load repetition) will be reduced continuously and by studying this it is possible to evaluate if there is any risk of further post compaction. As opposed to permanent deformation caused by shearing, the post compaction process will stop when it is not possible to reduce the pore volume of the unbound material any further at the current stress level. The post compaction process continues if the stress level is increased although only to a certain limit when shearing/dilatation of the structure may appear in the unbound material. It si

therefore important to clarify if there is any risk of shearing in the unbound material for the actual state of stress.

The reduced pore volume in the unbound material as a result of compaction and post compaction increases the number of contacts between the particles and also increases the contact areas between the particles. This will affect the elastic properties of the unbound material. However, the properties are also affected by the grain size distribution, the load level and in the field also by the other layers in the road structure. A constant elastic modulus is thus not a good indicator for identifying the conditions for post compaction. Unbound material has load (stress) hardening elastic properties and compaction and post compaction will influence these. The stress hardening can be evaluated by analyzing the elastic properties at different load levels.

According to the definition of post compaction used in the present thesis, post compaction occurs in real road structures in service. However, analogies to post compaction can also be seen in laboratory and field tests and there is a link between the three.

In the field it is possible to evaluate the stress hardening elastic properties by means of a multi load heavy falling weight deflectometer (FWD) test. If a road structure is exposed to post compaction from a wheel load for example, and FWD tests are performed before and after the post compaction, it is possible to relate post compaction to the change in stress hardening elastic properties. It is also possible to use this relationship if a FWD test is performed only after post compaction. Surfaces subjected to post compaction or not, i.e. within or outside the wheel track, may be analyzed. It is also important to be able to clarify in which structure layers the permanent deformation occurs.

It is, however, difficult to use field tests. The existing horizontal stresses and those caused by the load are unknown and impossible to control during post compaction and the FWD test. The horizontal stresses will probably also vary between the stations where the FWD tests are performed. There will also be influences from the other layers in the road structure and the subgrade. If the conditions for post compaction are to be studied, the field test can be complemented with a triaxial laboratory test. Here a single layer/material can be evaluated and horizontal stresses can be controlled. It is also easier to control the water content. Scale effects compared to field conditions are a disadvantage. However, it must be possible to test both the resilient and permanent deformation properties in the same laboratory triaxial test in order to relate post

compaction to the elastic properties. The stress hardening elastic properties can be evaluated in different ways. It is favorable to use as simple a relationship as possible between stress and resilient modulus when the results are from FWD tests due to the fact that only the vertical load and surface deflection are known.

In summary, this leads to three hypotheses in the present thesis:

1. Post compaction can be seen as a continuous decrease in the permanent deformation rate during repeated loading.
2. Post compaction occurs if the load characteristics of compaction and the loadings after compaction differ.
3. The stress hardening behavior is affected by compaction, post compaction and shearing.

1.4 Scope of work

In the present thesis post compaction is studied and evaluated by means of the following:

- A review of the literature and the theory of the subject in order to provide a theoretical and practical background and to improve the hypotheses.
- Use of results from laboratory triaxial tests for validating the hypotheses
- Use of results from field tests for validating the laboratory test results.
- Use of test results from unloaded and loaded road structures for comparison and validation.
- Discussion and conclusion

1.5 Limitations

For the unbound material evaluated, free drainage of water is assumed. Negative pore pressure values are assumed to be small compared to the stress from applied loads. Any separation of the total stress into effective stress and pore pressure is therefore not done.

2 LITERATURE REVIEW

2.1 Introduction

The unbound layers in a road construction act as a working platform for the overlying bound layers and through load distribution on the weaker subgrade. The unbound layers also act as drainage layers and help to avoid damage from frost-thawing processes (Smith & Collis 1993). For low-volume roads with a thin asphalt layer, the unbound granular layers carry most of the load (Dawson et al. 1994). It is therefore important to study the performance of the unbound material in a pavement structure. The present thesis focuses on identifying the conditions for post compaction and separates it from shearing/dilatation.

2.2 Mechanisms of deformation in unbound granular material

The deformation behavior of unbound granular material can be observed either by studying research roads with “normal” traffic or using accelerated tests and laboratory tests. The advantages of studying research roads with “normal” traffic are that many factors that influence the performance can be taken into account, such as climate, ageing and traffic load. If there is an interest in obtaining quicker results from performance tests, accelerated tests can be performed. The load level is easier to control in these tests. If the tests are performed in special test pits, the subgrade can be chosen. However, the climate factor and ageing cannot be taken into account, which also applies to any resting periods between load repetitions. A cheaper and even more controllable way is to perform laboratory tests. The most common laboratory test for evaluating resilient and permanent deformation behavior is the repeated load triaxial test. Strength parameters can also be evaluated using static triaxial tests.

From observations of the deformation behavior it is concluded that the granular material can be described as an elasto-plastic material (Wolf & Visser 1994, Baley et al. 1997, Uzan 1999, Ekdahl et al 2004b and Werkmeister 2003), which means that the total deformation consists of both a permanent and an elastic (resilient) deformation part during a load cycle. The resilient, elastic part is the dominant strain in every load cycle whilst the permanent strain increment is almost negligible and only needs to be taken into account after many load repetitions (El

Abd et al. 2005). An example of deformation measurement during a load cycle is shown in Figure 2.1 (Werkmeister (2003).

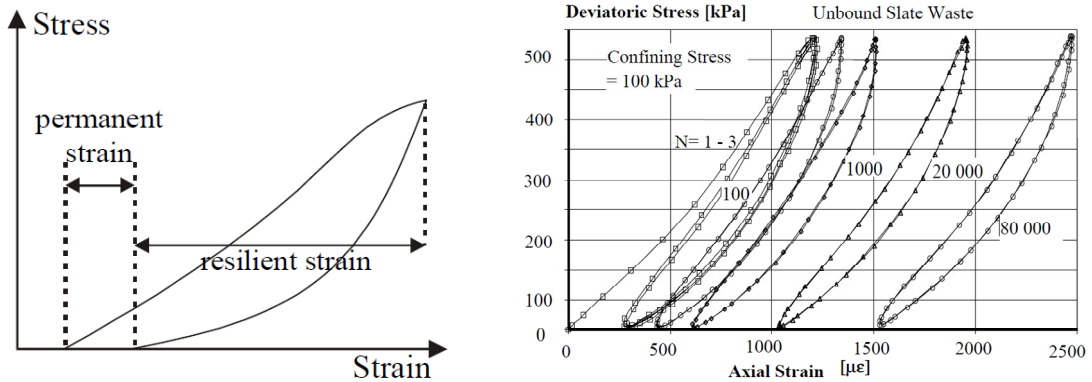


Figure 2.1. Load and unloading curves from a triaxial test. From Werkmeister (2003).

If different load levels are used as presented in Figure 2.2 (Thom 1988), it can be seen that an increase in load level increases the permanent strain rate, especially just after the increase in the load.

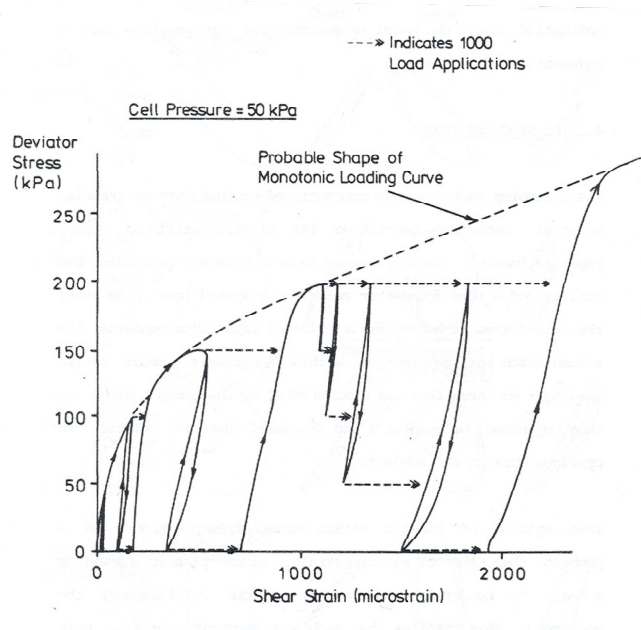


Figure 2.2. Load and unloading curves from a triaxial test. From Thom (1988).

After each unloading the permanent deformation increment can be seen in Thom (1988). At low loading levels, the permanent deformation can be negligible. If the load is increased, the elastic response increases in proportion to the increase in

load and the permanent deformation increases proportionally more than the elastic deformation (Tholén 1980).

The number of load repetitions, stress history, confining pressure, stress level and density are the parameters that influence the accumulation of permanent strain (Lentz & Baladi 1980). The stress history (previously applied stresses) reduces the permanent strain during repeated loading, i.e. the permanent strain rate for each load repetition. The increase in confining pressure results in a decrease in permanent strain whilst a reduction in density will increase the permanent strain. If the confining pressure is constant, an increase in principal stress level leads to an increase in the permanent strain (Barksdale 1972 and Yoder & Witzcak 1975), which also Thom (1998) concluded. Lenz & Baladi (1980) concluded that soils have non-linear behavior, which means that performance at low stress levels cannot be extrapolated to predict performance at high stress levels.

The development of permanent deformation in unbound granular materials as a result of repeated external wheel loads can be divided into two phases (Wolff & Visser 1994, Theys 1997, Núñez et al. 2004, Odermatt et al. 2004, Werkmeister et al (2004) and El-Basyouny et al. 2005). Firstly there is a rapid increase in permanent strain. The rate of increase in permanent strain is not constant but continuously decreasing. In the second phase, the permanent deformation strain rate is relatively slow and may approach a constant value, as illustrated in Figure 2.3.

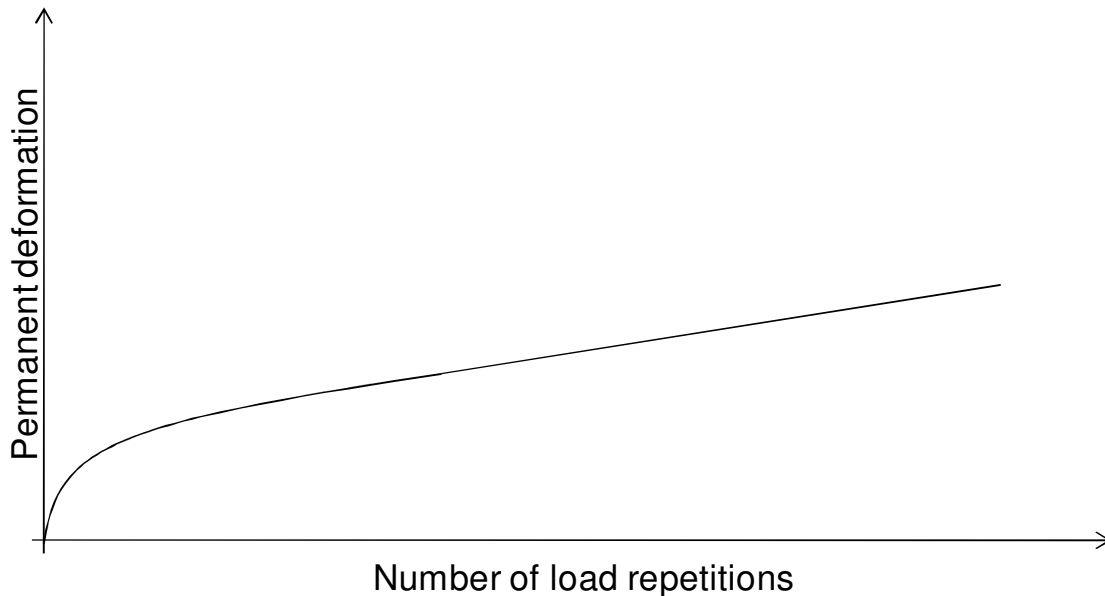


Figure 2.3. Example of development of permanent deformation in an unbound road material. After Theys (1997).

The initial phase is often described by, for example, Werkmeister et al. (2004) Núñez et al. (2004) and Odermatt et al. (2004) as post compaction. During post compaction there is densification of the material, a reduction in pore volume, and eventually crushing of the particles in the unbound material. This results in a volumetric change of the material (El-Basyouny et al. 2005). In a triaxial test an analogy with post compaction can be seen when the first load repetition causes considerable plastic strain. This can be described as a conditioning phase according to Baley et al. (1997), El Abd et al (2004) and El Abd (2005). Kolisoja (1998) and Hornyk et al. (1998) also noted an increase in material stiffness after a few load repetitions.

After the initial phase the deformation rate is more or less constant and the deformation is dominated by volume change although shear deformation rises at an increasing rate (Werkmeister et al. 2004). If failure occurs, there will be no volume change, just shear strain (El-Basyouny et al. 2005). Failure occurs when the deviatoric stress σ_d exceeds a threshold. Tholén (1980) stated that the permanent deformation is caused by compaction, crushing and material migration, both in the pavement and in the subgrade.

Werkmeister et al. (2004) divided the development of permanent deformation after the initial phase into three different types of behavior, which they labeled “A”, “B” and “C”, see Figure 2.4. Deformation behavior “A”, results in an initial phase of rapid increase in permanent strain. After this phase no further permanent strain is obtained. Behavior “B” involves a continuous increase in permanent deformation after the initial phase, and failure may eventually occur after a large number of load repetitions. In the case of behavior “C”, the material collapses almost immediately. Behaviors “A”, “B” and “C” are related to the stress - strength ratio.

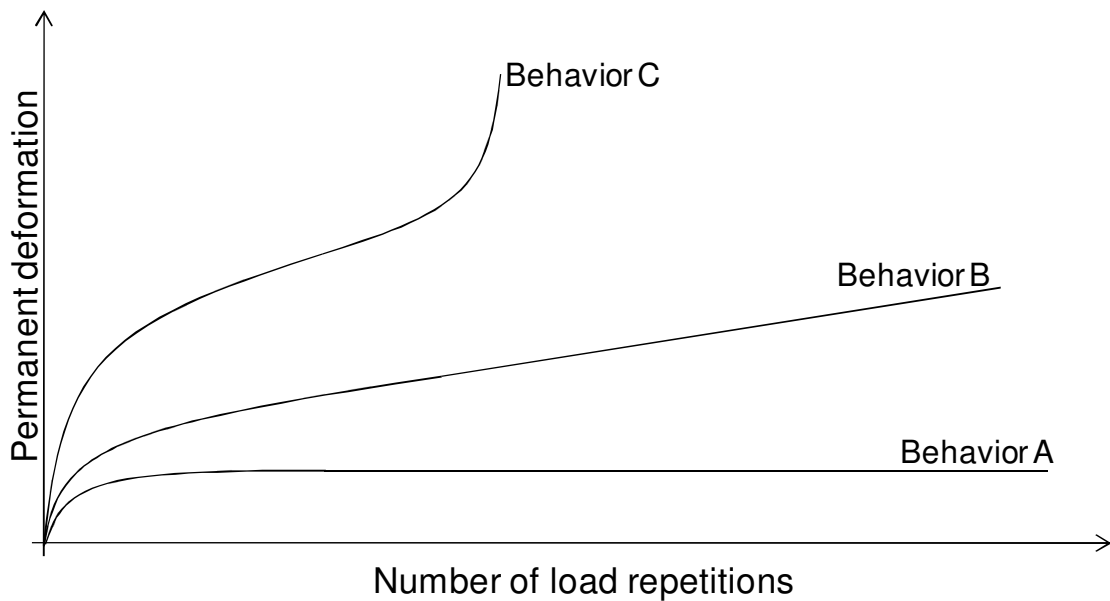


Figure 2.4. Permanent deformation behaviors “A”, B and “C” as described by Werkmeister et al. (2004).

Behaviors “B” and “C” can be described using the shake down approach. Lekarp & Isacsson (1998) among others explained the approach, which states that, if a material is loaded with a stress level above a specific limit known as the shake down load, there will be a progressive accumulation of plastic strain caused by repeated loading, which will lead to collapse or gradual failure. If the load level is below this limit, the plastic strain rate will be reduced to zero and the subsequent response will be elastic. Loads below the shake down limit results in a mainly elastic response that is significantly non-linear (El Abd et al 2004 and El Abd et al 2005). The stress level, at which the permanent strain must be considered, needs to be known for design purpose (Tholén 1980).

If rearrangement of the particles is prevented and if the particles are densely compacted, the only way deformation can occur is by means of an increase in volume, i.e. dilation. Hoff et al. (1998) observed an increase in volume of the sample during repeated triaxial load tests. This was a result of a shearing process, which in turn caused dilation (Figure 2.5).

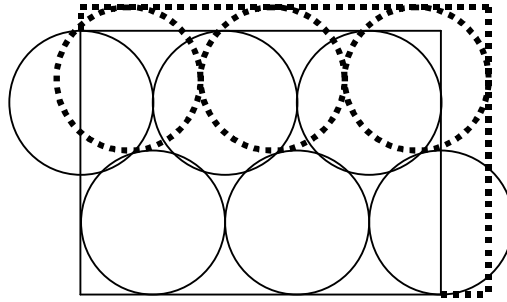


Figure 2.5. Increase in volume due to dilative behavior in the unbound material. After Hoff et al (1998).

This requires deformation in the opposite direction to the load. If the surrounded material prevents this, the stiffness of the granular material increases. Uzan (1999) states that granular material will dilate under high deviatoric stress.

The stress in the granular material is not evenly distributed. Ullidtz et al (1996), Ullidtz (1997), Ullidtz (1998), Kolisoja (1997), van Baars (1996), Troadec & Dodds (1993), Oda & Ivashita (1999) and Gervois & Bideau (1993) all concluded that the stresses within the material are distributed in stiff particle chains. Therefore some particles will be involved in the stress distribution and some will not. Due to permanent deformation, rearrangement of the particles will occur, which results in the development of new particle chains. These conclusions have been made by analyzing the deformation behavior of granular materials (Kolisoja 1997), simulations using laboratory tests (van Baars 1996, Troadec & Dodds 1993, (Oda & Ivashita 1999 and Gervois & Bideau 1993) and simulations using computer soft-ware (Ullidtz et al 1996, Ullidtz 1997, Ullidtz 1998, Kolisoja 1997). Due to the complexity of the problem the simulations were performed in two dimensions. Gervois & Bideau (1993) used photo elastic glass cylinders to perform a 2D simulation and concluded that approximately 15 % of the cylinders carried most of the external load and that approximately 50 % of the particles were not involved in the load distribution at all. Ullidtz (1998) used the Distinct Element Method (DEM), where forces and displacement of every particle were modeled individually. Kolisoja (1998) used Particle Flow Code (PFC) in 2D for his simulations. Hansson (2002) measured stresses in the contacts between unbound particles and a steel chamber and found a distribution of stresses from very high to very low.

The chain-like load distribution explains why larger grain size increases the stiffness of the unbound material. Kolisoja (1998) concluded that large particles result in fewer particles per chain and in turn fewer contacts where displacements take place. The total deformation therefore decreases.

Lindblom (1972) and Kolisoja (1998) described the permanent deformation process occurring in the unbound material at a discrete level. When the deviatoric stress q increases above a certain level this causes a decrease in the stiffness. The decrease in stiffness can be explained by sliding at the point of contacts between the particles when the shear stress exceeds the shear strength. The shear strength depends on the normal force and friction angle. The friction angle in turn depends on the surface roughness of the grains. If the deviatoric stress continues to increase, sliding occurs in more contacts. Until the system stabilizes, considerable rearrangement of the particles is necessary. Three types of process in the contacts were identified: elasto-plastic compression, shearing and crushing. Which one, dominate depends on the shape, strength and arrangement of the particles. The state of stress and stress history (pre-consolidation) also affects the permanent deformation process. The elasto-plastic compression in the contact depends on the normal force and material strength. If the normal force exceeds the strength the contact area will increase by crushing and around the area elastic compression will occur. The crushing process results in micro cracks in the material resulting from tension stresses. If the shear forces increase above the shear strength of the contact, sliding will occur. When the forces change in the contact, a new equilibrium will be found. If the stress state is below the pre-consolidation the deformation in the contact will be elastic compression, but as soon as the pre-consolidation stress is exceeded, sliding and crushing will start.

Werkmeister et al. (2004) reported that there is an associated change in resilient behavior, which is dependent on the “A”, “B” or “C” permanent deformation behavior (see Figure 2.4). The resilient response is constant for behavior “A” although the resilient modulus decreases with every load repetition when the permanent deformation behavior corresponds to “B”. El Abd et al (2005) conclude that the elastic strain is assumed to be unaffected by a large number of load repetitions, although the resilient strain decreases after the first few load repetitions.

The resilient (elastic) behavior of the unbound material is often referred to as non-linear, which is well known, (Dawson et al. 1994). Werkmeister (2003) termed the stiffer response in the unbound material during an increase in the stress level as “strain hardening”. Park & Lytton (2002) also reported that the non-linear behavior is apparent even at low stress levels and that this is dependent on the stress history and current stress state. The behavior observed in experiments shows that increasing hydrostatic stress levels also increase the

stiffness of the granular material. Niekerk et al. (1998) reported that an increase in confining pressure increases the stiffness of the material.

Kolisoja (1997) and Kolisoja (1998) explained the non-linear stress dependent behavior from a discrete perspective. Two particles in the unbound material are assumed to be spherical. Each of them consists of material with linear elastic properties and there is a linear relationship between stress and strain at the contact between the particles. If forces compress the particles against each other, there should be a linear elastic response between force and displacement. However, as the force increases, the contact area will increase. The larger the contact area, the higher the force must be to obtain the same rate of displacement between the particles (Figure 2.6).

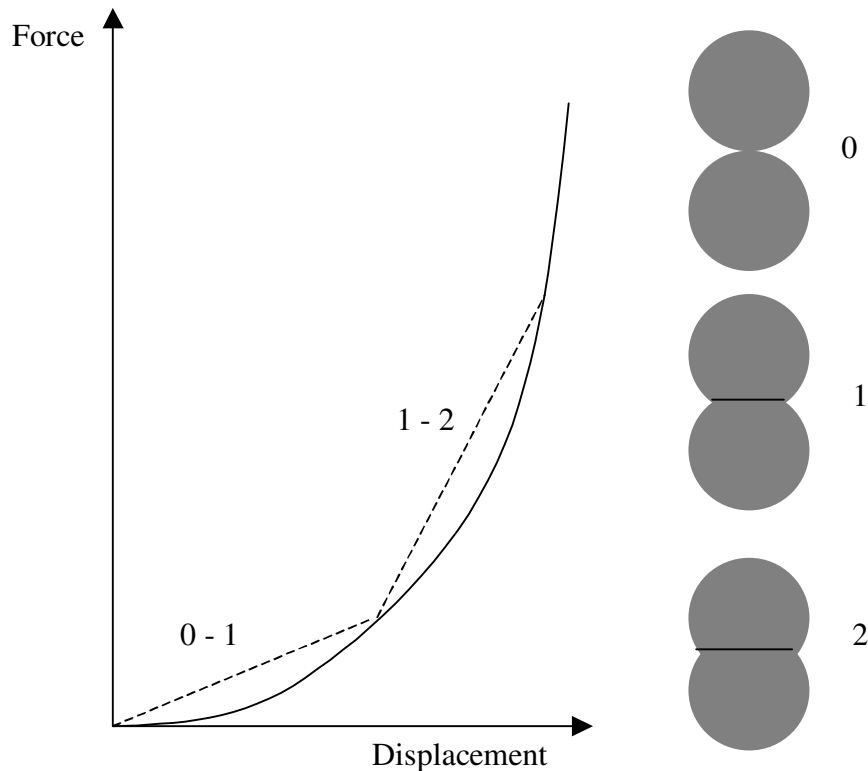


Figure 2.6. The principles of the non-linear behavior of unbound granular material. The increase of contact area increases the stiffness. After Kolisoja (1997).

Kolisoja (1998) concluded that the reduction in void content increases the number of contacts per particle with other particles, i.e. coordination number, which in turn increases the stiffness of the material. Kolisoja (1998) also stated that the particle assembly would react more stiffly at higher stress levels due to the non-linear behavior at the contacts between the particles. The effect becomes

even greater due to that fact that new contacts between the particles appear when the particles are subjected to increased compression and the number of contacts per particle will be increased.

Heydinger et al. (1996) described test results, where well-graded (containing different fractions) and open-graded (containing a single fraction) crushed lime stone was tested in a cyclic triaxial test. The behavior of the open-graded material was affected more by different stress levels than that of the well-graded one, although the latter had a higher deformation modulus. Material with well-graded grain size distribution will have many contacts between the particles and therefore higher shear resistance. If the material contains a lot of fines compared to the other fractions, the smaller grains may become positioned between the contacts of the larger particles, leading to a reduction in friction and thereby lower shear resistance. Smith & Collis (1993) say more about well-graded and open-graded materials and their properties.

2.3 Deformation behavior modeling

Theys (1997) described the permanent deformation behavior from a conceptual point of view. He found that permanent deformation is a dependent variable, not controllable during a test or in a real structure. It is dependent on the independent variables such as stress or strain and number of loads. The independent variables determine the rate and amount of the permanent deformation and can be controlled or measured. Theys (1997) divided the independent variables into primary and secondary. The primary variables are stress and strain levels and the number of load repetitions. These variables are needed to obtain permanent deformation. The secondary variables are moisture content, initial density and shear strength parameters. These variables influence the rate and amount of permanent deformation.

Ullidtz (1997) modeled the unbound material as consisting of discrete particles by using a Distinct Element Method (DEM). He simulated triaxial tests and observed large permanent strain after the first simulated load cycles, mostly due to particle sliding. Ullidtz (1997) obtained Poisson's ratios of more than 0.5 in his DEM simulations, which indicate a dilative behavior. By using the DEM, he showed that the first loading cycle caused more permanent than resilient (elastic) strain. At the end of the simulation Ullidtz observed that sliding and rotation of some particles caused the total permanent deformation but not all particles had moved.

Modeling the granular material as discrete particles can be useful to describe the deformation behavior but may be too complicated and time consuming for modeling the actual deformation (Kolisoja 1997). Therefore the continuum mechanical approach is still used. The granular material is simplified to be continuous and where stresses and strain describe the process instead of forces and displacement of particles.

In continuum mechanics the deformation behavior is related to stresses and there are different ways of describing them. The permanent deformation is often related to strength parameters. Resilient strain is also in some models related to the permanent strain. Stress, strength parameters, permanent deformation and resilient deformation modeling will therefore be described in the next chapter.

State of Stress in a Continuum Material

Ekblad (2004) and Samuelsson & Wiberg (1993) among others state that a continuum material can be represented by a three-dimensional cubic element as in Figure 2.7. External forces cause stresses in the material and therefore also in the cubic element. The state of stress of the element is represented by compressive stresses σ_x , σ_y , and σ_z , parallel to the x , y and z directions and shear stresses τ will also be present. For easier determination of the state of stress, the element in Figure 2.7 can be rotated, i.e. transformed to a coordinate system, where only principal stresses σ_1 , σ_2 , and σ_3 appear, in the principal directions 1, 2 and 3 as in Figure 2.8. Note that $\sigma_1 > \sigma_2 > \sigma_3$.

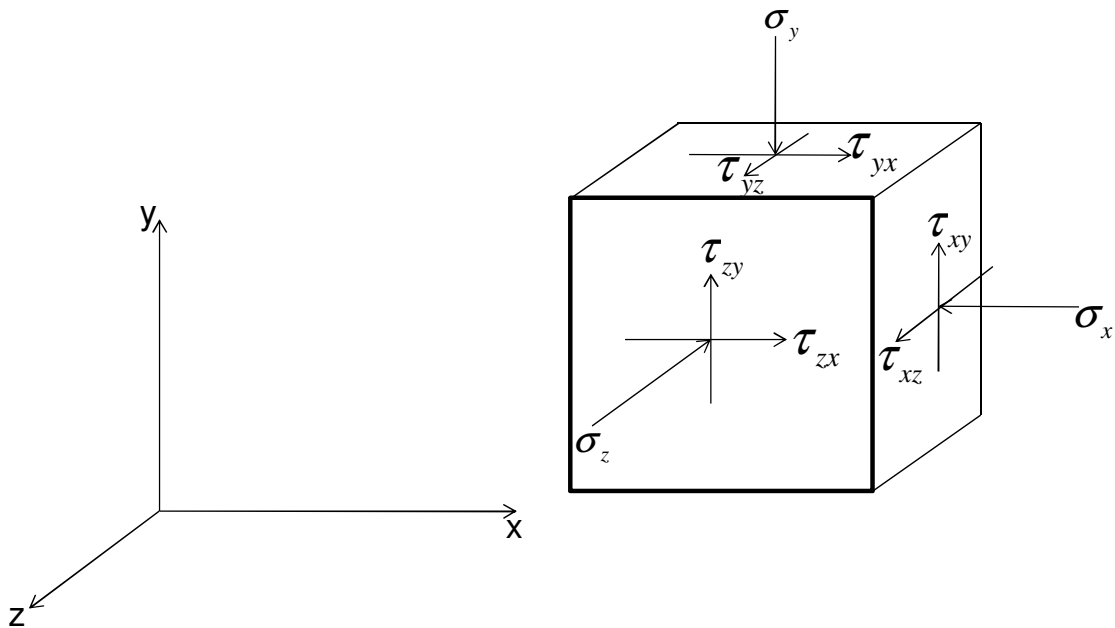


Figure 2.7. Stresses in x , y and z directions on a cubic element due to external forces.

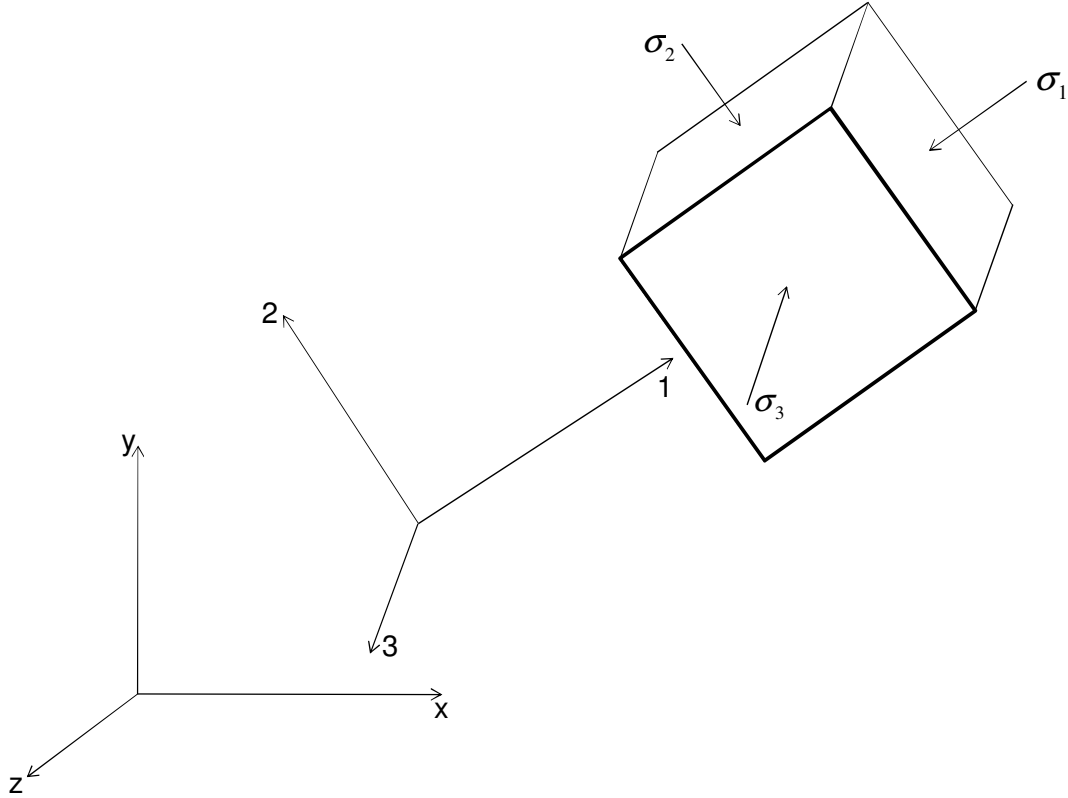


Figure 2.8. Stresses in the principal stress direction on a cubic element due to external forces after translation from the x, y, z coordinate system.

The state of stress can be described in the $\sigma_1, \sigma_2, \sigma_3$ - stress space as in Figure 2.8 and the state of stress can be expressed using the first stress invariant I_1 and the second deviatoric stress tensor J_2 . The first invariant I_1 for the three dimensional case is described in Equation 2.1. The second deviatoric stress tensor J_2 is expressed in Equation 2.2. For evaluation of the state of stress for a cylindrical load, $\sigma_2 = \sigma_3$ is valid.

$$I_1 = \sigma_1 + \sigma_3 + \sigma_3 = \sigma_1 + 2\sigma_3 \quad (2.1)$$

$$J_2 = \frac{1}{6} [(\sigma_1 - \sigma_3)^2 + (\sigma_1 - \sigma_3)^2 + (\sigma_3 - \sigma_3)^2] = \frac{1}{3} (\sigma_1 - \sigma_3)^2 \quad (2.2)$$

In different models for describing resilient and permanent deformation behavior it is also common to use deviatoric stress q , which for a cylindrical load is as described in Equation 2.3.

$$q = \sigma_1 - \sigma_3 \quad (2.3)$$

The mean stress p and bulk stress θ as described in Equation 2.4 and Equation 2.5 respectively.

$$p = \frac{\sigma_1 + \sigma_2 + \sigma_3}{3} = \frac{I_1}{3} \quad (2.4)$$

$$\theta = \sigma_1 + \sigma_2 + \sigma_3 = I_1 \quad (2.5)$$

In most cases the axial or vertical stress σ_v is higher than the confining stress σ_c or horizontal stress σ_h , which results in Equation 2.6 and Equation 2.7.

$$\sigma_1 = \sigma_v \quad (2.6)$$

$$\sigma_3 = \sigma_c = \sigma_h \quad (2.7)$$

The last two equations are only valid below the center of a circular load.

Permanent deformation behavior models

In the most common permanent deformation models the permanent deformation is related to the number of load applications N using a form of regression model. A model is calibrated by using test data from laboratory or field tests. The regression parameters can be related to physical parameters such as stresses, strength, moisture content and initial density (Theys 1997).

Barksdale (1972) described the relationship between the numbers of load repetitions N and accumulated permanent strain ε_p as a straight line in a semi logarithmic plot and this can be described mathematically using a logarithmic function as in Equation 2.8 (Lentz & Baladi 1980).

$$\varepsilon_p = a + b \ln N \quad (2.8)$$

The parameter a describes the permanent deformation at load application 1 and b the slope of the straight line in the semi logarithmic plot.

Yoder & Witzcak (1975) instead described the relationship as a straight line in a log-log plot. Sweere (1990) described this using a power law function as in Equation 2.9.

$$\varepsilon_p = aN^b \quad (2.9)$$

Again, the parameter a describes the permanent deformation at load application 1 and b the slope of the straight line in the log-log plot.

A logarithmic function describes a larger and more distinct initial post compaction phase and a relatively slower strain rate which is then compared to the power function. The results from permanent deformation tests can be used to calibrate the models. In other words, the parameters a and b are determined by regression analysis (i.e. curve fitting).

According to Lekarp (1999), Veverka (1979) found a relationship between permanent and resilient strain as in Equation 2.10.

$$\varepsilon_p = a\varepsilon_r N^b \quad (2.10)$$

Sweere (1990) did not find this relationship. However, all three equations more or less describe the initial post compaction phase. The continuing phase shows a continuously decreasing permanent strain rate. No asymptotic value can be seen, which puts the described behavior between behavior A and B as in Figure 2.4 (Werkmeister et al 2004). In other, words the strain will never be zero but no failure behavior is modeled. To model behavior A, in Figure 2.4 (Werkmeister et al 2004), a final permanent deformation (asymptotic value) can be set (or calculated) and the development toward the final deformation can be described in a manner similar to the power function as suggested by Paute (Dawson et al. 1994) (Equation 2.8). The final permanent deformation (the asymptotic value) is described by the parameter J and the strain rate to the final deformation is controlled by parameter H . The shape of the curve described by Equation 2.11 has, however, a problem describing the initial post compaction behavior. The development for the first 100 load applications is therefore excluded.

$$\varepsilon_p(N) = J \left[1 - \left(\frac{N}{100} \right)^{-H} \right] \quad (2.11)$$

Huurman (1997) suggested a power function that excluded the first 1 000 load applications. Excluding the initial post compaction is rather common in permanent deformation modeling. According to Werkmeister (2003) this phase is not as interesting to describe as it happens only once in the service life of a road structure.

The regression parameters can be given physical meaning by, for example, relating them to stress level and stress at failure. Parameter J in Equation 2.11 can, for example, be related to deviatoric stress q and mean stress p as in Equation 2.12 (Dawson et al. 1994).

$$J = \frac{\frac{q}{p}}{a - b \frac{q}{p}} \quad (2.12)$$

The higher the deviatoric stress, the higher the final permanent deformation, which is reasonable. Huurmann (1997) related the model parameters to the stress/strength ratio $\sigma_1 / \sigma_{1,f}$, where σ_1 = axial stress and $\sigma_{1,f}$ = axial stress at failure according to the Mohr-Coulombs failure criterion by using regression analysis. The Huurmann expression shows that the closer the stress level is to the strength, the higher the permanent strain rate, which is logical due to the observations of permanent deformation behavior described above.

Werkmeister et al. (2004) used the Huurmann model but found it difficult to determine $\sigma_{1,f}$ for crushed materials. It was therefore not possible to use the stress/strength ratio. Other relationships were developed with consideration given to vertical stress and confining pressure, different for behavior A and B. The relationship showed that the higher the confining pressure, the lower the permanent strain rate, which is reasonable.

Sweeres power function (Equation 2.9) was complemented by Korkiala-Tanttu (2005) in order to consider the shearing in the material. The deviatoric stress q was assumed to have most influence the permanent strain development. Korkiala-Tanttu found that the permanent deformation of the first loading cycle is dependent on the degree of compaction and water content. When identical materials were studied, the permanent strain rate was higher in the field compared to the laboratory.

A model created by Paute, developed by Gidel (2001) and used by El Abd et al. (2004) used both the empirical relationship to the number of load applications and an elastoplastic model. Here the applied cyclic stresses p_{\max} and q_{\max} were combined with the failure envelope in the $p - q$ stress space (Equation 2.13).

$$q = Mp + S \quad (2.13)$$

Where M describes the slope and S the cohesion intercept as in Figure 2.9, see also Equation 2.3 and Equation 2.4.

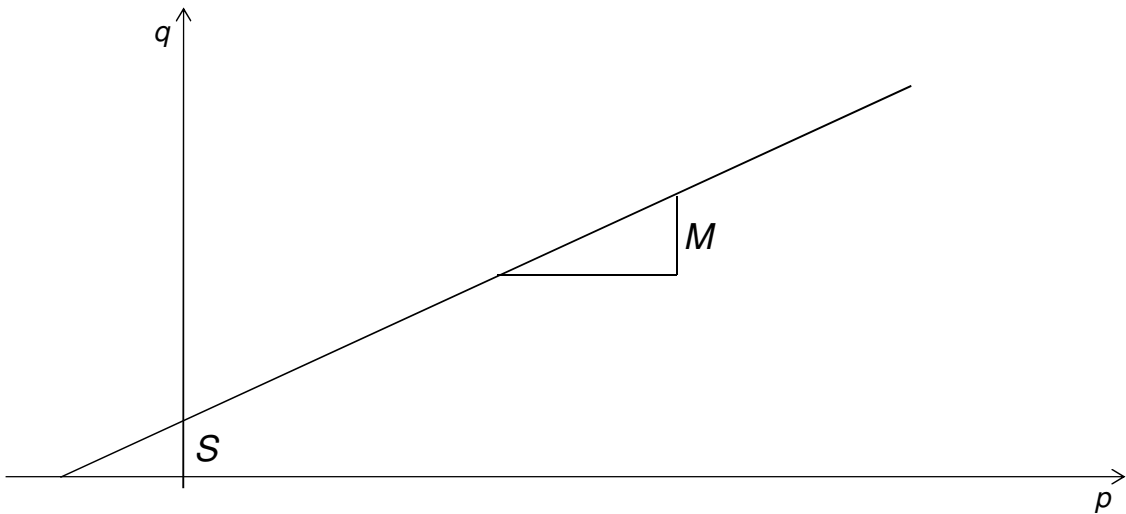


Figure 2.9. Failure criterion in the $p - q$ stress space.

The model by Gidel and Paute showed that high strength and low deviatoric stress result in low permanent strain.

Núñez et al. (2004) found relationships between the permanent strain during post compaction and the permanent strain rate at the phase after the initial post compaction (deformation behavior B according to Werkmeister et al 2004 Figure 2.4). Deviatoric stress, the stress/strength ratio and initial permanent deformation showed a good fit in regression.

There are also attempts to relate the resilient strain response to the permanent strain. An example of this is a model developed by Tseng & Lytton (1989). This was used by for example El-Basyouny et al. (2005) and Erlingsson & Ingasson (2004). El-Basyouny et al calibrated the model by evaluating old structures. Erlingsson & Ingasson assumed that the ratio between permanent and resilient strain obtained from the laboratory test was also valid in the field. The model was

used to predict the results of an accelerated pavement test using a Heavy Vehicle Simulator (HVS). Two different design types were used and the model provided good predictions of both. Werkmeister et al. (2005) found a linear relationship between $\log(\varepsilon_p)$ and $\log(\varepsilon_{el})$ in the cyclic load test.

There is a difference between the measured permanent deformation in the field and in the laboratory. This can be described by introducing a shift factor S_f as in Equation 2.14.

$$S_f = \frac{\varepsilon_{p,field}}{\varepsilon_{p,lab}} \quad (2.14)$$

According to Werkmeister et al. (2005), the shift factor is probably dependent on the material used and stress level. They found that the shift factor could vary between 2.9 and 3.3. The shift factor can be explained by the rotation of the principal stress axes, which occurs in the field due to a moving wheel load causing larger permanent deformation. The load in a laboratory test is often uniaxial.

In many of the models described above the stress level and the stress/strength ratio are used to describe the permanent deformation behavior. Lekarp & Isacsson (1998) and Werkmeister (2003) among others described the shake down approach, where stresses below a stress threshold result in stable behavior where the permanent strain rate is reduced to zero after the post compaction phase. Stresses above this threshold result in shearing and the permanent strain rate could be stable or result in failure depending how close to the strength the stress level is. Bonaquist & Witzak (1997) described and used a model to consider this behavior, developed by Desai (1986). The model describes the behavior of geological materials during yielding. Permanent strain is assumed to be a function of the state of stress and strain and can be described using a yield function in the $I_1 - \sqrt{J_2}$ stress space, Equation 2.15 (see Figure 2.10).

$$\frac{J_2}{p_a^2} - \left[\gamma \left(\frac{I_1}{p_a} \right)^2 - \alpha \left(\frac{I_1}{p_a} \right)^n \right] = 0 \quad (2.15)$$

Where J_2 = second invariant of the deviatoric stress tensor, I_1 = first invariant of the stress tensor, p_a = atmospheric pressure (100 kPa) as a reference and γ, α, n = material parameters.

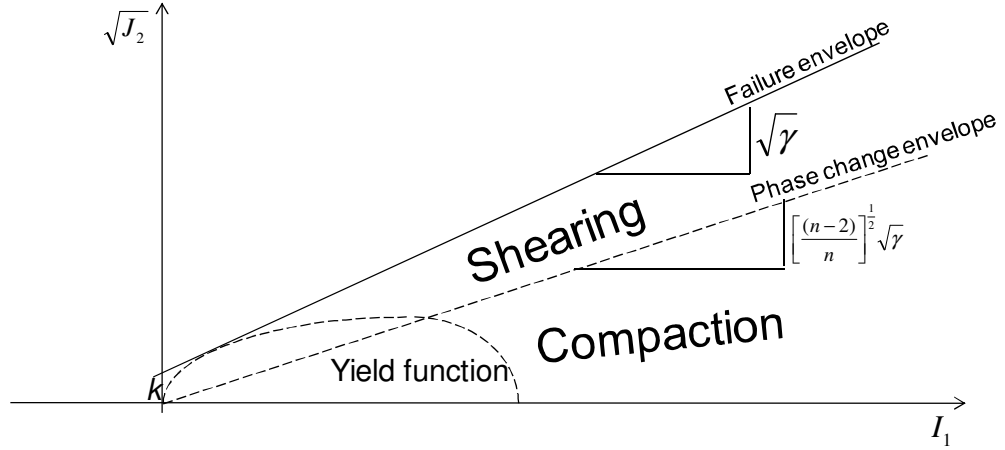


Figure 2.10. Failure criterion of Drucker-Prager combined with a phase change envelope for separating dilative and compaction behavior during permanent deformation and a series of yield surfaces to describe the permanent strain behavior. After Bonaquist & Witczak (1997).

When the plastic strain of the material increases, the yield surface expands. The size of the yield surface is controlled by the hardening parameter α . When the value of α decreases, the yield surface expands. At failure, α is infinite and the yield function in Equation 2.15 is reduced to the Drucker-Prager failure envelope, which is described in Figure 2.10 and Equation 2.16.

$$\sqrt{J_2} = \sqrt{\gamma}I_1 + k \quad (2.16).$$

$\sqrt{\gamma}$ is the slope of the failure envelope of Drucker-Prager and the parameter k is the cohesion intercept.

The parameter n in Equation 2.15 is related to the volume change behavior. The direction in which the yield surface expands is described by the normal of the yield surface. If the normal of the yield surface has a component in the positive I_1 direction, the material will be compacted when plastic strain occurs. This takes place when the ratio $\sqrt{J_2}/I_1$ is low. At higher $\sqrt{J_2}/I_1$ ratios, the component is in the negative I_1 direction and the material will instead dilate as a result of plastic strain. If the normal is perpendicular to the I_1 - axis there will be no volume change at all. This point on the yield surface can be found if the derivate of

Equation 2.15 with respect to I_1 is equal to zero. The result is introduced into the yield function giving the expression in Equation 2.17.

$$\frac{\sqrt{J_2}}{I_1} = \left[\frac{(n-2)}{n} \right]^{\frac{1}{2}} \sqrt{\gamma} \quad (2.17)$$

This new expression represents the phase change envelope in Figure 2.10. At a low $\sqrt{J_2}/I_1$ ratio, i.e. high confining pressure compared to axial stress, the material will be compacted when plastic strain occurs, which will result in a stable behavior. At higher $\sqrt{J_2}/I_1$ ratios, the material will instead dilate as a result of plastic strain due to shearing. The stress states on this phase envelope indicate conditions where no volume change occurs.

For n values close to 2, the phase change envelope is approaching the I_1 axis, which will describe a behavior where all permanent deformation will be caused by shearing. For n values approaching ∞ , all permanent deformation will be caused by compaction.

Resilient Deformation Behavior Models

The granular material has in many cases been simplified to be linear elastic due to easier expressions for calculating stresses and strains. However, when the deformation modulus is studied it is clear that it is stress dependent. The deformation modulus is therefore referred to as a resilient modulus M_r instead of a constant elastic modulus.

The non-linear behavior of unbound granular material has been described by Dawson et al. 1994, Ullidtz et al. (1996), Heydinger et al. (1996), Kolisoja (1998), Niekerk et al. (1998) and Park & Lytton (2002) among others. Stress dependency is analyzed by evaluating the modulus at different stress levels. The parameters describing stress dependency are often evaluated by means of regression, where the modulus is the dependent parameter. Brown & Pell (1967, after Kolisoja 1998) described the relationship of the resilient modulus M_r to the stress level using the well-known $k - \theta$ model, presented in Equation 2.18. The bulk stress θ is equal to the sum of the principal stresses, described using Equation 2.19. The regression parameters in this power function (log-log) model are k_1 and k_2 . If M_r is plotted versus the bulk stress θ , k_2 is the slope of the line in the log-log space. The higher the k_2 -value, the more stress dependent the resilient modulus (Heydinger et al. 1996). The regression parameter k_1^* describes the extrapolated

value of M_r for $\theta = 1$ kPa if the plotted values are in the log-log scale and the unit of θ is in kPa.

$$M_r = k_1^* \theta^{k_2} \quad (2.18)$$

$$\theta = \sigma_1 + \sigma_2 + \sigma_3 \quad (2.19)$$

There is some confusion about the use of the $k - \theta$ model in the form described in Equation 2.18, due to the fact that factor k_1^* is not dimensionless i.e. the dimension of k_1^* is dependent of the value of k_2 . Consequently Niekerk et al. (1998) used a form of the $k - \theta$ model where a reference stress $\theta_0 = 1$ kPa in order to render k_1^* in the same unit as M_r (Equation 2.20) (described as k_1) or as k_1^{**} in Equation 2.21 where k_1^{**} is dimensionless.

$$M_r = k_1 \left(\frac{\theta}{\theta_0} \right)^{k_2} \quad (2.20)$$

$$M_r = k_1^{**} \theta_0 \left(\frac{\theta}{\theta_0} \right)^{k_2} \quad (2.21)$$

The values of the parameters k_1 or k_2 are not affected by the inclusion of the reference stress $\theta_0 = 1$ kPa. Instead of using a reference stress of $\theta_0 = 1$ kPa, there are examples of using the atmospheric pressure $p_a = 100$ kPa instead in Equation 2.19 (Erlingsson & Ingasson (2004) and Andrei et al. (2004)). In the latter case the k_2 -value is not affected but the k_1 - value is.

There is a relationship between k_1 and k_2 . Boudali & Roberts (1998) reported that a low k_2 value is compensated for by a higher k_1 - value and Niekerk et al. (1998) described this relationship using Equation 2.22.

$$k_1 = C_1 k_2^{c_2} \quad (2.22)$$

A relationship between the k_2 - value and the grain size distribution, represented by the ratio d_{60}/d_{10} , was also found by Niekerk et al. (1998). The parameter d_{60} represents the sieve size that allows 60% of the material to pass through the mesh while d_{10} is the sieve size that allows 10% of the material to pass through the mesh. A larger ratio represents a well-graded grain size distribution while a low ratio indicates a more single size grain distribution. The relationship is presented

in Equation 2.23 and the results indicate that the more well-graded the material, the higher the k_2 -value. An explanation could be that well-graded material has a greater number of contacts between the grains compared to a single grain size material. This in turn results in a more stress dependent modulus, which confirms the analysis made by Kolisoja (1998). Boudali & Robert (1998) on the other hand did not observe any difference in the modulus for different grain size distributions. Instead, the k_1 value appeared to be affected by the strength of the individual grains. A larger k_1 was obtained for lower grain strength. A higher void content of the structure (grain skeleton) resulted in a lower k_1 value, and k_2 appeared to be unaffected by other parameters, although it should relate to certain cohesion in the material. Suction also affected the k_1 value.

$$k_2 = C_0 + C_1 \left(\frac{d_{60}}{d_{10}} \right)^{C_2} \quad (2.23)$$

The stiffening effect on granular material of a higher confining pressure is clear. Dunlap (1963) (after Boudali & Robert 1998) reported that the modulus of coarse-grained materials increases in line with increasing confining pressure. The increased axial stiffness of the granular material caused by higher confining pressure is due to the dilatancy characteristics. If the confining pressure is high, the material resists shearing, which in turn results in a higher axial modulus.

The, $k - \theta$ model, Equation 2.20 is useful for analyzing triaxial laboratory test results (Irwin 1994). However, difficulties arise when pavement structures are analyzed. The unbound layers bend under the load, which may cause tensile stresses at the bottom of this layer, which may give a negative θ . For this state of stress, the resilient modulus is undefined. Instead, semi-logarithmic models can be used. In these models, only the resilient modulus data are transformed into their logarithms as in Equation 2.24.

$$M_r = k_1 e^{\theta k_2} \quad (2.24)$$

Another shortcoming with the $k - \theta$ model is that it is not valid for simulating a moving wheel (Correia & De Almeida 1998). Dawson et al. (1994) concluded that the $k - \theta$ model is valid, i.e. gives a good fit in regression analysis at higher stress levels but not at stress levels close to failure. A high stress level appears beneath thin asphalt layers. In line with this, Niekerk et al. (1998) used the $k - \theta$ model for stress levels far lower than the strength of the material and Equation 2.25 for stress levels closer to failure stress, where the stress/strength ratio is considered.

$$M_r = k_1 \left(\frac{\sigma_3}{\sigma_{3,0}} \right)^{k_2} \left(1 - k_3 \left(\frac{\sigma_1}{\sigma_{1,f}} \right)^{k_4} \right) \quad (2.25)$$

Here $\sigma_{3,0} = 1.0$ kPa and $\sigma_{1,f}$ = axial stress at failure.

A positive k_2 -value in the $k - \theta$ model for granular material indicates stress hardening behavior. A negative value indicates stress softening behavior. Unlike granular material, fine grained materials such as clay have softening behavior, which is described by Park & Lytton (2002) among others. Regression analysis using deviatoric q stress instead of bulk stress θ in a log-log model shows better fit, which means that Equation 2.26 is more valid for fine grained materials than Equation 2.20.

$$M_r = k_1 q^{k_2} \quad (2.26)$$

Some materials can have both coarse and fine grained properties and therefore combined models can be used instead (Andrei et al. 2004). Witczak & May (1981) and Uzan (1985) proposed one such model, described by Bouladi & Robert (1998) and presented in Equation 2.27.

$$M_r = k_1 \left(\frac{\theta}{p_a} \right)^{k_2} \cdot \left(\frac{q}{p_a} \right)^{k_3} \quad (2.27)$$

The parameter $p_a = 100$ kPa is the atmospheric pressure while k_1 to k_3 are regression parameters. Bouladi & Robert (1998) concluded that Equation 2.27 provided a better fit than the $k - \theta$ model (Equation 2.20).

Park & Fernando (1998) performed a sensitivity analysis of the Universal Soil Model, Equation 2.27. The regression parameters $k_1 - k_3$ were determined by evaluating repeated load triaxial tests. Mohr-Coulomb's strength parameters, cohesion and angle of inner friction were determined by evaluating static strength tests. The resilient modulus and permanent strain were predicted by means of Equation 2.26 and a relationship was established between the resilient modulus, strength parameters and plastic strain. The sensitivity analysis was performed in order to determine the influence of the different parameters on the resilient modulus and plastic strain. The strength parameters and the different k -values were therefore varied $\pm 30\%$ from the base value, one at a time and stress,

resilient and permanent strain calculations of a pavement structure were performed. The parameter k_1 was assumed to have the greatest influence on the resilient modulus while the predominance of hardening or softening behavior depends on the stress level and geometry. These relationships were used to predict plastic strain. The sensitivity analysis showed that k_1 has the greatest influence on the plastic strain. When k_1 was increased, the plastic strain in the base layer also increased. This can be explained by the fact that higher stiffness increases the stress level and therefore the plastic strain. The effect of change in k_2 was somewhat confusing. An increase in k_2 results in greater stiffness, which in turn increases the stress, thus leading to greater plastic strain. A decrease in k_2 results in a softer response, which in turn causes increased plastic strain. The k_3 value had no effect whatsoever on the plastic strain. The Mohr Coulomb strength parameters were also varied. The friction angle had the most significant influence. It was also concluded that base and subgrade are important for bearing capacity. Adequate support increases the confining pressure and reduces bending in the overlying layer.

Dawson et al. (1994) reported that instead of describing the resilient behavior by resilient modulus and Poisson's ratio, the stress dependent volumetric and shear stiffness can be used. Boyce (1980) suggested an expression for volumetric stiffness K , which was dependent on mean normal stress and deviatoric stress. An expression of the shear stiffness and G was also suggested, which was dependent on the mean stress. Correia & De Almeida (1998) used the expressions of K and G when evaluating Variable Confining Pressure triaxial tests. From the expressions of K and G the resilient modulus M_r and Poisson's ratio ν can be evaluated. El Abd et al. (2005) used the Boyce model to calculate volumetric and shear strain and completed it with an anisotropy variable.

Werkmeister et al. (2005) described a stress-dependent resilient model developed in Dresden. The modulus of elasticity E and Poisson's ratio ν are determined using Equation 2.28 and Equation 2.29,

$$E = p_a \left(Q + C \left(\frac{\sigma_3}{p_a} \right)^{Q_1} \right) \cdot \left(\frac{\sigma_1}{p_a} \right)^{Q_2} + D \quad (2.28)$$

$$\nu = R \frac{\sigma_1}{\sigma_3} + A \frac{\sigma_1}{p_a} + B \quad (2.29)$$

Where D is a constant term for the modulus of elasticity that is stress independent but affected by compaction degree, fine content, grain shape and water content. This parameter cannot be determined by repeated load triaxial tests due to the fact that the residual stress needs some time to develop in real pavement constructions.

2.4 Measuring deformation behavior

The deformation behavior that has been observed and modeled is formulated from the results from laboratory triaxial tests or field measurements. The measurements provide input data for the deformation models. From the triaxial test, the resilient response or permanent deformation performance of the material can be evaluated. The field measurements that are considered in the present thesis are the Falling Weight Deflectometer (FWD), see Tholén (1980) and the HVS, see Rust et al. (1997). The FWD measures the bearing capacity of the pavement. The HVS is an accelerated pavement testing method for evaluating permanent deformation performance of the pavement.

From the measurements of stresses and strains in the field, the resilient properties can be evaluated by using backcalculation, which is also studied in the present thesis. The bearing capacity is measured indirectly and the stress-strain relationship be evaluated and expressed as layer modulus, surface modulus, deflection, and surface curvature (Tholén 1980).

Laboratory triaxial tests

According to Brown & Pappin (1981), repeated load triaxial tests can be performed in two different ways, either with Constant Confining Pressure, CCP, or Variable Confining Pressure, VCP. In a VCP test both confining pressure and deviatoric stress are cycled while only the deviatoric stress is cycled in CCP tests. The variable confining pressure tests make it possible to use different stress path slopes in the $p - q$ space. Vehicle load also induces rotation of the principal stresses according to Correia & De Almeida (1998) and Chou & Tutumluer (2001). This behavior increases the rate of both shear and volumetric strain. The use of a variable confining pressure test is better for simulating the wheel load but cannot simulate the principal stress rotation (Correia & De Almeida (1998), Chou & Tutumluer (2001), Balye et al. (1997) and Boudali & Robert (1998)). For this a hollow cylinder test can be used instead (Thom (1988)). The deformation modulus seems to be overestimated in constant confining tests.

Irwin (1994) discussed the difference in confining pressure between laboratory and field. In the laboratory tests, equal confining pressure is used in the vertical and horizontal direction, but in a road structure the vertical confining stress is greater than the horizontal, which results in an anisotropic stress state. The anisotropic consolidation ratio describes this state and has a major effect on the resilient modulus. This means that the isotropic consolidation used in the triaxial test is incorrect. The problem is how to identify which lateral earth pressure coefficient at rest K_0 should be used during the consolidation, due to the fact that it is influenced by the degree of compaction of the unbound material. The lateral earth pressure coefficient at rest K_0 describes the relationship between the horizontal effective stress σ_h and the vertical effective stress σ_v as in Equation 2.30.

$$K_0 = \frac{\sigma_h}{\sigma_v} \quad (2.30)$$

Instrumentation in the field

Lytton (1989) stated that in most cases the elastic stiffness is the property obtained from non-destructive testing on pavements. The various sets of test equipment for non-destructive testing have different methods for applying loads to the pavement as well as a different number of sensors for evaluating the response. Examples of load modes are static or slowly moving loads, vibration loads, near field impulse methods and wave propagation methods. Response measurements can be performed on the pavement surface or using in-depth instrumentation. The sensors used for response measurements can be accelerometers for acceleration measurements, geophones for velocity measurements or Linear Voltage Differential Transformers (LVDT) (see Mork (1994)) for displacement measurements. Near field impulse loads can be applied by means of the FWD.

Falling Weight Deflectometer

Tholén (1980) described the principles of FWD tests, see Figure 2.11.

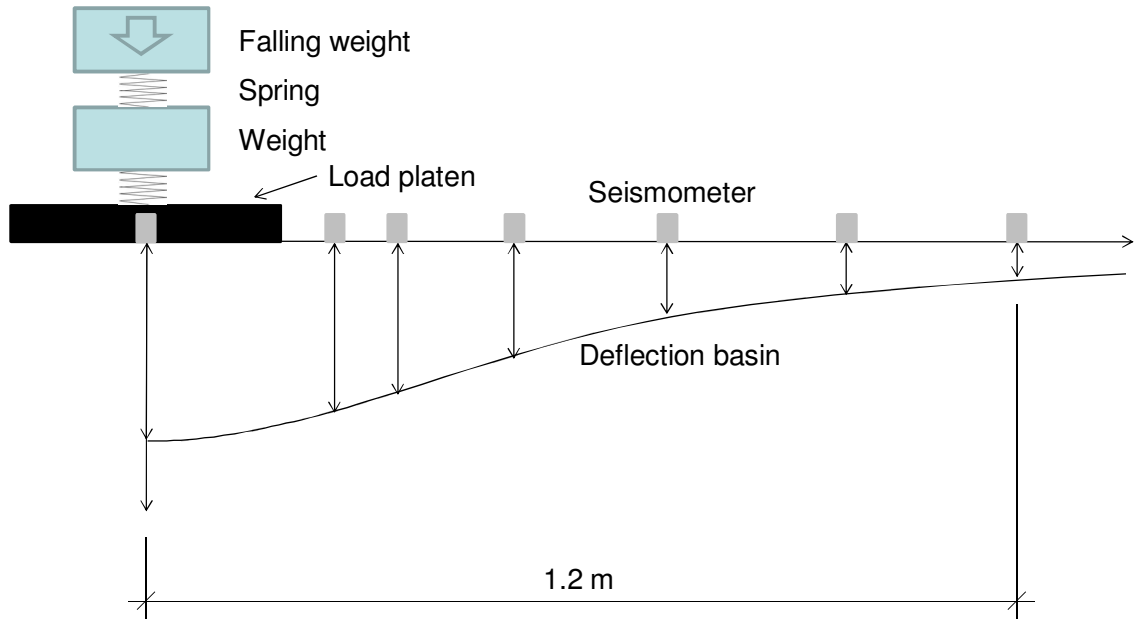


Figure 2.11. The principle of the Falling Weight Deflectometer.

A weight is dropped onto a spring system connected to a load platen, which transmits the load to the pavement surface. The peak value of the force on the pavement surface and the shape of the loading and unloading curve are determined by the mass of the weight, as well as the height and properties of the spring system. The FWD load is designed to mimic that of heavy traffic. Deflection is measured at the center of the load as well as at a number of other points away from the load. Deflections close to the load are influenced by the material properties of the upper layers of the structure and vice versa. Due to the viscoelastic properties of asphalt and the dependence of the strain rate on fine-grained materials, it is important that the load pulse of the FWD has the same temporal duration as heavy traffic. For this reason, Tholén (1980) improved the FWD device by adding a two mass system where the falling weight first hits one spring system, after which the load is transmitted to another load shape and continues to the second spring system and then to the load platen. This results in a near half sine load pulse shape. The load platen was also improved by being divided into different segments. As a result, a better contact surface between the load platen and the pavement surface was obtained when uneven pavement surfaces were tested.

Lenngren (1994) reported that when the FWD load impacted on the surface of the pavement, the stresses are propagated from the load center and out. In the case of a moving wheel load, the deflection basin follows the wheel in a stationary fashion. In most cases only the maximum deflection is recorded by the

deformation sensors in FWD tests, but it will not be at the same time for all sensors. If time history data are used, the deflection development from impact to recovery is recorded, which in turn contains valuable information on the material properties, such as dynamic and non-linear elastic behavior.

Backcalculation of FWD data

The measured “deflection basin” can be used for different ways of calculation, such as calculating curvature and horizontal strain at the bottom of the bitumen bound layer. The deflection basin can also be used as input data in the backcalculation process. In this process the elastic modulus of the different layers of the tested structure are reasonably assumed from experience. A forward calculation is performed with these elastic modules and a deflection basin is calculated. The thickness of the different layers must also be known. The calculated deflection basin is compared with the measured one, and if necessary the assumed elastic modules are adjusted and used in a new forward calculation for better fit to the measured deflection basin. In the backcalculation process, the moduli of the deepest layers are first determined by using the outer sensors, after which the sensors closer to the load are used to calculate the moduli of the upper layers. To obtain the best fitting an iterative process is applied that continues until the root mean square value (RMS) is less than a certain pre-defined limit. For a quicker result a backcalculation program can be used. A number of programs are available for backcalculation. The deflections are calculated by assuming that the pavement system can be described as a multilayered elastic system. In this system, the pavement is described as a homogeneous half space, with an infinitely large area and an infinite depth. The analytical method for determining the stresses and strains assumes that the material in each layer is homogenous, isotropic and can be described using the elastic modulus and Poisson’s ratio. The layers must have a finite thickness except for the lowest layer and the load is a uniform pressure applied on the surface over a circular area with a known radius. Full friction between the layers is normally also assumed.

Same source data have been used for backcalculation of moduli with different programs. The results show a difference of up to 37 % for the asphalt layer on top and 14% for unbound material. The layer thickness is a very important parameter according to Von Quintus & Killingsworth (1998). It must be accurate in order to provide a good backcalculation result. Flintsch et al. (2003) stated that common problems in performing backcalculations are the determination of the depth to rigid bottom, stress dependency of granular material and plastic deformation in thin surfaces.

The relationship between FWD results and rut depth progress was investigated by Lenngren & Fredriksson (1998) and Lenngren & Fredriksson (2002). Regression analysis was performed with FWD data as an independent variable and rut depth as a dependent variable. Best fit was obtained for the top of the subgrade stress, which is a function of the load spreading capacity of the structure and therefore the bearing capacity.

The difference between laboratory and in-situ measurements was discussed by Von Quintus & Killingsworth (1998). The former are made on homogenous specimens while the latter indicate the influence of the surrounding material, thickness and density variations and cracking on the modulus. The density of the material can differ between laboratory and field conditions, which affect the modulus. The stress dependency of unbound materials makes it necessary to determine the modulus in the laboratory with the correct state of stress. The state of stress in the road structure varies both horizontally and vertically and is influenced by the load and at rest stress. Quintus & Killingsworth performed backcalculation on FWD test results. The backcalculated layer moduli for each unbound layer and subgrade were used to determine the stress states for use in the laboratory in such a way that the laboratory modulus is equal to the backcalculated modulus. The ratio between the laboratory modulus and the FWD modulus varied between 0.1 and 3.5 anyway.

Flintsch et al. (2003) performed a similar study and found that the laboratory modulus was consequently higher, which can be explained by the fact that the subbase layer modulus was average while the bulk stress in the middle of the subbase was probably lower than average. Meshkani et al. (2003) discussed when backcalculated FWD data and triaxial data should be used when performance of unbound materials is to be evaluated using non-linear models as in Equation 2.27. They found it difficult to determine a correct k_1 value in the laboratory that is valid for field conditions. The internal structure of the granular material differs under field and laboratory conditions due to different preparation techniques, i.e. compaction. The k_2 and k_3 values are not influenced to the same extent by the internal structure, i.e. difference in compaction technique and the k_2 and k_3 values from laboratory test results may thus also be valid for field conditions. The conclusions from the investigation are that a modulus determined in the laboratory must be adjusted in order to predict the structural response of pavement structures to wheel load. Difficulties in determining the stress state in laboratory tests and the influence of the other layers may partly explain why such adjustment is necessary.

FWD test as quality control

Livneh & Goldberg (2001) described the use of the FWD and the Light Falling Weight Deflectometer as a quality control method for formation, i.e. compacted subgrade or capping layer and foundation (subbase). They argued that the FWD might be too sophisticated for measurements performed on unbound layers. They compared the results with the static plate bearing test and found that the E_{V2} from the static plate bearing test was about 85% of the backcalculated FWD value for clay material and 55% for sandy material. Results described by Fleming et al. (1998) showed a relationship of 110%. The FWD may be used as a form of quality control for unbound material layers, subgrade and especially for the identification of weak spots. Solminihac et al. (2004) also found that quality control can be carried out using peak deflection values from FWD tests.

The FWD test can also be used to detect non-resilient, plastic behavior in pavement structures according to Orr (2003). Plastic behavior indicates bad compaction or loss of bearing capacity. It is assumed that all material in a pavement is resilient in nature and linear or non-linear elastic. No permanent deformation occurs in a perfectly resilient material. If a permanent deformation exists, it is usually very small compared to the resilient behavior of each cycle of a repeated loading sequence. If plastic strain occurs, it cannot be differentiated from resilient strain and is therefore not measurable as it can only be observed after unloading. If the load is sufficiently large, non-resilient behavior will occur in the granular material. In the case of several drops per load level, it is possible to identify whether or not the plastic response decreases after each drop due to compaction or increases as a result of liquefaction. This identification is similar to that of a triaxial test during the confining phase or close to failure.

Full Scale Tests and HVS Tests

Full-scale tests with a wheel load can be performed in different ways such as Long Term Pavement Performance (LTPP) and Accelerated Pavement Testing (APT) according to Metcalf (2004) and Sharp (2004). In Long Term Pavement Performance Tests, mainly “normal” traffic conditions account for the load and instrumentation for deformation and stress measurements may be used. Climate and ageing of the materials and the structures can be considered in these tests. There are two kinds of Accelerated Pavement Testing, test roads and test tracks. In test roads, sections of pavements are loaded by traffic, usually typical trucks operating under controlled load and speed conditions. An example is the AASHO test road in the USA in the 1960s. In test tracks, linear or circular loading systems are used to apply loads over short pavement sections and these are often located in a kind of test pit. While it is more difficult to consider the

effects of climate and ageing in Accelerated Pavement Tests, the results do not take as long to obtain as Long Term Pavement Performance Tests and are a good complement to laboratory testing.

Accelerated Pavement Tests are often used to evaluate new materials and design types as well as calibrating of different design models. The Heavy Vehicle Simulator (HVS) is a mobile loading device for accelerated tests. The test tracks do not need to be constructed in a special test pit, which means, for example, that field sections at highway construction sites can be evaluated. The HVS was developed in South Africa (Rust et al. 1997). The first equipment was a static (not mobile) device from the 1960s. In 1970, a mobile prototype was developed and until 1976 different tests were performed. The present HVS device has been produced since 1978. In Sweden and Finland, HVS-Nordic is used and is owned by the Swedish Road and Transport Research Institute (VTI) and previously the Technical Research Center of Finland (VTT) (Odermatt et al. 2004). This HVS device is 23 m long, 4 m wide and 4 m high. A single or dual wheel configuration can be used and a test section with a length of 8 m can be loaded at a speed of 12 km/h for 6 of those meters. The wheel load can be varied between 30 and 110 kN. The capacity is approximately 22000 passes per day. The principles of the HVS are presented in Figure 2.12.

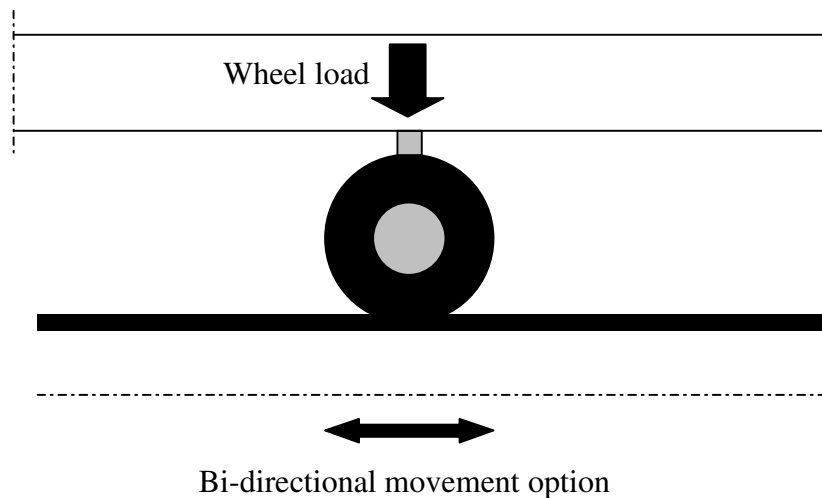


Figure 2.12. The principle of the HVS.

In HVS tests both resilient and permanent deformation properties can be evaluated. All layers are considered and the rotation of the principal stresses can be considered. Compared to long term performance tests, ageing and rest period

effects cannot be evaluated, although accelerated tests, e.g. with HVS, can be seen as a link between laboratory and real pavement performance.

2.5 Conclusions from the literature review

The conclusions from the literature review are summarized and the hypotheses are discussed.

Summary of the literature review

The post compaction process in the literature is described both in repeated load triaxial laboratory tests and field tests. It is often referred to as a conditioning phase. In the initial post compaction process the permanent strain rate is high but decreasing. However, some permanent deformation models do not consider the initial post compaction or only consider it briefly, e.g. Equation 2.11. Permanent deformation behaviors A, B and C, described by Werkmeister et al. 2004 can be related to the phase change envelope described by Bonaquist and Witczak (1997). Stresses below the phase change envelope result in compaction (deformation behavior A). Stresses above the phase change envelope results in shearing (deformation behavior B). This obstructs post compaction. Compaction and shearing will probably affect the stress hardening behavior. However, this must be confirmed further through evaluation of laboratory and field test results.

As regards measurement methods, there is a difference between the conditioning (compaction) and confining pressure in laboratory triaxial test and field tests. Furthermore, the confining pressure varies according to depth. This affects the evaluation of the resilient modulus, which can be up to three times higher in the laboratory. Stress dependency can be evaluated both in laboratory tests and in the field by using different load levels. If the $k-\theta$ model is used for the evaluation (Equation 2.19), the regression parameter k_2 does not seem to be affected by the test type (laboratory or field), although the k_1 value is affected. The load pulse time may affect the results at the same peak load as well as viscoelasticity and damping effects. Asphalt concrete and saturated clay in particular are influenced by the load time. Extra care should be taken when static and dynamic test results are compared as well as if static calculations are used to evaluate dynamic test results. The FWD can be used as a quality control method and permanent deformation due to lack of compaction can be studied by means of statistical analysis of peak deflections after repeated drops. A pure elastic response results in a random difference between two drops, but if permanent

deformation occurs, there are significant differences between the drops and the standard error increases.

First hypothesis

Post compaction can be seen as a continuous decrease in the permanent deformation rate during repeated loading.

According to Wolff & Visser (1994), Theys (1997), Núñez et al. (2004), Odermatt et al. (2004), Werkmeister et al (2004) and El-Basyouny et al. (2005) the development of permanent deformation in unbound granular materials as a result of repeated external wheel loads can be divided into two phases. During the initial phase there is a rapid increase in permanent strain. The rate of increase in permanent strain is not constant and decreases continuously. This can also be seen in laboratory triaxial tests referred to as the conditioning phase. In the literature this phase is referred as “post compaction”, but this definition is not exactly the same as the one used in the present thesis. Analyses of the laboratory and field test results will be used for further verification of the hypothesis.

Second hypothesis

Post compaction occurs if the load characteristics of compaction and loadings after compaction differ.

According to Thom (1988) it can be seen that an increase in load level immediately increases the permanent strain rate if different load levels are used in a laboratory test. This is probably also the case for wheel load although the literature does not consider that kind of loading. The field and the triaxial laboratory test will therefore be used to verify the hypothesis.

Third hypothesis

The stress hardening behavior is affected by compaction, post compaction and shearing.

According to Ullidtz et al (1996), Ullidtz (1997), Ullidtz (1998), Kolisoja (1997), Van Baars (1996), Troadec & Dodds (1993), Oda & Ivashita (1999) and Gervois & Bideau (1993) the stresses within the material are distributed in stiff particle chains. Some particles will therefore be involved in the stress distribution and some will not. Due to permanent deformation, rearrangement of the particles will occur, which results in the development of new particle chains. The chain like load distribution explains why larger grain size increases the stiffness of the unbound material. Kolisoja (1997) and Kolisoja (1998) explained the non-linear

stress dependent behavior of granular material that the contact area between the particles increases when the particles are pressed against each other. This affects the elastic behavior of the whole particle assembly. Kolisoja (1998) also concluded that the reduction in void content increases with the number of contacts per particle with other particles, i.e. the coordination number, which in turn increases the stiffness of the material. Kolisoja (1998) also stated that the particle assembly would react more stiffly at higher stress levels due to the non-linear behavior at the contacts between the particles. The effect becomes even greater due to the fact that new contacts between the particles appear when the particles are subjected to increased compression and the number of contacts per particle is increased. According to Werkmeister et al. (2004) Núñez et al. (2004) and Odermatt et al. (2004) there is densification of the material, reduction in pore volume, and eventually crushing of the particles of the unbound material during post compaction. This leads to the conclusion that post compaction causes an increase in the non-linear behavior, which can be seen as a change in the stress hardening behavior (for example the increase in the regression parameter k_2 in the $k - \theta$ model after post compaction). However, further evaluation of laboratory and field test results must confirm the results of this discussion in order to verify the third hypothesis.

3 CONCEPTUAL MODEL AND EVALUATION METHOD

3.1 Evaluation of the condition of post compaction

Post compaction in unbound materials in a real road structure is the unintended compaction by wheel loads from heavy traffic after a road structure is brought into service by the definition of the present thesis. The objective is to identify the conditions for post compaction and shearing of unbound granular material.

Post compaction continuously reduces the pore volume of the unbound material resulting in a decrease in volume. It is also assumed to result in a change of the stress hardening behavior. The permanent deformation rate is the proof that post compaction occurs and the stress hardening behavior is the evaluation method, which is intended to be used for identifying post compaction in the field. Increased load will also cause post compaction if shearing/dilatation not occurs.

The relation between permanent deformation rate and stress hardening behavior must be verified in both laboratory and field tests where it is possible to evaluate both parameters at the same time. In the laboratory test the load is more controllable, the deformation is easier to measure and the material properties are more controllable than in a field test. The field tests are used to validate the laboratory test and will continued to be used in the future.

The laboratory test used in the present thesis is the triaxial test with constant confining pressure. Eight load steps with increasing load each load step are applied for each test sample. Both the elastic and permanent deformation are measured at different number of loadings. Increased load is expected to cause post compaction until the load level is high enough to cause shearing. This is another reason for using the laboratory test in the present thesis due to an easier way of evaluating the theory of stress hardening behavior, post compaction and shearing.

The field test used is the multi load FWD. This makes it possible to also evaluate stress hardening behavior in the field. The FWD tests are performed before and after a HVS test. This test simulates wheel loads from heavy traffic, which is supposed to cause permanent deformation and post compaction. Measurements of elastic and permanent deformation are performed in the unbound base layer

of the test road structure. An evaluation of the triaxial and FWD test is described below.

According to the literature review there have been earlier attempts to find relationships between elastic and permanent deformation, but it has been found that it could be difficult. For post compaction evaluation in the field, the method must be quick for it to be used during the construction phase as a means of finding a way to minimize the post compaction. According to the literature review, the stress hardening behavior seems to influence compaction.

3.2 Conceptual model of the triaxial laboratory test

The vertical resilient and permanent deformations are measured simultaneously during the laboratory triaxial test. Each test sample is subjected to eight load steps with several load repetitions each load step. Post compaction is therefore expected at each load step. The total number of load repetitions varies depending on the strength of the test sample but in most cases it is more than 200 000. Measurements are performed every 100 load repetition the first 4 000 repetitions and then up to every 10 000 repetitions with denser measurements for each new load step. A post compaction process can be seen when the permanent strain rate is evaluated. The strain rate should clearly decrease towards zero when the sample is post compacted to the least possible pore volume for the actual stress level.

The stress hardening behavior can be evaluated in different ways. If the loading sequence is measured continuously both regarding load and deformation as in the example in Figure 3.1a it is possible to evaluate the curvature of the stress-strain line (the blue line represents a lower dynamic load and the red line a higher dynamic load).

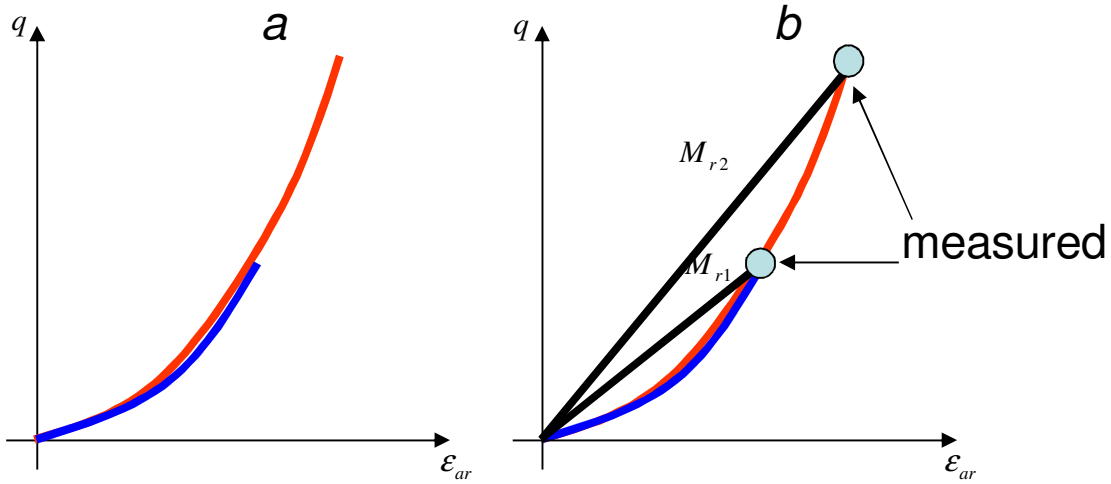


Figure 3.1 Unbound granular materials have stress hardening behavior which can be evaluated by study of the deformation in detail or by calculating the resilient modulus M_r at different stress levels.

During the triaxial tests used in the present thesis, the loading sequence is not measured, only the peak values (e.g. one peak value for the lower dynamic load and one for the higher dynamic load as shown in Figure 3.1a). Instead the peak values are used to calculate the resilient modulus M_r , which is a secant modulus as shown in the example in Figure 3.1b (one resilient modulus for each of the dynamic load levels).

The equation for calculating the resilient modulus from the peak values is presented in Equation 3.1.

$$M_r = \frac{q}{\epsilon_{ar}} \quad (3.1)$$

Where q is the applied dynamic deviatoric stress and ϵ_{ar} is the axial resilient peak strain. In Figure 3.1b it can be seen that the resilient modulus M_r is larger (steeper slope) for the higher dynamic load level compared to the lower one, i.e. the elastic behavior is stress hardening. According to the literature, the stress hardening behavior is often describes as the relationship between the resilient modulus and the bulk stress as shown in Figure 3.2.

3. Conceptual model and evaluation method

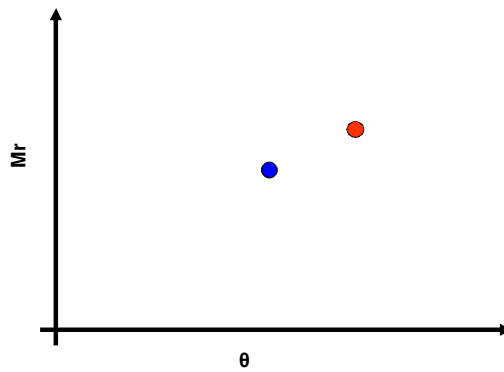


Figure 3.2. Evaluation of the stress hardening behavior by relating the resilient modulus at different stress levels with each other.

The blue dot in Figure 3.2 represents the resilient modulus M_r at the lower dynamic load and the red dot the higher load level.

Unbound granular material is said to be a stress hardening material, as shown in Figure 3.2 above. However, there could also be behaviors that show no increase or decrease in M_r when the load increases. In that case it may indicate that shearing occurs in the material, as described in Figure 3.3 and Figure 3.4.

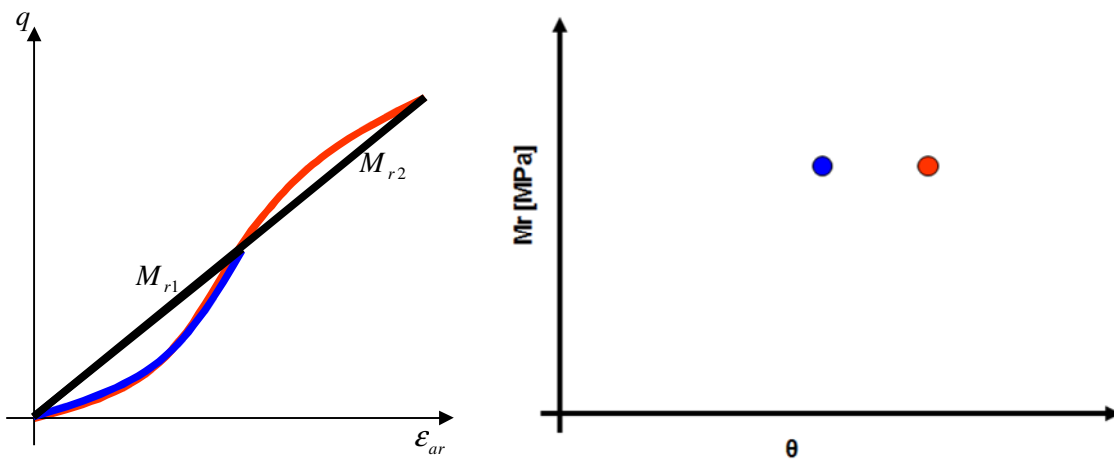


Figure 3.3. Shearing in the unbound granular material may erase the stress hardening behavior and instead cause no increase of the resilient modulus M_r .

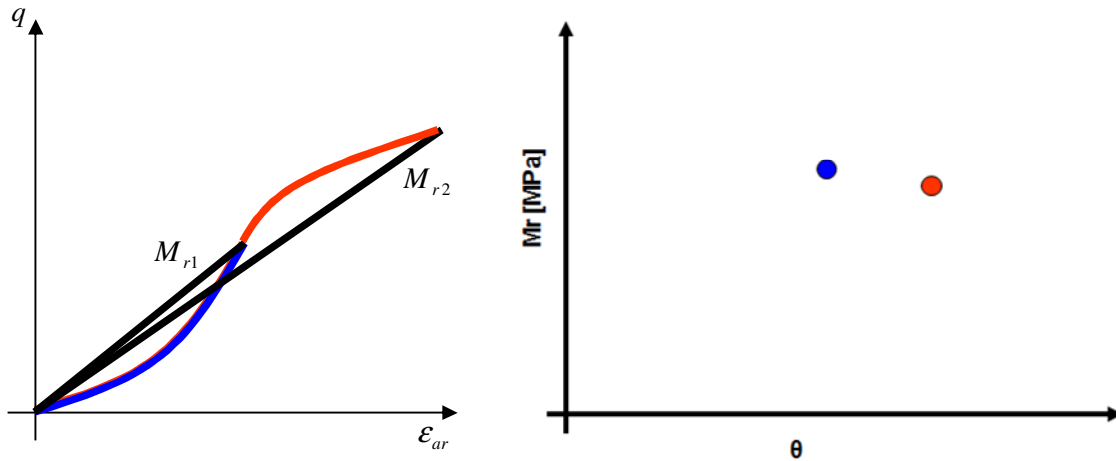


Figure 3.4. Shearing in the unbound granular material may erase the stress hardening behavior and instead cause a decrease in the resilient modulus M_r .

Due to the assumed shearing, the resilient modulus M_r can be evaluated to be constant as described or decreasing for higher load levels (stress softening).

3.3 Conceptual model of the FWD test

From the FWD test the elastic modulus of the different layers in the road structure is obtained for the different load levels by backcalculation. This makes it possible to evaluate the resilient modulus M_r and any stress hardening or softening behavior as described in Section 3.2.

In the backcalculation of the FWD deflection basins, the load and the deflection are known but the stress and strain unknown. Instead the resilient modulus and the stresses and strains are backcalculated for different load. If the backcalculated resilient modulus increases for each load level, the behavior indicates a stress hardening as shown in Figure 3.5.

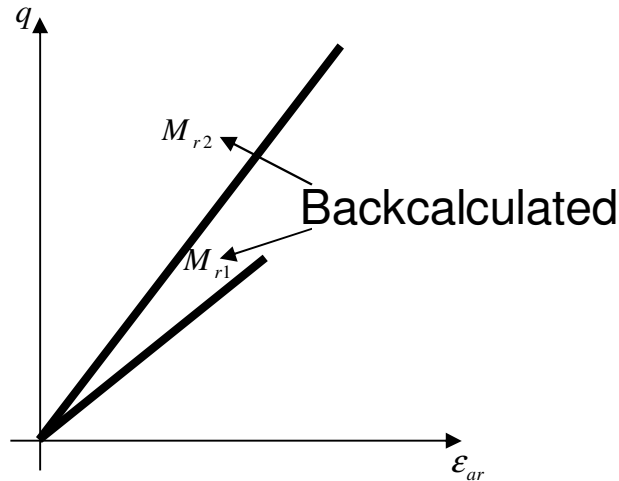


Figure 3.5. Resilient modulus evaluated by backcalculation for different load levels.

The resilient modulus for the different load levels can be related to the calculated bulk stress θ as mentioned before. However the bulk stress is related to the lateral earth pressure coefficient K_0 (see Equation 2.30), which in turn is related to the Poisson's ratio, Equation 3.2.

$$K_0 = \frac{\nu}{1-\nu} \quad (3.2)$$

The Poisson's ratio is unknown in field condition. A common value used for unbound materials is 0.40. The Poisson's ratio for clay is often set at 0.45, asphalt at 0.35 and concrete at 0.15 (Huang 2004). If the backcalculated resilient modulus is related to the bulk stress calculated from the assumed Poisson's ratio, the stress hardening behavior can be evaluated in the same manner as for the triaxial test.

3.4 Conceptual model for describing the relationship between stress hardening, post compaction and shearing

The stress hardening and stress softening behavior described in Figure 3.1, Figure 3.3 and Figure 3.4 could be affected by repeated loading. Increased stress hardening behavior could be a result of permanent deformation caused by compaction (post compaction) and decreased stress hardening behavior as a result of shearing. The reason for this is described conceptually below.

Unbound granular material consists of single grains with different sizes, described conceptually in Figure 3.6.

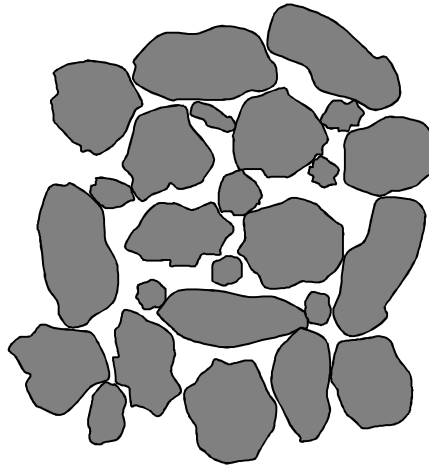


Figure 3.6. Unbound granular material consists of single grains with different sizes.

When the material is subjected to external stress it will be deformed both elastically and permanently. The elastic deformation is caused mainly by deformation in the contact between the particles as described in Figure 3.7.

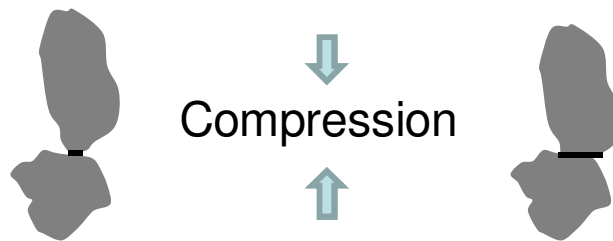


Figure 3.7. Elastic increase in the contact area between the particles due to compression.

The contact area of each contact is deformed and the area between the contacts is increased. During elastic compression more contacts are created, as described in Figure 3.8.



Figure 3.8. More contacts between particles are created elastically due to compression of the unbound granular material represented by the black lines.

The increased contact area and the creation of new contacts between the particles make it more difficult to deform the unbound material elastically the higher the stress level. The response is thus stress hardening as also described in Figure 2.6.

Repeated loadings cause permanent deformation, in turn caused by crushing and sliding in the contacts between the grains, and the grains start to move and rotate as shown in Figure 3.9.

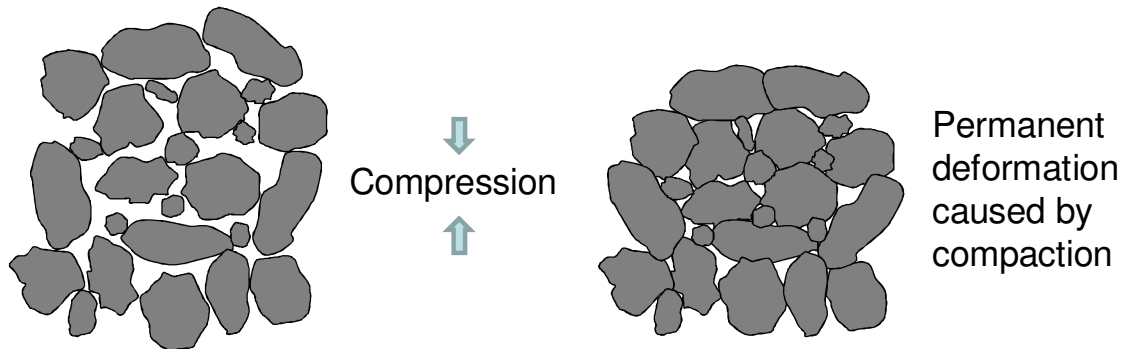


Figure 3.9. *Permanent deformation cause crushing and sliding in the contacts between the particles and the grains start to move and rotate.*

The pore volume is reduced and the volume of the unbound material decreases. When the pore volume is decreased, the number of contacts between the particles increases. This increases the deformation modulus but also the stress hardening due to the higher number of contacts, the area of which can be larger during the elastic deformation. The denser structure also makes it possible to increase the number of contacts during the elastic deformation, which will cause even greater stress hardening.

Relationship between stress hardening, post compaction and shearing evaluated in a laboratory triaxial test

As mentioned before the triaxial test is performed by using eight load steps. Elastic and permanent deformation measurements are performed at different load repetitions from the 100th load repetition to the last for each load step. In the present thesis results from the 100th load repetition and the last load repetition will be used to describe the effect of permanent deformation on the stress hardening behavior. As mentioned above, the triaxial test is assumed, according to the second hypothesis, to create permanent deformation (post compaction or shearing) for each load step.

Below conceptual description of the first two load steps of the triaxial test starting with Figure 3.10.

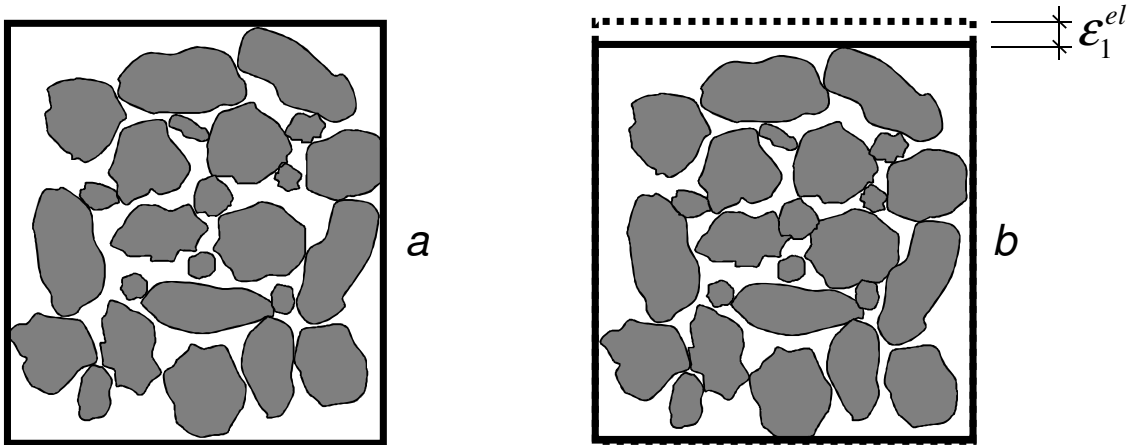


Figure 3.10. After sample preparation, the first elastic deformation measurement is performed after 100 load repetitions.

After sample preparation (Figure 3.10a), the test starts with the first load step and 100 load repetitions are performed on the test sample. The first elastic deformation ϵ_1^{el} is done after 100 load repetitions (Figure 3.10b). Some permanent deformation is expected to occur in the material. However, the permanent deformation that occurs the first 100 load repetitions for each load step is ignored. The elastic deformation appears in the contacts between the grains by increasing contact area. The test then continues, as described in Figure 3.11.

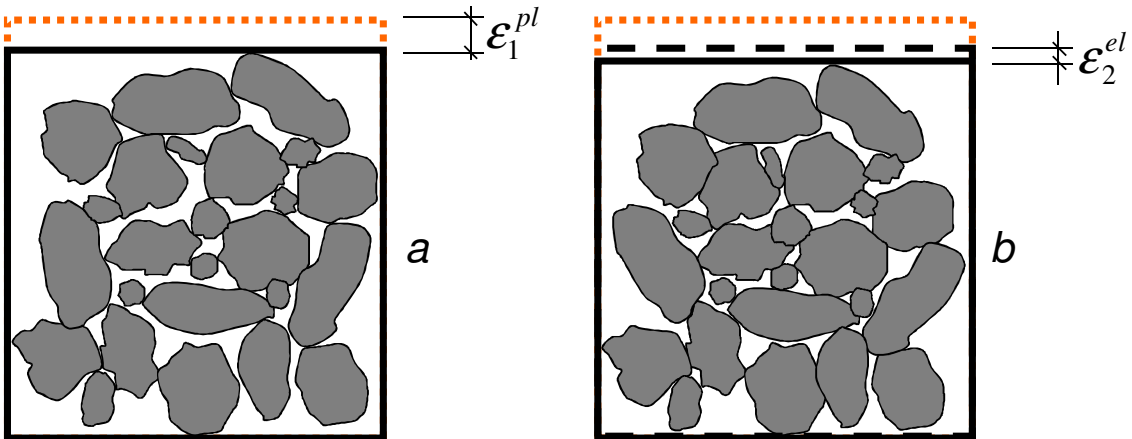


Figure 3.11. Permanent and elastic deformation measurements the last load repetition load step 1.

At the first load step, 1000 load repetitions are applied and permanent deformation develops in the sample through sliding and rotation of the particles until the last load repetition. A permanent deformation measurement is

3. Conceptual model and evaluation method

performed (ϵ_1^{pl}) at the 1000th load repetition (Figure 3.11a). At the same time, the second elastic deformation measurement ϵ_2^{el} is made (Figure 3.11b). The structure becomes denser after the permanent deformation, the number of contacts increases and the contact areas between the grains becomes larger. That is why $\epsilon_2^{el} < \epsilon_1^{el}$. The test continues with the second load step, which is described in Figure 3.12.

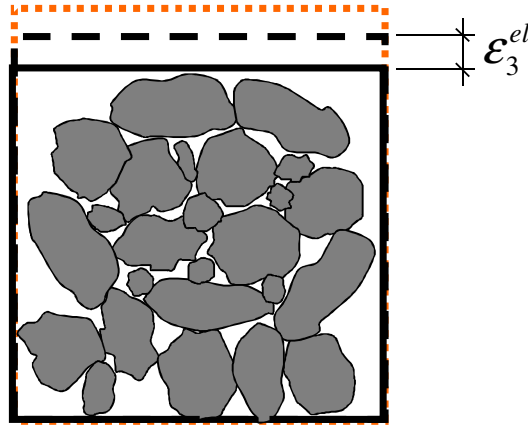


Figure 3.12. Elastic deformation measurement performed after 100 load repetitions load step 2. The red box represents the size of the sample before the test.

The third elastic deformation measurement ϵ_3^{el} is made at the 100th load repetition load step 2. The elastic strain increases due to the higher load ($\epsilon_3^{el} > \epsilon_2^{el}$). The test continues with further load repetitions and permanent deformation occurs in the sample as described in Figure 3.13.

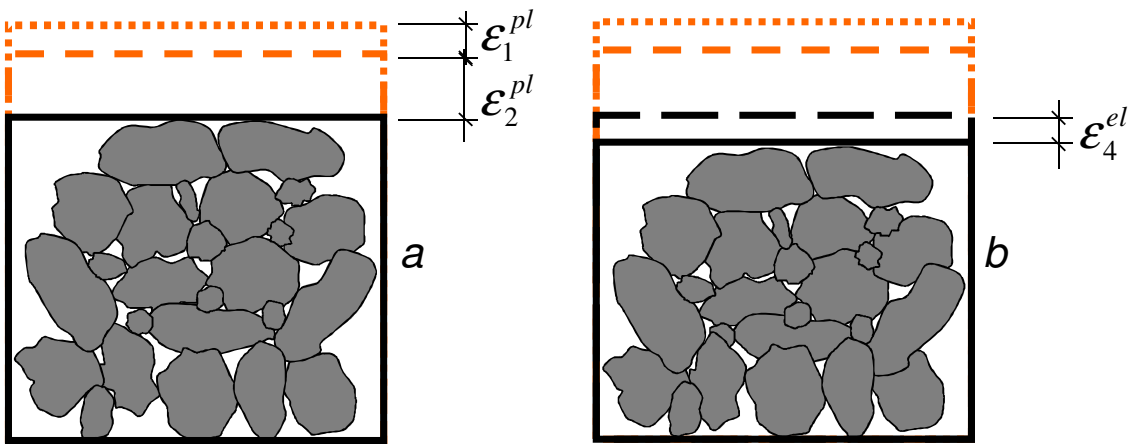


Figure 3.13. Permanent and elastic deformation measurement the last load repetition of load step 2

The permanent deformation is again caused by sliding and rotation of the particles until the last load repetition of the second load step. The second permanent deformation measurement ϵ_2^{pl} (Figure 3.13a) is made. The structure becomes even denser. The number of contacts increases and the contact areas becomes larger. This results in a stiffer response in the fourth elastic deformation measurement ϵ_4^{el} (Figure 3.13b) performed at the last load repetition of the second load step compared to the third elastic deformation measurement, i.e. $\epsilon_4^{el} < \epsilon_3^{el}$. The elastic deformation measurements ϵ_1^{el} to ϵ_4^{el} presented in Figure 3.10 to Figure 3.13 are summarized in Figure 3.14.

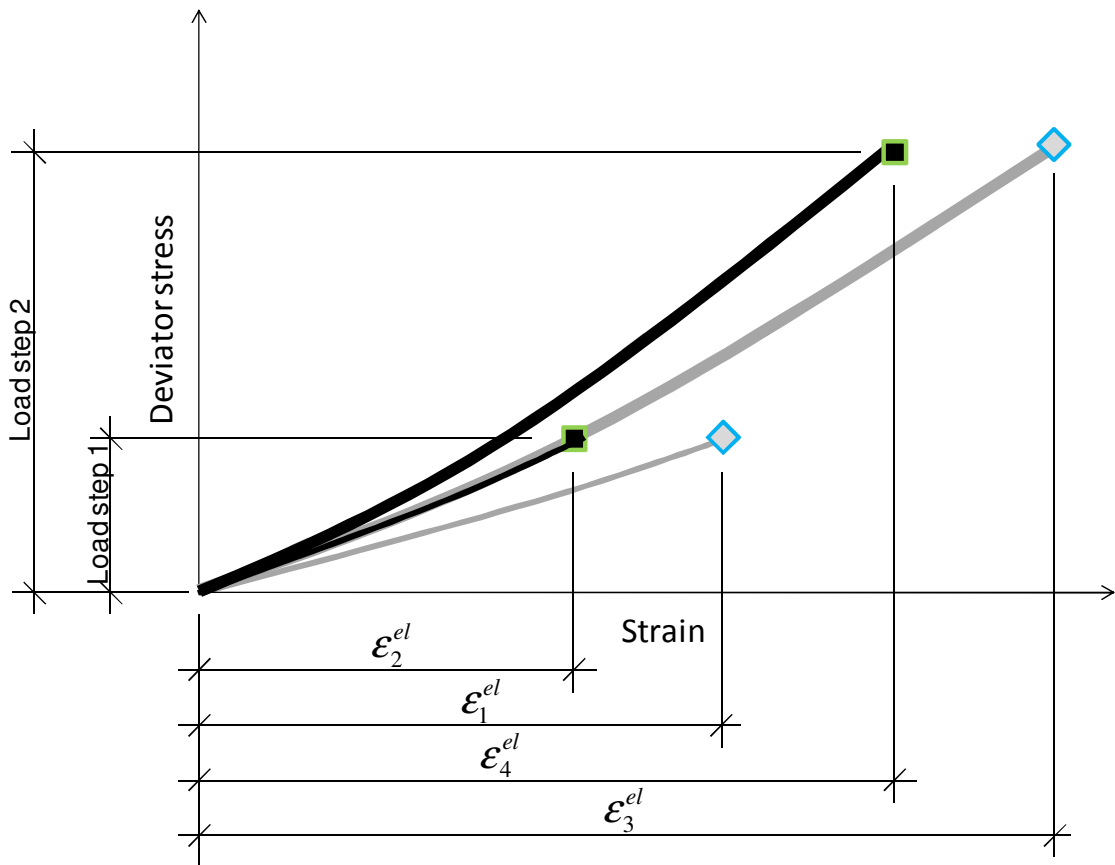


Figure 3.14. The elastic deformation measurements performed at the 100th and the last load repetition of load step 1 and 2 summarized as a stress – strain relationship.

In the conceptual model the permanent strain occurred during load step 1 ϵ_1^{pl} cause a stiffer response, i.e. $\epsilon_2^{el} < \epsilon_1^{el}$ as mentioned before. The same applies to load step 2. The stiffer response results in an increased resilient modulus M_r and this is summarized in Figure 3.15.

3. Conceptual model and evaluation method

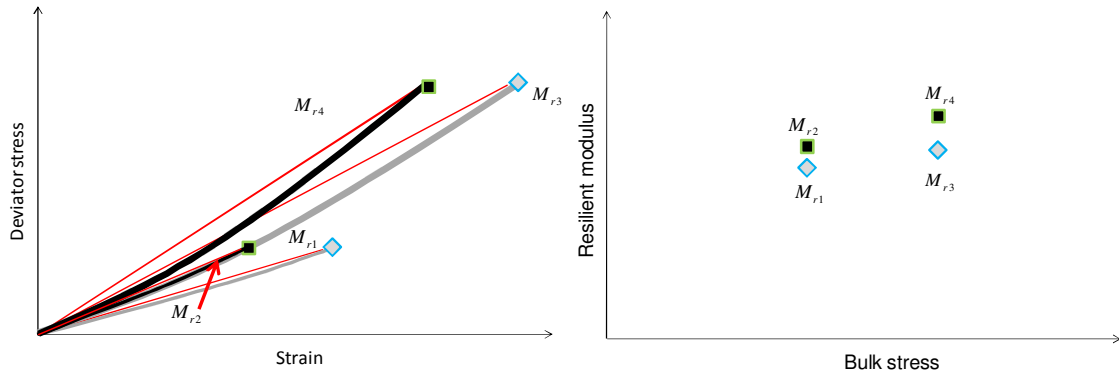


Figure 3.15. The resilient modulus increases due to post compaction.

If the load of the second load step is too high compared to the strength of the structure compared to the example in Figure 3.9, shearing instead of compaction may cause permanent deformation during the repeated loading, see Figure 3.16.

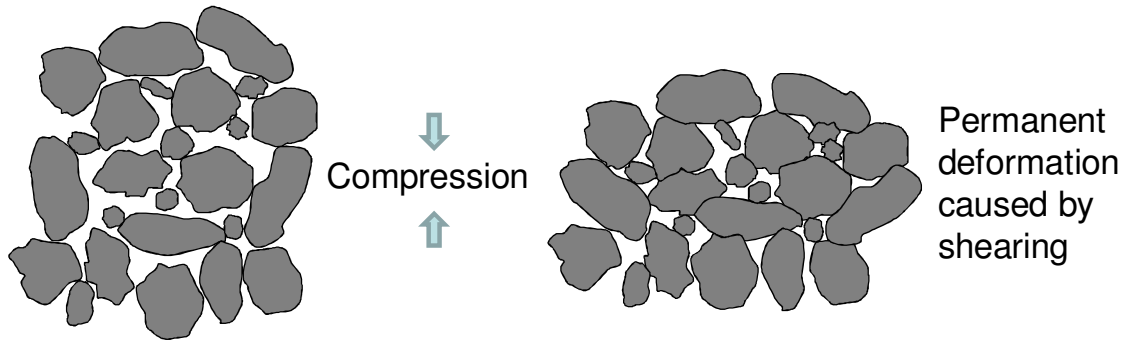


Figure 3.16. Permanent deformation causes crushing and sliding in the contacts between the particles, the grains start to move and rotate and shearing instead of compaction occurs.

The shearing results in a more open structure compared to if pure compaction is obtained. The open structure causes a larger elastic strain compared to if the structure is denser. The conceptual description of the first two load steps of the triaxial test will be the same as earlier described in Figure 3.10 to Figure 3.13 but the repeated loading the second load step will cause shearing, which can be seen in Figure 3.17.

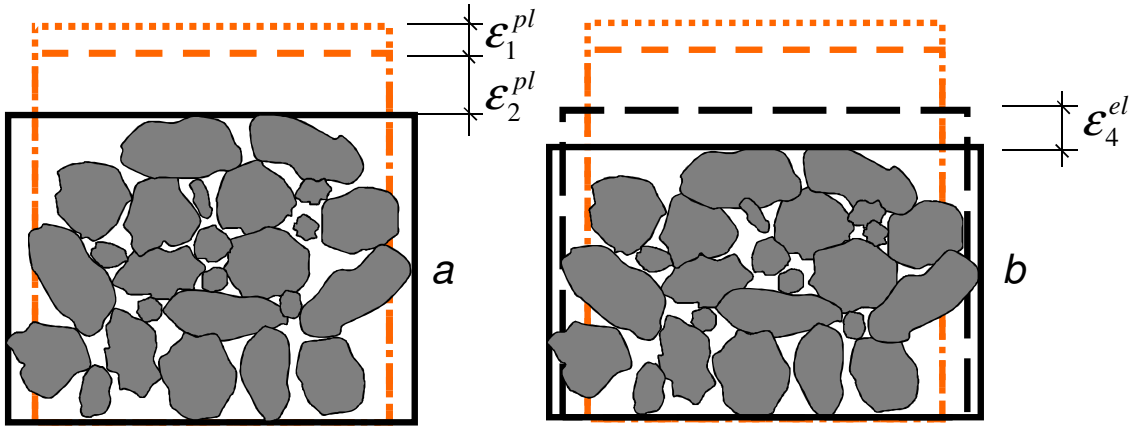


Figure 3.17. Permanent and elastic deformation measurement performed the last load repetition load step 2 during assumed shearing.

As can be seen, ϵ_4^{el} in Figure 3.17b is larger than ϵ_4^{el} in Figure 3.13b and also somewhat larger than ϵ_3^{el} . Note that shearing is not assumed to occur until the 100th load repetition in the second load step. The situation described in Figure 3.12 will therefore be the same for both scenarios (compaction or shearing). The shearing scenario is summarized in Figure 3.18.

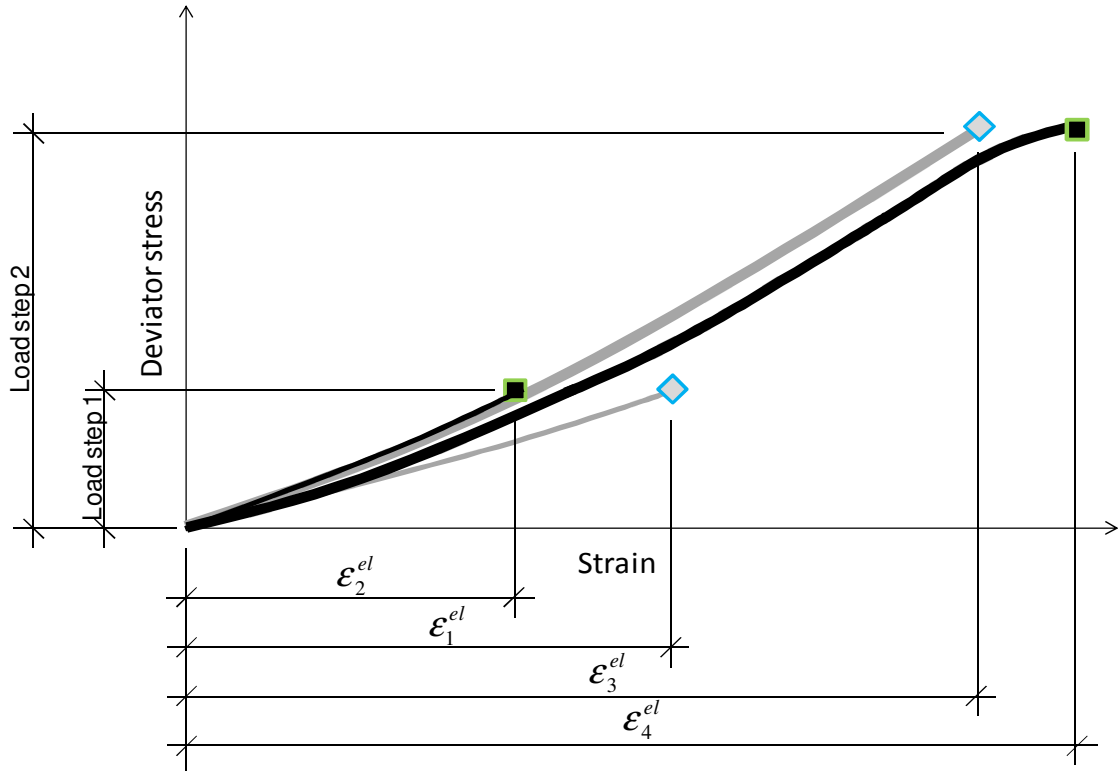


Figure 3.18. The elastic deformation measurements performed at the 100th and the last load repetition of load step 1 and 2 summarized as a stress – strain relationship shown for assumed shearing.

As can be seen compared to Figure 3.14 $\varepsilon_4^{el} > \varepsilon_3^{el}$. This result affects the resilient modulus compared to Figure 3.15 and this is presented in Figure 3.19.

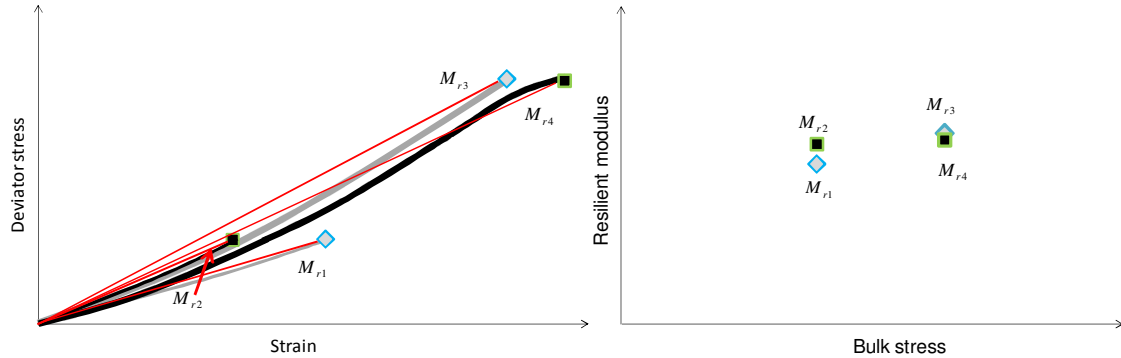


Figure 3.19. The resilient modulus decreases due to shearing.

However, there is still a stress hardening behavior when the resilient modulus of the last load repetition for load step 1 and 2 is combined, i.e. $M_{r4} > M_{r2}$, the stress hardening decreases.

Relationship between stress hardening, post compaction and shearing evaluated in FWD and HVS tests

Almost the same evaluation can be made for the FWD test although the test is performed in a different order compared to the triaxial test. Different load levels are used before the assumed post compaction as well as after the assumed post compaction (before and after the HVS test). This is presented in Figure 3.20.

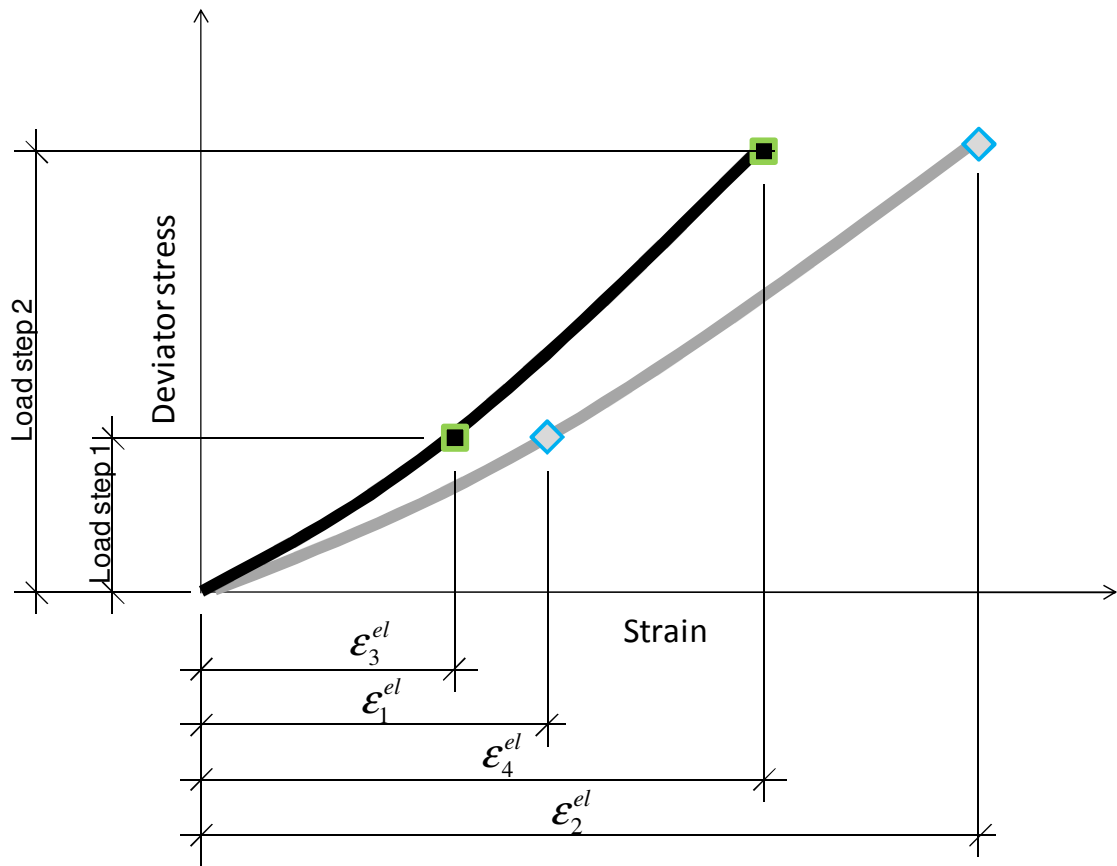


Figure 3.20. The elastic deformation measurements performed before and after the HVS test as a stress – strain relationship shown for assumed post compaction.

The resilient modulus increases after the HVS test for both the presented load steps and especially at the higher load level. This gives the same pattern as described in Figure 3.15 (compaction) or Figure 3.19 (shearing) for the triaxial test.

Evaluation of the stress hardening parameter

The stress hardening behavior must be quantified in order to see whether it increases due to post compaction or not. According to the literature review, it is common to relate M_r to the bulk stress $\theta = \sigma_1 + \sigma_2 + \sigma_3$ (sum of the principal stresses) when stress hardening behavior of unbound granular material is described. In many cases a log-log relationship has been found between M_r and θ . The relationship between M_r and θ can in turn be described using a regression model reported in the literature review, the so called $k-\theta$ model (Equation 3.3).

$$M_r = k_1 \left(\frac{\theta}{\theta_0} \right)^{k_2} \quad (3.3)$$

The regression parameter k_2 is related to the stress hardening rate, i.e. k_2 should increase due to post compaction. In order to give the regression parameter k_1 the same unit as the resilient modulus M_r , a reference stress θ_0 of Equation 3.3 will be used. This stress is set to 1 kPa.

There are many models used to describe the stress hardening behavior of unbound granular material. In the present thesis the stress hardening behavior will be evaluated by using FWD data as well as laboratory triaxial data. Backcalculated elastic modulus can be compared with backcalculated stresses. The number of available evaluated parameters is limited. The evaluation methods should therefore be as simple as possible, which is in line with Occam's Razor (see among others Barbour & Krahn 2004).

The $k - \theta$ model is supposed to be used to evaluate the stress dependent resilient modulus. The stress dependency is described in Figure 3.1. The resilient modulus is evaluated for the different load levels for determining the k_1 and k_2 values.

In order to see the effect of post compaction on the stress hardening behavior evaluated from the laboratory triaxial test, the resilient moduli evaluated after the 100th load repetition each load step are combined to evaluate the stress hardening behavior. In the same way the resilient moduli evaluated during the last load repetition for each load are combined. However, the resilient moduli evaluated the 100th load repetition, load steps 2, 3 and onwards have all been subjected to post compaction the earlier load step. This effect on the stress – strain relationship that can be seen in Figure 3.21.

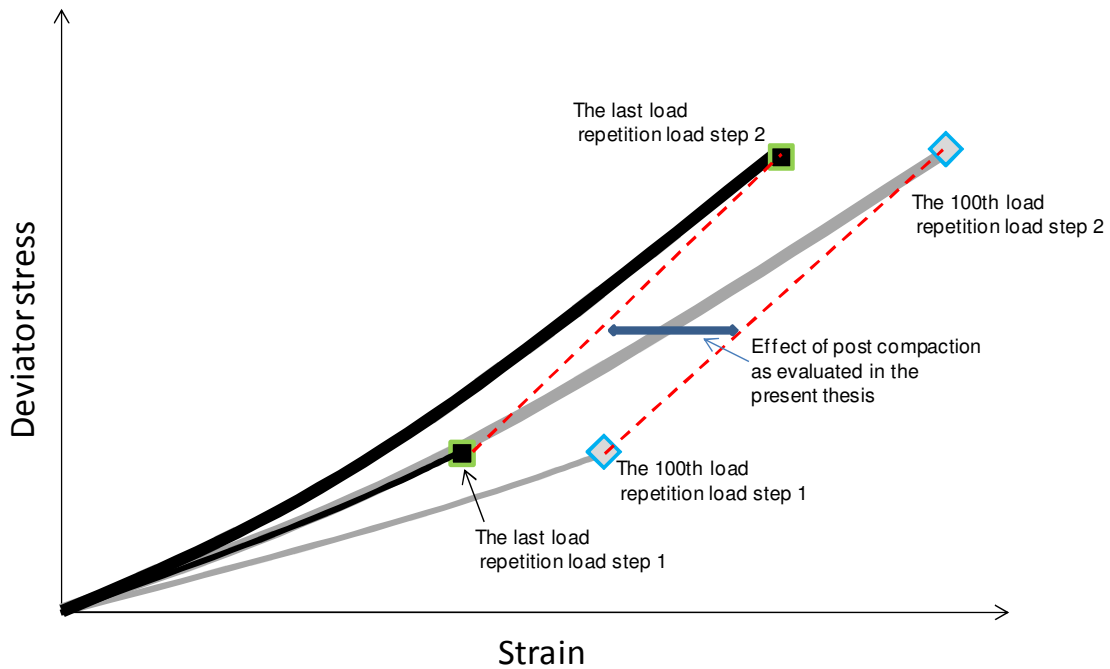


Figure 3.21. Evaluation of the stress hardening behavior. The red broken lines combine the measurements used for evaluation of the stress hardening used in the $k - \theta$ model.

The resilient modulus evaluated at the 100th load repetition for load step 1 does not follow the same stress – strain curve as the load step 2 at the 100th load repetition. The same applies to the resilient moduli evaluated at the last load repetition. However, the resilient modulus at the last load repetition load step 1 follow the same stress – strain curve as the resilient modulus at the 100th load repetition load step 2. When the stress hardening behavior is evaluated by using the $k - \theta$ model one stress – strain curve is supposed to be analyzed in time. In this case instead the red broken lines in Figure 3.21 are used to evaluate the stress hardening behavior before and after post compaction. They represent a sort of fictive stress – strain relationship.

In other words, when the $k - \theta$ model is used for comparing resilient moduli evaluated after 100 load repetitions with resilient moduli evaluated at the last load repetition, the intended use of the model is not followed. Consequently, the evaluated regression parameters can only be used to evaluate patterns related to post compaction and shearing and not for design purposes. However, it seems reasonable to use the $k - \theta$ model in this way. When triaxial laboratory tests were planned the intension was not to use the results in the way they have been analyzed in the present thesis.

In the present thesis, three load steps at a time are used for evaluating k_1 and k_2 in order to minimize deviations in the measurements and this makes the problem even clearer, as described in Figure 3.22.

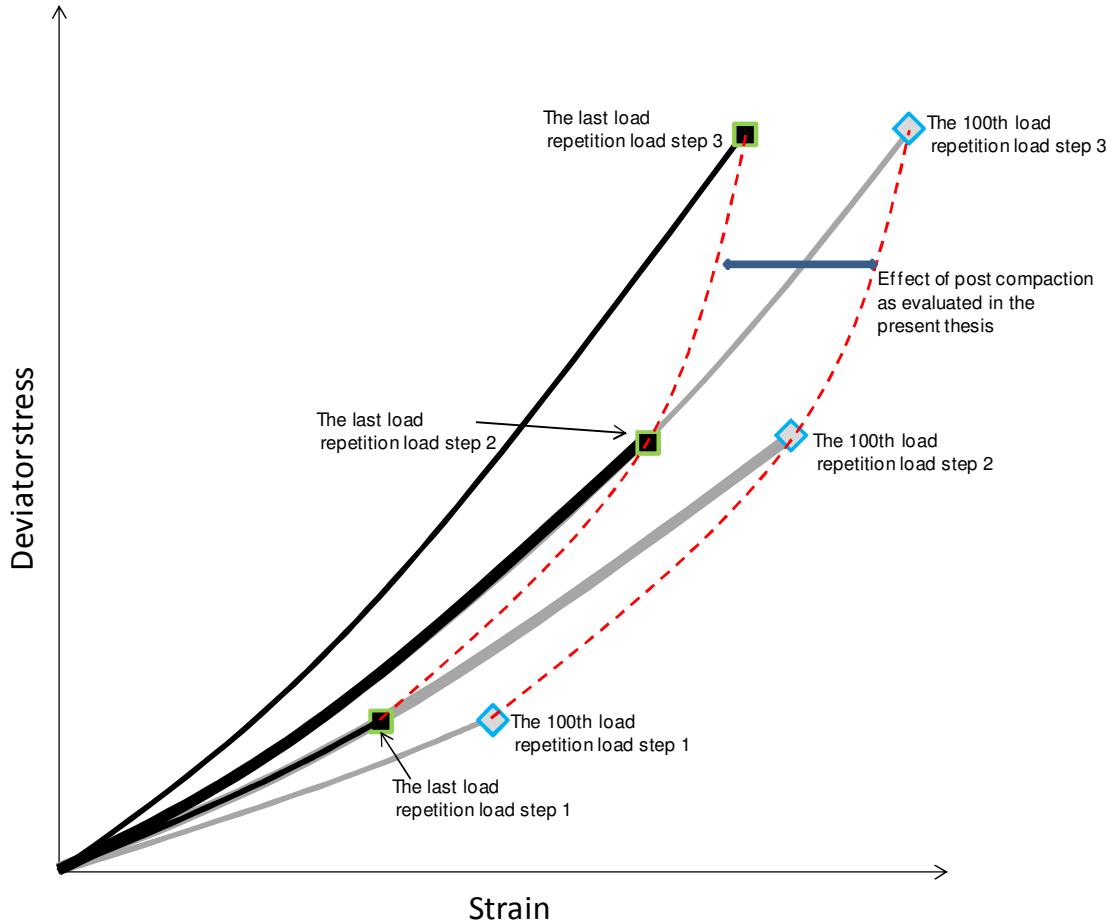


Figure 3.22. Evaluation of the stress hardening behavior. The red lines combines the resilient modulus used in the $k - \theta$ model.

For the FWD and HVS tests, this problem does not occur. The FWD test performed before the HVS test is done using three load levels and there is no post compaction between the load steps. For the FWD test after the HVS test, all load steps have been exposed to the same post compaction. This is summarized in Figure 3.23.

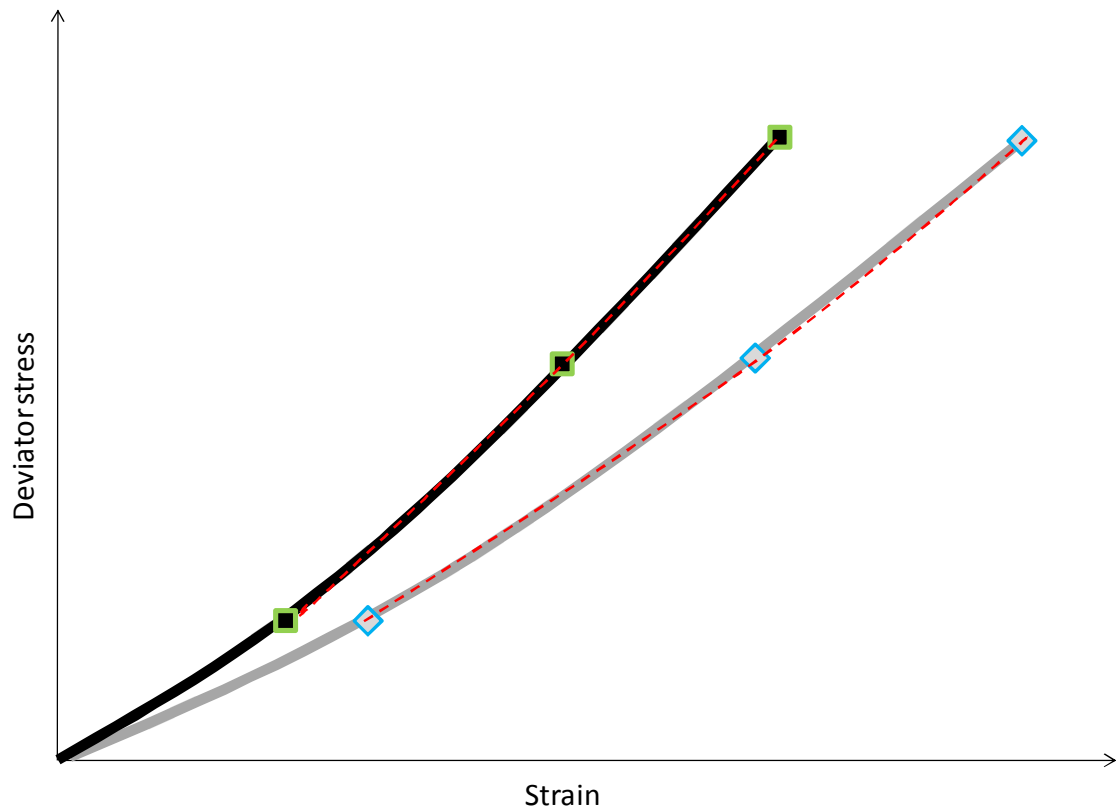


Figure 3.23. Evaluation of the stress hardening behavior for the FWD test before and after the HVS test.

As can be seen, the red dotted lines follow the stress – strain relationships.

Examples of regression analysis performed in order to evaluate the stress hardening behavior before and after supposed post compaction is shown in Figure 3.24.

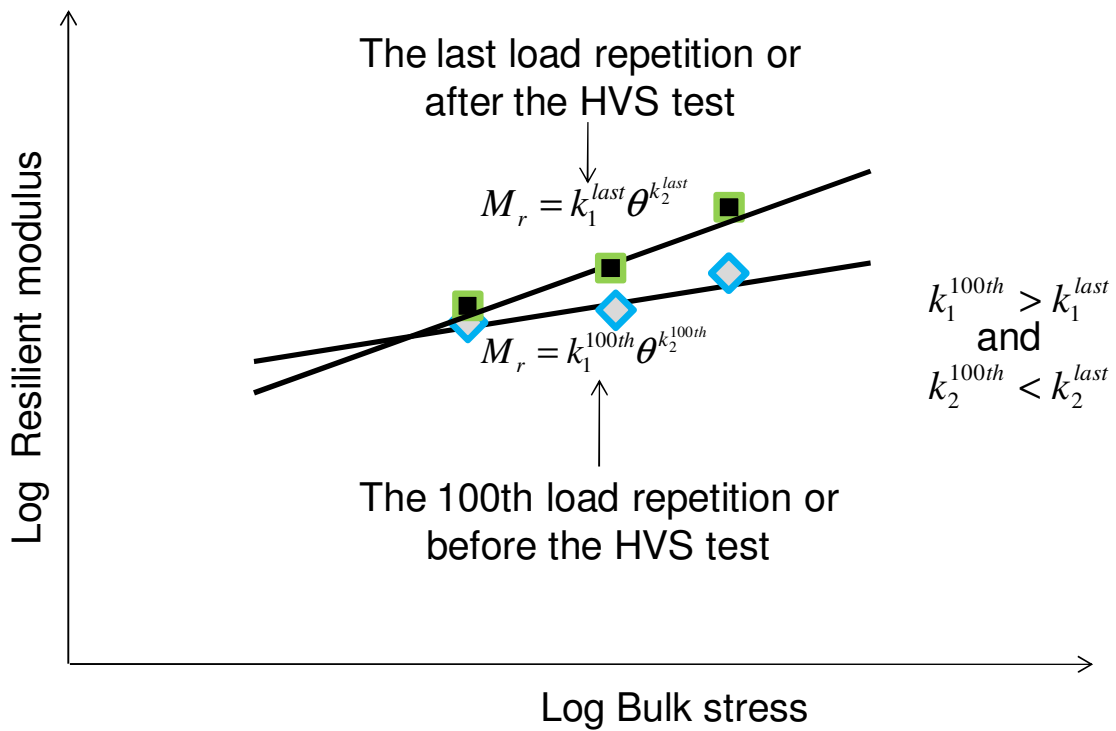


Figure 3.24. Evaluation of the stress hardening behavior parameters k_1 and k_2 for post compaction behavior.

As mentioned before, the k_2 – value increases and the k_1 – value decreases as a result of post compaction. In Figure 3.25 the effect of shearing instead of post compaction is presented.

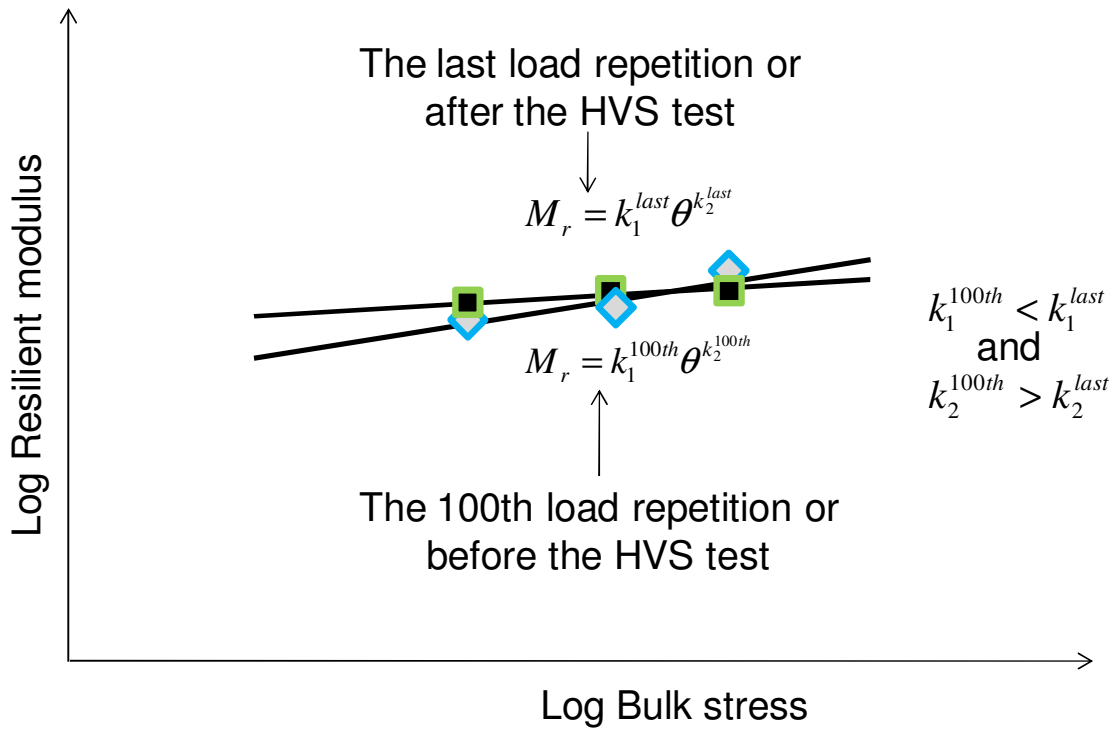


Figure 3.25. Evaluation of the stress hardening behavior parameters k_1 and k_2 for shearing behavior.

As can be seen, the conceptual model results in a decrease in parameter k_2 and increase of the k_1 – value. These two scenarios will be used to describe post compaction and shearing in the present thesis.

4 IDENTIFICATION OF THE CONDITIONS FOR POST COMPACTION USING SMALL SCALE TESTS

4.1 Introduction

In the present thesis the aim is to identify the conditions for post compaction and to separate it from shearing/dilatation. If post compaction has thus occurred there should be a change of the stress hardening behavior and some permanent deformation according to the hypothesis. This is also described using the conceptual model in Section 3. The permanent deformation process will be compared to the stress hardening behavior in order to see if there are any links between the two.

One way of identifying the condition for post compaction is a controlled test on a small scale. In a controlled test it is possible to choose the test conditions. The test parameters can be adjusted for the purposes of the test. The small scale makes it easier to control the test and the boundary conditions are better known.

Results from laboratory repeated load triaxial tests are used. The tests were performed by the Swedish National Road and Transport Research Institute (VTI) on behalf of the Swedish Road Administration. The results of the triaxial tests can be found in a database available from the Swedish Road Administration (see Ekdahl et al 2004a). In these tests four different unbound base layer materials were tested. All the material was stock piled crushed rock and the grain size distribution was 0-40 mm. The aim of these tests was to identify the influence of fine grained mica with different moisture contents on the permanent deformation behavior and thus find the maximum permitted mica content. The mica content was measured in the grain size range of 0.125-0.250 mm and in the unbound base layer the material it was, from #1 to #4, 14 %, 34 %, 6 % and 30% respectively. The results were also used as input to test different existing material models for elastic and permanent deformation and to eventually develop new ones.

These tests are used to investigate if there are any differences in loading conditions during compaction of the specimen and during the test, any permanent deformation during the test due to post compaction and if the stress hardening behavior is affected during the test.

4.2 Description of the triaxial laboratory test

The triaxial cell used by VTI for the tests had a diameter of 150 mm and a height of 300 mm. A rubber membrane held the material in place. It was possible to have constant cell pressures during the test but with adjustable levels. The test specimen was prepared (compacted) as described in Arvidsson (2006). The test specimen was placed on a vibrating table while a vertical load was applied and it was then compacted until the desired degree of compaction was achieved.

Each test specimen was loaded with increasing dynamic loading and cell pressure in eight steps, see Table 4.1. The bulk stress θ is calculated by using Equation 4.1.

Table 4.1. Loading steps of the laboratory triaxial test for each test sample.

Loading Step	Dynamic load (Deviatoric stress) q [kPa]	Cell pressure σ_c [kPa]	Static load σ^s [kPa]	Bulk stress θ [kPa]	Number of loadings N
1	100	60	20	300	1000
2	200	60	20	400	1000
3	400	60	20	600	1000
4	400	120	20	780	1000
5	600	120	20	980	100000
6	800	120	20	1180	100000
7	1000	120	20	1380	10000
8	1200	120	20	1580	10000

$$\theta = q + 3 \cdot \sigma_c + \sigma^s \quad (4.1)$$

The use of different load levels made it possible to evaluate the stress hardening behavior. The first three load steps had a cell pressure of 60 kPa and the dynamic loading was increased from 100 kPa to 200 kPa and 400 kPa. For each load step 1 000 load repetitions were performed. At the fourth load step, the constant confining pressure was increased from 60 kPa to 120 kPa although the dynamic loading was still at 400 kPa and a further 1 000 load repetitions were performed. For the fifth and sixth load steps (600 and 800 kPa) 100 000 load repetitions were performed and for the last two load steps (1 000 and 1 200 kPa) 10 000 load repetitions were performed.

The four unbound materials were tested at three different water contents, 60 %, 80 % and 100 % of optimum, evaluated from modified Proctor compaction tests (SS-EN 13286-2:2004 2004). Two tests were performed with each of the water contents of the material, resulting in a total of 24 tests. All test results are evaluated with regard to the deformation behavior. However, only the results from the test with water content 80% of optimum (8 tests) will be used for a detailed presentation of the deformation behavior. The water content of 80% of optimum was closed to the one measured in the unbound base layer during the field test.

4.3 Description of the tested unbound material

The four tested materials were crushed rock from different quarries. They were stock piled for some months before testing. All materials are igneous rocks and some of them have been exposed to metamorphism. The rock materials were chosen in order study the influence of fine grained mica on the permanent deformation properties. The mica content was measured in the grain size range of 0.125-0.250 mm by using the Swedish Road Administration method VVMB 613 (2001).

Material 1 consisted of a granitic to granodioritic gneissic rock material with a small number of micro cracks (in most cases within the microcline). The color is gray with some red spots. The mica content is relatively high and the number of micro cracks is low. The mineral content is determined using point counting of three thin sections and the results are shown in Table 4.2. Classification of Material 1 is presented in Appendix A, Figure A1.

Table 4.2. Mineral content of Material 1

Mineral	Content [%]
Quartz	34 - 36
Microcline	6 - 11
Plagioclase	27 - 36
Biotite	2 - 5
Muscovite	1 - 7
Chlorite	5 - 7
Epidote	8

4. Identification of the conditions for post compaction using small scale tests

Material 2 is a mixture of a tonalitic gneissic rock and a coarse grained granite. The tonalitic rock had a very low microcline content but a high content of biotite. The coarse grained granite (mineral grain size up to 7 mm) with some muscovite was weakly foliated and the number of micro cracks was rather high. The mineral content is determined using point counting of three thin sections and the results are shown in Table 4.3. Classification of Material 2 is presented in Appendix A, Figure A2.

Table 4.3. Mineral content of Material 2

Mineral	Content [%]
Quartz	29 - 36
Microcline	0 - 46
Plagioclase	16 - 46
Biotite	0 - 24
Muscovite	0 - 2

Material 3 was a granitic rock with no foliation. The mineral grains were well distributed and the grains size was up to 5 mm. The color was red to grey. The number of micro cracks was rather high. The mineral content is determined using point counting of three thin sections and the results are shown in Table 4.4. Classification of Material 3 is presented in Appendix A, Figure A3.

Table 4.4. Mineral content of Material 3

Mineral	Content [%]
Quartz	32
Microcline	31
Plagioclase	33
Biotite	1
Clorite	2

Material 4 was a fine grained tonalitic gneissic rock with a low amount of microcline but a high amount of plagioclase. The grain size of the plagioclase was large. The content of biotite was also high. The number of micro cracks was low. The mineral content is determined using point counting of three thin sections and the results are shown in Table 4.5. Classification of Material 4 is presented in Appendix A, Figure A4.

Table 4.5. Mineral content of Material 4

Mineral	Content [%]
Quartz	19
Plagioclase	37
Biotite	31
Muscovite	2
Epidote	9

The grain size was 0-40 mm for all materials. The abrasion strength was also tested using Micro Deval (MD) Test (SS-EN 1097-1) and Nordic Ball Mill Test (NBMT) (SS-EN 1097-6) and the impact strength was tested using the Los Angeles Test (LA) (SS-EN 1097-2). The results of the tests are present in Table 4.6 (see Ekdahl et al. 2004a).

Table 4.6. Material strength properties.

Material	MD	NBMT	LA	Mica content [%]
1	7.5	13.7	21	14
2	9.3	18.2	26	34
3	9.1	23.0	38	6
4	15.0	19.2	24	30

4.4 Results

From the triaxial test results it is possible to evaluate the elastic resilient and permanent deformation. Some of the results are also presented by Hansson & Lenngren (2005). First the results of the permanent deformation evaluation are presented.

Permanent deformation

According to the second hypothesis, post compaction occurs if the load characteristics of compaction and the loads after compaction are different. In this case the specimen was placed on a vibrating table while a vertical load was applied and it was compacted until the desired degree of compaction was achieved. The loading after compaction was a 100 kPa dynamic load. Post compaction should thus be expected. After the sample preparation the degree of compaction was 97 %, 96 %, 97 % and 95% of optimum for materials 1, 2, 3 and 4 respectively (compared to the Modified Proctor Test).

The measurements show that permanent deformation occurs in the unbound material. An example from one of the two tests on material 1 with 80% water content (test b) can be seen in Figure 4.1 (the first four load steps) and Figure 4.2 (all load steps) (the results of the other three materials and water content 80% are presented in Appendix B Figure B1 and Figure B2).

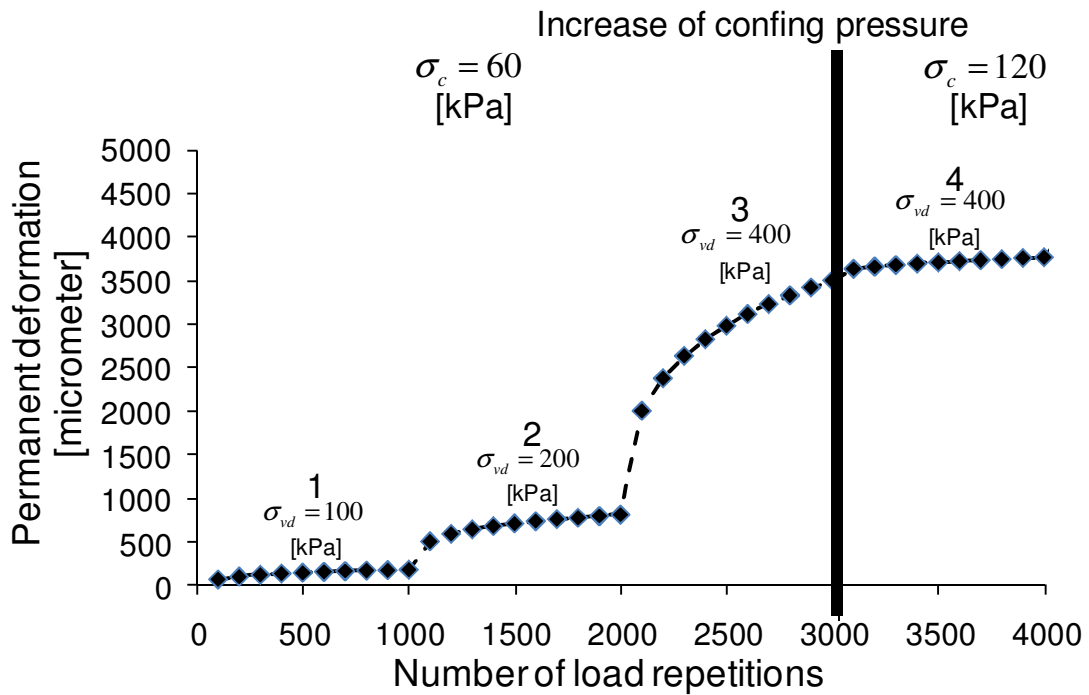


Figure 4.1. Permanent strain development during the triaxial test of Material 1 (test b) the first 4000 load repetitions (load step 1 to 4).

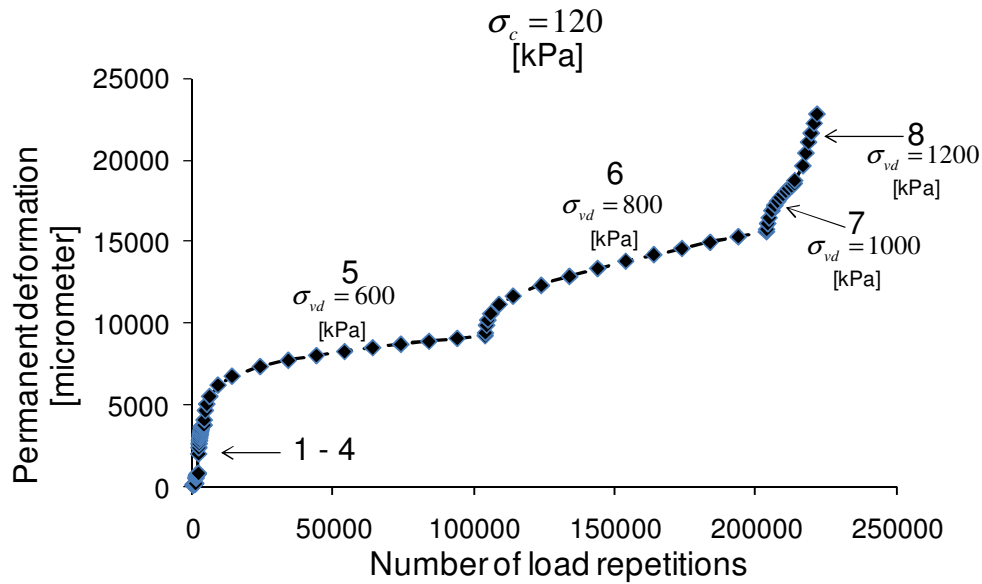


Figure 4.2. Permanent deformation during the triaxial test of Material 1 (test b) for all load repetitions.

The permanent deformation occurs directly during the first load step and the deformation rate increases for each new load step. It can also be seen that the deformation rate decreases for each load repetition at each load step, except for the 8th load step. The decrease in deformation rate is lower the higher the stress level although the cell pressure exerts a great influence when load steps 3 and 4 are compared (Figure 4.2). For the 8th load step failure probably occurs in the test sample. The measured permanent deformation in load step 1 is rather low.

It can be seen clearly that when the characteristics of the loading change (the load level increases), the permanent deformation rate increases directly, which is expected according to the second hypothesis.

Resilient deformation and stress hardening behavior

In Figure 4.3 the elastic deformation in the different load cycles is presented for Material 1 (test b) at 80% water content of optimum.

4. Identification of the conditions for post compaction using small scale tests

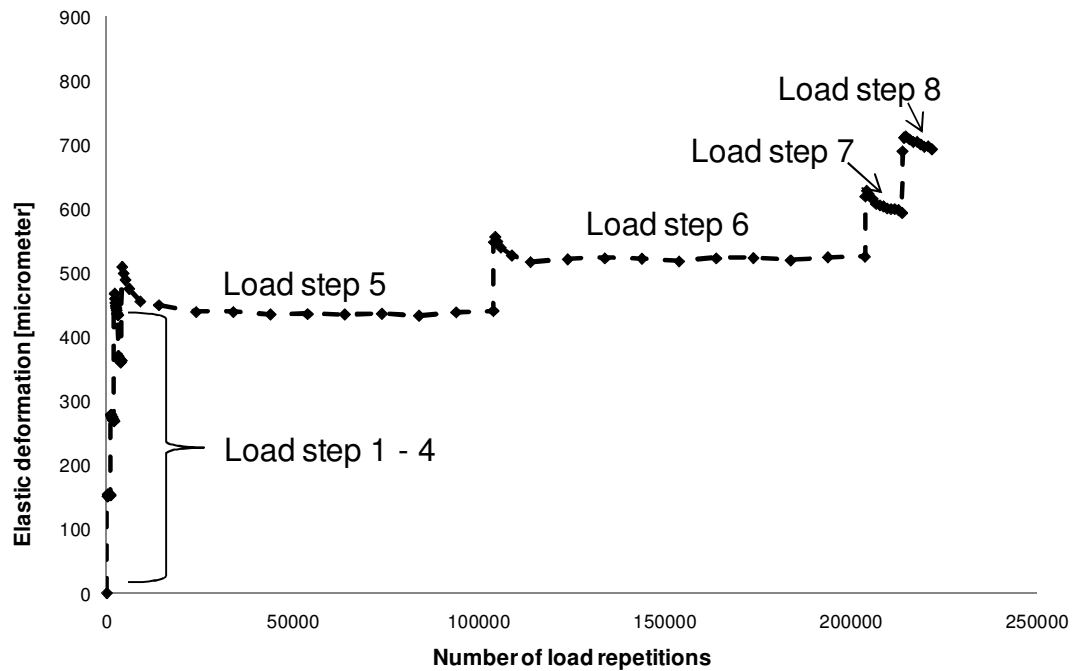


Figure 4.3. Elastic deformation during the triaxial test of Material 1 for all load repetitions and load levels.

As can be seen there are tendencies that the elastic deformation decreases during each load cycle. The same results can be seen for the other tests on the other three materials with water content 80% and these are presented in Appendix B, Figure B3.

The peak deformation for each load step was measured and divided by the sample height for calculating the strain. This evaluation of the result was performed for the 100th and the last load repetition for each load step. The resilient strain was plotted against the deviatoric stress and the results for Material 1 (test b) at 80% water content of optimum are presented in Figure 4.4.

4. Identification of the conditions for post compaction using small scale tests

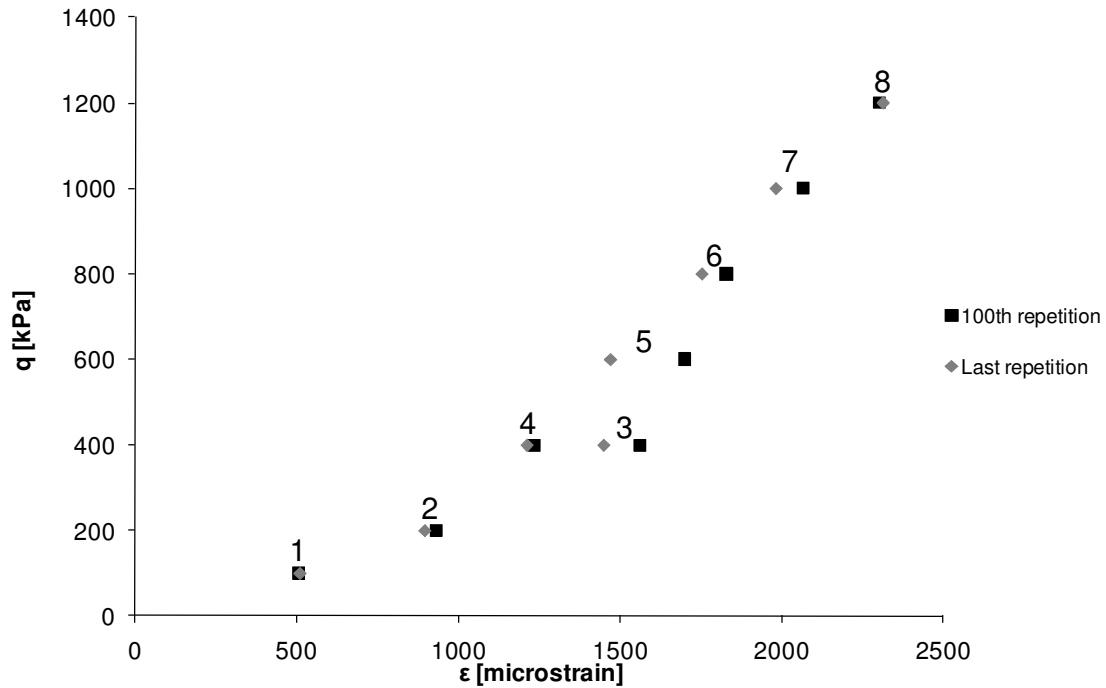


Figure 4.4. The stress-strain relationship for all eight load steps in the triaxial test at the 100th and the last load repetition for Material 1 and at a water content of 80% of optimum.

The resilient strain decreases from the 100th to the last load repetition for load steps 2 to 7 although the tendency is only small for load steps 2 and 4. Load steps 1 and 8 do not show any changes in resilient strain. The increase of the confining pressure from load step 3 to 4 can be seen as a decrease of the strain. The same patterns can be seen for all the other tests as presented in Appendix B, Figure B4 to Figure B7 apart from an increase of strain for load step 8 in about half of the tests.

By using the results from Figure 4.4, the resilient modulus can be calculated as presented in Figure 3.1 and by using Equation 3.1. This was done for all load steps and the results are presented in Figure 4.5 where the resilient modulus is related to the bulk stress on a log-log scale for material 1 and a water content of 80% of optimum.

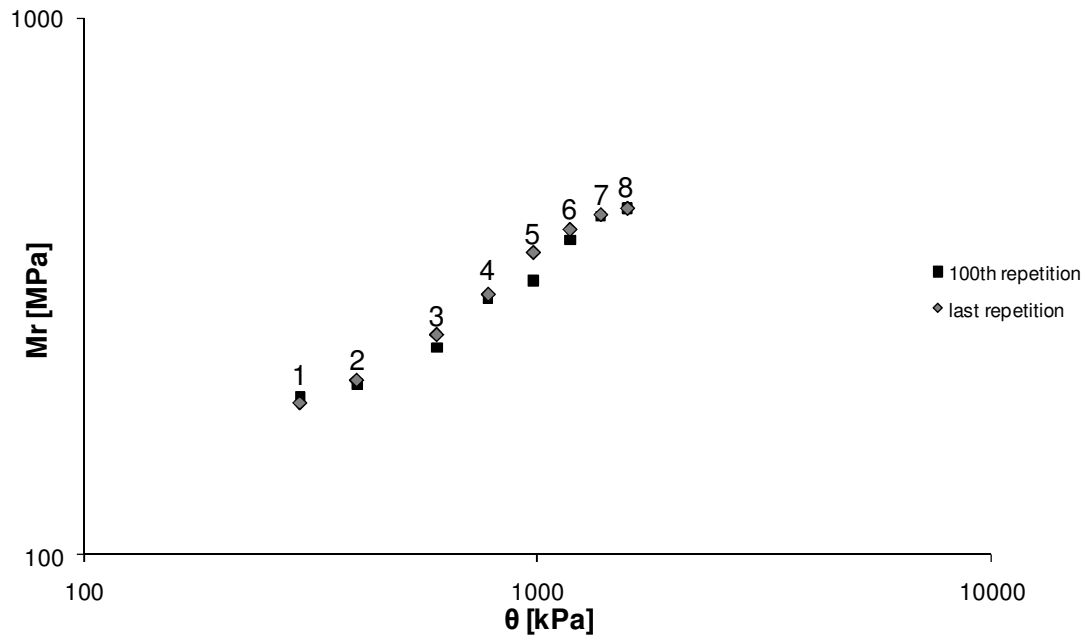


Figure 4.5. Relationship between bulk stress and the resilient modulus for material 1 water content 80% of optimum.

Load steps 2 to 6 show an increase in the resilient modulus from the 100th to the last load repetition and load steps 1, 7 and 8 do not show any changes.

The stress hardening behavior is evaluated stepwise using Equation 3.3. To obtain the stress hardening behavior for each load step, a regression analysis for three load steps at a time was performed. A total of six regression analyses were performed named A to F stepwise. The first regression analysis A considers bulk stresses 300, 400 and 600 kPa, the second regression analysis B bulk stresses 400, 600 and 780 kPa and C analysis 600, 780 and 980 kPa and so on (for load steps see Table 4.1). This is summarized in Figure 4.6.

Thus, it was possible to study the change in the stress hardening behavior for different bulk stresses. The results of the regression analysis A are presented in Figure 4.7.

4. Identification of the conditions for post compaction using small scale tests

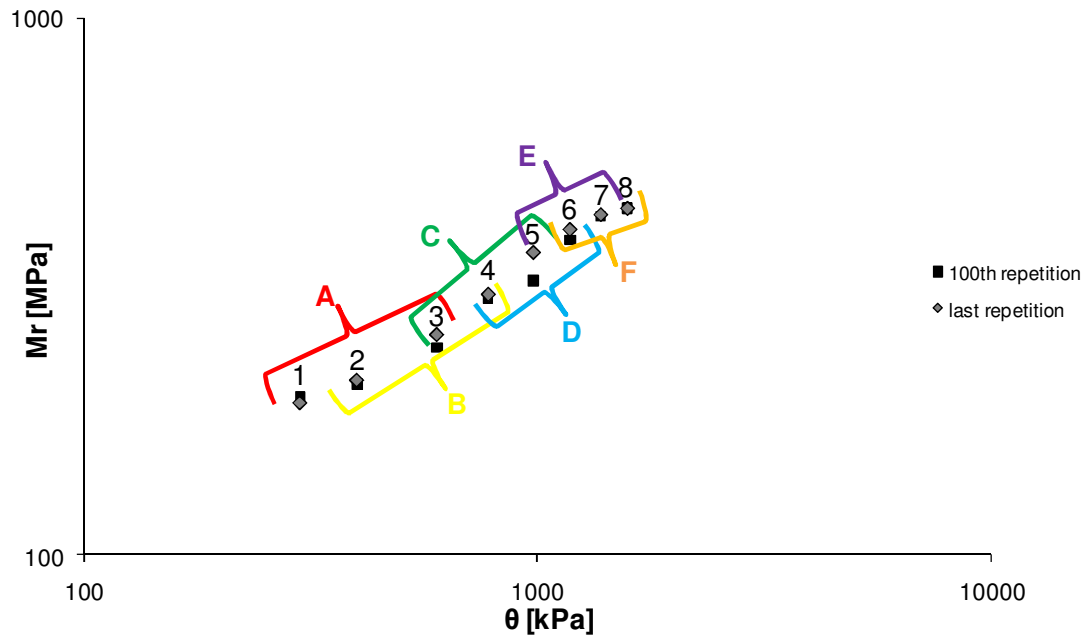


Figure 4.6. Resilient modulus at different bulk stresses evaluated from the triaxial test of material 1 and water content 80% of optimum. A to F represent the different regression analyses.

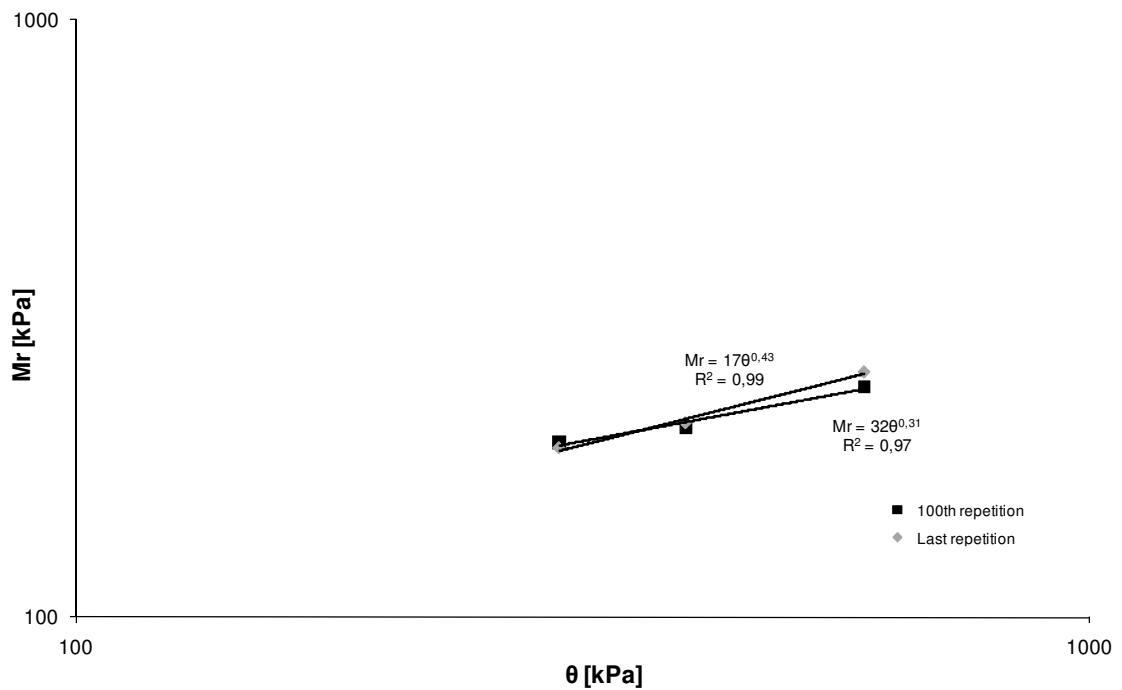


Figure 4.7. Regression analysis A for bulk stresses 300, 400 and 600 kPa Material 1 and with a water content of 80% of optimum.

4. Identification of the conditions for post compaction using small scale tests

It is possible to see that the regression parameter k_2 increases from the 100th load repetition to the last repetition (0.31 to 0.43) and the regression parameter k_1 decreases from 32 to 17. The results of all load steps of Material 1 80 % water content of optimum are summarized in Table 4.7.

Table 4.7. Regression analysis and load steps in the laboratory triaxial test Material 1 80% water content of optimum.

Regression analysis	Bulk stresses θ [kPa]	Regress. Param. 100 th rep. k_1 [MPa]	Regress. Param. 100 th rep. k_2 [-]	Regress. Param. Last rep. k_1 [MPa]	Regress. Param. Last rep. k_2 [-]
A	300, 400 and 600	22.1	0.37	10.4	0.5
B	400, 600 and 780	4.5	0.63	5.1	0.62
C	600, 780 and 980	2.9	0.7	1.2	0.84
D	780, 980 and 1180	2.2	0.74	1.4	0.81
E	980, 1180 and 1380	0.47	0.96	5.3	0.63
F	1180, 1380 and 1580	5.4	0.62	19.1	0.45

In Figure 4.8 and Figure 4.9 the parameters k_1 and k_2 respectively are plotted against the bulk stress θ for all tests and highlighted Material 1 and 80 % water content of optimum.

4. Identification of the conditions for post compaction using small scale tests

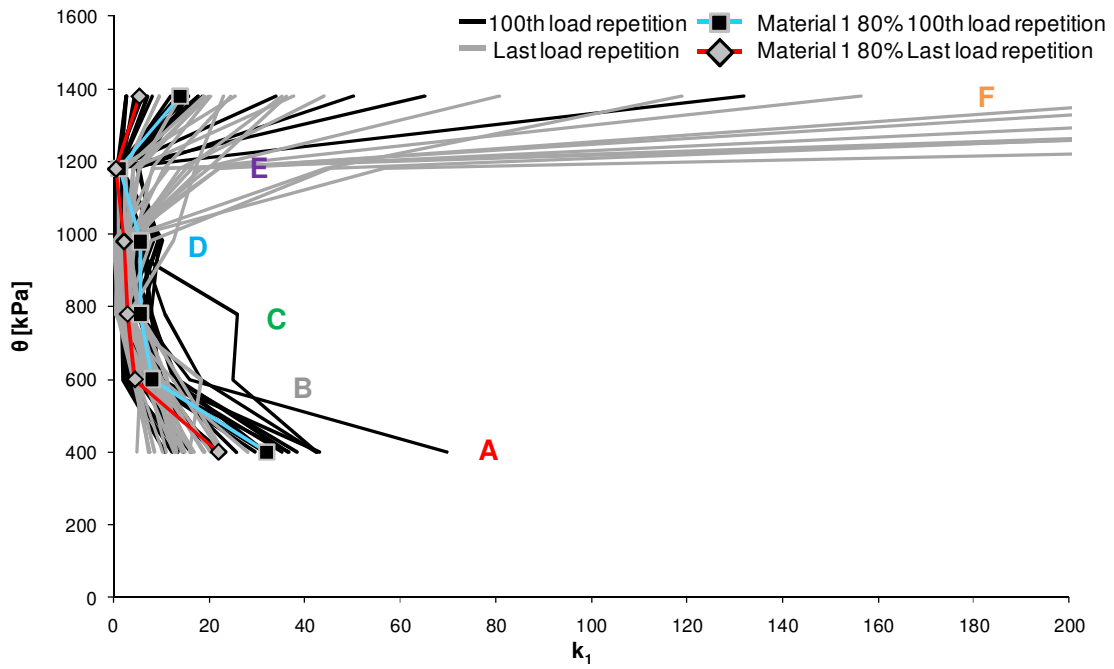


Figure 4.8. Stress hardening behavior parameter k_1 at different bulk stresses at the 100th and the last load repetition for all tests on all materials. Label A to F represents the different regression analyses

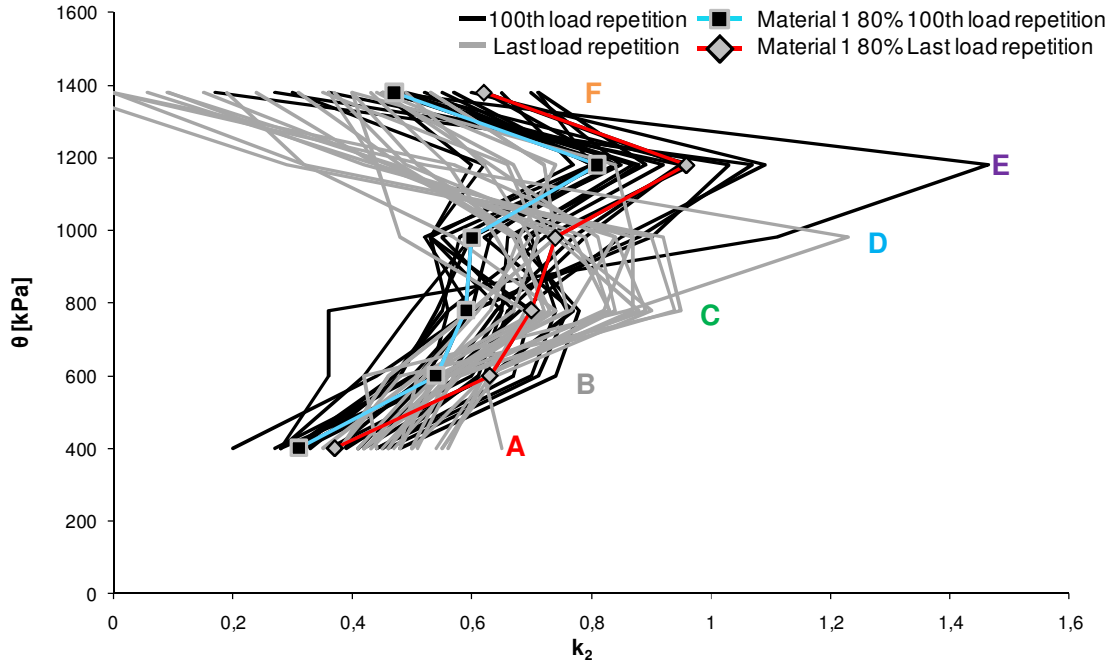


Figure 4.9. Stress hardening behavior parameter k_2 at different bulk stresses at the 100th and the last load repetition for all tests on all materials. Label A to F represents the different regression analyses

It is possible to see regression analyses A, C and D show a clear decrease of k_1 and increase of k_2 from the 100th to the last load repetition. Regression analysis B does not show any change but E and F show a clear increase of k_1 and decrease of k_2 . The “middle” point in each regression analysis represents the actual load step that is analyzed. Load step 1s and 8 can therefore not be analyzed. The parameter k_1 decreases to a minimum and parameter k_2 increases to a maximum around the bulk stress 1200 kPa after 100 load repetitions and 1000 kPa for the last load repetition.

The results of the evaluation of the maximum mica content

The results of the evaluation of the maximum mica content in base layer material are presented in Ekdahl et al. (2004a). The conclusions were that it was difficult to relate the performance to the mica content but at higher water content the influence of mica is clearer. In Ekdahl et al. (2004a) the usefulness of the results as input for testing different existing material models for elastic and permanent deformation are also presented.

5 IDENTIFICATION OF POST COMPACTION USING FULL SCALE TESTS

5.1 Introduction

In order to extend the amount of data describing the deformation process, results from a field test are evaluated. Such a test was carried out at a Swedish Road Administration field site during the summer of 2003. The Swedish Road and the Transport Research Institute (VTI), performed an accelerated pavement test for the Swedish Road Administration. A HVS was brought to the site to test functional properties of mica-rich aggregates of crushed rock and also light-fill materials at a realignment construction project on the E6 Freeway close to Uddevalla, approximately 100 km north of Gothenburg. A Multi Load FWD was also brought to the site. From the HVS test, the permanent deformation behavior could be analyzed and from the FWD test the stress hardening behavior could be evaluated in the same manner as for the triaxial test described in Section 3.

The tests formed part of a large project involving the laboratory triaxial tests referred to in section 4. The aim of these studies was primarily to find the maximum mica content in unbound material that can be permitted according to bearing capacity and water influence. The properties that were found to be most important to evaluate were the permanent deformation and stiffness. For this purpose four test cells were constructed for the HVS test. Here, test cells are defined as test areas, finite in size and with controllable properties. The subgrade, subbase and the asphalt surface were equal for all test cells although the unbound base layer of each test cell consisted of crushed rock of four different rock types and mica content. It was the same rock materials that were tested in the triaxial tests described previously. The four test cells were constructed in the same way and the compaction and grain size of the material in the unbound base layer were also kept as equal as possible.

Field tests, such as static plate bearing test, light falling weight deflectometer test, ground penetrating radar test, degree of compaction and moisture content were also performed on the test cells. The test cells were equipped with precise deflection measurement devices (EMU-coils) and pressure cells in the unbound base layer (see Figure 5.1) (Ekdahl et al. (2004a).

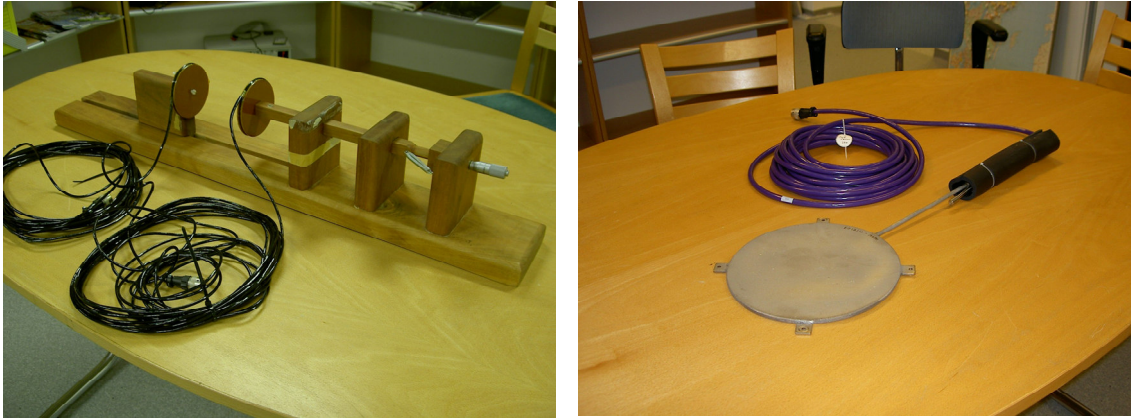


Figure 5.1. EMU-coils to the left for deformation measurements and pressure cell to the right for stress measurements in the unbound layers.

The size of the EMU-coil is 100 mm in diameter and the thickness is 8 mm. The EMU-coils measure the displacement that takes place between pairs of inductive coils placed in the granular material. The pairs of coils are not in contact and displacement of one coil does not affect the displacement of one other. When the coil is subjected to an alternating current, a magnetic flux field is generated. When another coil is placed within the generated magnetic flux field, an alternating current is generated in the EMU-coil. The current generated corresponds to the flux density at that specific position. The generated current can thus be related to the distance between the coils. An average strain between a pair of coils can be calculated by dividing the displacement by the distance between the coils. Both dynamic and static measurements for resilient and permanent deformation measurements can be performed.

The pressure cells used in the evaluation of vertical stresses are 200 mm in diameter and are 10 mm thick. The pressure cell contains oil and when the cell is subjected to stress from the unbound material, the pressure cell is compressed. The pressure in the oil obtained in the pressure cell corresponds to the vertical stress in the unbound material. Temperature and moisture were also recorded. Further details of how the entire test was conducted can be found in Ekdahl et al. (2004a).

The FWD tests were carried out before and after the HVS test. Three different stress levels were used and for each stress level the drop was repeated. In this way it was possible to evaluate an increase in the stress hardening behavior in the unbound base layer from drop 1 to drop 2 in the same way as the laboratory triaxial tests. It was also possible to evaluate if the stress hardening behavior changed after the HVS test and if the permanent deformation that resulted from

the HVS loading might be caused by post compaction. All test results are available in a data base provided by the Swedish Road Administration, see Ekdahl et al (2004a).

5.2 HVS Test Design and Evaluation

The field test site was constructed as four test cells, Cells #1 - #4, see Figure 5.2.

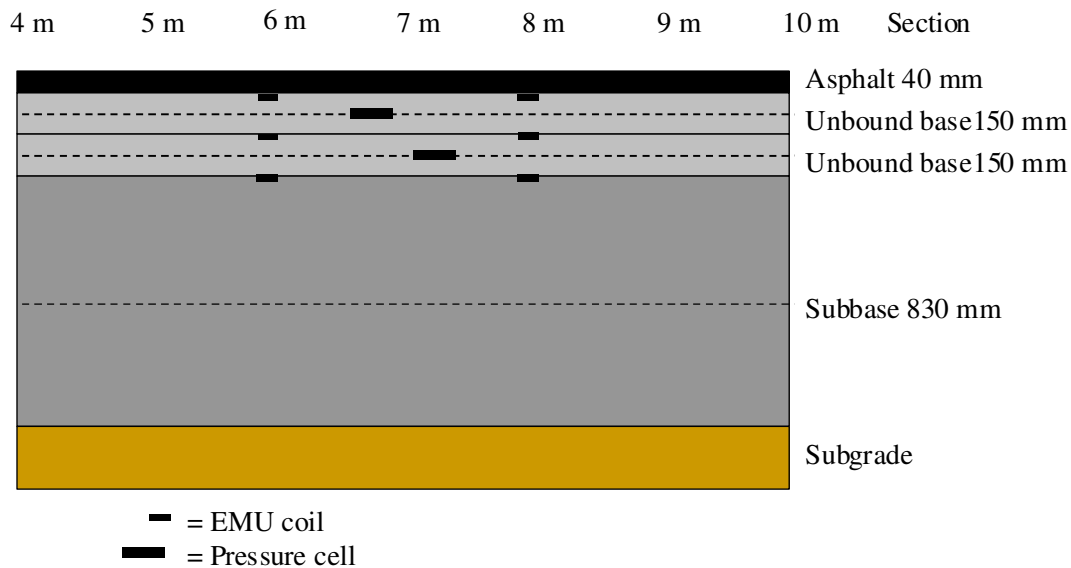


Figure 5.2. Design of Test Cells #1-#4. The broken lines represent surfaces where compaction was performed in addition to the compaction of each layer.

The test cells were designed to be equal apart from different mica content in the unbound base layer of crushed rock. The mica content was measured in the grain size range of 0.125-0.250 mm and in the unbound base layer of Test Cells #1 to #4, it was 14 %, 34 %, 6 % and 30 % respectively, i.e. Material 1 of the triaxial test was placed in Test Cell #1 and so on (see Ekdahl et al 2004a). All cells were constructed on the same clay subgrade. Each cell was designed with three layers from subgrade to surface, 830 mm of subbase layer, 300 mm of unbound base and on top 40 mm of bituminous surface layer. The subbase was the same for all test cells and consisted of crushed rock with a gradation size of 0 - 90 mm. It was arranged in two layers and each layer was compacted six times using a vibrating roller with a weight of 6 700 kg and a compaction depth of approximately 450 mm. The aim of the compaction was to reach a bearing capacity of $E_{v2} = 125$ MPa (evaluated from the static plate bearing test performed according to the Swedish Road Administration method VVMB 603:1993 which follows DIN

18134) at the surface of the subbase layer. The base layer consisted of crushed rock with a gradation size of 0 - 40 mm with different mica content. The 300 mm layer was arranged into four sublayers and each layer was compacted with a static roller with a line load of 50 kN/m in order to avoid damage to the instrumentation. The aim of the compaction of the base layer was to achieve a degree of compaction (DOC), comparable to the compaction level of a modified Proctor test, of 95% for all test surfaces. The surface layer was the same for all test cells.

The degree of compaction and water content (degree of optimum from a modified Proctor test), was measured before and after the HVS test at the surface of the unbound base layer and in the middle of the layer at six points for each test cell.

In addition, the light falling weight deflectometer tests on the subgrade surface and the static plate bearing test on the subbase surface, in the middle of the base layer and on the base layer surface were performed as a quality control of the test cells.

Each test cell was made fifteen meters long and the track length of the HVS was eight meters. One meter on each side was a turning area for the wheel for a change of direction. The full speed (12 km/h) length was therefore six meters. A dual-wheel configuration was used for the load. For the test, 100 000 bidirectional passes, were employed. As is common, the test was initiated by a lower load level of 30 kN the first 200 000 passes. The tire pressure was also low, 700 kPa. After 20 000 passes, the actual test commenced with an 80 kN total load and a tire pressure of 1000 kPa. Lateral wander was engaged over a width of 500 mm in eleven increments. The lateral position followed a normal distribution, with the highest frequency of passes in the center track (24%). All tests were enclosed in a climate chamber, keeping the temperature at 10°C and thus minimizing the variation in temperature for the different cells. A standard axle load of 100 kN is normally used (50 kN on either side of the axle) in the design in Sweden. This means that the 80 kN load used in the tests is 1.6 times higher than the design load. During the test, permanent and elastic deformation and stress were recorded. These measurements were carried out for load pass 0 (before the test), and at approximately 20 000 (after pre-loading and before the ordinary test), 21 000, 25 000, 40 000, 60 000 and 100 000 passes. As the HVS was stopped temporarily (before the start of the test and after 20 000, 40 000, 60 000 and 100 000 passes), rut progression was monitored on the surface at three locations for

each cell; one near the pressure cells and the other two three meters on either side from that location along the HVS track.

During the HVS test, resilient deformation and stress during a passing of wheel load were measured by the EMU-coils and pressure cells respectively in the upper and lower unbound base layer. At around pass 40 000, four different load levels of the HVS wheel, 30, 50, 60 and 80 kN, were exerted during these measurements. The measurements at the different load levels were performed with the dual wheel in lateral position 0 and 150 mm. Lateral position 0 means that the gap between the wheels is centered directly above the instrumentation and in lateral position 150 mm, one of the dual wheels is directly above the instrumentation, see Figure 5.3.

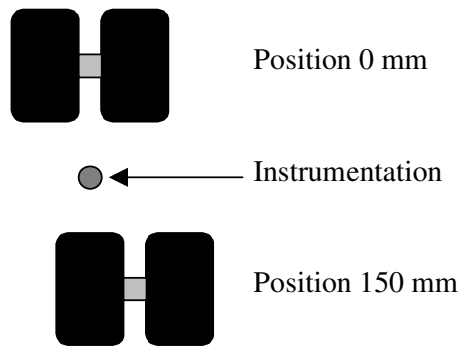


Figure 5.3. The dual wheel configuration of the HVS in lateral position 0 and 150 mm.

The resilient strain was evaluated as the average strain between the pair of EMU-coils. The stress and resilient strain were evaluated for each of the four load levels in the upper and lower base layer separately. The HVS equipment is shown in Figure 5.4.



Figure 5.4. The HVS with climate chamber at the test site in Uddevalla. A dual wheel configuration was used during the tests.

5.3 FWD test design and evaluation

In the FWD test at the HVS test site three load levels were used, 30, 50 and 63 kN. The VTI research FWD, a dual-mass, was used for this purpose (see Tholén 1980). The drop of the falling weight at each load level was repeated once for a total of six drops per station, not counting the 50 kN seating drop. The FWD stopped at one-meter increments along the projected line of the HVS test wheel, sections 0 to 14 (see Figure 5.5).

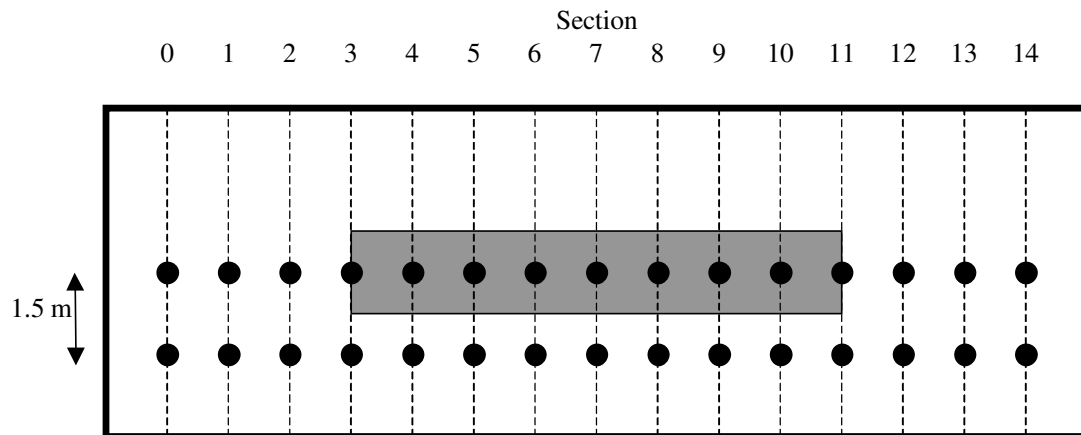


Figure 5.5. Basic sketch of Test Cells #1 - #4 as seen from above. The dots represent FWD stations. The shadowed area represents the area loaded with the HVS wheel load. From Ekdahl et al. 2004a.

A second set of tests along a line, 1.5 meters parallel to the HVS track was also measured. As each test cell was 15 meters long, several stations were outside the loading area, namely sections 0-3 and 11-14.

The deflection sensors of the FWD recorded a peak deflection at the center and 200, 300, 450, 600, 900 and 1200 mm away from the load. The linear elastic backcalculation program CLEVERCALC 3.9 was used for the backcalculation of the elastic modulus. The program is based on the software EVERCALC 3.0, developed at the University of Washington, Seattle and was adapted to evaluation practice in Sweden. In many cases a three layer system is used and the structure is divided into a bound top layer, an unbound layer in the middle and the subgrade in the bottom. As the layer-thickness was known to a high degree of accuracy in the present study, a four-layer model was used directly. The structures of the four test cells were divided in the asphalt surface layer, unbound base layer, subbase layer and subgrade. The constructed layer thicknesses differed somewhat from the designed ones and the measured thicknesses were

therefore used in the evaluation. Determined by ground penetrating radar, rock was detected near the subgrade surface for some sections close to the end of Cells #1 and #4 with a steep surface slope. The common option of using a rigid base was rejected in this case, as it did not improve the fit, most likely due to the steep slope of the rock surface. RMS-values around one percent or less were achieved for most of the basins.

5.4 Results

In this section the results from the quality control are presented first, followed by the HVS test results of permanent deformation. After that the FWD results are presented and finally these results are compared to the resilient deformation results of the HVS test. Some results are also presented in Lenngren & Hansson (2004).

Quality control during construction

The degree of compaction and the water content were measured at different depths before and after the HVS test. These are presented in Table 5.1 and Table 5.2.

Table 5.1. *The degree of compaction of the unbound base layer for Test Cells #1 to #4 before and after the HVS test as an average value of six points.*

Test Cell	1	2	3	4
DOC before HVS [%] at the surface	99.3 ± 1.2	99.7 ± 1.1	100.1 ± 1.2	100.5 ± 1.6
DOC before HVS [%] in the middle	96.8 ± 1.0	94.9 ± 3.0	96.6 ± 1.6	95.9 ± 1.5
DOC after HVS [%] at the surface	99.7 ± 1.8	99.3 ± 1.5	99.3 ± 2.3	100.6 ± 2.0

Table 5.2. *Water content as a % of the optimum for Test Cells #1 to #4 before and after the HVS test.*

Test Cell	1	2	3	4
WC before HVS [%] at the surface	73.1 ± 9.0	84.9 ± 3.4	31.4 ± 3.6	84.3 ± 5.0
WC before HVS [%] in the middle	89.6 ± 4.4	106.7 ± 15.2	76.6 ± 10.6	121.7 ± 11.0
WC after HVS [%] at the surface	63.8 ± 5.4	69.9 ± 4.7	29.1 ± 3.0	82.1 ± 8.6

Here it is possible to see that the degree of compaction is close to maximum at the surface of the unbound base layer and close to the target value of 95% in the middle of the base layer before the test. After the test the degree of compaction had not changed very much at the surface of the base layer. The water content decreased after the test especially for Test Cells #1 and #2. The water content is quite similar for all test cells except Test Cell #3, which has a much lower content. The water content in the middle of the unbound base layer is higher compared to the surface probably caused by evaporation (the test was performed in May).

The light falling weight deflectometer results are shown in Table 5.3 as E_{vd} value (dynamic surface modulus compared to the static plate bearing tests E_{v2}).

Table 5.3. Light falling weight deflectometer results for the subgrade surface.

Test Cell	1	2	3	4
Subgrade E_{vd} [MPa]	23.1 ± 1.8	18.2 ± 4.0	17.9 ± 5.1	9.5 ± 6.4

The recommend E_{vd} values in the SRA standard (ATB Väg) are 4 to 5 MPa when the total thickness of the unbound layers is 1130 mm. All the tested points achieve this. However, the subgrade of test cell #4 seems to be much softer than the other ones.

Table 5.4 shows the results of the static plate bearing test.

Table 5.4. Static plate bearing test results of the subbase layer and in the middle and on the surface of the unbound base layer.

Test Cell	1	2	3	4
Subbase E_{v2} [MPa]	112 ± 18	104 ± 13	116 ± 12	99 ± 9
Base layer middle E_{v2} [MPa]	160 ± 12	156 ± 3	158 ± 15	163 ± 13
Base layer surface E_{v2} [MPa]	164 ± 13	152 ± 7	160 ± 11	158 ± 14

According to the Swedish Road Administration standard (ATB Väg) the E_{v2} value should be at least 125 MPa for the subbase and on top of the unbound base layer at least 140 MPa. As can be seen the E_{v2} values are lower in the subbase layer for all test cells. The E_{v2} values in the middle of the base layer and on top of it are much higher than the requirement of 140 MPa.

The compaction ratio is E_{v2}/E_{v1} and its result is presented in Table 5.5 (the requirements in brackets). Note that the requirements values are linked to the E_{v2} value obtained for each specific test point, the higher the E_{v2} , the higher ratio is allowed.

Table 5.5. *Static plate bearing test results for the subbase subbase layer and in the middle and on the surface of the unbound base layer, compaction ratio (the requirements in brackets).*

Test Cell	1	2	3	4
Subbase E_{v2}/E_{v1} (demand) [-]	2.2 ± 0.6 (4.1)	2.3 ± 0.6 (3.9)	2.6 ± 0.7 (4.2)	2.1 ± 0.3 (3.8)
Base layer middle E_{v2}/E_{v1} (demand) [-]	2.5 ± 0.4 (3.7)	2.5 ± 0.4 (3.6)	2.6 ± 0.2 (3.7)	2.8 ± 0.4 (3.7)
Base layer surface E_{v2}/E_{v1} (demand) [-]	2.6 ± 0.7 (3.7)	2.8 ± 0.6 (3.6)	3.0 ± 0.6 (3.7)	3.2 ± 0.6 (3.7)

In the static plate bearing test the load is applied twice at each test point. The first one gives E_{v1} and the second one E_{v2} . If the E_{v2} -value is much higher than the E_{v1} -value, the ratio is high and shows that the compaction is bad. This is because the test equipment can compact the material. As can be seen in Table 5.5 the requirements are met.

As a summary of the quality control the subgrade had sufficient bearing capacity according to the total thickness of the unbound layers. However the bearing capacity of the subbase was not sufficient although the compaction ratio indicates good compaction. One interpretation of the results could be that the lower part of the subbase is not as well compacted but the upper part is. The compaction result for the unbound base layer seems to be very good.

Permanent deformation measurements

The total permanent deformation of the pavement structure measured at the surface of the asphalt in the middle of the wheel track is presented in Figure 5.6. Note that the wheel load was increased after approximately 20 000 passes from 30 kN to 80 kN.

5. Identification of post compaction using full scale tests

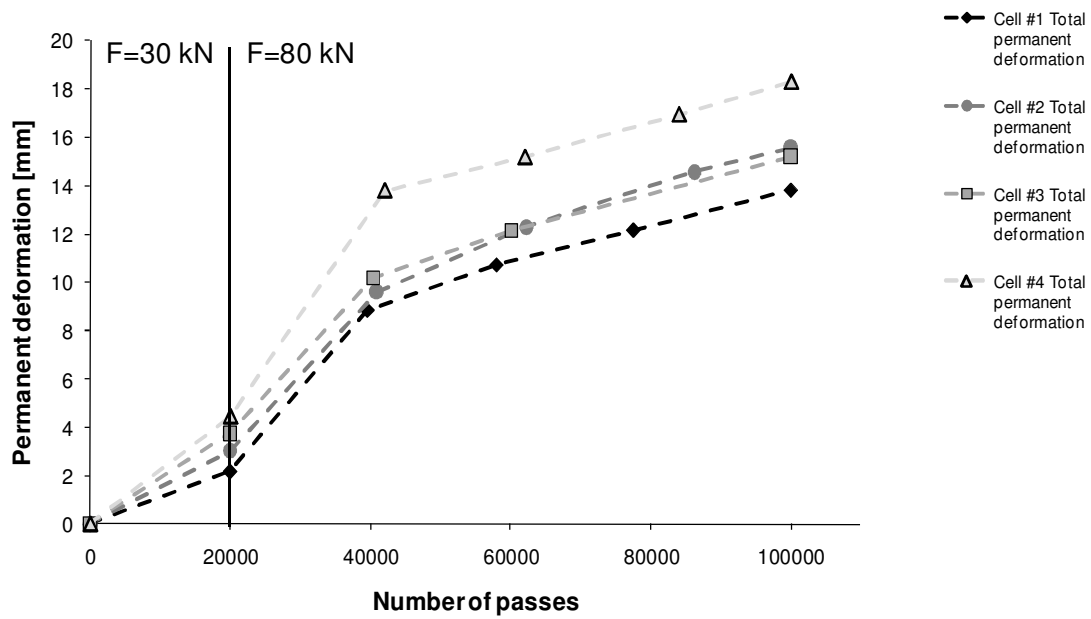


Figure 5.6. Total permanent deformation measured on top of the asphalt layer.

The total permanent deformation is the average of the measurements at the three locations (sections 5, 7 and 9, see Figure 5.2). The permanent deformation rate is high at the beginning of the test, and the rate decreases after passing 40 000 for all test cells. The permanent deformation rate seems to be quite even after passing 40 000 for all test surfaces and the deformation rate does not show any tendency to decrease. The permanent deformation obtained during the first 40 000 passes shows some differences between the test surfaces. The total permanent deformation of test cell #4 shows by far the highest and test cell #1 the lowest, with test #2 and #3 in between.

The permanent deformation measured in the unbound base layer is the average of the measurements at the two locations of the EMU-coils (Figure 5.2) and is presented in Figure 5.7.

5. Identification of post compaction using full scale tests

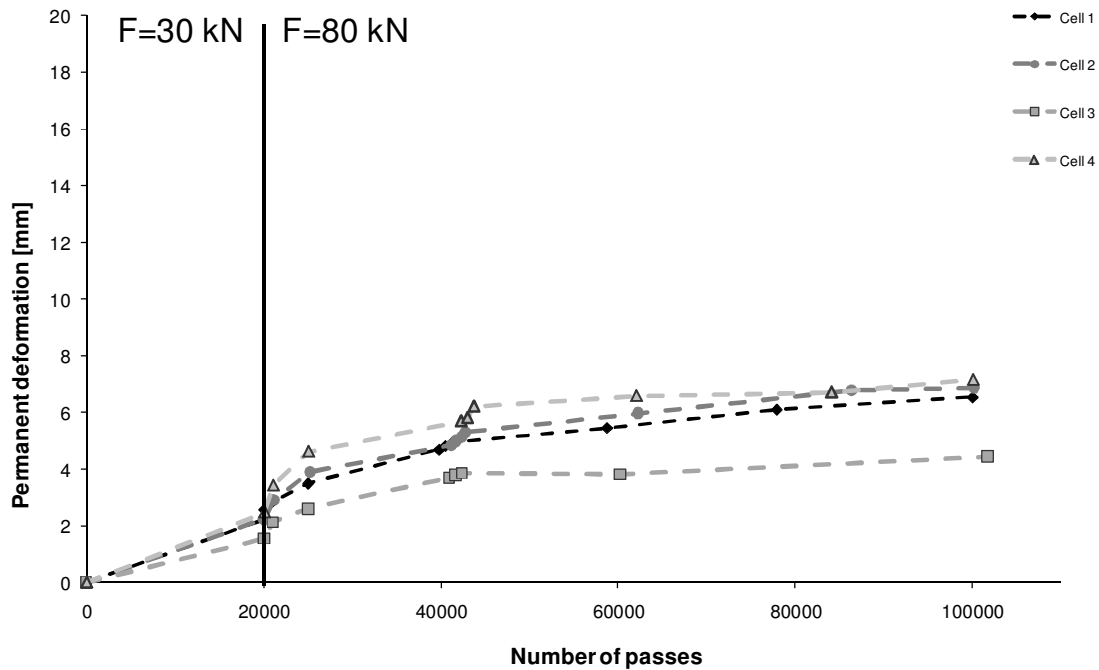


Figure 5.7. Permanent deformation in the unbound base layer.

For the unbound base layer the permanent deformation rate seems to be decreasing for all test cells and test cell #3 shows a slightly lower permanent deformation than the other cells. Around passing 40 000 an irregularity can be seen. This could be explained by the special test program where the resilient properties were tested for different load levels and wheel positions. This may have disturbed the deformation measurements.

The permanent deformation in the subbase and subgrade is evaluated by subtracting the deformation in the base layer from the total rutting. In this case the permanent deformation in the asphalt layer is assumed to be negligible due to the small thickness. The results are presented in Figure 5.8.

5. Identification of post compaction using full scale tests

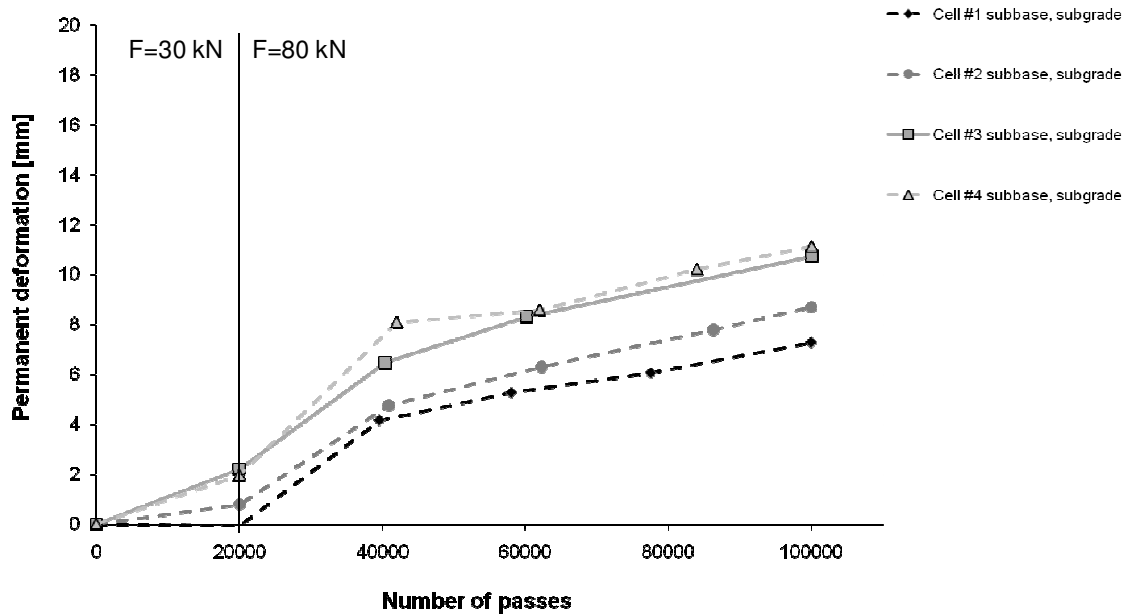


Figure 5.8. Sum of the permanent deformation in the subgrade and subbase layer.

The subbase and subgrade also show a high permanent deformation rate between passing 20 000 and 40 000. However, the rate probably decreases in the same way as for the unbound base layer presented in Figure 5.7. After 40 000 passes the deformation rate is more or less constant with almost the same rate for test cells #2 to #4 and a slightly lower rate for test cell #1. The first 40 000 passes for the subbase of test #4 followed by test cell #3 showed the highest strain rate and test cell #1 and #2 much lower.

The average distances between the EMU coils for each of the test cells are presented in Table 5.6.

Table 5.6. Layer thicknesses for the unbound base layer

Test Cell	1	2	3	4
Lower base layer [mm]	113	129	123	132
Upper base layer [mm]	130	145	136	125
Unbound base layer total [mm]	243	274	260	256

The thickness of the unbound base layer was found to vary somewhat. In the design it was supposed to be the same. The influence of the permanent deformation measurements is difficult to evaluate. These results are influenced by the difference in material properties (mica content) of the unbound base layer,

see also Table 4.6, and the thickness of the asphalt layer and subbase, which probably vary from test cell to test cell. If the thinner unbound base layer of Test Cell #1 is compensated with a thicker subbase layer, this is probably of benefit to the total deformation due to the higher bearing capacity of the coarser subbase material and vice versa for Test Cell #2.

Permanent Strain Evaluation in the Unbound Base Layer

In order to normalize permanent deformation to the layer thickness, the permanent strain can be determined instead. The permanent strain is likely to vary through the layer and the calculated strain in this case is an average strain over the layer thickness. The instrumentation design made it possible to measure the deformation in the upper and lower half of the base layer individually and the permanent strain is thus calculated for the upper and lower base layers separately.

The permanent strain development in the upper and lower base layer of Test Cell #1 to #4 is presented in Figure 5.9 and Figure 5.10.

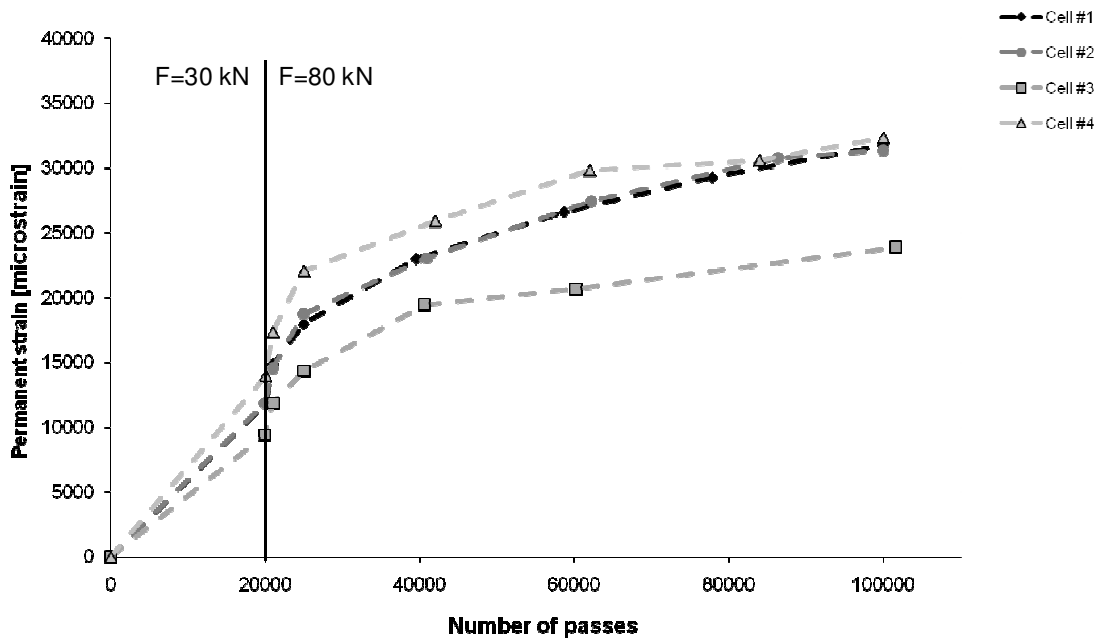


Figure 5.9. Permanent strain in the upper base layer.

5. Identification of post compaction using full scale tests

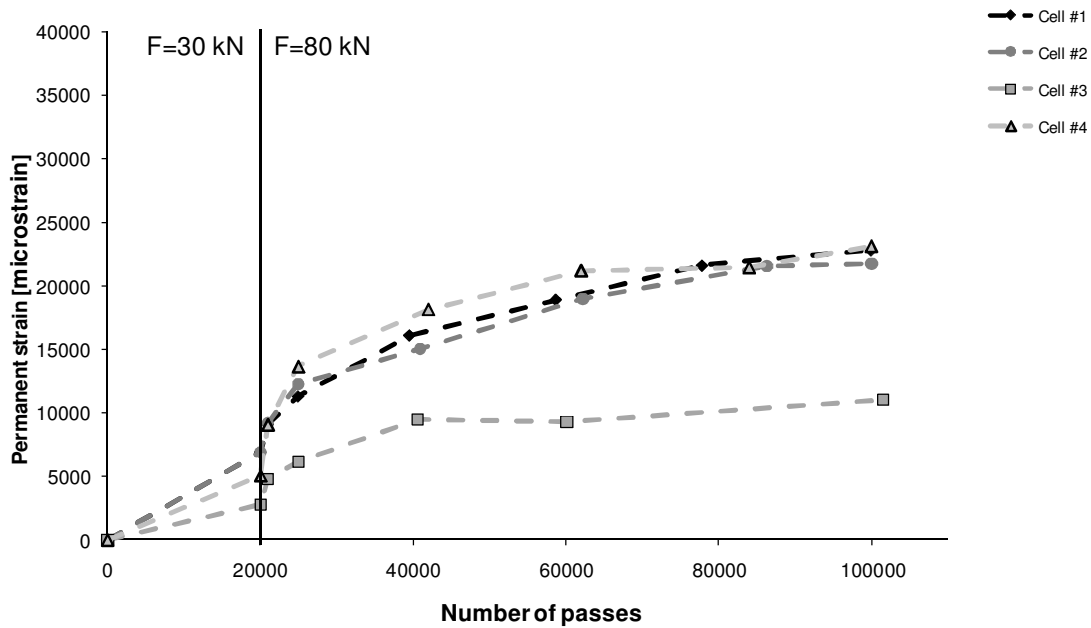


Figure 5.10. Permanent strain in the lower base layer.

In the lower base layer the permanent strain rate decreases from a high level although these tendencies are not very clear. The higher strain rate of both the upper and lower base layers for test cell #1 up to load passing 40 000 cannot be explained by the degree of compaction, water content or the bearing capacity of the subbase or the base layer.

Elastic Strain Evaluation in the Unbound Base Layer

The results of the elastic deformation measurements are shown in Figure 5.11 and Figure 5.12 for all test cells.

5. Identification of post compaction using full scale tests

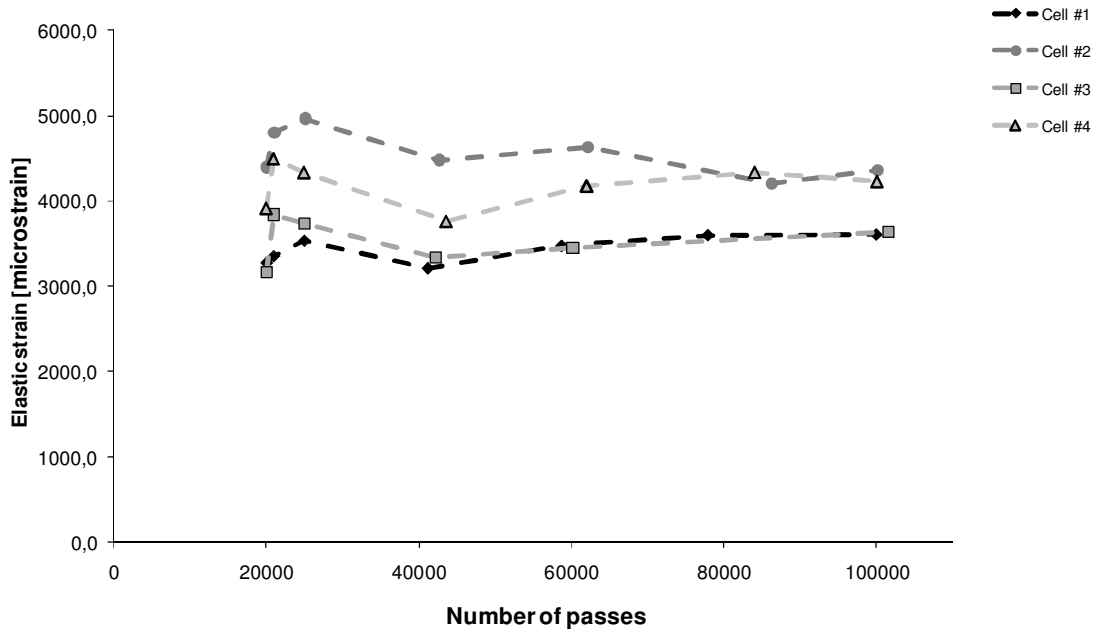


Figure 5.11. Elastic strain evaluated in the upper base layer of all test cells.

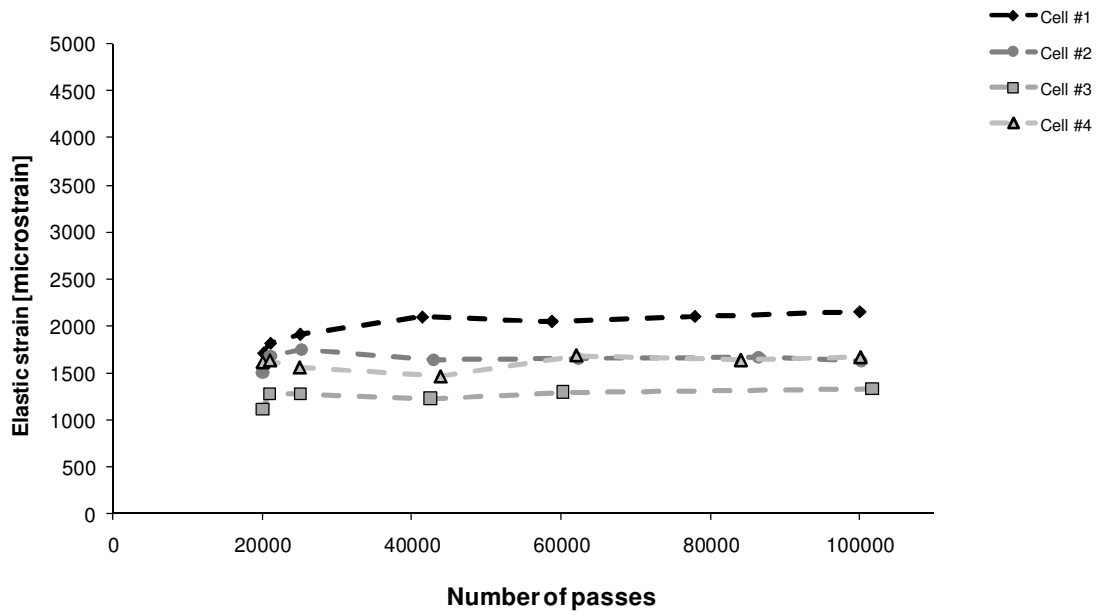


Figure 5.12. Elastic strain evaluated in the lower base layer of all test cells.

For all test cells the elastic strain seemed to be quite constant for all test cells during the test.

5.5 Results of the FWD test and the stress hardening evaluation

Linear Elastic Behavior of the Subgrade and Subbase

The average backcalculated elastic modulus of the subgrade and subbase for all test cells is presented in Table 5.7 and Table 5.8 respectively. The backcalculated moduli of elasticity of the subbase layer and subgrade before and after the HVS test for Test Cells #1 to #4 are presented in Figure 5.13.

Table 5.7. Average backcalculated elastic modulus \pm the standard deviation for the subgrade for the different test cells before and after the HVS test.

Test Cell	<i>E</i> -modulus before the HVS test [MPa]	<i>E</i> -modulus after the HVS test [MPa]
1	197 \pm 29	222 \pm 27
2	141 \pm 7	160 \pm 9
3	116 \pm 7	131 \pm 9
4	119 \pm 12	138 \pm 14

Table 5.8. Average backcalculated elastic modulus \pm the standard deviation for the subbase for the different test cells before and after the HVS test.

Test Cell	<i>E</i> -modulus before the HVS test [MPa]	<i>E</i> -modulus after the HVS test [MPa]
1	121 \pm 16	130 \pm 10
2	161 \pm 8	147 \pm 11
3	158 \pm 13	154 \pm 14
4	122 \pm 15	124 \pm 15

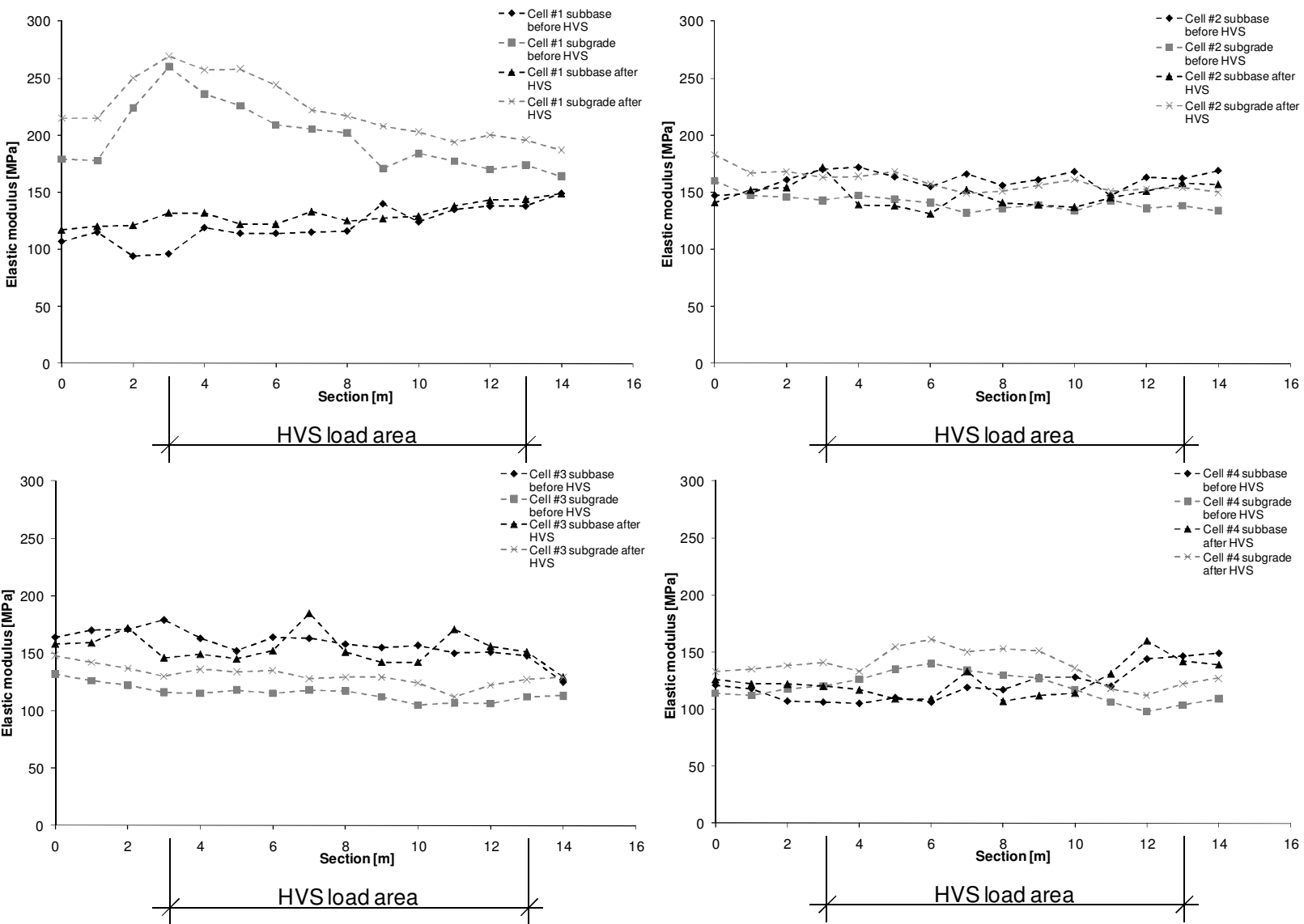


Figure 5.13. Backcalculated elastic modulus for the different sections of the subbase and subgrade in Test Cell #1 to #4 before and after the HVS test.

It can be seen that the subgrade modulus varies for the different sections for Test Cell #1. The reason for this may be the influence of rock present beneath the subgrade clay at different depths in the different sections. It can also be seen that the subbase modulus varies in the opposite way as in the subgrade. This could be due to an over compensating error in the backcalculation program or that the compaction is disturbed by reflection waves due to a stiff layer beneath, rock apparently close to the surface. The subgrade modulus is slightly higher for Test Cell #1 and lower for Test Cell #4. The subgrade is stiffer than both the unbound base and the subbase. As the subgrade soil was classified as clay the outcome seems to be slightly odd. It must be borne in mind, however, that the modulus is based on outer sensor surface deformation and that the modulus expresses a deformation by load ratio. Clay subjected to rather low deviatoric stresses also exhibits rather high values. Georadar measurements showed rock present near the surface. The modulus should thus be regarded as a combination of clay and rock; a very common cause of high backcalculated subgrade moduli. There are methods to determine the depth to a stiff layer in a pavement structure, but since the subgrade was regarded to of less interest in the present test this was not done. After the HVS test, the subbase and subgrade seem to be virtually unaffected by the HVS load for all test cells.

Linear Elastic Evaluation of the Base Layer

In Table 5.9 the average backcalculated elastic modulus evaluated from the center line, is presented for Test Cells #1 to #4 before and after the HVS test. The backcalculated unbound base layer modulus for Test Cells #1 to #4 is presented in Figure 5.14 (results along the center line of the HVS test and in Figure 5.15 (1.5 m beside the center line i.e. outside the wheel load area).

Table 5.9. Average backcalculated elastic modulus of the stations in the centre line for the unbound base layer before and after the HVS test.

Test Cell	<i>E</i> -modulus before the HVS test [MPa]	<i>E</i> -modulus after the HVS test [MPa]
1	56	133
2	48	119
3	67	129
4	74	153

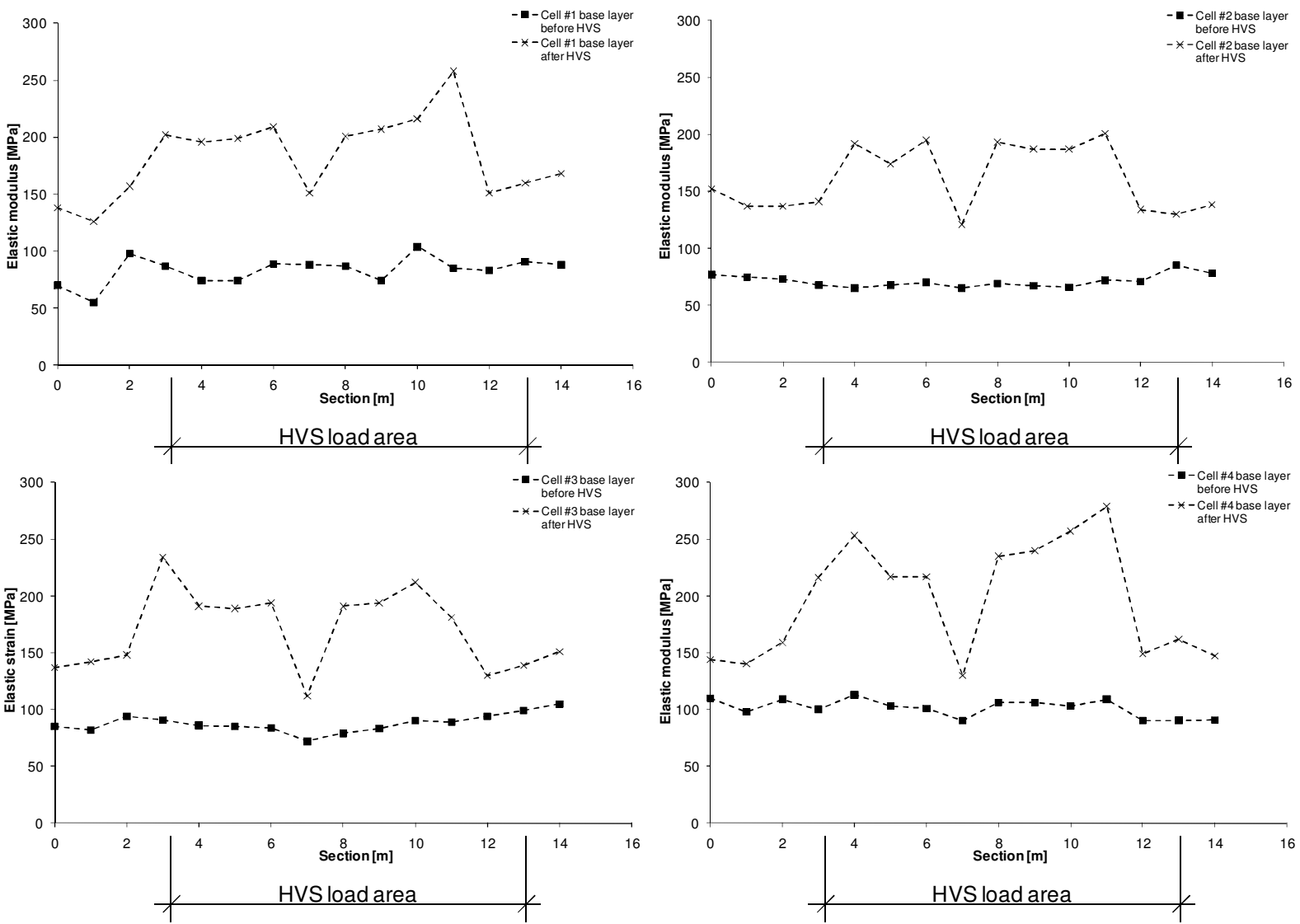


Figure 5.14. Backcalculated elastic modulus for the different sections of the unbound base layer of Test Cells #1 to #4 in the center line before and after the HVS Test.

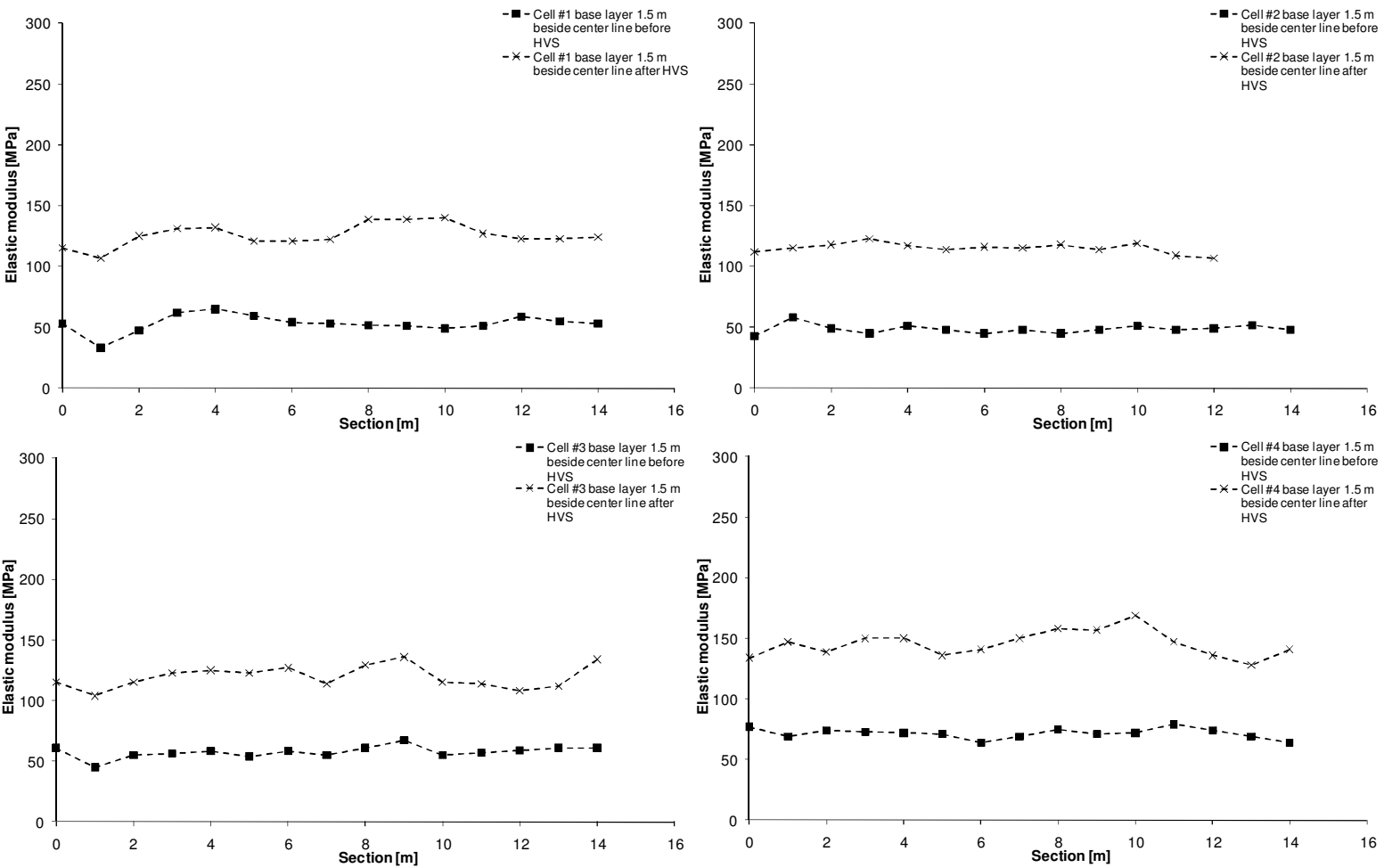


Figure 5.15. Backcalculated elastic modulus E for the different sections 1.5 m beside the center line of the base layer (i.e. outside the wheel load area) of Test Cells #1 to #4 before and after the HVS Test.

The unbound base layer modulus is quite constant along the sections but is unexpectedly low before the HVS test. However, the modulus of the base layer increases after the HVS test for all test cells and especially in the wheel track of the HVS loading. The modulus 1.5 m beside the center line is slightly lower compared to the center line. It was a ditch close to the line, 1.5 m beside the center line. It can be seen that the modulus increases after the HVS 1.5 m beside the center line. The elastic modulus thus increases regardless of whether the area has been subjected to a wheel load or not, but, as mentioned before, the increase is more significant in the wheel load area.

The base layer modulus varies between the test cells and the stiffness of the unbound base layer of Test Cell #4 is higher compared to the other test cells. The construction, including the compaction, was the same and the subgrade consisted of the same clay. The only intended differences were the source of the material in the unbound base layer. Any difference in post compaction or the permanent deformation behavior in the unbound layers in general might thus be affected by a difference in material strength properties (see Table 4.6). If the effect of compaction on the post compaction should be studied properly, the design of the test should be different. Then different compaction should be used on test cells with same design and materials.

The results of the HVS are presented in Ekdahl et al. (2004a). The material with the smallest mica content (Material 3) had the smallest permanent deformation although the difference was too small to draw any clear conclusion.

Stress hardening evaluation of the base layer

The stress hardening behavior was evaluated from FWD test results by performing backcalculation of each load level as described in Section 3, by using all three load levels to evaluate one stress hardening parameter per station. The influence of the increased or decreased load level of the stress hardening behavior could therefore not be evaluated as in the triaxial test. The FWD test was performed with two drop sequences for each station, each of them containing the three load levels 30, 50 and 65 kN. This was done for all FWD stations, both inside and outside the wheel track of the HVS. As mentioned earlier, the loaded area of the HVS test extends from Section 4 to Section 10 with turning points in Section 3 and 11 (see Figure 5.2).

Figure 5.16 shows details of the results before and after the HVS test from section 6, Test Cell #1 within the HVS wheel load area.

5. Identification of post compaction using full scale tests

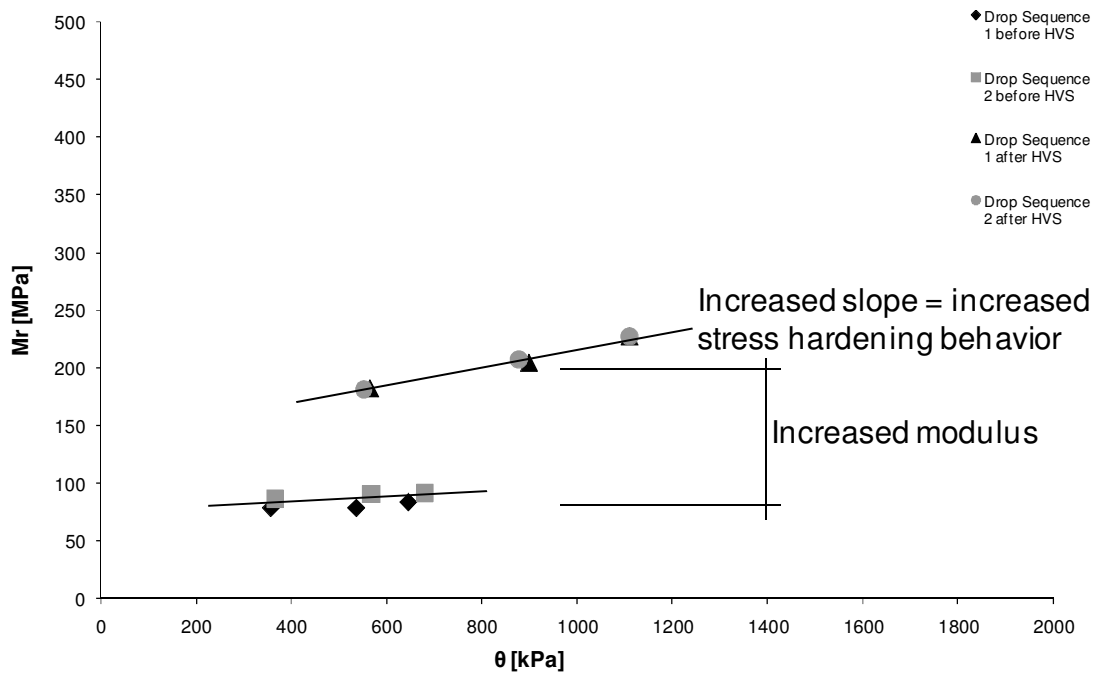


Figure 5.16. Backcalculated resilient modulus M_r and bulkstresses in the unbound base layer at different load levels of the FWD. Test Cell #1, section 6 before and after the HVS Test.

Here, the modulus of elasticity is presented as the resilient modulus M_r . M_r is plotted against the bulk stress θ . The bulk stress represents the stress level in the middle of the unbound base layer and is evaluated by using an assumed value of the Poisson's ratio of 0.35 for estimation of the horizontal stress. The backcalculated resilient modulus, M_r seems to be somewhat independent of the bulk stress θ before the HVS test (small slope of the $\theta - M_r$ relationship). The second drop per load level obviously results in a somewhat higher stiffness. After the HVS test, the resilient modulus, M_r of the unbound base layer seems to be clearly dependent on the bulk stress level (higher slope of the $\theta - M_r$ relationship), i.e. higher with stress hardening. There is only a small difference between the first and second drop from the FWD test at the same load level indicating that the unbound base layer is compacted to a level where the FWD equipment cannot compact it any further. However, the most significant is that the elastic modulus of the layer has increased after the HVS test, which could also be seen in Figure 5.13. The increased elastic modulus also results in an increased stress level. The higher elastic modulus increases the load spreading capacity of the layer, which in turn results in a higher stress level within this layer. The stress hardening behavior of the unbound base layer measured using the FWD test can

be evaluated by using the $k-\theta$ model in the same way as for the laboratory triaxial test results. An example is shown for Test Cell #1, section 6 after the HVS test, the second drop sequence (see Figure 5.17).

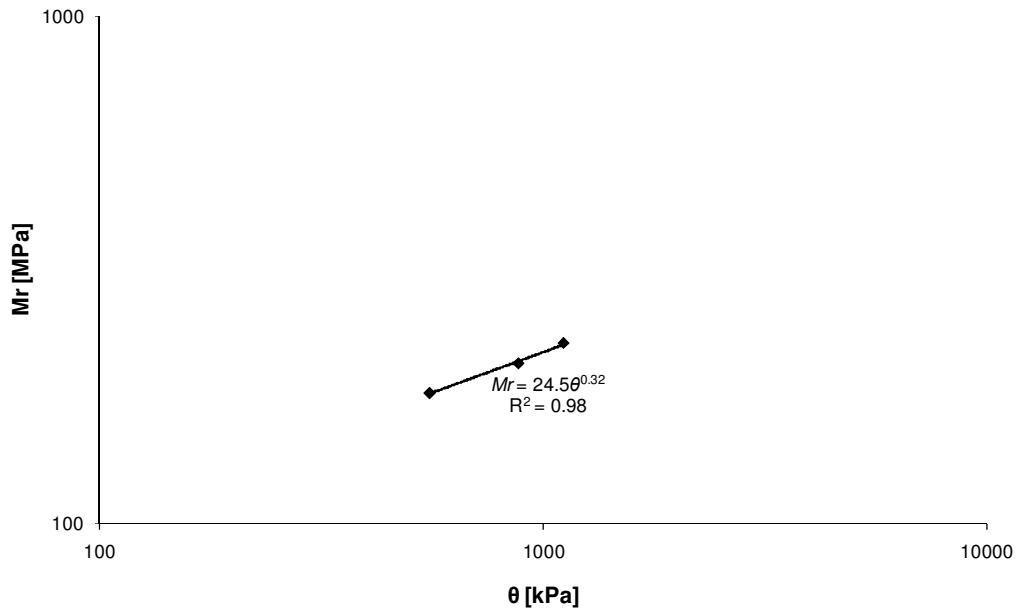


Figure 5.17. Regression analysis with the $k - \theta$ model. The second drop per load level is shown for FWD test results of Test Cell #1, section 6 before the HVS test.

Regression analyses were performed for all drop sequences for all sections within the wheel load area and outside for all test cells before and after the HVS test by using the $k-\theta$ model in the same way as described in Figure 5.17. The stress hardening behavior is represented by the regression parameters k_1 and k_2 . In Figure 5.18 and Figure 5.19 the k_1 and k_2 – values respectively for the different sections of Test Cells #1 to #4 is presented.

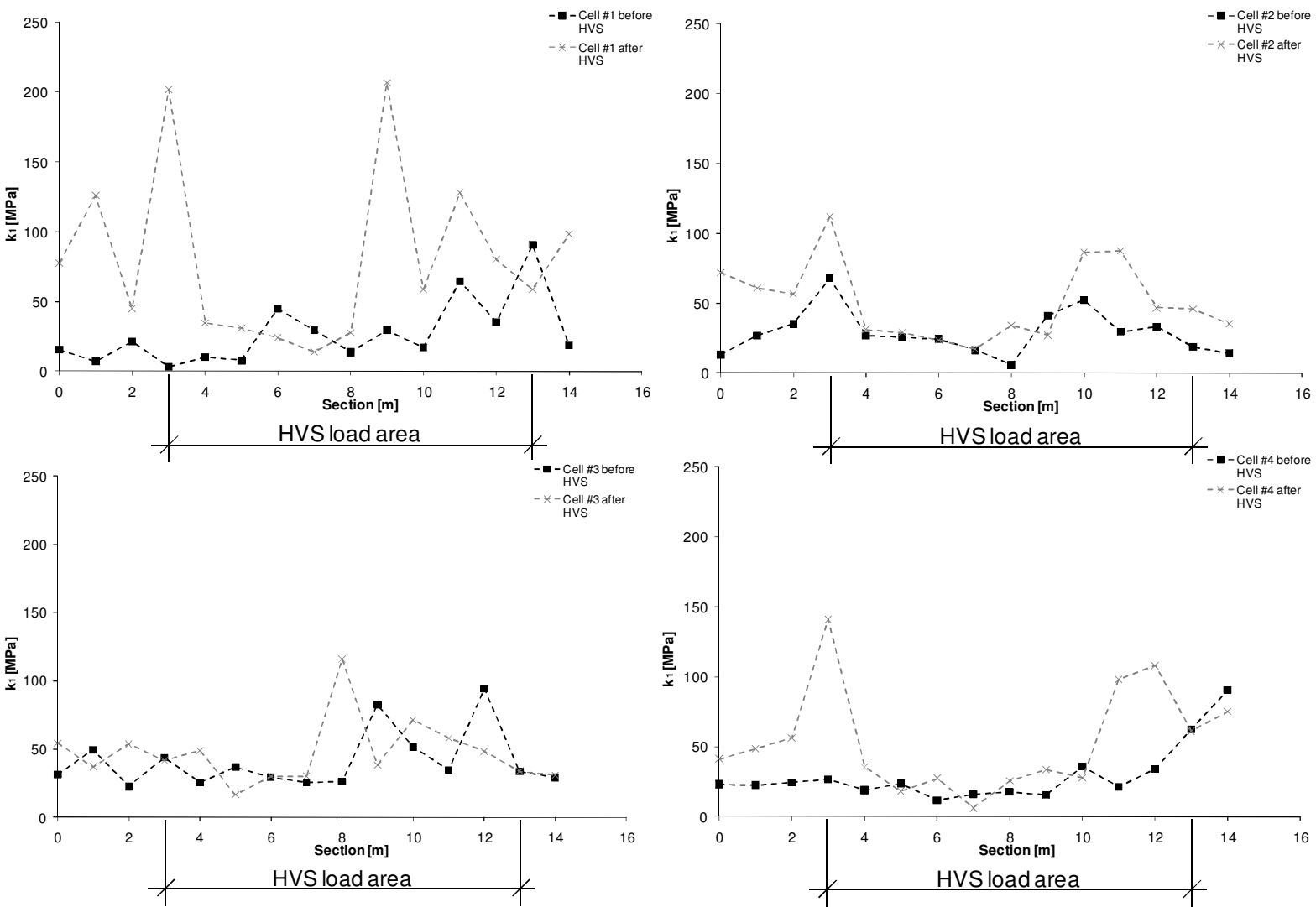


Figure 5.18. The regression parameter k_1 of the $k - \theta$ model evaluated by means of backcalculation of FWD test results in the center line of Cell #1 to #4 performed before and after the HVS test.

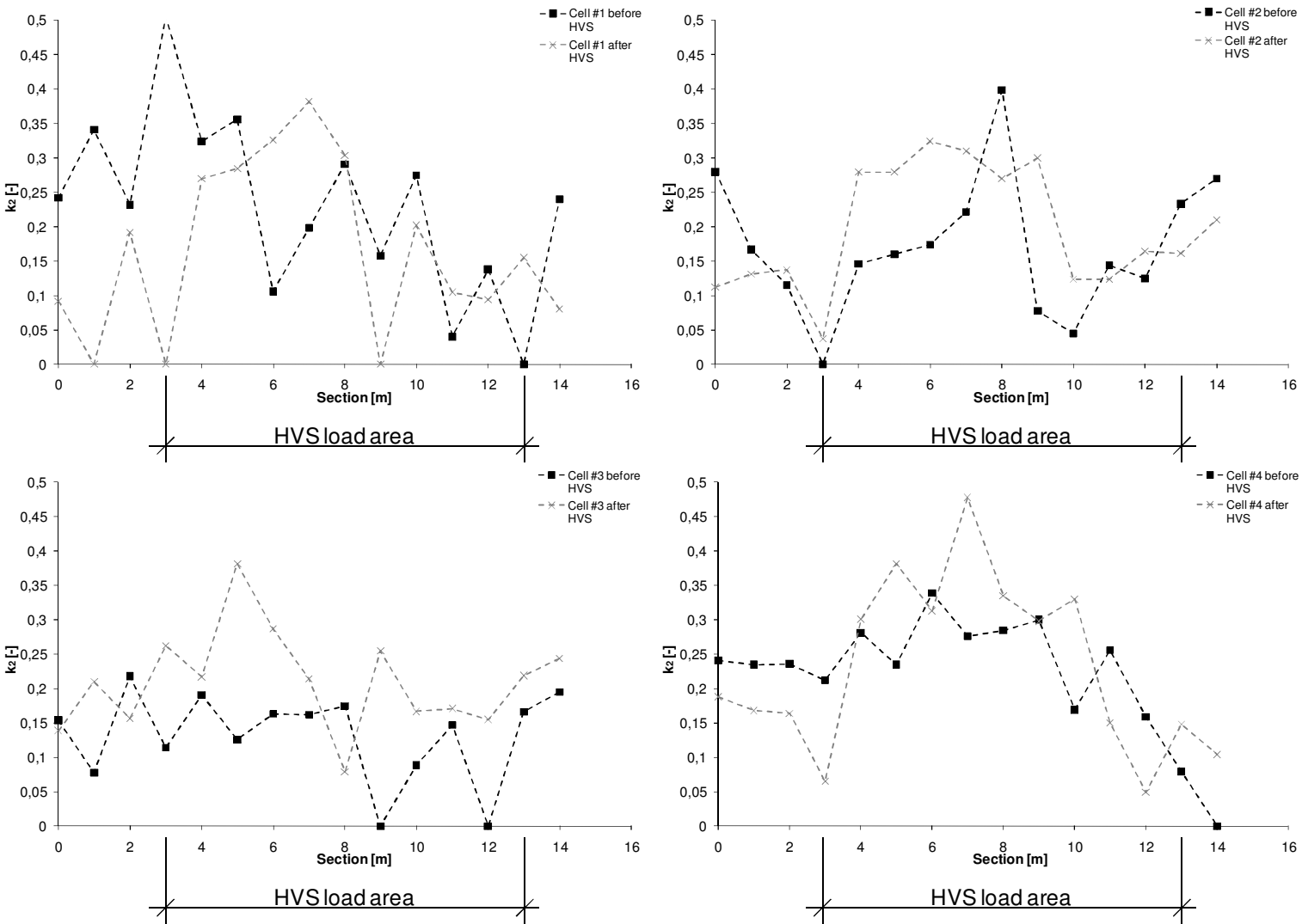


Figure 5.19. The regression parameter k_2 of the $k - \theta$ model evaluated by means of backcalculation of FWD test results in the center line of Cell #1 to #4 performed before and after the HVS test.

5. Identification of post compaction using full scale tests

As can be seen there are some indications that the stress hardening behavior parameter k_1 do not change so much in the wheel track but increases outside the wheel track after the HVS test. In same time there are some indications that the stress hardening behavior parameter k_2 is higher in the wheel track after the HVS test (especially for Test Cells #2 and #4). However, this is not as clear as for Test Cell #1, section 6 described in Figure 5.16.

6 ANALYSIS

6.1 Introduction

The analysis process is summarized in Figure 6.1.

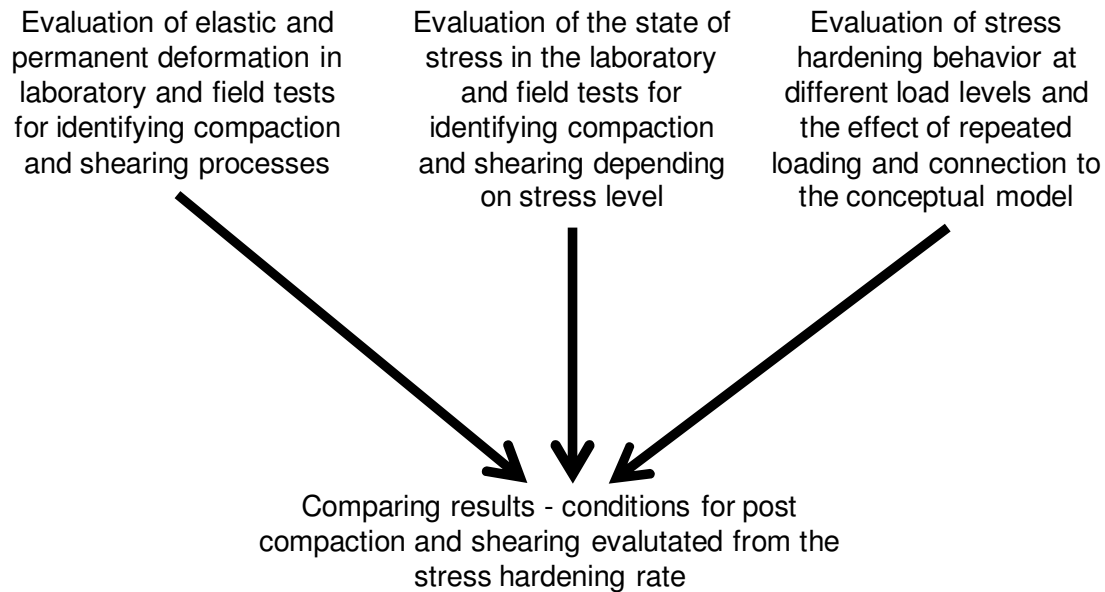


Figure 6.1. Description of the analysis process in the present thesis.

Firstly, the compaction and shearing processes are identified by means of an evaluation of the state of stress and an evaluation of the elastic and permanent deformation behavior. The relationship between elastic and permanent strain will be analyzed for both the laboratory and field tests in order to identify post compaction and shearing processes. The permanent strain is also compared to existing models. Analyses of the state of stress for the laboratory and field test will give an indication of whether there is a risk of shearing or not for the different load levels in the triaxial test, HVS test and FWD test.

By comparing the results from these methods, it will be possible to see which load levels cause compaction or shearing. Parallel to this, the stress hardening behavior is evaluated at different load levels. The effect of repeated loading on the stress hardening behavior will also be analyzed. The stress hardening behavior is then compared to the elastic and permanent deformation behavior

and the state of stress in order to see if it can be used to evaluate the conditions for compaction and shearing.

6.2 Relationship between permanent and elastic deformation and comparison with permanent strain models

Relationship between permanent and elastic deformation

A relationship between stress hardening behavior and post compaction requires a relationship between elastic and permanent deformation. According to Lekarp (1999) Veverka (1979) found a direct relationship between permanent and elastic strain and he developed a model where higher elastic strain renders a higher permanent strain. Lekarp stated that other researchers have not found these relationships.

From the laboratory triaxial tests presented here, it was possible to evaluate both elastic and permanent deformation at eight different load levels. In Figure 4.3 it is possible to see that the elastic deformation seems to decrease for some load steps for every load repetition. According to Figure 4.1 and Figure 4.2 the permanent deformation rate seems to decrease every load repetition for all load steps.

To facilitate comparison, the permanent deformation rate for every loading is calculated (permanent deformation/load repetition) and plotted together with the elastic deformation for material 1 and water content 80% of optimum (test b). The result for all 224 000 loading cycles is presented in Figure 6.2. The first 4 000 loading cycles in Figure 6.3, loading cycle 4 000 to 204 000 in Figure 6.4 and finally the last 20 000 loading cycles in Figure 6.5. The same figures for materials 1 to 4 with water content 80% are presented in Appendix C, Figure C1 to Figure C12. In Appendix C Figure C13 to Figure C18, the elastic deformation and permanent deformation rate for all tests are presented.

6. Analysis

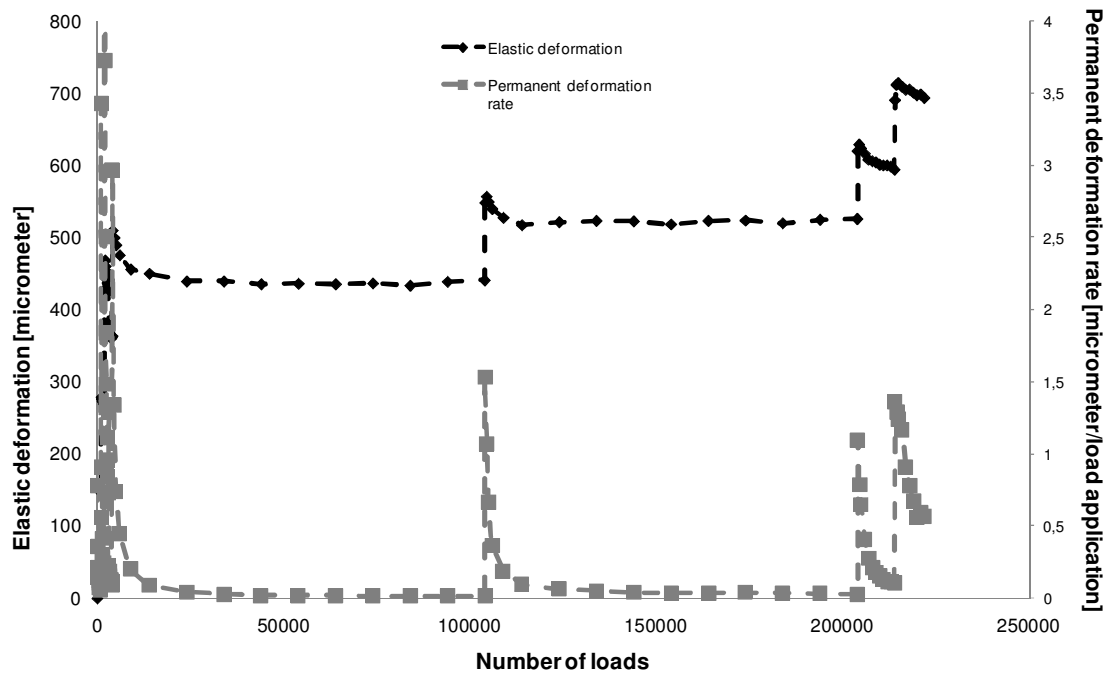


Figure 6.2. Comparison of the elastic deformation and permanent deformation rate for all load cycles of Material 1, water content 80% of optimum.

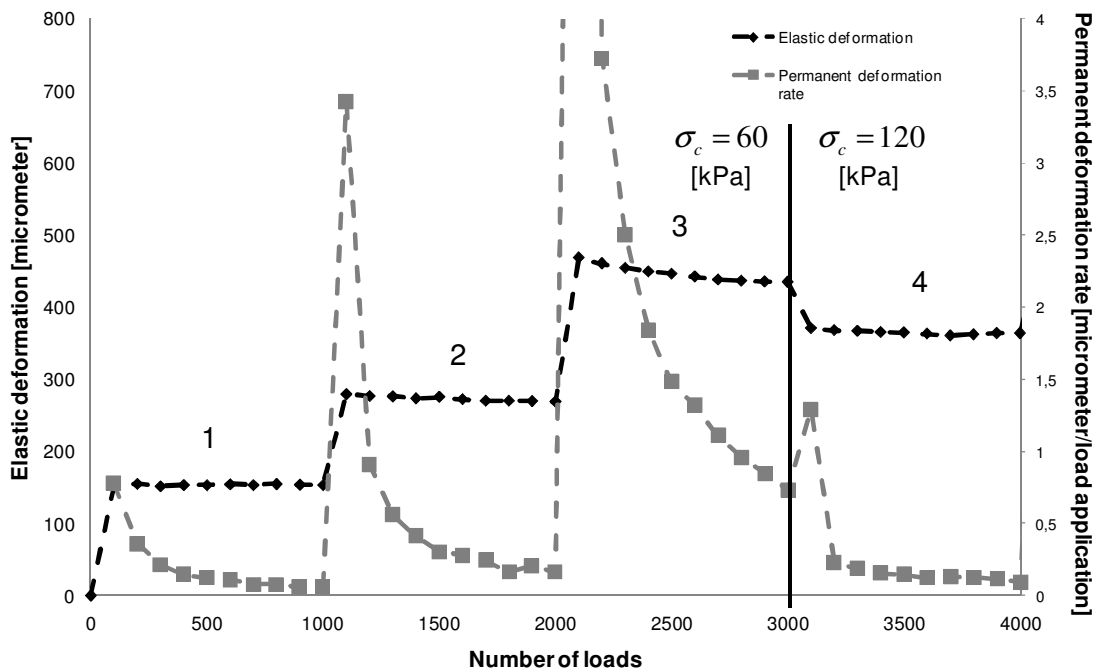


Figure 6.3. Comparison of the elastic deformation and permanent deformation rate for load cycles 0 to 4000 (load steps 1 to 4) of Material 1, water content 80% of optimum.

6. Analysis

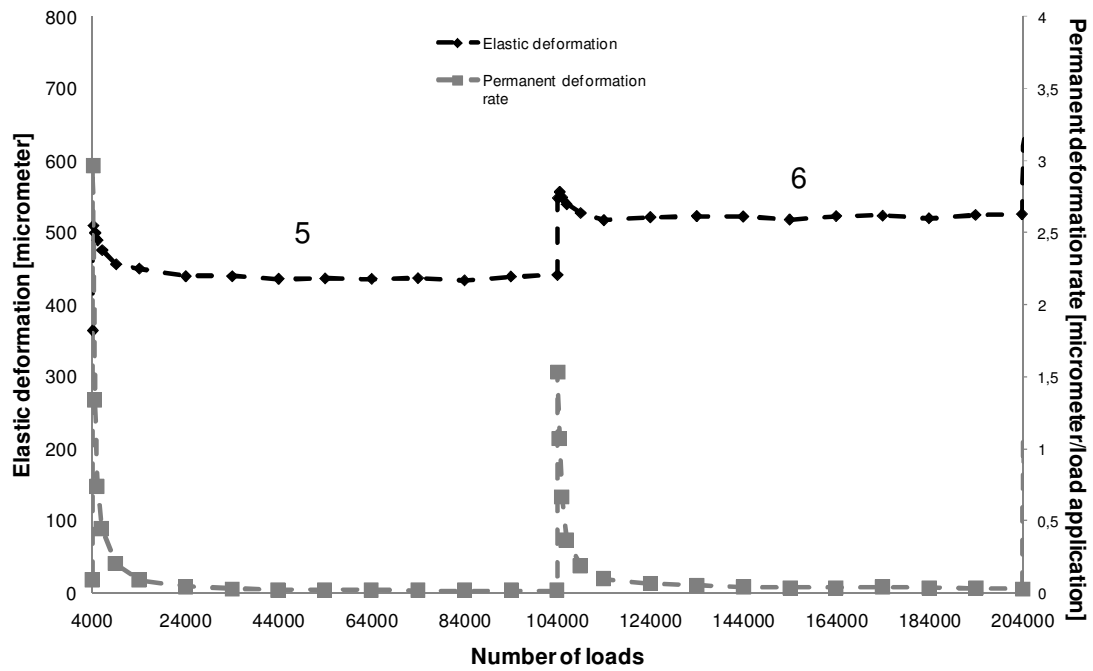


Figure 6.4. Comparison between the elastic deformation and permanent deformation rate for for load cycles 4000 to 204000 (load steps 5 and 6) of Material 1, water content 80% of optimum.

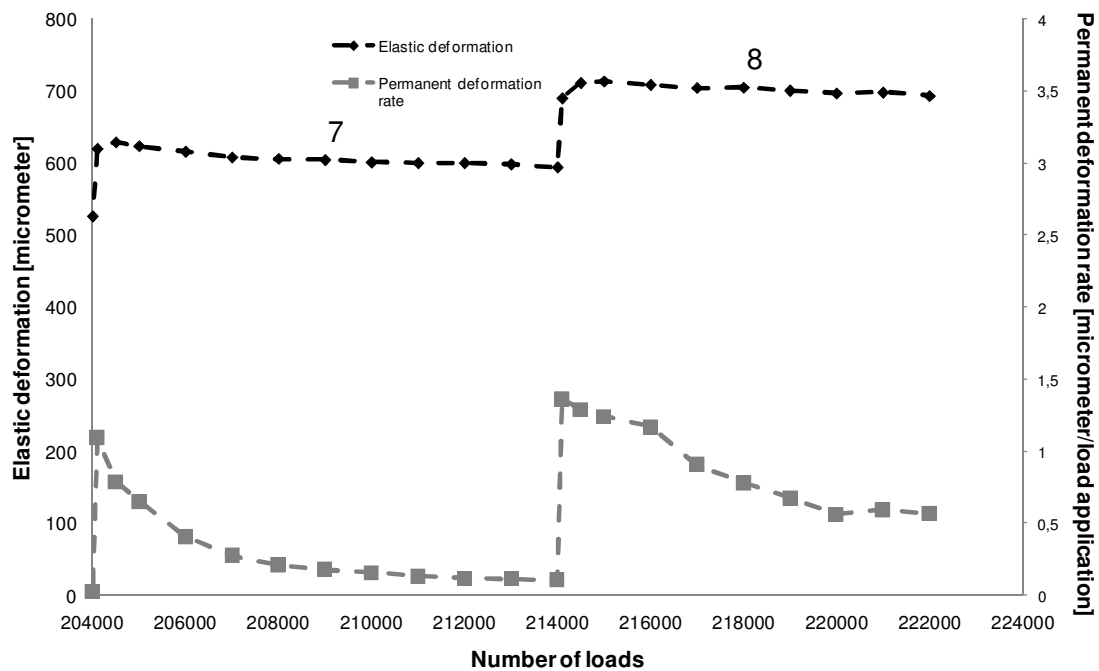


Figure 6.5. Comparison of the elastic deformation rate and permanent deformation rate for load cycles 204000 to 224000 (load steps 7 and 8) of Material 1, water content 80% of optimum.

For the first 4 000 loading cycles one can see that the elastic deformation is almost constant or decreases slightly for all four load steps but that the permanent deformation rate decreases rapidly towards zero, except for load step 3. The increase in the confining (horizontal) stress can be seen both as a decrease in the elastic strain and as a reduction in the permanent strain rate. For load steps 5 and 6 (load cycles 4 000 to 204 000) the pattern for elastic deformation becomes similar to the permanent deformation rate. The elastic deformation decreases rapidly as well as the permanent deformation rate and both reach a more or less constant level at the same load cycle (towards zero for the permanent deformation rate). The permanent deformation rate for load step 6 may show the same rate in the last load repetition. For the last two load steps the elastic deformation decreases slowly while the permanent deformation rate decreases rapidly to a constant value but not towards zero. The permanent deformation rate in particular indicates that the deformation behavior is similar to behavior B according to Werkmeister et al (2004), see Figure 2.4. This behavior is said to be unstable indicating that there is shearing involved and not just post compaction for the last two load steps. No increase in the permanent deformation rate is observed, which is why deformation behavior C can be excluded.

Comparison of the permanent strain rate and the elastic strain could also be made for the HVS test. From the results of the field test it was found that initial post compaction could be observed in the unbound base layer for all test cells, see Figure 5.9 and Figure 5.10. The deformation behavior after post compaction of the unbound materials in the test cells was between material behavior “A” and “B”. In Figure 6.6 the deformation measurements of the base layer of Cell #1 are presented as elastic strain and permanent strain rate (obtained from the EMU-coil measurements). The same is presented for Cells #2 to #4 in Appendix C, Figure C19 to Figure C21.

6. Analysis

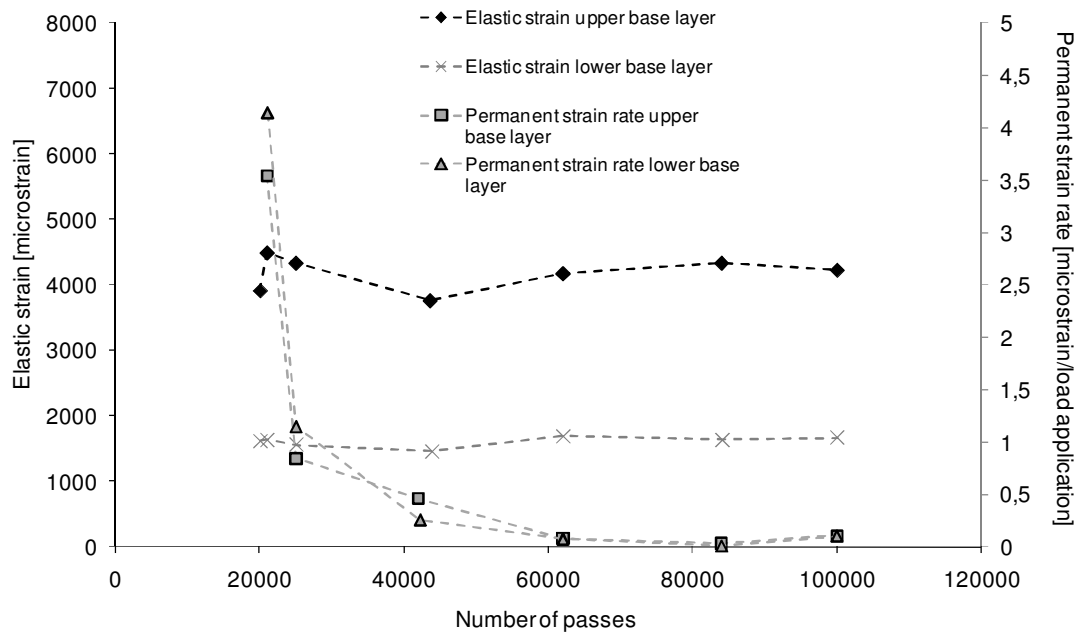


Figure 6.6. The relationship between the elastic deformation and permanent deformation rate in the unbound base layer of Test Cell #1 obtained from the EMU-coil measurements.

Overall there is no tendency towards decreasing elastic strain. In Test Cell #1 it does not seem that the permanent strain rate decreases to zero and for test cells #3 and #4 the permanent strain rate increases at the end of the test. For all test cells the behavior is similar to that of load step 5 in the triaxial test i.e. similar to Behavior A according to Werkmeister et al (2004), see Figure 2.4. This may indicate compaction for all test cells.

Summary of the relationship between permanent and elastic deformation

In summary, in the laboratory triaxial test load steps 5 and 6 the permanent deformation rate and the elastic deformation show the same pattern for an increasing number of load repetitions. For load steps 1 to 4, the elastic deformation decreases slightly although the permanent strain rate shows a clear decrease. For load steps 7 and 8 the elastic deformation increases slightly during the first load repetitions in each load step and then decreases while the permanent deformation rate clearly decreases. The results of the HVS test shows similar patterns regarding the permanent strain rate as for load steps 6 and 7. If the permanent deformation or strain rate seems to reach zero or at least approaches it, this means compaction while the opposite indicates shearing.

Based on the permanent strain rate test it seems that shearing occurs for load steps 3, 7 and 8 in the triaxial test as well as for the HVS test (3 of 4 test cells) i.e. Behavior B according to Werkmeister et al. (2004). Note that the confining pressure in the triaxial test increases from load step 3 to load step 4.

Comparison with permanent strain models

In the literature two types of equations describe the relationship between permanent strain and number of load repetitions, Equation 2.8 (lin-log relationship) and Equation 2.9 (log-log relationship). These equations were compared to deformation behaviors representing assumed compaction behavior (load step 2 in the laboratory triaxial test) and assumed shearing behavior (load step 8). The HVS test (passing 20000-100000) represents both shearing and compaction behavior as it was difficult to identify the deformation behavior.

In summary it can be seen that the lin – log relationships (Equation 2.8) show the best relationships (straight line) for permanent deformation obtained from assumed compaction behavior, see Figure 6.7 (load step 2 in the triaxial test). For assumed shearing behavior the log – log relationship (Equation 2.9) shows the best relationship, see Figure 6.8 (load step 8 of the triaxial test). For the HVS test the log – log relationship (Equation 2.9) showed the best relationship indicating shearing behavior, see Figure 6.9.

In Appendix D Figure D1 to Figure D15 the relationships of in triaxial test load steps 2, 5 (assumed compaction behavior) and 8 and the HVS test, the upper and lower base layers are presented on lin – lin, lin – log and log – log scales.

6. Analysis

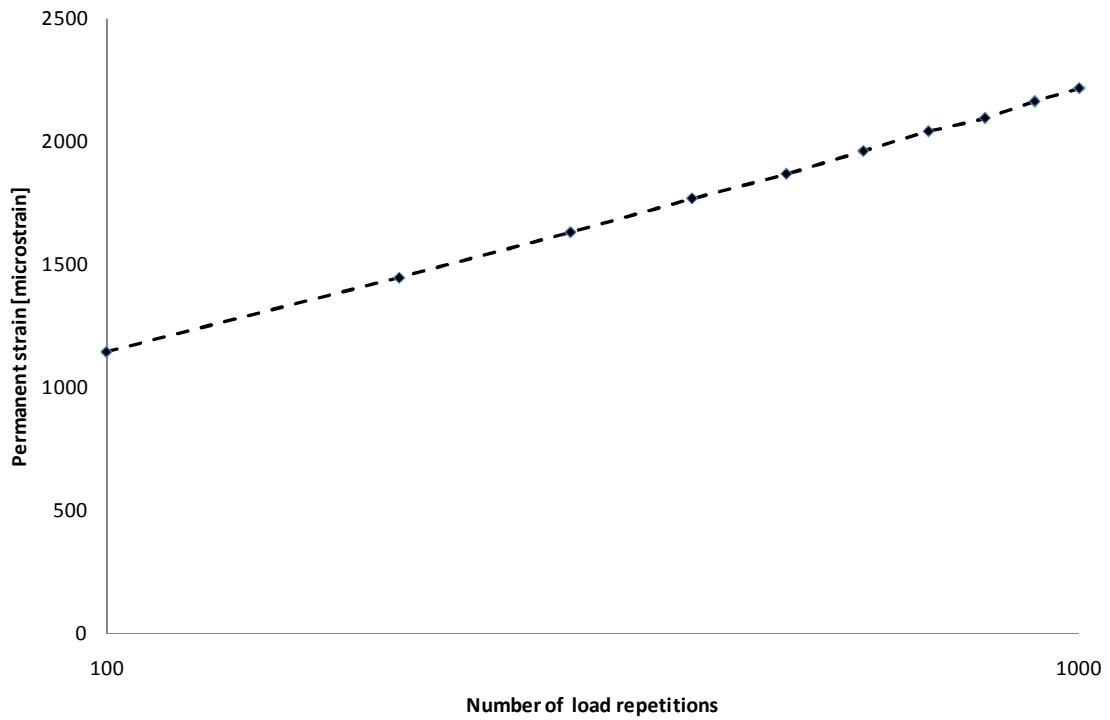


Figure 6.7. Material 1 80% water content of optimum load step 2 (load repetition 1000 - 2000), lin – log relationship.

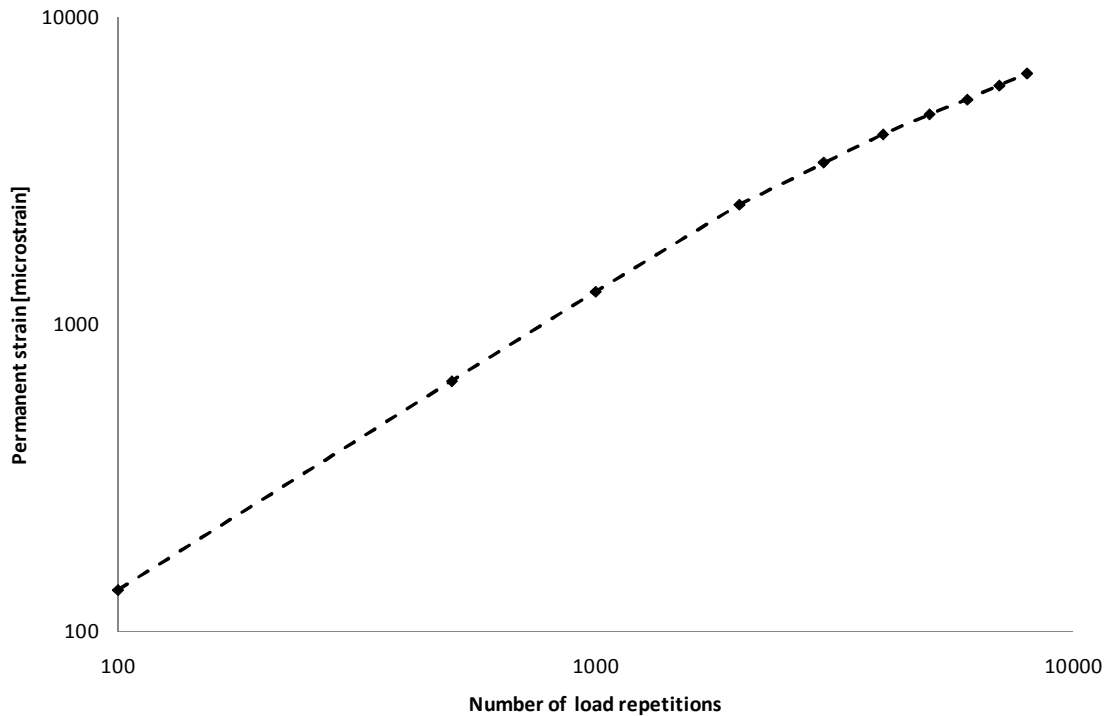


Figure 6.8. Material 1 80% water content of optimum load step 8 (load repetition 214000 - 224000), log – log relationship.

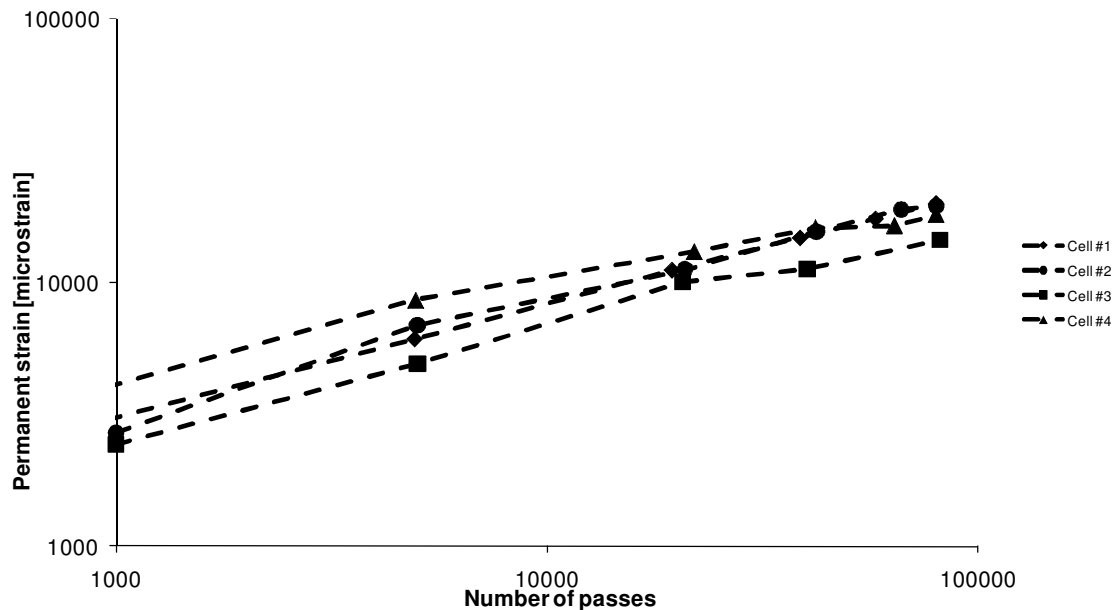


Figure 6.9. HVS test upper base layer passing 20000 – 100000, log – log relationship.

6.3 State of stress

To clarify the conditions for post compaction and shearing a study of the state of stress is done. An example of this kind of analysis is given by Bonaquist & Witzcak (1997) (see Chapter 2 above). The permanent deformation behavior in unbound granular material is dependent on the state of stress. At low deviatoric stress levels, the deformation is more or less elastic and regardless of permanent deformation occurs it is caused by decreased volume, i.e. compaction. Stress states closer to failure, i.e. at high deviatoric stress, result in larger permanent deformation caused by shearing, resulting in a dilative behavior. This also affects the resilient behavior. A determination of state of stress is therefore performed by using the theory described by Bonaquist & Witzcak (1997).

Evaluation of the failure envelope

Bonaquist & Witzcak (1997) uses the Drucker-Prager failure criterion, Equation 2.16. The failure envelope must be determined from static triaxial strength tests. No such tests have been performed on the unbound material used. Consequently, assumed strength parameters must be used and the failure envelope can just be used for discussion purposes. Ekdahl et al. (2004a), describe a project where invited researchers performed predictions of the performance of the unbound material used in triaxial tests. Strength parameters used by Hornyh in Ekdahl et

al. (2004a) are thus used. These strength parameters are based on the $p - q$ stress space (Equation 2.13) and the values here were $S = 20$ MPa and $M = 2.55$. See also Figure 2.9

In order to make an evaluation of the state of stress according to Bonaquist & Witzcak (1997), the strength parameters S and M must be translated into the corresponding Drucker-Prager strength parameters (Equation 2.16) k and $\sqrt{\gamma}$ see also Figure 2.10. The parameter k can be calculated from S as in Equation 6.1, see Appendix E.

$$k = \frac{S}{\sqrt{3}} \quad (6.1)$$

For $S = 20$ MPa, k becomes 11 kPa.

The slope of the failure envelope of Equation 2.16 $\sqrt{\gamma}$ can be calculated from M as Equation 6.2, see Appendix E.

$$\sqrt{\gamma} = \frac{M}{3\sqrt{3}} \quad (6.2)$$

For $M = 2.55$, $\sqrt{\gamma}$ becomes 0.49

Hence, the failure envelope is given using Equation 6.3 below.

$$\sqrt{J_2} = 0.49I_1 + 11.5 \quad (6.3)$$

It is also possible to present the failure envelope in $\tau - \sigma_n$ stress space (Mohr-Coulomb failure criterion). ϕ can be related to M as in Equation 6.4 and c to S as in Equation 6.5 (compression), see Appendix E.

$$\phi = \arcsin \frac{3M}{6 + M} \quad (6.4)$$

$$c = \frac{S \tan \phi (3 - \sin \phi)}{6 \sin \phi} \quad (6.5)$$

For $M = 2.55$, ϕ becomes 63° and for $S = 20$ MPa c becomes 19 kPa.

Evaluation of the phase change envelope

The phase change envelope is described using Equation 2.17, where parameter n describes the volume change (compaction or shearing). To evaluate this parameter, triaxial tests with variable confining pressure must be performed. No such tests results were available for the unbound material used in the triaxial test. Instead the value of parameter n is taken from Bonaquist & Witzcak (1997). They determined the parameter n by using a statistical optimizing process of triaxial test results with variable confining pressure with different stress paths. This gave $n = 3.05$ for a crushed gneiss, which is assumed to be similar to the crushed rock material used in the tests described. The phase change envelope can thus just be used simply for discussion purposes. The n value is probably affected by the compaction effort and hence, also by post compaction. The phase change envelope for the value of $n = 3.05$ is given using Equation 6.6.

$$\sqrt{J} = \left[\frac{n-2}{n} \right]^{\frac{1}{2}} \sqrt{\gamma} I_1 = \left[\frac{3.05-2}{3.05} \right]^{\frac{1}{2}} 0.49 I_1 = 0.59 \cdot 0.49 I_1 = 0.29 I_1 \quad (6.6)$$

Similar to the failure envelope, this assumed phase change envelope can be used simply for discussion purpose. A corresponding ϕ is calculated by using Equation 6.2 and Equation 6.4 and becomes 37° .

An empirical expression described by Hansbo (1975), see Appendix F, shows that the actual material should have $\phi = 44^\circ$. By using Equation 6.4 M is calculated to be 1.81. From Equation 6.2 the slope of this “phase change envelope” is calculated to be 0.35. This corresponds to an n value of 4.08 (by using Equation 6.6). This is presented in Equation 6.7

$$\sqrt{J} = \left[\frac{n-2}{n} \right]^{\frac{1}{2}} \sqrt{\gamma} I_1 = \left[\frac{4.08-2}{4.08} \right]^{\frac{1}{2}} 0.49 I_1 = 0.71 \cdot 0.49 I_1 = 0.35 I_1 \quad (6.7)$$

The phase change envelope of Equation 6.6 and Equation 6.7 together with the failure envelope of Equation 6.3 is presented in Figure 6.10.

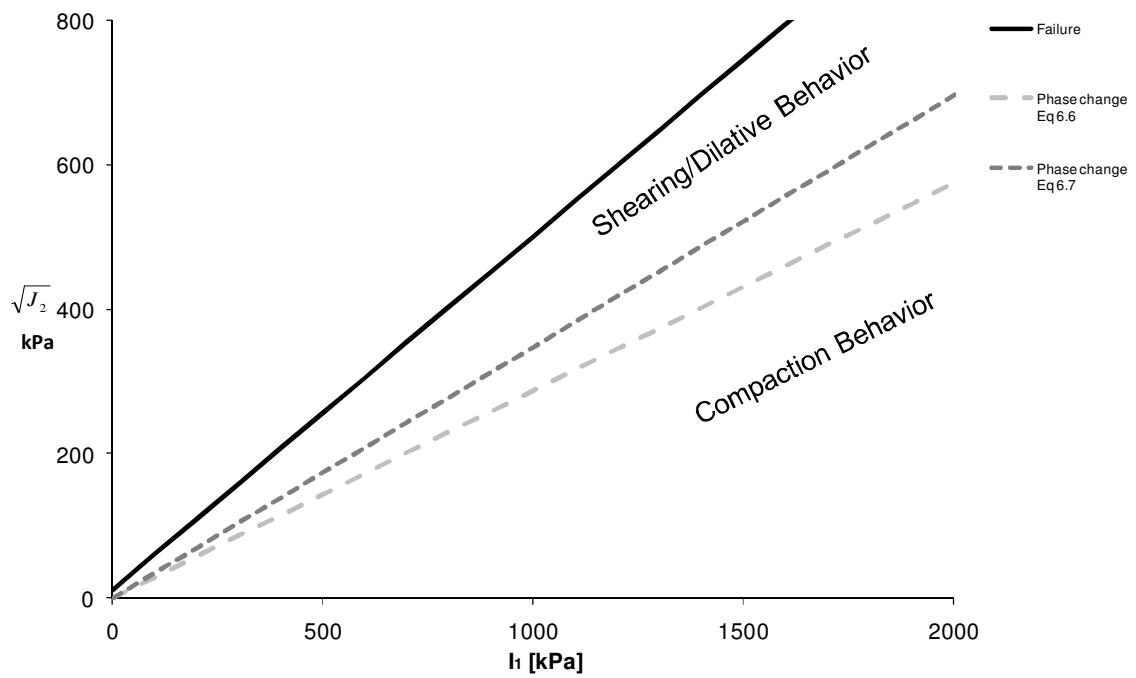


Figure 6.10 Failure envelope and phase change envelope used for evaluating the state of stress.

State of stress in the triaxial test

The stresses of the eight load steps were calculated to be fitted in the $I_1 - \sqrt{J_2}$ stress space. This was done in order to indicate whether the stress levels of the eight load steps may cause compaction or shearing. The deviatoric stress q is related to \sqrt{J} using Equation 6.8, rewritten from Equation (2.2).

$$\sqrt{J_2} = \frac{q}{\sqrt{3}} \quad (6.8)$$

The bulk stress θ is related to I_1 using Equation 6.9 rewritten from Equation (2.1).

$$I_1 = \theta \quad (6.9)$$

The result is presented in Table 6.1.

Table 6.1. The calculated I_1 and $\sqrt{J_2}$ for the eight load steps of the triaxial test.

Load step	I_1 [kPa]	$\sqrt{J_2}$ [kPa]	$\Delta\sigma_v$	σ_h
1	300	23	160	60
2	400	81	260	60
3	600	196	460	60
4	780	162	520	120
5	980	277	720	120
6	1180	393	920	120
7	1380	508	1120	120
8	1580	624	1320	120

The eight load steps were compared to the results of the permanent deformation behavior in Chapter 6.2 in order to create a phase change envelope by assessment. Load steps 3, 7 and 8 indicated shearing behavior, which is why the phase change envelope may be close to these states of stress. In Figure 6.11 an assessment of the phase change envelope is shown together with the failure envelope and phase change envelopes of Equation 6.6 and Equation 6.7 as already presented in Figure 6.10.

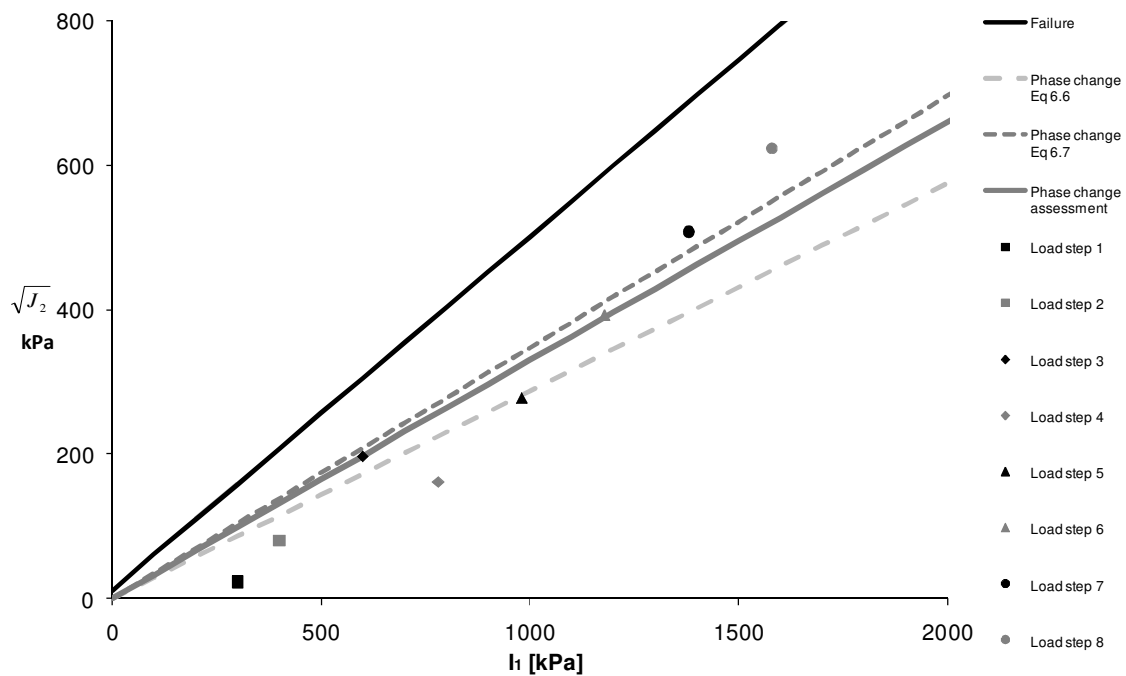


Figure 6.11. The state of stress for the eight load steps used in the triaxial test.

As can be seen, the stress levels of loading steps 1, 2, 4 and 5 are within the zone of compaction behavior and 3, 6, 7 and 8 are within the zone of shearing/dilative behavior according to the phase change envelope of Equation (6.6). For the phase change envelope of Equation (6.7) only stresses from load steps 7 and 8 are within the shearing/dilative zone. The phase change envelope from assessment has a slope of " $\sqrt{\gamma}$ " = 0.33, which corresponds to $M = 1.71$ and $\phi = 42^\circ$. This is very close to the empirical phase change envelope (Equation 6.7). The empirical phase change envelope is built on input from the actual material properties, which is why it is reasonable that the one from the assessment is close to it. The phase change envelope from the assessment considers both the shearing behavior in load step 3 and load steps 7 and 8. Thus, the phase change envelope from the assessment will be used further.

State of stress in HVS and FWD test

The state of stress of a HVS load was analyzed in order to indicate whether compaction or shearing caused the permanent strain in the unbound base during the HVS test. The FWD load is also analyzed in the same way. As an aid a forward calculation program for analyzing a multilayer system is used.

In a forward calculation program, stresses at different depths in a pavement structure can be calculated by using input data such as the modulus of elasticity E or the parameter k_1 and k_2 from the $k - \theta$ model. The input data can be evaluated using backcalculating FWD data.

The forward calculation of stress and strain was obtained in the pavement structure by using the software Nelapav 4 developed by Irwin (2001). This software uses the multilayer elastic theory and 15 different constitutive models can be evaluated. One of them is linear elastic, stress independent and the other 14 are stress dependent regression models. As input data, the material properties such as elastic modulus, Poisson's ratio, non-linear material parameters, density and layer thickness are needed. The program reports stresses and strain due to load and overburden separately. The stresses and strains are calculated at specific points determined when creating the input data file. Irwin (2001) describes a test where Nelapav 4 was compared to a Finite Element Method program and the difference in displacement was within one percent.

In the program the loaded area is assumed to be circular. Using the very same HVS equipment as in the present study, Korkiala-Tanttu & Laksonen (2004) performed a Finite Element Method calculation on the data from a field test in

Finland. They simulated a load distributed over a circular area with a radius of 200 mm for the dual wheels. In Huvstig (2003) the relationship between contact pressure between the road surface and tire for different wheel loads is presented. For a tire pressure of 1000 kPa, the contact pressure on the road surface was just above 700 kPa for a wheel load of 80 kN. This requires a load area with a radius of 190 mm, which is what is used. For the FWD load simulation the radius is 150 mm as is the size of the load plate.

The input data used in the forward calculation are evaluated from backcalculated FWD results for the subgrade, subbase and the unbound base layer. For the asphalt layer it is difficult to obtain reliable results from backcalculation when the layer is thin. Therefore, an assumed value was used. The linear elastic material model is used for subgrade, subbase and asphalt layer. For the unbound base layer both the linear elastic model and the stress dependent $k - \theta$ model are used. In Table 6.2 the input data are summarized. The calculated stress distribution was compared to the measured values, obtained from the pressure cell recordings of the response measurements, see Figure 5.2. The result is presented in Figure 6.12.

Table 6.2. Parameters used for the calculations in Nelapav 4 for evaluation of the stress distribution.

Model parameter	Subgrade	Subbase	Unbound base	Asphalt
Linear model E [MPa]	100	125	174	6000
$k - \theta$ model FWD k_1 [MPa]			49	
$k - \theta$ model FWD k_2 [-]			0.24	

6. Analysis

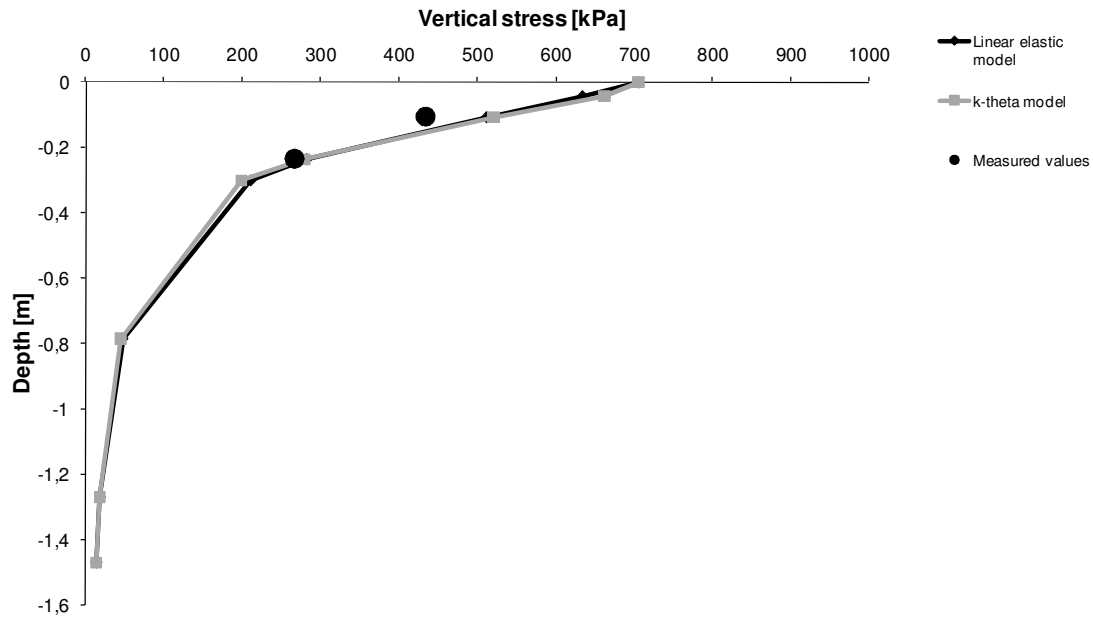


Figure 6.12. Results from calculation of vertical stress distribution by depth below the center of the load. Different models and input data are used and the results are compared with measured values calculated using the instruments presented in Figure 5.2.

As can be seen, the stress does not seem to be influenced significantly by the model used. There is good agreement with the measured values, especially for the lower base layer. In the upper base layer, the measured stress values are somewhat lower than the calculated. The measured values are presented for recordings when the dual wheel is in lateral position 0 and the gap between the wheels is directly above the instrumentation, see Figure 5.3. In the upper base layer, the wheel load is not evenly distributed. When the wheel is in lateral position 150 mm the measured stress in the upper unbound base layer was 650 kPa compared to 430 kPa at lateral position 0. In the lower base layer, there is no difference between the stress measured in lateral position 0 or at 150 mm due to the load distribution.

Brown (1996), stated that the lateral earth pressure coefficient at rest K_0 (Equation 6.10) will increase due to compaction and over consolidated clays show larger values than normal consolidated clays.

$$K_0 = \frac{\sigma_h}{\sigma_v} \quad (6.10)$$

This is the result of an increase in the horizontal (confining) stress. Which horizontal stress should be used in the evaluation of the state of stress during HVS and FWD test is unknown. In order to see the effect of different horizontal stresses, two different calculations were performed in Nelapav. It was not possible to directly regulate the horizontal stress or K_0 in Nelapav. However, the Poisson's ratio ν is possible to set in the program. The relationship between K_0 and ν is described in Equation 6.11. This expression is valid if the stress path starts at $\sigma_v = \sigma_h = 0$, which is so the present case.

$$K_0 = \frac{\nu}{1-\nu} \quad (6.11)$$

An increase in the Poisson's ratio will result in an increase in K_0 , resulting in turn in an increase in the horizontal pressure in the program Nelapav. Poisson's ratio of pavement materials is often set at 0.35 for asphalt, 0.40 for unbound material and 0.45 for clay. These values have been evaluated in laboratory tests but are dependent on the stress path. Water is said to be incompressible, which corresponds to a Poisson's ratio of 0.5. If a value of the ratio is measured to be more than 0.5, it indicates an increase in volume due to dilation (Hoff et al. 1998).

In pavement layers, the surrounding material reduces the horizontal strain and this reduction causes an increase in horizontal stress. The increased horizontal stresses result in a stiffer material, which is one of the aims of the compaction work. It is therefore reasonable to simulate an increase in the horizontal stress with an increase in Poisson's ratio (in this case it of no interest to consider the strains). A sensitivity analysis was therefore made to see the effect of an increased Poisson's ratio from 0.4 to 0.5, which corresponds to a change in K_0 from 0.67 to 1.0 according to Equation 6.11. During loading, the horizontal stress level is influenced by both the compaction induced stress, which can vary according to depth and the stress distribution.

The software Nelapav 4 was used to calculate the stress levels ($\sqrt{J_2}$ and I_1) just below the asphalt layer, in the middle of the upper unbound base layer and in the middle of the lower unbound base layer ($z = 43, 107$ and 235 mm respectively). The calculated stress levels were then compared to the failure envelope and phase envelope from assessment. Calculations were made for input data obtained from FWD measurements before and after the HVS test in order to see the effect on the stress for different input data. The input data for the calculation of $\sqrt{J_2}$ and I_1 is presented in Table 6.3 (material parameters) and Table 6.4 (load specifications).

6. Analysis

Table 6.3. Parameters used for stress calculations for evaluating the state of stress.

Model parameter	Subgrade	Subbase	Unbound base	Asphalt
Before HVS test E [MPa]	100	125	75	6000
After HVS test E [MPa]	100	125	174	6000
Poisson's ratio	0.45	0.40	0.40 or 0.50	0.35

Table 6.4. Surface stress level used for stress calculations to evaluate the state of stress.

Loading	Load [kN]	Load radius [mm]	Stress [kPa]
HVS load 80 kN	80	190	705
FWD load 65 kN	65	150	919
FWD load 50 kN	50	150	707
FWD load 30 kN	30	150	424

In Figure 6.13 the calculated stresses for the HVS load 80 kN at depths of $z = 43$, 107 and 235 mm before and after the HVS test at $K_0 = 0.67$, are presented.

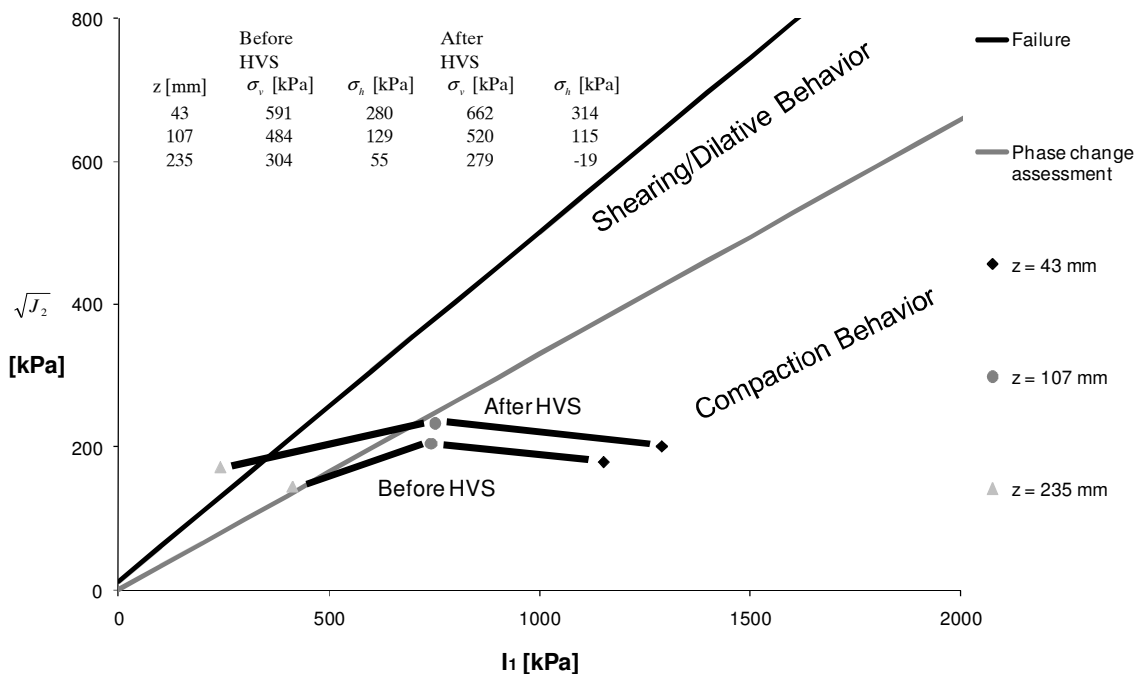


Figure 6.13. The state of stress before and after the HVS test for a K_0 -value of 0.67. an HVS wheel load of 80 kN is used.

On top of the upper unbound base layer, $z = 43$ mm, the state of stress is in the zone, where compaction of the material is expected due to permanent strain. In the middle of the upper layer, $z = 107$ mm, the state of stress is within the compaction zone but closer to the shearing/dilative zone, especially after the HVS test. In the middle of the lower unbound base layer, $z = 235$ mm, the state of stress can be in the shearing/dilative zone before the HVS and after the test, above the failure envelope. In reality no stresses should be above the failure envelope, only on the failure envelope. However, the failure envelope as mentioned before is not performed for the material in question and the tensile stress the Nelapav program calculated will not occur in reality. In Figure 6.14 the same result is shown but for $K_0 = 1.0$

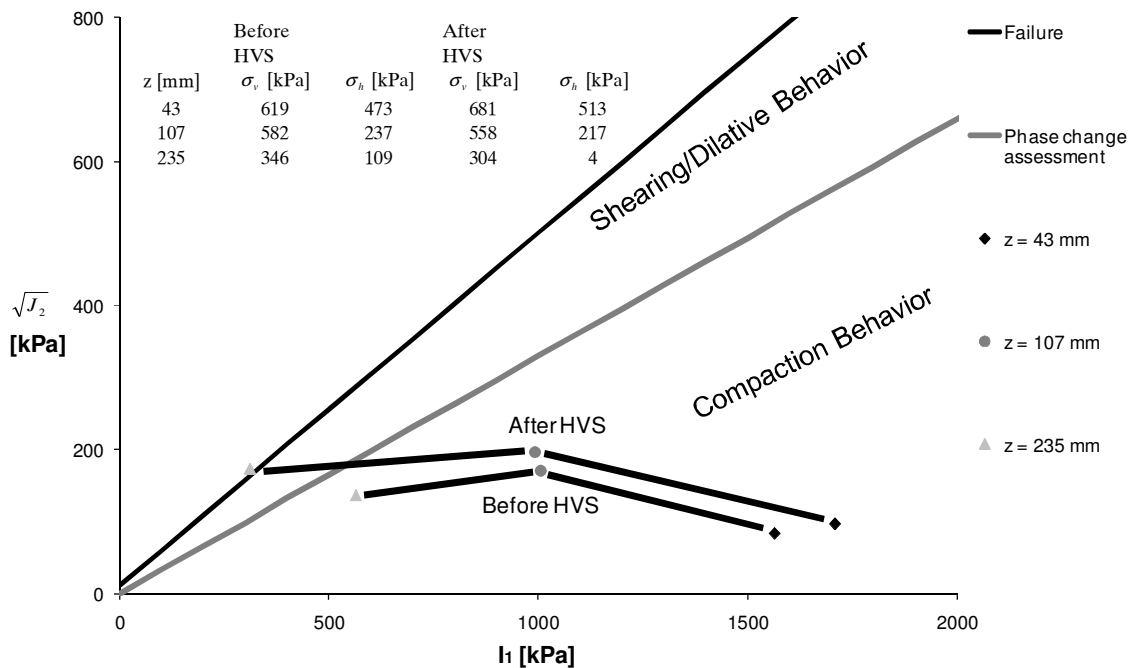


Figure 6.14. The state of stress before and after the HVS test for a K_0 -value of 1.0. an HVS wheel load of 80 kN is used.

As can be seen the stresses in the middle of the upper base layer are within the compaction zone instead. This is also the case for the stresses in the middle of the lower base layer before the HVS test. This indicates that higher horizontal stresses increase the possibility of compaction behavior and that $K_0 = 0.67$ is too small for the case in question.

6. Analysis

In Figure 6.15 the states of stress for the FWD loads 30, 50 and 65 kN after the HVS test, are presented at depths $z = 107$ and 235 mm respectively for a K_0 value of 0.67.

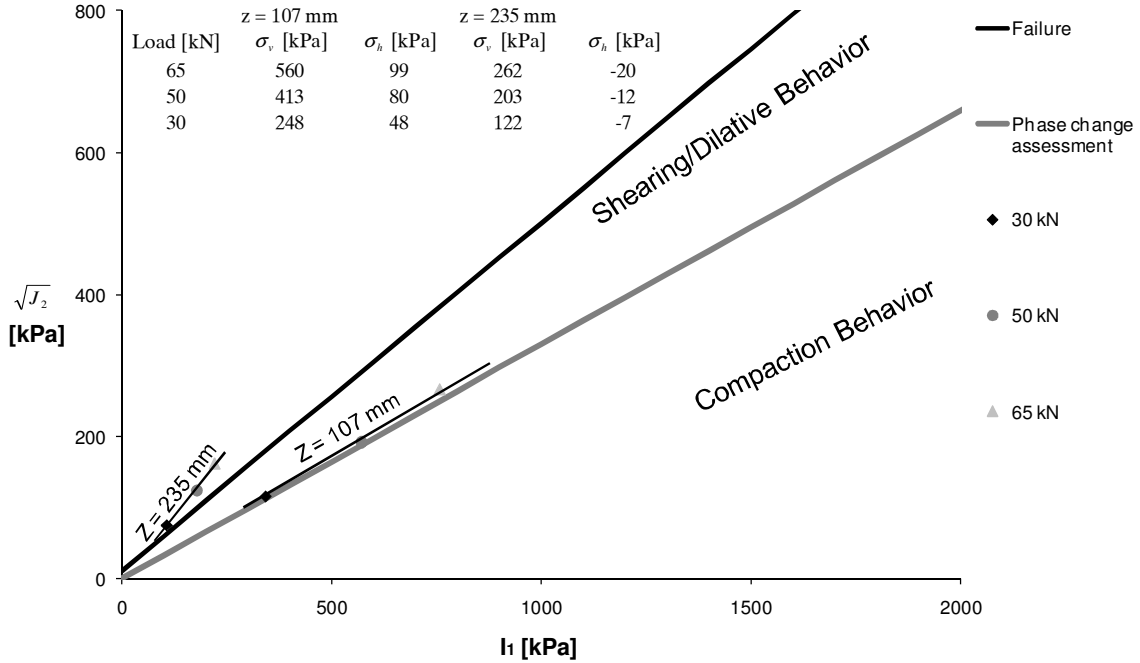


Figure 6.15. The state of stress after the HVS test for a K_0 – value of 0.67 at different load levels of the FWD.

It can be seen that in the middle of the upper base layer, $z = 107$ mm, the state of stress for all load levels of the FWD is the phase change envelope. In the middle of the lower base layer, $z = 235$ mm, the state of stress is above the failure envelope for all load levels. In Figure 6.16 the state of stress is presented for a $K_0 = 1.0$.

6. Analysis

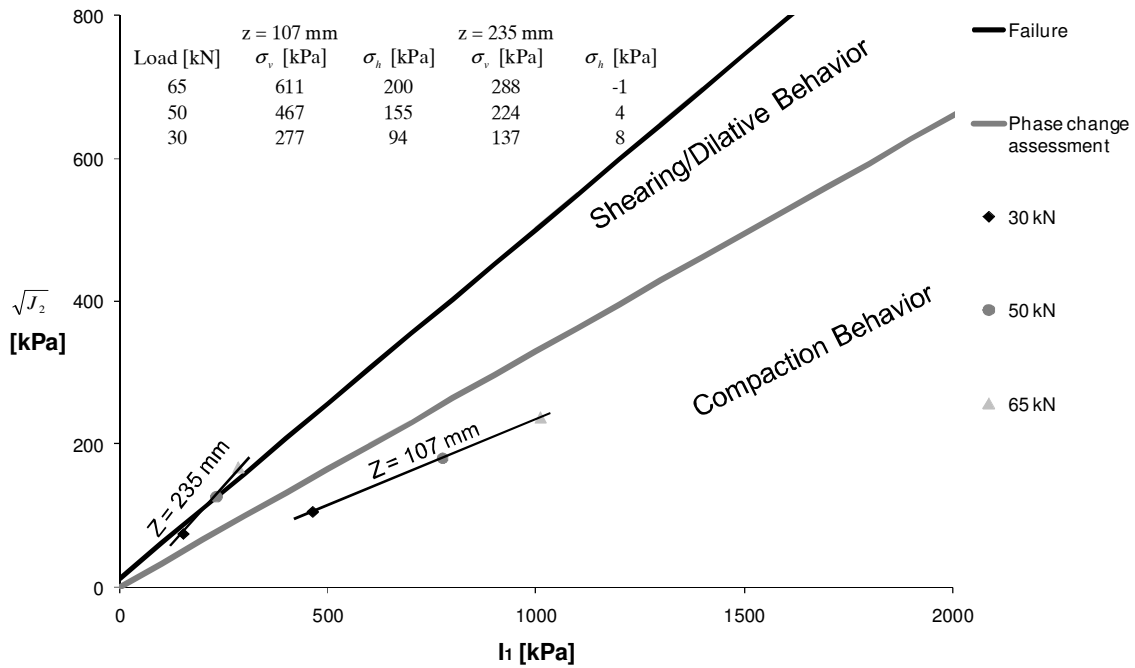


Figure 6.16. The state of stress after the HVS test for a K_0 -value of 1.0 at different load levels of the FWD.

In the middle of the upper unbound base the state of stress can instead be in the compaction zone for all load levels. In the lower base layer, the state of stress is on the failure envelope. It should be mentioned that failure of the material during the FWD test was not noticed, which again indicates that $K_0 = 0.67$ is too small.

The reason why dilative behavior or shearing seems to occur in the lower base layer due to HVS or FWD loading when the state of stress is analyzed can be explained by Figure 6.17.

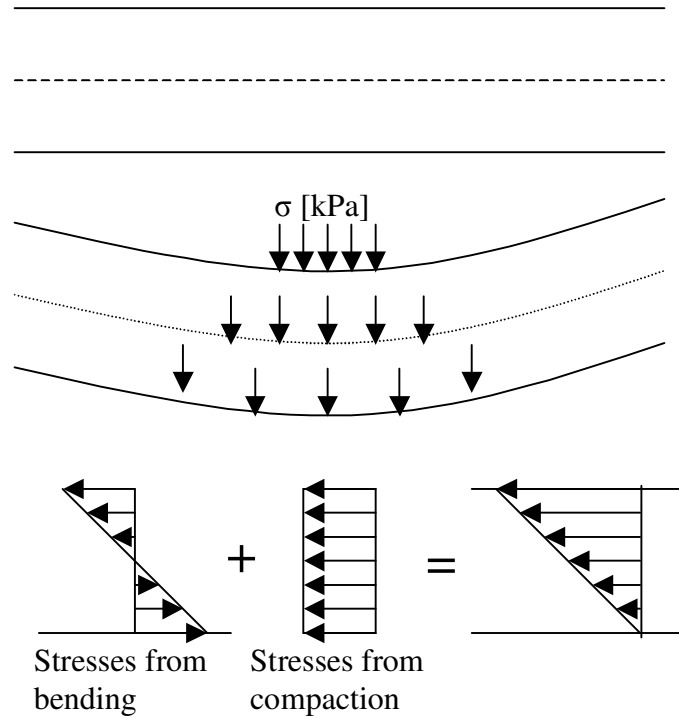


Figure 6.17. Principle sketch of the influence of compaction and bending due to vertical loading on the horizontal stress distribution by depth.

Figure 6.17 is a principle sketch of the vertical and horizontal stress distribution due to external load. The horizontal stresses due to compaction often vary with depth. The horizontal stress, induced by the vertical stress, also decreases with depth due to the decrease in the vertical stress caused by the stress distribution. “Bending” of the unbound material layer due to the vertical load on the surface will cause a reduction in the horizontal stress in the lower part of the layer and an increase in the horizontal stress in the upper part of the layer. However, the “bending” and its effect on the horizontal stress distribution may be an effect of the model being used to calculate the stresses and strains. In Figure 6.18 the calculated horizontal stresses for the assumed values of $K_0 = 0.67$ and 1.0 are presented for Test Cell #1.

6. Analysis

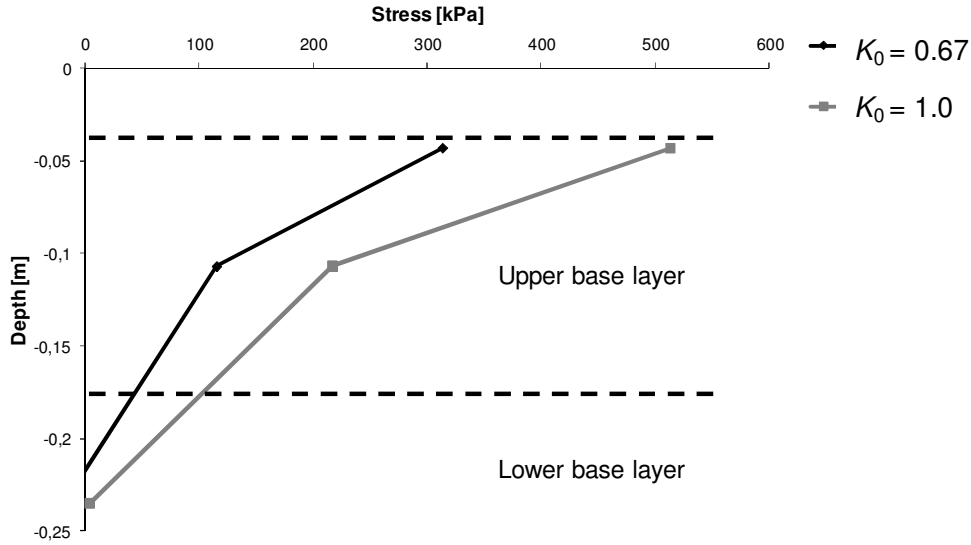


Figure 6.18. Calculated horizontal stresses at different Poisson's ratios in the upper and lower unbound base layer by using Nelapav 4 and the $k - \theta$ model. The input data used are presented in Table 6.3.

As can be seen, the horizontal stress decreases with depth. In this case, for the assumed value of $K_0 = 0.67$, the horizontal stress is tensile at the bottom of the lower unbound base layer. When K_0 is increased, the confining pressure also increases. The effect of different K_0 on the state of stress is presented in Figure 6.19.

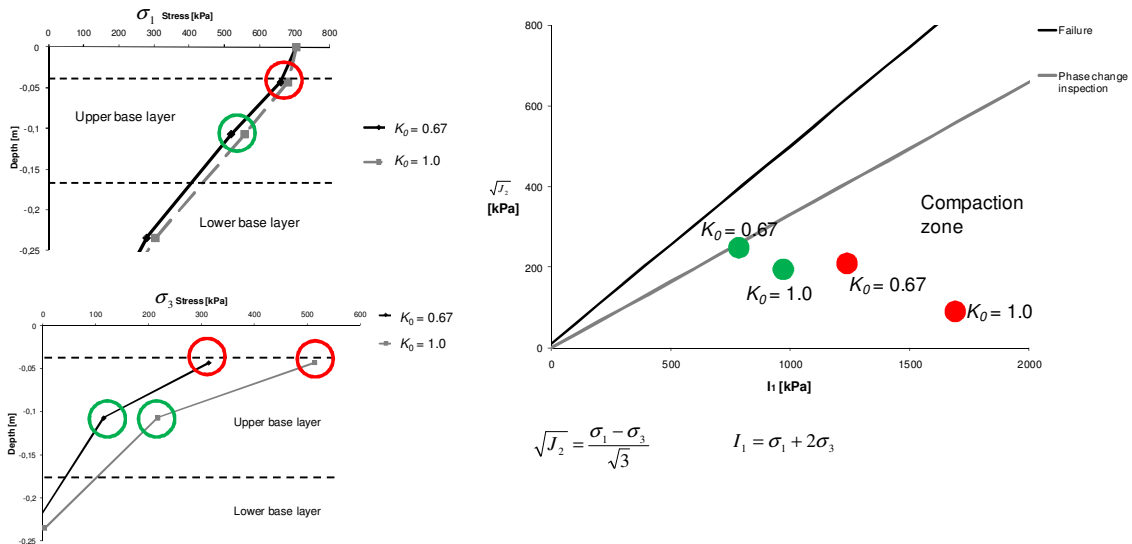


Figure 6.19. The effect of different K_0 - values on the vertical and horizontal stress and the $I_1 - \sqrt{J_2}$ stress space.

If K_0 is assumed to be 0.67, the state of stress on top of the unbound base layer and in the middle of the upper base layer can also be in the compaction zone both before and after the HVS test. In the middle of the lower base layer, the state of stress can be in the compaction zone before the test and in the shearing zone after the test, see Figure 6.13. This means that the risk of shearing or failure is reduced at a higher K_0 (see Figure 6.14), which is summarized in Figure 6.19.

Summary of the state of stress

Based on the interpretation of the state of stress, compaction may occur for load steps 1, 2, 4 and 5 in the triaxial test as well in the upper base layer the HVS and FWD loads. The state of stress for load steps 3 and 6 is on the phase change envelope. Shearing may occur for load steps 7 and 8 and in the lower base layer for HVS and FWD loads.

6.4 Stress hardening behavior

The stress hardening parameters are evaluated from the triaxial test and FWD/HVS test and compared to the conceptual model described in Chapter 3. This is done in order to connect the stress hardening parameters to post compaction and shearing behaviors.

Analysis and evaluation of the triaxial test results

From the triaxial test, the elastic modulus was evaluated for the different bulk stresses as already shown in Figure 4.5 (material 1 and water content 80%). As can be seen, the resilient modulus increases for each increase in load. The $k - \theta$ model (Equation 3.2) could therefore be used to describe the resilient behavior of the actual unbound material.

The effect of load level on the stress hardening behavior parameters k_1 and k_2 in the $k - \theta$ model are presented in Figure 4.8 and Figure 4.9. The conceptual explanation of the meaning of increasing and decreasing k_1 and k_2 parameters was described in Chapter 3.

In order to provide a conceptual explanation for Figure 4.8 and Figure 4.9, the stress - strain plot of material 1 and a water content of 80% of optimum shown in Figure 4.4 is completed in Figure 6.20 by showing the intervals of regression analyses A to F.

6. Analysis

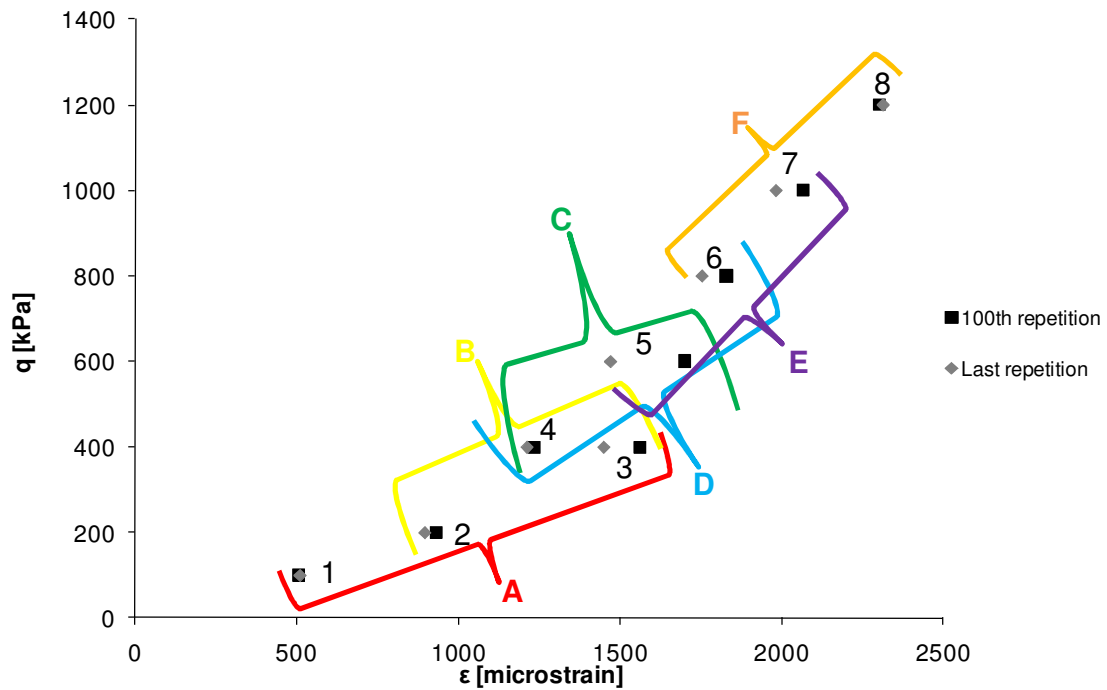


Figure 6.20. The stress – strain relationship evaluated from material 1 and a water content of 80% of optimum. A to F represents the different regression analyses.

Each interval of the regression analyses can be compared to the expected scenarios described in Figure 3.14 and Figure 3.18. However, the stress hardening behavior of the triaxial test results is evaluated for three load levels at time and examples of such a scenario are shown in Figure 3.22. This increases the number of possible scenarios. Consequently, more scenarios are needed. For regression analysis A, the scenario shown in Figure 6.21 can be used.

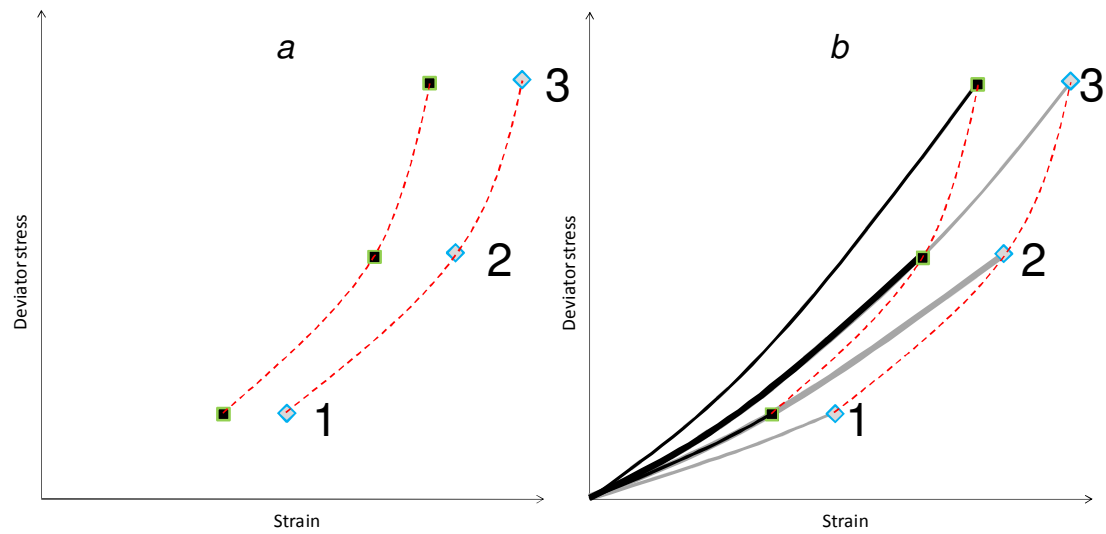


Figure 6.21. Scenario describing post compaction behavior for all load steps in regression analysis A. In Figure a, the red dotted lines represent the stress – strain used in the evaluation of the stress hardening behavior. In Figure b, the black and grey lines represent the assumed stress – strain relationship in reality. Numbers 1 to 3 represent load steps 1 to 3 in the triaxial test.

The red dotted lines in Figure 6.21a represent the sort of fictive stress – strain relationships used to evaluate the stress hardening behavior from the triaxial test. Figure 6.21b shows the possible stress – strain relationship from the triaxial test in the same way as described in Figure 3.21 and Figure 3.22. This scenario describes compaction behavior for all load steps. For regression analysis F, the scenario described in Figure 6.22 can be used.

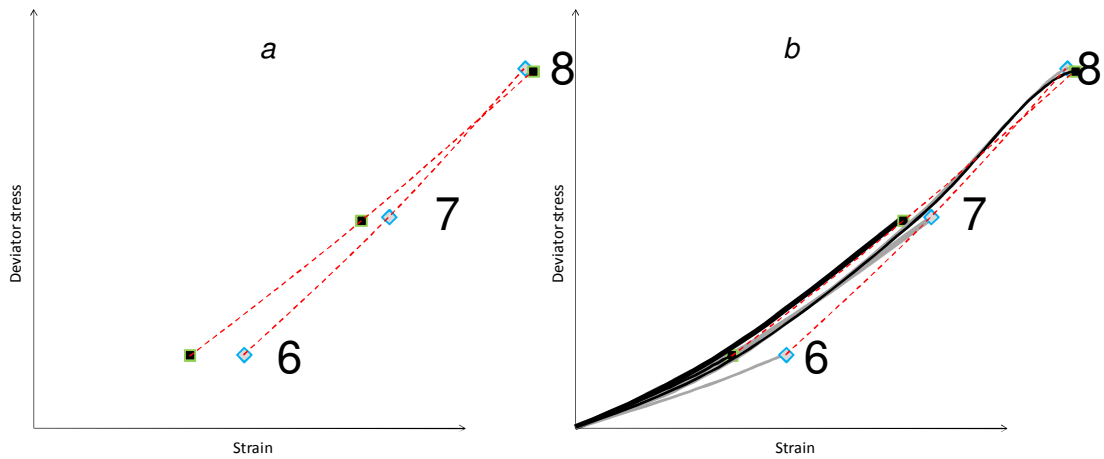


Figure 6.22. Load steps 6 to 8 in the triaxial test involved in regression analysis F. Scenario describing shearing behavior for load steps 6 to 7 as well as and shearing for load steps 7 to 8. Figure a, the red dotted lines represent the stress – strain used in the evaluation of the stress hardening behavior. Figure b, the black and grey lines represent the assumed stress – strain relationship in reality.

This scenario describes shearing for load steps 6 to 7 and load steps 7 to 8. For regression analyses B, C and D it is difficult to evaluate the stress - strain behavior due to the influence of the increased confining pressure of load step 4, see Figure 6.20. For regression analysis E, the scenario described in Figure 6.23 can be used.

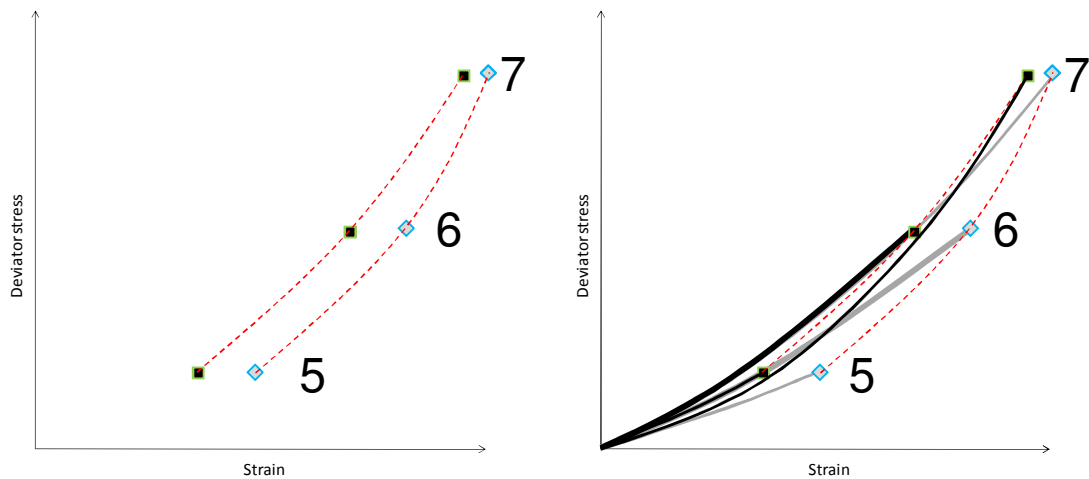


Figure 6.23. Load steps 5 to 7 in the triaxial test involved in regression analysis E. Scenario describing shearing for load steps 5 to 6 and 6 to 7. Figure a, the red dotted lines represent the stress – strain used in the evaluation of the stress hardening behavior. Figure b, the black and grey lines represent the assumed stress – strain relationship in reality.

For load steps 5 to 6 there are indications that shearing starts (the strain is greater during the last load repetition compared with Figure 6.21). For load steps 6 to 7, shearing starts clearly. In summary, load steps 1, 2 and 3 show compaction behavior and load steps 6, 7 and 8 show shearing behavior. Load steps 4 and 5 may show compaction behavior but this is not as clear.

Niekerk et al. (1998) described a relationship between the regression parameters k_1 and k_2 in the $k-\theta$ model (Equation 2.20). If there is a strong relationship between the regression parameters k_1 and k_2 , the influence of one parameter might be described by the other parameter. Hence, by incorporating such a relationship into the expression for the elastic modulus it might be sufficient to study just one of them.

Regression analysis results A to F for all tests on all materials used in the triaxial test are presented in Figure 6.24 for the parameters k_1 and k_2 .

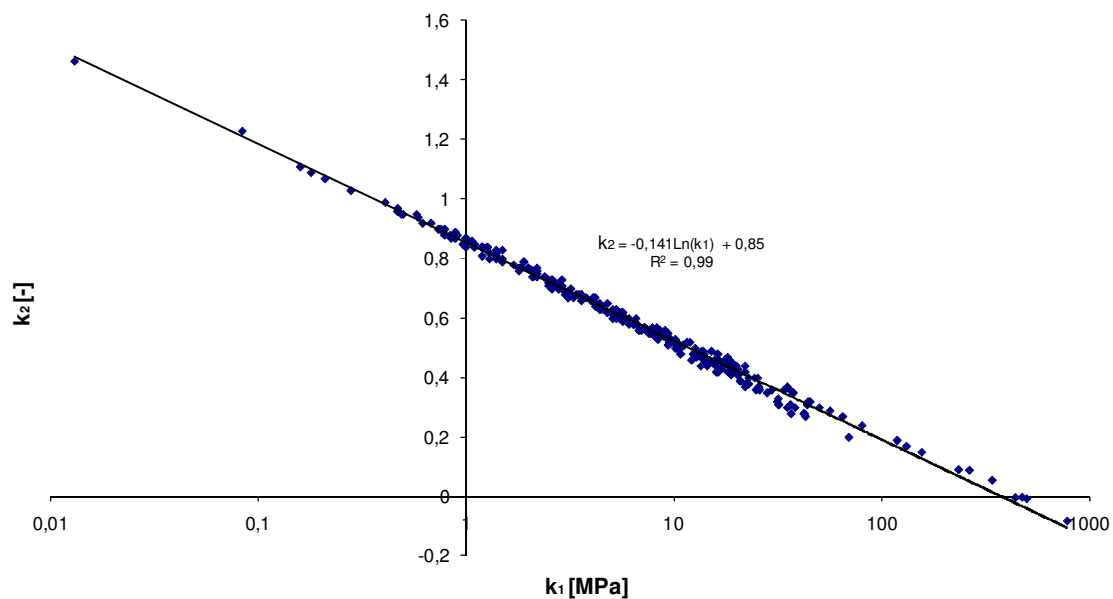


Figure 6.24. Regression analysis of the regressed k_1 and k_2 values from the triaxial test results used in the present thesis, lin-log model.

As can be seen, a very clear relationship between k_1 and k_2 was found, which shows that the $k-\theta$ model works well. The relationship is linear in the lin - log space (Equation 6.12) and not in log-log as was found by Niekerk et al. (1998).

$$k_2 = -D_1 \ln k_1 + D_2 \quad (6.12)$$

D_1 describes the slope of the $k_1 - k_2$ relationship and D_2 the k_2 value for $k_1 = 1$. From Appendix G D_1 is derived to be related to θ as described in Equation 6.13.

$$D_1 \approx \frac{1}{\ln[\theta]} \quad (6.13)$$

According to Equation 2.20 $M_r = k_1$ for $k_2 = 0$, why D_2 could be related to M_r by using Equation 6.14.

$$D_2 = D_1 \ln[M_r] \quad (6.14)$$

The relationship between k_1 and k_2 is thus determined by the bulk stress and the resilient modulus. This can be seen when D_1 and D_2 values are calculated for $\theta = 400$ kPa (load step 2 representing regression analysis A) and a resilient modulus of $M_r = 214$ MPa (representing an average modulus for load step 2) by using Equation 6.14 and Equation 6.15. The same is done for $\theta = 1380$ kPa (load step 7 representing regression analysis F) and corresponding $M_r = 474$ MPa. The calculated D_1 and D_2 values are used in Equation 6.13 to calculate a relationship between k_1 and k_2 for each bulk stress. The result is presented in Figure 6.25. As can be seen the evaluated k_1 and k_2 values can be related to the calculated values.

6. Analysis

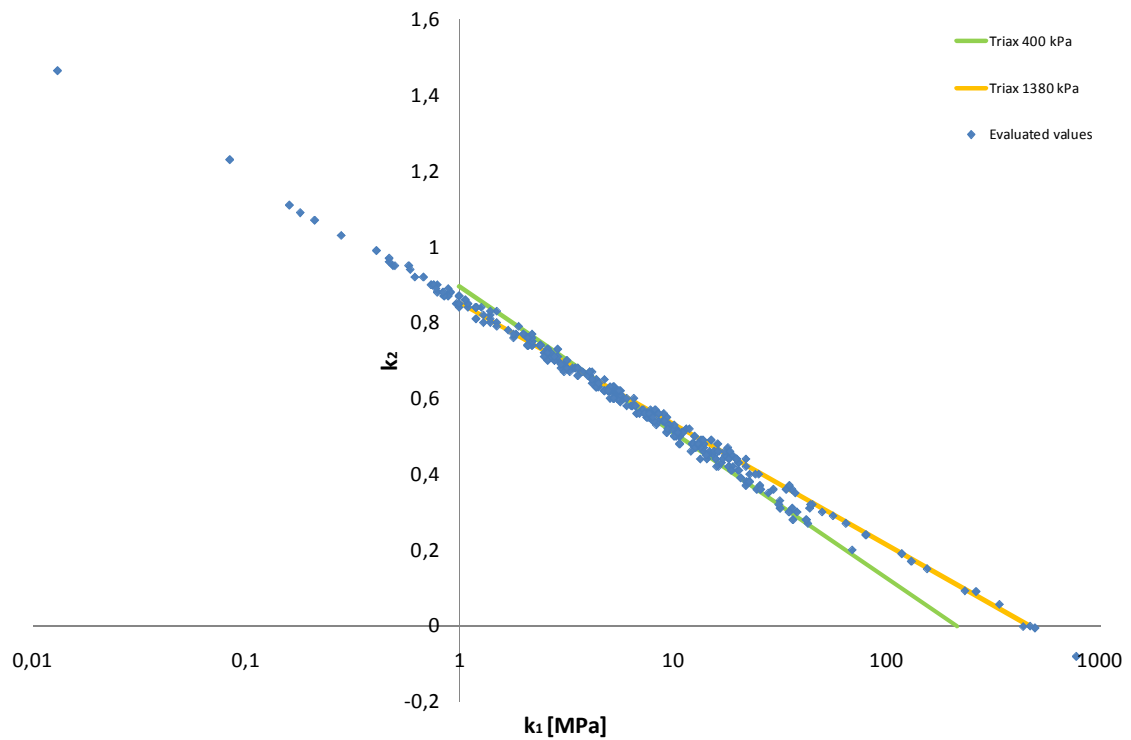


Figure 6.25. Comparison between calculated relationships between k_1 and k_2 and the results of the regression analyses A to F of the triaxial test results.

Figure 4.8 and Figure 4.9 show the effect of increased load and permanent deformation on parameters k_1 and k_2 . In Figure 6.26 this is presented in the $k_1 - k_2$ space for material 1 and with water content 80% of optimum.

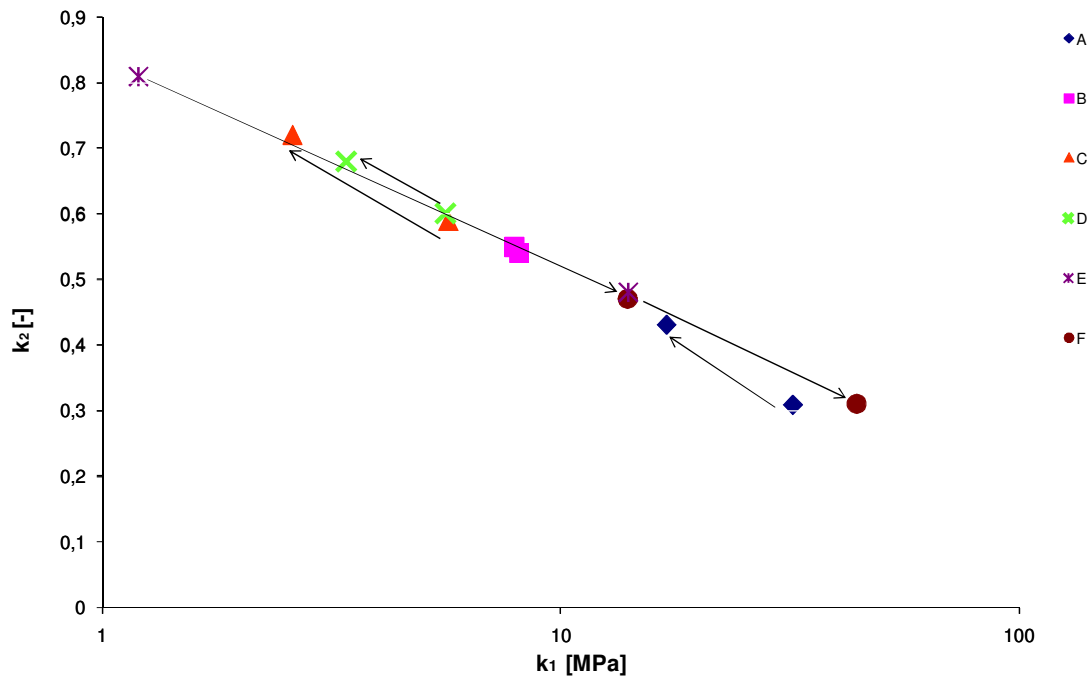


Figure 6.26. The influence of permanent deformation on the k_1 and k_2 values.

As already indicated, the load steps up to regression D results in a decrease in the k_1 parameter and an increase in the k_2 parameter from the 100th to the last load repetition. This indicates post compaction behavior according to the conceptual model described in Chapter 3. Load steps E and F result in an increase in the k_1 parameter and a decrease in the k_2 parameter. This indicates that shearing occurs immediately or after load application, at least from stresses representing regression analyses E and F according to the conceptual model described in Chapter 3. Regression analysis B shows an unclear picture.

Analysis and evaluation of the FWD test results

The most significant result from the evaluation of the HVS and FWD test was that the backcalculated elastic modulus after the HVS test showed an increase (see Figure 5.14 and Figure 5.15). The increase was most significant in the wheel load area. However, the elastic modulus also increased outside the wheel track. It seems that two processes cause an increase, both the wheel load inside the wheel track and “resting” outside the wheel track.

The stress hardening behavior parameters k_1 and k_2 were also evaluated, as described in Figure 3.23, Figure 5.16 and Figure 5.17. The results are presented in Figure 5.18 and Figure 5.19. As can be seen, the results were not as clear as the evaluation of the elastic modulus. There are some indications that the stress

hardening behavior parameter k_1 does not change so much inside the wheel track but increases outside the wheel track after the HVS test. At the same time, there are some indications that the stress hardening behavior parameter k_2 is higher inside the wheel track after the HVS test (especially for Test Cells #2 and #4).

In the same way as for the triaxial testing an attempt was made to find a relationship between the parameter k_1 and k_2 obtained from the FWD test. The regressed k_1 and k_2 values for all test cells are presented in Figure 6.27. It should be noted that there were two drops per load level, which made it possible to perform two regression analyses per station. The relationship between k_1 and k_2 can be seen and compared to the ones calculated for bulk stresses 400 and 1380 kPa in the triaxial test (see Figure 6.25).

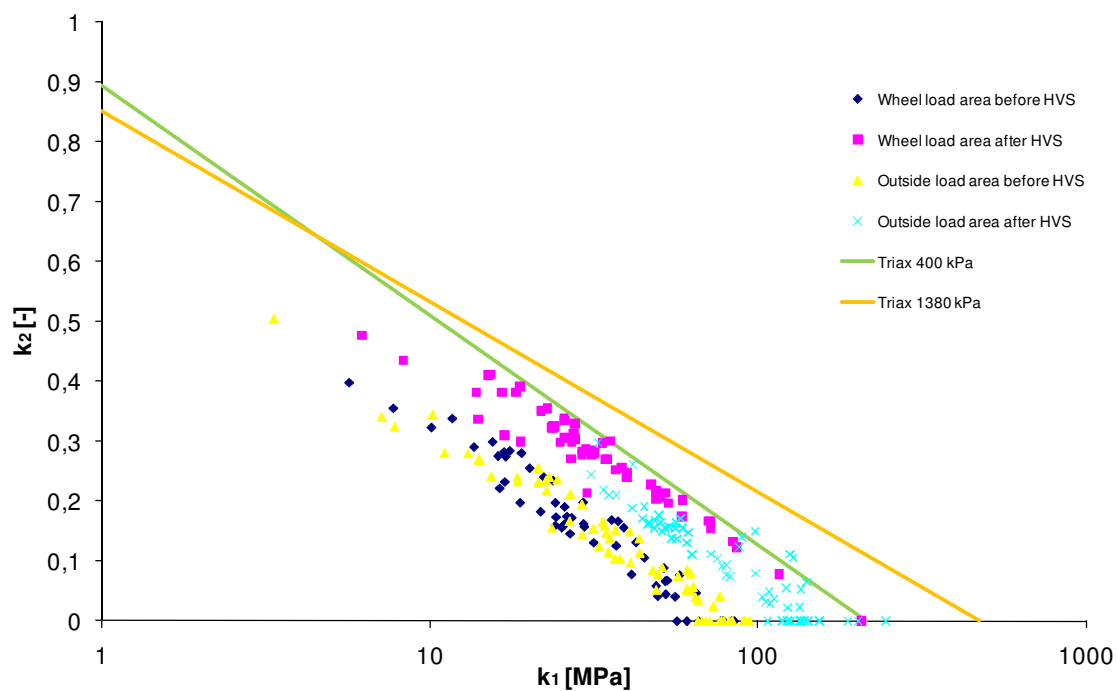


Figure 6.27. Relationship between k_1 and k_2 for the FWD test results of all test cells. The green line represents the calculated value for bulk stress 400 kPa and 1380 kPa for the triaxial test as shown in Figure 6.25.

It can be seen that there is a relationship between the k_1 and k_2 values for each FWD test, similar to the laboratory triaxial testing. However, the scatter is larger. It is significant that the relationships differ depending on whether the test is performed before or after the HVS test and inside or outside the wheel load area. This is clearer compared to the indications in Figure 5.18 and Figure 5.19, where the k_1 and k_2 values were shown alone. By using the average backcalculated bulk stress and resilient modulus for load level 50 kN, a relationship between k_1 and k_2

can be calculated in the same way as presented in Figure 6.25 by using Equation 6.12, Equation 6.13 and Equation 6.14 and the values of bulk stresses and resilient moduli in Table 6.5. The result is presented in Figure 6.28 for all test cells. In Figure 6.28 the average values for k_1 and k_2 inside and outside the wheel load area, before and after the HVS test, are also presented. For each individual test cell, see Appendix H, Figure H1 to Figure H4.

Table 6.5. Average backcalculated resilient modulus and bulk stress of the FWD test before and after the HVS-test, inside and outside the wheel load area.

	Average backcalculated resilient modulus for an FWD load of 50 kN [MPa]	Average backcalculated bulk stress for an FWD load of 50 kN [kPa]
Before the HVS test inside the wheel load area	79	557
After the HVS test inside the wheel load area	193	635
Before the HVS test outside the wheel load area	78	449
After the HVS test outside the wheel load area	162	450

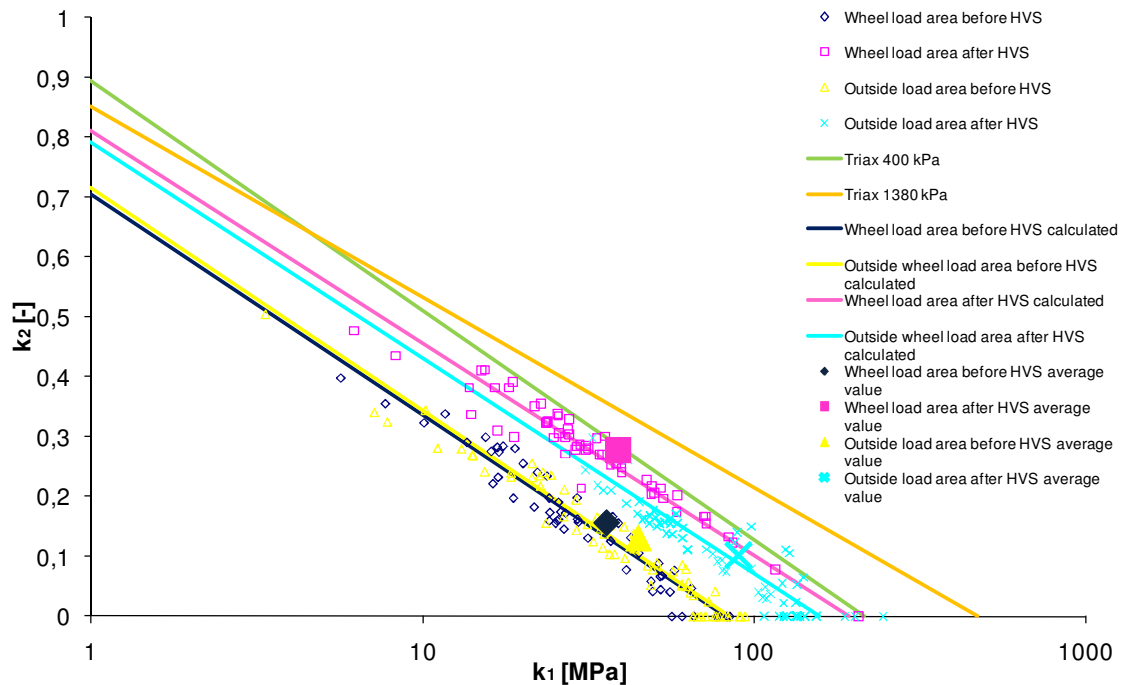


Figure 6.28. Relationship between k_1 and k_2 for the FWD test results of Test Cell #1 compared to the calculated values. The green line represents the calculated value for bulk stress 400 kPa and 1380 kPa of the triaxial test as shown in Figure 6.25

As can be seen there is a good fit between the calculated relationship between k_1 and k_2 and regressed k_1 and k_2 . The slope of the relationship between the k_1 and k_2 values is quite equal for all FWD tests and similar to the triaxial test with bulk stress of 400 kPa, which must obviously be the result as the bulk stress levels are similar, see Table 6.5. The tendencies are rather clear, -the increase in the resilient modulus after the HVS test is caused by an increased k_1 value outside the wheel load area and by an increased k_2 value inside the wheel load area. By only analyzing the average values of all test cells this is even clearer. The scatter of the results however, is very large. The increase in the k_2 – value after the HVS test inside the wheel load area indicates that post compaction occurred in the unbound base layer.

6.5 Summary of the analysis

In Table 6.6 the stress hardening behavior evaluated from the triaxial and FWD/HVS tests and the conceptual model is compared with analysis of the permanent deformation behavior and the state of stress.

Table 6.6. Summary of the results of the analysis

Load	Permanent deformation rate (Compaction or Shearing)	Evaluation of the state of stress (Compaction or Shearing)	Stress hardening behavior	Werkmeister Behavior according to Figure 2.4
Triaxial load step 1	Compaction	Compaction		A
Triaxial load step 2	Compaction	Compaction	Compaction	A
Triaxial load step 3	Shearing	Shearing/ Compaction	Compaction	A/B
Increase in confining pressure between load steps 3 and 4				
Triaxial load step 4	Compaction	Compaction	Compaction	A
Triaxial load step 5	Compaction	Compaction	Compaction	A
Triaxial load step 6	Compaction	Shearing/ Compaction	Shearing	A/B
Triaxial load step 7	Shearing	Shearing	Shearing	B
Triaxial load step 8	Shearing	Shearing		B
HVS load 80 kN	Compaction	Compaction in the upper base layer Shearing in the lower base layer	Compaction	A/B

The evaluation of deformation behavior in the triaxial test indicated post compaction for load steps 1, 2, 4 and 5 for stress hardening behavior, permanent deformation rate and state of stress. This corresponds to behavior A (Werkmeister 2003). Load steps 7 and 8 indicated shearing behavior for all evaluation methods. For load step 3 the picture is unclear. The number of load repetitions was not sufficient to see a reduction in the permanent deformation rate to zero (Figure 6.3). The state of stress was on the assessed phase change envelope (Figure 6.11) and the increased confining pressure in load step 4 made it more difficult to evaluate the stress hardening behavior. For load step 6 it is not totally clear that the permanent deformation rate decreased to zero (Figure 6.4) and also the state of stress is on the phase change envelope (Figure 6.11).

Permanent deformation caused by post compaction or shearing also affects the stress hardening behavior (Figure 6.26). In summary there are strong indications that the stress hardening behavior could be used to separate post compaction behavior from shearing behavior. This will be discussed in the next chapter.

The evaluation of the deformation behavior of the FWD/HVS test indicated post compaction. It was not totally clear that the permanent deformation rate decreased to zero. The state of stress indicated compaction in the upper base layer and shearing in the lower base layer. The result of the evaluation of the stress hardening rate showed a clear pattern although there was a large scatter for the stress hardening parameters k_1 and k_2 . The most significant result from the HVS and FWD tests was the increase in the resilient modulus inside the wheel track after the HVS test. However, the resilient modulus also increased after the HVS test outside the wheel track but not as much as inside the wheel track. The increase in the resilient modulus inside the wheel track is a known phenomenon. Repeated loading in the form of compaction increases the resilient modulus and this is used for performance control measurements after compaction.

A lin – log relationship between the stress hardening behavior parameters k_1 and k_2 was found (Figure 6.28). The slope of the relationship is determined by the actual bulk stress for which the evaluation of k_1 and k_2 is made. The intercept on the log k_1 – axis is determined using the resilient modulus. The results of the stress hardening analysis are summarized in Figure 6.29.

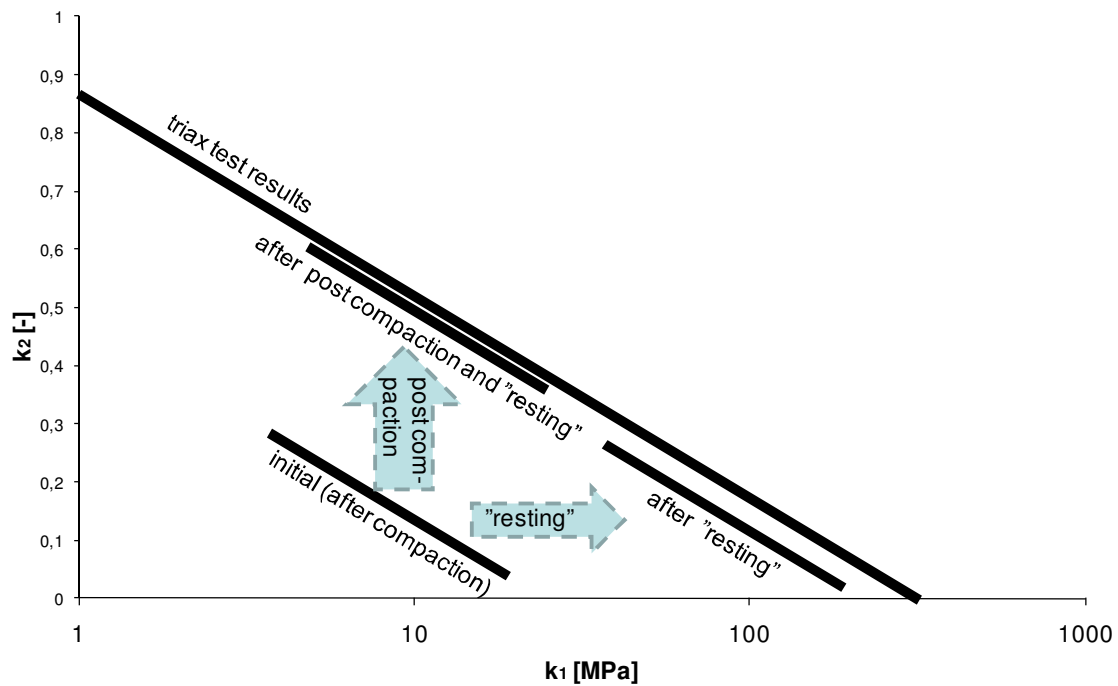


Figure 6.29. Model for describing the effect of resting and post compaction.

Before the HVS test, almost the same relationships between k_1 and k_2 were found inside and outside the wheel track as well as the resilient modulus and bulk stress. After the HVS the resilient modulus was higher inside the wheel track than outside. In the wheel track both the evaluated resilient modulus and the bulk stress was almost the same as for load step 1 in the triaxial test. This result in k_1 and k_2 values close to the ones evaluated from the triaxial test and with the same slope of the $k_1 - k_2$ relationship.

Inside the wheel track a higher k_2 value was obtained while outside the wheel track a higher k_1 value was obtained after the HVS test. The difference inside and outside the wheel track is that inside the wheel track, the material is exposed to post compaction. Outside, the material has simply “rested”. Both processes lead to increased resilient modulus as mentioned above

7 DISCUSSION

The results and findings will be discussed and suggestions for how they can be used will be presented. The discussion is summarized by evaluating the three hypotheses.

7.1 Discussion of the results

The objective of the present thesis is to identify the conditions for post compaction and separate it from shearing/dilatation. This could be done by evaluating the stress hardening behavior parameters k_1 and k_2 of the $k - \theta$ model as shown in the analysis. Both the laboratory triaxial test and FWD test show that the resilient modulus of the unbound granular material is stress dependent, which is why it is reasonable to use this model. Analysis of the resilient modulus alone cannot separate post compaction from shearing due to the fact that it increased for all the load steps in the triaxial test irrespective of whether the state of stress or permanent deformation rate indicated compaction or shearing behavior furthermore. The FWD test showed that k_1 and k_2 could be used to separate wheel loaded surfaces from unloaded (rested) although the resilient modulus showed an increase in both cases. Both k_1 and k_2 are therefore more useful to use compared to just using the resilient modulus to describe permanent deformation behavior.

In the relationship $\ln k_2 - \log k_1$ as described in Figure 6.29, the slope is determined by the bulk stress (Equation 6.13) and the intercept on the $\log k_1$ - axis using the resilient modulus (Equation 6.14). Both the results from the evaluation of the triaxial test and the FWD test showed a good fit. This is thus a stable relationship at least for the state of stress and materials used in the present thesis. The relationship between k_1 and k_2 can then be used when the results from the laboratory triaxial tests and FWD/HVS tests are analyzed as shown in Figure 6.29.

The effect of post compaction and shearing on the k_1 and k_2 values was also conceptual explained by an increased and decreased number of contacts between the particles in the unbound material, see Chapter 3. The reason why “resting” during the HVS test increases the resilient modulus and consequently, the k_1 - value, as described in Figure 6.29 is unclear. No increase in number of contacts is expected and that is probably why the k_1 - value has increased and not the k_2 - value. The increase in the resilient modulus (k_1 - value) must then be caused by

strengthening in the contact area between the particles. Suction effects in the unsaturated material could be one cause of this strengthening.

Whether there is any effect of resting after post compaction or resting before post compaction can be studied by using the HVS/FWD test. After finishing the asphalt surface, the HVS test started on the surface of test cell #1. After a week the test proceeded on test cell #2 and so on. After the HVS test was finished on all test cells, the second FWD test was performed. This means that test cell #1 rested for at least three weeks after the HVS test and test cell #4 rested for three weeks before the HVS test. The FWD test does not reveal any significant differences between the test cells in the wheel track after the HVS and resting thus has no effect on post compaction. This result is summarized in Figure 7.1.

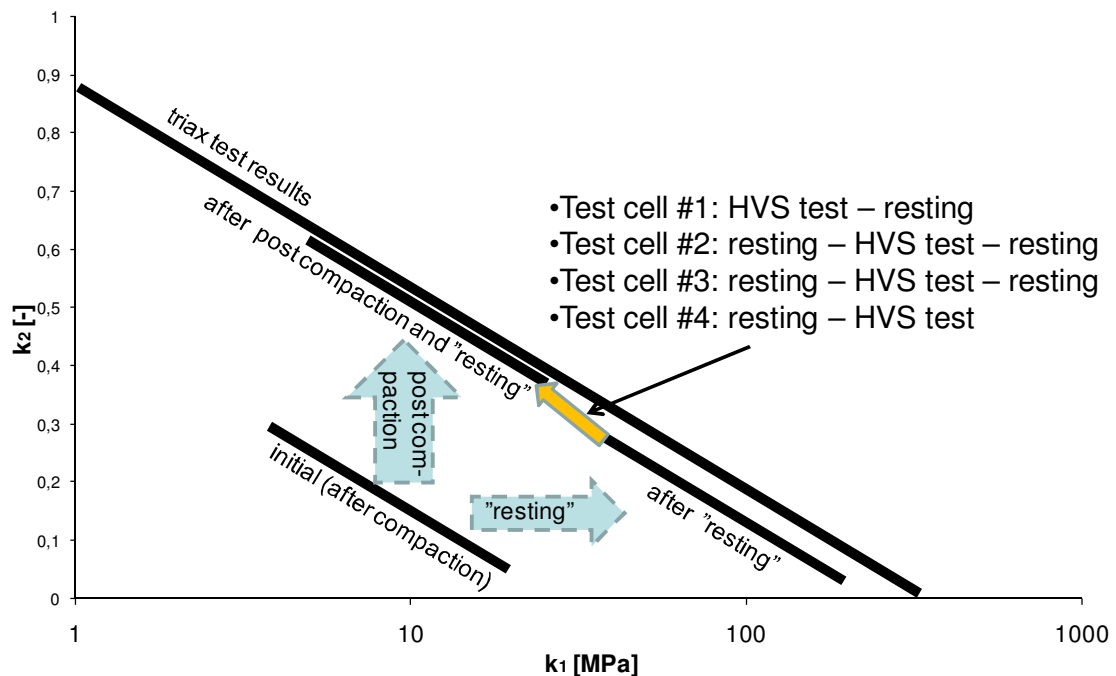


Figure 7.1. Model for describing the effect of resting and post compaction.

The evaluation of the state of stress showed the importance of horizontal support in order to avoid shearing or failure in the unbound layers in the road structure, Figure 6.17 to Figure 6.19. The decrease in the horizontal support due to bending of the layers of the road structure increased the chance of shearing or failure in the unbound layers. The calculated effect of the bending could be affected by the models used, such as the friction between the layers, or the dividing of the unbound material into two layers (subbase and unbound base layer) in the calculations. The stiffness of the underlying layers and subgrade is of course of

importance. Better support causes a lower bending effect in the overlaying unbound layers and thus higher horizontal stress. However, the properties the clay in the subgrade were not known enough to perform any deeper analysis.

7.2 Use of the result

It is of interest to know during the construction phase if the compaction work is sufficient to avoid post compaction and control so that the future traffic load does not cause shearing in the unbound layers. The results of the present thesis show that this could be possible. For this purpose a multi load field test must be performed, possibly supplemented by a triaxial laboratory test.

From the laboratory test it is possible to evaluate target values for k_1 and k_2 for the actual state of stress in the unbound layers. The field test (e.g. an FWD test) is used for controlling the status versus the target values from the triaxial test. The triaxial test is performed with repeated loading to evaluate the permanent deformation properties. The stress hardening parameters k_1 and k_2 are evaluated before and after the repeated loading in order to see if the k_1 value is decreasing and the k_2 value is increasing (indicating compaction) or vice versa (indicating shearing) due to permanent deformation. To make it possible to evaluate k_1 and k_2 before and after the repeated loading, a special elastic deformation test could be performed. In that case the lower load and the higher load are applied in order to make it possible to perform a regression analysis (including the load level for the repeated loading). The performance of the triaxial test used in the present thesis does not make this possible. The resilient moduli evaluated the 100th load repetition. Load steps 2, 3 and onwards have all been subjected to post compaction or shearing in the earlier load step (see Figure 3.22).

If there is no possibility of performing a triaxial test, repeated loading could be done in the field by using repeated drops during the FWD test. To find the limit where shearing starts, more than three load levels could be used in order to see the effect on k_1 and k_2 of an increasing load. If there is a risk of shearing for the load level of future traffic, a redesign of the road structure may be necessary.

The effect of resting to avoid post compaction was small, as described in Figure 7.1. Increasing the resilient modulus by resting thus does not solve the problem of post compaction. However, an increased modulus due to resting or compaction results in a higher bearing capacity, which is of benefit to the asphalt layer. During paving and compaction of the asphalt layer the load from the asphalt

layer is relatively low, which in turn probably do not change the position in $k_1 - k_2$ space significantly (see Figure 7.1). However, a better support from the unbound layers due to resting or compaction increases the possibility to provide a better compaction result of the asphalt layer and in turn reducing the risk of fatigue cracking.

To decrease post compaction during construction, the compaction work must be increased as well as the possibility of verifying the compaction work according to the suggestions above.

If transportation on the road using haulers during construction is encouraged, the unbound layers are subjected to “post compaction” during the construction phase. This could take place if the material is capable of with standing traffic directly on the unbound material and if there is any solution to deal with mud from the wheels of the haulers. The mud could be compressed through the unbound material and thus increase the amount of fines.

To avoid the effect of decreased horizontal stress due to “bending” of the unbound layers, the stability of the upper part of the subgrade could be increased. To use as coarse grained aggregate in the subbase as possible could also be a possibility. Coarser grained material has better stability and internal friction angle and thus resists decreased horizontal stresses better.

7.3 Hypotheses and objective

As a summary of the discussion, the three hypotheses are evaluated as follows.

First hypothesis

The first hypothesis is that post compaction can be seen as a continuous decrease in the permanent deformation rate during repeated loading.

The literature review showed that the permanent deformation rate decreased during post compaction. Consequently, the literature review alone provides support for the first hypothesis.

The deformation rate was evaluated for both the laboratory triaxial test and the HVS test. The permanent deformation rate was related to an analysis of the state of stress, which indicates if the permanent deformation is caused by compaction or shearing for the actual stress levels in the triaxial test and HVS tests. In a majority of the load steps in the triaxial test (six out of eight) there was

agreement between permanent deformation rate and assumed compaction or shearing behavior according to the analysis of the state of stress. For the HVS test the analysis of the state of stress indicates either shearing or compaction depending on whether it is the upper or lower base layer that is being analyzed. All other tests indicated compaction behavior.

Second hypothesis

The second hypothesis is that if the load characteristics of compaction and loadings after compaction differ, post compaction occurs.

The literature review showed that post compaction will occur if the load characteristics change, at least for laboratory tests. In the laboratory tests used, the loadings during the sample preparation differed from the loadings during the real test. Therefore post compaction occurred during the first load step. When the stress level increased the next load step, post compaction started again due to the different (higher) load.

In the HVS test there was also a difference in loading during the compaction of the test cells before the test and the wheel load during the test, which caused post compaction in the first loadings of the test. After 20000 wheel passes, the wheel load was increased, which again caused a post compaction process.

Third hypothesis

The third hypothesis is that the stress hardening behavior is affected by compaction, post compaction and shearing.

The conclusions of the literature review were that post compaction causes an increase in the non-linear behavior, which for example influence the regression parameters k_1 and k_2 in the $k - \theta$ model after post compaction. The conceptual model also showed that post compaction should affect the stress hardening behavior by decreasing the k_1 - value and increasing the k_2 - value. Shearing on the other hand contradicts compaction and post compaction. It may cause a reduction in coordination number due to an increase in void content when the material is permanently deformed. Shearing will therefore affect the stress hardening behavior in an opposite way compared to compaction, through an increased k_1 - value and a decreased k_2 - value.

From the triaxial test a specific bulk stress was found, where lower stress gave a decreased k_1 - value and an increased k_2 - value due to repeated loadings and the opposite at higher stress. The HVS and FWD test results showed a large scatter

7. Discussion

although the mean values showed an increased k_2 – value in the wheel track after the repeated wheel loading.

8 CONCLUSIONS

It is possible to describe the permanent deformation behavior of unbound road material by examining resilient behavior. However, it is not sufficient to use the resilient deformation or resilient modulus. For an adequate description it is necessary to evaluate the stress hardening behavior. This can be evaluated by using the $k - \theta$ model and its stress hardening behavior regression parameters k_1 and k_2 .

There is a specific bulk stress level that separates compaction behavior and shearing behavior as a result of repeated load. Below that specific bulk stress parameter k_1 decreases and parameter k_2 increases as a result of repeated load. This could be related to post compaction behavior. Above the specific bulk stress level, repeated loading will cause an increase in k_1 and a decrease in k_2 , which can be related to shearing behavior. Hence, it is not sufficient to only study the resilient modulus due to the fact that it increases with repeated loadings at bulk stresses below and above the specific bulk stress level. These results were found by studying the laboratory triaxial test results and the processes could be followed by means of graphic presentation in $\log k_1 - \ln k_2$.

An increase in the k_2 - value due to post compaction could be explained conceptually by an increase in the number of contacts between the grains of unbound material. An increase in the number of contacts is a result of increased density caused by the post compaction. A decrease in the k_2 - value due to shearing could be explained by a more open structure compared to the structure caused by post compaction.

There is a clear relationship between the stress hardening behavior parameters k_1 and k_2 of the $k - \theta$ model. The relationship is a straight line in a $\log k_1 - \ln k_2$ graphic presentation. The slope of the relationship is determined by the bulk stress, the higher the bulk stress, the smaller the slope. The intercept on the $\log k_1$ axis is determined using the resilient modulus.

The resilient modulus increases both due to post compaction and to resting. However, the increase due to post compaction is more significant. Analysis of the stress hardening behavior shows that the increase in the resilient modulus from post compaction is caused by an increased k_2 - value and from resting by an increased k_1 -value. The processes could be followed by graphic presentation in $\log k_1 - \ln k_2$.

8. Conclusions

Target values for k_1 and k_2 to avoid post compaction could be evaluated by using the repeated load laboratory triaxial test. These target values can then be used to check the compaction.

Increased bearing capacity caused by resting could be of benefit to the paving and compaction of the overlaying asphalt layer. However, the k_1 or k_2 values are not influenced whether post compaction occurs directly after compaction or after resting. Hence, a road structure is not improved by resting if post compaction or compaction has caused a dense structure and resting does not protect a structure from post compaction.

9 RECOMMENDATION OF FUTURE WORK

- Suggest a working method, where a triaxial test is used in order to find the optimal k_1 and k_2 values in field and the stress limit where shearing starts. The limit, where shearing starts, should be used in design purpose. The optimal k_1 and k_2 values should be used as target values in field when the compaction effort is evaluated in order to avoid post compaction. If it is not possible to achieve the optimal values of k_1 and k_2 , post compaction is expected and an evaluation can be performed after the road is taken in service in order to see if more post compaction should be expected.
- The FWD tests should be performed with more than three load levels for making it possible to evaluate the load limit where shearing starts.
- Laboratory triaxial tests should be performed in such way that it is possible to evaluate the effect of post compaction or shearing in a specific load step. The last load repetition for a specific load should be continued by load repetitions with a lower followed by a higher load. In this way it is possible evaluate the stress hardening parameters where they are not affected by repeated load at a lower load step, which was the case for the triaxial test used for the evaluation in the present thesis.
- Study the “resting” effect further in order to evaluate its effect on the resilient modulus and the stress hardening behavior parameters.
- Evaluate the effect of water content in order to see the effect of drying at wetting on the k_1 and k_2 parameters of the $k - \theta$ model.
- Evaluate the effect of different properties of the other structure layers and subgrade on the layer that is of specific interest.

REFERENCES

- Andrei D., Witczak M.W., Schwartz C.W., Uzan J., 2004: Harmonized Resilient Modulus Test Method for Unbound Pavement Materials. Transport Research Board 83th Annual Meeting January 2004, Washington, D.C, USA.
- Arvidsson H. 2006: Dynamiska treaxialförsök på VTI – jämförelse mellan VTI metoden och EN 13286-7. VTI 21-2006, VTI, Linköping, Sweden. (In Swedish).
- Baars van S., 1996: Discrete element analysis of granular materials. PhD thesis, Department of Geotechnics, Technical University of Delft, Delft, The Netherlands.
- Baley J., Correia A.G., Jouve P., Hornych P., Paute J-L., 1997: Mechanical behaviour of soils and unbound granular materials, modelling of flexible pavements - recent advances. Eighth International Conference on Asphalt Pavements, August 1997, Seattle, Washington, USA.
- Barbour S.L., Krahn J., 2004: Numerical Modelling – Prediction or Process. Geotechnical News, Geospec.
- Barksdale R.D., 1972: Laboratory Evaluation of Rutting in Base Course Materials. Third International Conference on the Structural Design of Asphalt Pavements, London, UK.
- Bonaquist R.F., Witczak M.W., 1997: A Comprehensive Constitutive Model for Granular Materials in Flexible Pavement Structures. Eighth International Conference on Asphalt Pavements, August 1997, Seattle, Washington, USA.
- Boudali M., Robert C., 1998: Laboratory determination of base material resilient moduli. The 5th International Conference on the Bearing Capacity of Roads and Airfields, vol 3, pp. 1235-1245, July 1998, Trondheim, Norway.
- Boyce J.R., 1980: A non-linear model for elastic behaviour of granular materials under repeated loading. International Symposium on Soils under Cyclic and Transient Loading, pp. 280-294, Swansea, UK.
- Brown S.F., Pappin J.W., 1981: Analysis of Pavements with Granular Bases. Transport Research Record No 810 pp 17 - 23. Washington DC, USA.
- Brown S.F., 1996: Soil mechanics in pavement engineering. Géotechnique 46, No. 3, pp 383-426, Thomas Telford Services Ltd, London, UK.
- Chatti K., Ji Y., Harichandran R., 2004: Dynamic Time Domain Backcalculation of Layer Moduli, Damping and Thicknesses in Flexible Pavements. Transport Research Board 83th Annual Meeting January 2004, Washington, D.C, USA.

References

- Chou F.-J., Tutumluer E., 2001: Stress path testing for a proper characterization of unbound aggregate base behavior. Transport Research Board 80th Annual Meeting January 2001, Washington, D.C, USA.
- Correia A.G., De Almeida J.R., 1998: Mechanical behavior of unbound granular materials for modeling of flexible pavements. The 5th International Conference on the Bearing Capacity of Roads and Airfields, July 1998, Trondheim, Norway.
- Dawson A.R., Correia A.G., Jouve P., Paute J.-L., Galjaard P.J., 1994: Modelling Resilient and Permanent Deflection in Granular and Soil Pavement Layers. The 4th International Conference on the Bearing Capacity of Roads and Airfields, July 1994, Minneapolis, Minnesota, USA.
- Desai C.S., Somasundaram S., Frantziskonis G., 1986: A Hierarchical Approach for Constitutive Modeling of Geological Materials. International Journal for numerical and Analytical Methods in Geomechanics, John Wiley and sons, vol. 10, pp. 225-257.
- Dunlap W.A., 1963: A Report on a Mathematical Model Describing the Deformation Characteristics of Granular Materials. Technical Report 1, Project 2-8-62-27, TTI, Texas A & M University, Texas, USA.
- Ekblad J., 2004: Influence of Water on Resilient Properties of Coarse Granular Materials. Licentiate Thesis, Royal Institute of Technology, Stockholm, Sweden.
- Ekdahl P., Hansson J., Huvstig A., Thorén H., 2004a: Test of the influence from mica and LWA on permanent deformations and calculations of the elastic and permanent response under HVS testing. Proceedings of the 6th international symposium on pavements unbound (UNBAR 6) July 2004, Nottingham, England, UK.
- Ekdahl U., Bengtsson, P.-E., Rydén N., 2004b: A new framework for analytical pavement design based on systematic control during construction work. NGM 2004, Ystad, Sweden.
- El Abd A., Hornych P., Breyse K., Denis A., Chazallon C., 2004: A simplified method of prediction of permanent deformations of unbound pavement layers. Proceedings of the 6th international symposium on pavements unbound (UNBAR 6) July 2004, Nottingham, England, UK.
- El Abd A., Hornych P., Breyse D., Denis D., 2005: Prediction of permanent deformations of unbound pavement layers. The 7th International Conference on the Bearing Capacity of Roads and Airfields, June 2005, Trondheim, Norway.
- El-Basyouny M.M., Witczak M., Kaloush K., 2005: Development of the Permanent Deformation Models for the 2002 Design Guide. Transport Research Board 84th Annual Meeting January 2005, Washington, D.C, USA.
- Erlingsson S., Ingasson T., 2004: Performance of two thin pavements structures during Accelerated Testing using a Heavy Vehical Simulator. 2nd International Conference on Accelerated Pavement Testing, September 2004, Minneapolis, Minnesota, USA.

References

- Fleming P.R., Rogers C.D.F., Frost M.W., 1998: Performance Parameters and Target Values for Construction of UK Road Foundations. The 5th International Conference on the Bearing Capacity of Roads and Airfields, vol 3, pp 1491 - 1501, July 1998, Trondheim, Norway.
- Flintsch G.W., Al-Qadi I.L., Park Y., Brandon T.L., Appea A., 2003: Relationship Between Backcalculated and Laboratory-measured Resilient Moduli of Unbound Materials. Transport Research Board 82th Annual Meeting January 2003, Washington, D.C, USA.
- Gervois A., Bideau D., 1993: Some geometrical properties of two-dimensional hard disk packings. Random materials and processes, Disorder and granular media, pp 1 – 34, Elsevier, Amsterdam, The Netherlands.
- Hansbo S., 1975: Jordmateriallära. Almqvist & Wiksell, Uppsala, Sweden. (In Swedish).
- Hansson J., 2002: Fatigue of unbound material in a road structure. Licentiate thesis, department of Geology (A 102), Chalmers University of Technology, Gothenburg, Sweden. (In Swedish)
- Hansson J., Lenngren C.A., 2005: Unbound Material Resilient Behavior due to Post Compaction –A study Comparing FWD and Tri-axial Tests. The 7th International Conference on the Bearing Capacity of Roads and Airfields, June 2005, Trondheim, Norway.
- Heydinger A.G., Xie Q., Randolph B.W., Gupta J.D., 1996: Analysis of Resilient Modulus of Dense- and Open-Graded Aggregates. Transport Research Record No 1547.
- Hoff I., Nordal S., Nordal, R.S., 1998: New hyperelastic material model for granular materials in pavement structures. The 5th International Conference on the Bearing Capacity of Roads and Airfields, July 1998, Trondheim, Norway.
- Hornych P., Kazai A., Piau J-M., 1998: Study of the resilient behaviour of unbound granular materials. The 5th International Conference on the Bearing Capacity of Roads and Airfields, July 1998, Trondheim, Norway.
- Huang Y.H., 2004: Pavement analysis and design, Pearson Prentice Hall, New Jersey, USA.
- Huurman M., 1997: Permanent Deformation in Concrete Block Pavements. PhD dissertation, Delft University of Technology, Delft, The Netherlands.
- Huvstig A., 2003: Notes from Work shop regarding the Heavy Vehicle Simulator test at Uddevalla, September 11 – 12 2003, Ellös, Sweden.
- Irwin L.H., 1994: Practical Realities and Concerns Regarding Pavement Evaluation. The 4th International Conference on the Bearing Capacity of Roads and Airfields, July 1994, Minneapolis, Minnesota, USA.

References

- Irwin L.H., Directions For Use of Nelapav 4. Cornell Local Roads Program, Ithaca, New York, USA.
- Kolisoja P., 1997: Resilient deformation characteristics of granular materials. Thesis for the degree of Doctor of Technology, Tampere University Technology, Tampere, Finland.
- Kolisoja P., 1998: Resilient deformation behaviour of aggregates determined by means of cyclic loading triaxial tests. The 5th International Conference on the Bearing Capacity of Roads and Airfields, July 1998, Trondheim, Norway.
- Korkiala-Tanttu L., Laaksonen R., 2004: Modelling of the stress state and deformations of APT tests. 2nd International Conference on Accelerated Pavement Testing, September 2004, Minneapolis, Minnesota, USA.
- Korkiala-Tanttu L., 2005: A new material model for permanent deformations in pavements. The 7th International Conference on the Bearing Capacity of Roads and Airfields, June 2005, Trondheim, Norway.
- Lekarp F., Isacsson U., 1998: Permanent deformation in granular material - state of the art. The 5th International Conference on the Bearing Capacity of Roads and Airfields, July 1998, Trondheim, Norway.
- Lekarp F., 1999: Resilient and Permanent Deformation Behavior of Unbound Aggregates under Repeated Loading. Division of Highway Engineering, Royal Institute of Engineering, Stockholm.
- Lenngren C.A., 1994: Non-Destructive Testing Utilizing Controlled Variable Rise Time. The 4th International Conference on the Bearing Capacity of Roads and Airfields, July 1994, Minneapolis, Minnesota, USA.
- Lenngren C.A., Fredriksson R., 1998: Initial rutting on reconstructed roads and how to relate it to FWD testing. The 5th International Conference on the Bearing Capacity of Roads and Airfields, July 1998, Trondheim, Norway.
- Lenngren C.A., Fredriksson R., 2002: Initial Rutting on Reconstructed Roads and How It Relates to FWD Testing II. The 6th International Conference on the Bearing Capacity of Roads and Airfields, June 2002, Lisbon, Portugal.
- Lenngren C.A., Hansson J., 2004: Comparing FWD Initial Tests with HVS Induced Initial and Long-Term Rutting. 2nd International Conference on Accelerated Pavement Testing, September 2004, Minneapolis, Minnesota, USA.
- Lentz R.W., Baladi G.Y., 1980: Prediction of Permanent Strain in Sand Subjected to Cyclic Loading. Transport Research Record No. 759, pp 54-58, Washington DC, USA.
- Lindblom U.E., 1972: Kompressionsegenskaper hos traktorutbredda sprängstensfyllningar, med särskild hänsyn till sättningar hos grundplattor. Institutionen för geoteknik med grundläggning, Chalmers tekniska högskola, Göteborg. (In Swedish).

References

- Livneh M., Goldberg Y., Use of Falling-Weight Deflectometer and Light Drop-Weight for Quality Assessment during Road Formation and Foundation Construction. Transport Research Board 80th Annual Meeting January 2001, Washington, D.C, USA.
- Lytton R.L., 1989: Backcalculation of Pavement Layer Properties. Nondestructive Testing of Pavements and Backcalculation of Moduli, ASTM STP 1026, pp 7-38, Philadelphia, USA.
- Meshkani A., Abdallah I.N., Nazarian S., 2003 Feasibility of Backcalculation of Nonlinear Parameters of Flexible Pavement Layers from Nondestructive Testing. Transport Research Board 82th Annual Meeting January 2003, Washington, D.C, USA.
- Metcalf J.B., 2004: Full Scale Accelerated Pavement Testing – A Nort American and European Perspective. 2nd International Conference on Accelerated Pavement Testing, September 2004, Minneapolis, Minnesota, USA.
- Mork H., 1994: Backcalculation of in-depth deflection measurements with linear theory and stress dependent material models. The 4th International Conference on the Bearing Capacity of Roads and Airfields, July 1994, Minneapolis, Minnesota, USA.
- Niekerk van A.A., Houben L.J.M., Molenaar, A.A.A., 1998: Estimation of Mechanical Behaviour of Unbound Road Building Materials from Physical Material Properties. The 5th International Conference on the Bearing Capacity of Roads and Airfields, vol 3, pp 1221 - 1233, July 1998, Trondheim, Norway.
- Núñez W.P., Malysz R., Ceratti J.A., Gehling W.Y.Y., 2004: Shear strength and permanent deformation of unbound aggregates used in brazilian pavements. Proceedings of the 6th international symposium on pavements unbound (UNBAR 6) July 2004, Nottingham, England, UK.
- Oda M., Ivashita K., 1999: Mechanics of granular materials. AA Balkema, Rotterdam, The Netherlands.
- Odermatt N., Wiman L.G., Arm M., Magnusson R., 2004: Deformation of Unbound Pavement Materials - Heavy Vehicle Simulator and Cyclic Load Triaxial Tests. 2nd International Conference on Accelerated Pavement Testing, September 2004, Minneapolis, Minnesota, USA.
- Orr D.P., 2003: Detection of Non-resilient Behavior in Pavements Using a Falling Weight Deflectometer. Transport Research Board 82th Annual Meeting January 2003, Washington, D.C, USA.
- Park S-W., Fernando E.G., 1998: Sensitivity Analysis of Predicted Stress-dependency and Plastic Behavior for Load Zoning. The 5th International Conference on the Bearing Capacity of Roads and Airfields, July 1998, Trondheim, Norway.

References

- Park S-W., Lytton R.L., 2002: Prediction of Flexible Pavement Response Using Non-Linear Stress-Dependent Material Models. The 6th International Conference on the Bearing Capacity of Roads and Airfields, vol 1, pp. 231-240, June 2002, Lisbon, Portugal.
- Quintus von H.L., Killingsworth B.M., 1998: Comparison of Laboratory and Insitu Determined Elastic Layer Moduli. Transport Research Board 77th Annual Meeting January 1998, Washington, D.C, USA.
- Rust F.C., Kekwick S.V., Kleyn E.G., Sadzik E.S., 1997: The Impact of Heavy Vehicle Simulator (HVS) Test Programme on Road Pavement Technology and Management. Eighth International Conference on Asphalt Pavements, vol 2, pp 1073-1085, August 1997, Seattle, Washington, USA.
- Samuelsson A., Wiberg N-E., 1993: Byggnadsmekanik – Hållfasthetslära. Studentlitteratur, Lund.
- Sharp K.G., 2004: Full Scale Accelerated Pavement Testing – A Southern Hemisphere and Asian Perspective. 2nd International Conference on Accelerated Pavement Testing, September 2004, Minneapolis, Minnesota, USA.
- Smith M.R., Collis L., 1993: Aggregates – Sand, gravel and crushed rock aggregates for construction purposes. The Geological Society, London, UK.
- Solminihaç H., Cabrera C. & Bengoa E., 2004: Asphalt Pavement Structural Evaluation during Road Construction Using Falling Weight Deflectometer. Transport Research Board 83th Annual Meeting January 2004, Washington, D.C, USA.
- SS-EN 13286-2:2004, 2004: Obundna och hydrauliskt bundna vägmateriäl - Del 2: Provningsmetod för laboratoriemässig bestämning av referensdensitet och vatteninnehåll – Proctorinstämning. SIS - Bygg och anläggning, Stockholm.
- Sweere G.T.H., 1990: Unbound granular bases for roads. PhD Thesis, Delft University of Technology, Delft, The Netherlands.
- Theyse H.L., 1997: Mechanistic-Empirical Modelling of the Permanent Deformation of Unbound Pavement Layers. Eighth International Conference on Asphalt Pavements, August 1997, Seattle, Washington, USA.
- Tholén O., 1980: Falling weight deflectometer – a device for bearing capacity measurements: properties and performance. Department of highway engineering, Royal Institute of Technology, Stockholm.
- Thom N.H., 1988. Design of road foundation. PhD Thesis, Civil Engineering, University of Nottingham, Nottingham, UK.
- Troadec J.P., Dodds J.A., 1993: Global geometrical description of homogeneous hard sphere packings. Random materials and processes, Disorder and granular media, pp 1 – 34, Elsevier, Amsterdam, The Netherlands.

References

- Tseng K., Lytton R., 1989: Prediction of Permanent Deformation in Flexible Pavement Materials. Implication of Aggregates in the Design, Construction, and Performance of Flexible Pavements, ASTM STP 1016, ASTM
- Ullidtz P., Askegaard V., Sjolín F.O, 1996: Normal Stresses in a Granular Material Under Falling Weight Deflectometer Loading. Transport Research Board 75th Annual Meeting January 1996, Washington, D.C, USA.
- Ullidtz P., 1997: Modelling of Granular Materials Using the Discrete Element Method. Eighth International Conference on Asphalt Pavements, August 1997, Seattle, Washington, USA.
- Ullidtz P., 1998: Modelling Flexible Pavement Response and Performance. Polyteknisk Forlag, Lyngby, Denmark.
- Uzan J. 1999: Permanent Deformation of a Granular Base Material. Transport Research Board 78th Annual Meeting January 1999, Washington, D.C, USA.
- Uzan J., 1985: Characterization of Granular Materials. Transport Research Record No 1022, Washington DC, USA.
- Yoder E.J., Witczak M.W., 1975: Principles of pavement design. Wiley-interscience publication, New York, USA.
- VV (2005): Användarmanual PMS Objekt. http://www.vv.se/templates/page3____7818.aspx.
- Werkmeister S., 2003: Permanent Deformation Behaviour of Unbound Granular Materials. PhD Thesis, University of Technology Dresden, Germany.
- Werkmeister S., Wellner F., Oeser M., Moeller B., 2004: Design criteria of granular pavements layers. Proceedings of the 6th international symposium on pavements unbound (UNBAR 6) July 2004, Nottingham, England, UK.
- Werkmeister S., Steven B., Alabaster D., Arnold G., Oeser M., 2005: 3D Finite Element analysis of accelerated pavement test results from New Zealand's CAPTIF Facility. The 7th International Conference on the Bearing Capacity of Roads and Airfields, June 2005, Trondheim, Norway.
- Witczak M.W., May R.W., 1981: Effective Granular Modulus to Model Pavement Response. Transport Research Record No 810, pp. 1-9, Washington DC, USA.
- Wolff H., Visser A.T., 1994: Incorporating elasto-plasticity in granular layer pavement design. Proc. Instn Civ. Engrs Transp., 1994, 105, Nov., pp 259-272.

References

APPENDICES

- Appendix A: Classification of the tested materials
- Appendix B: Results from the laboratory test
- Appendix C: Evaluation of deformation behavior
- Appendix D: Evaluation of material models
- Appendix E: Derivation of strength parameters
- Appendix F: Evaluation of the empirical expression of internal friction angle
- Appendix G: Derivation of the relationship between k_1 , k_2 , θ and M_r
- Appendix H: Graphic presentation of the $k_1 - k_2$ relationship for each test cell separately

Appendix

Appendix A

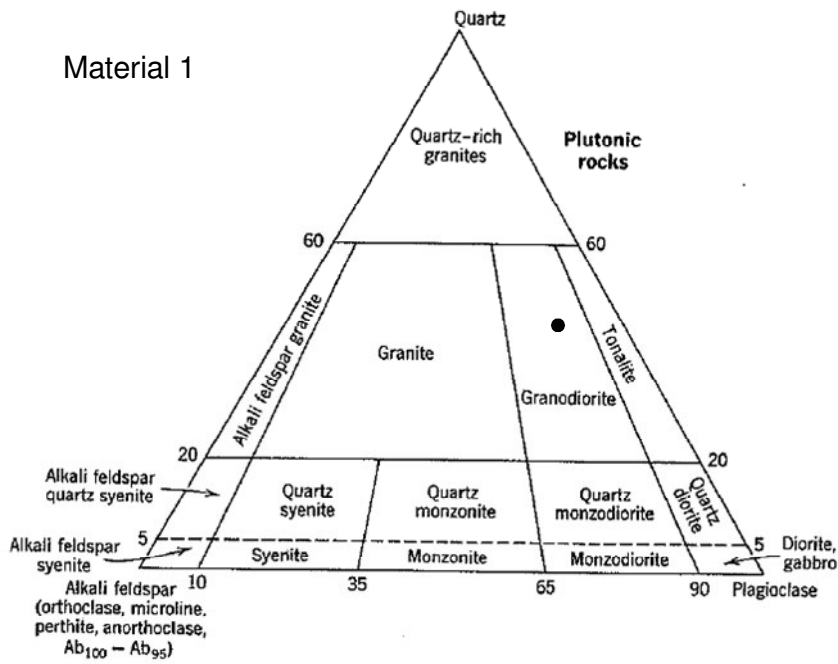


Figure A1. Classification of Material 1 as a Granodiorite.

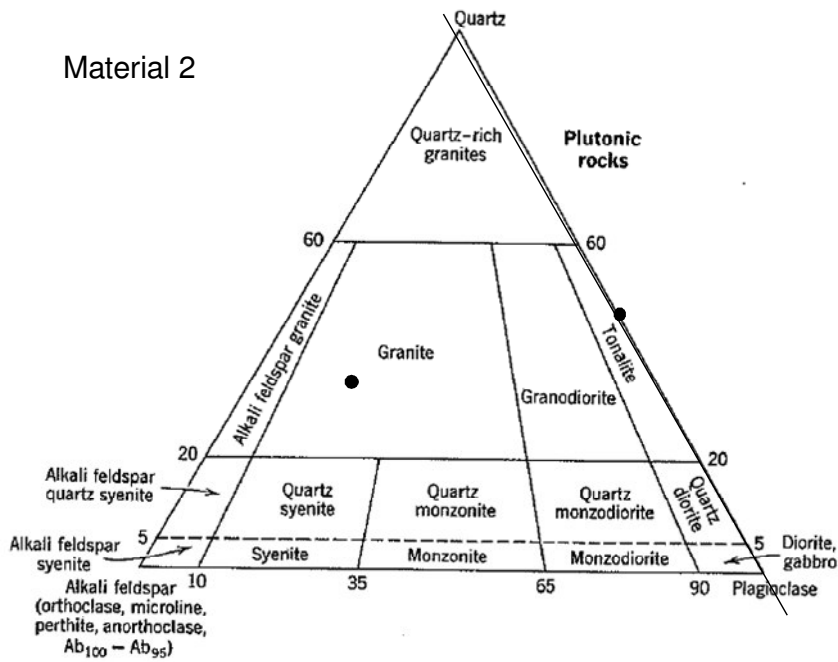


Figure A2. Classification of Material 2 as a mixed of a Granite and a Tonalite.

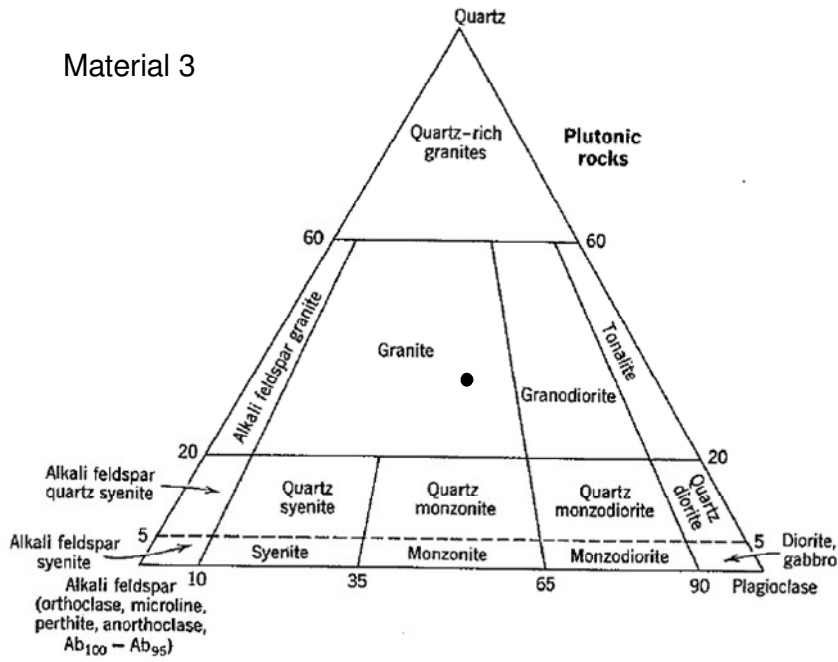


Figure A3. Classification of Material 3 as a Granite.

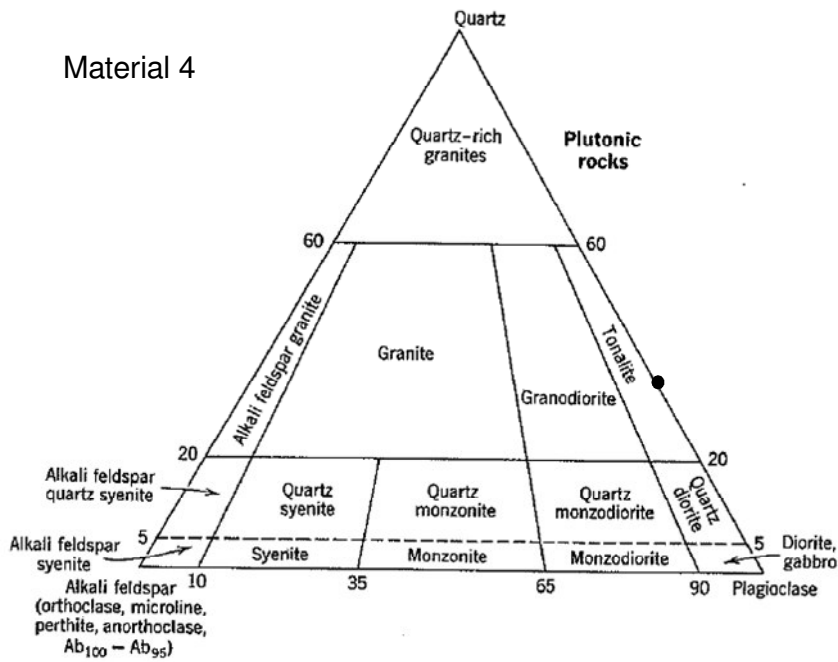


Figure A4. Classification of Material 4 as a Tonalite.

Appendix B

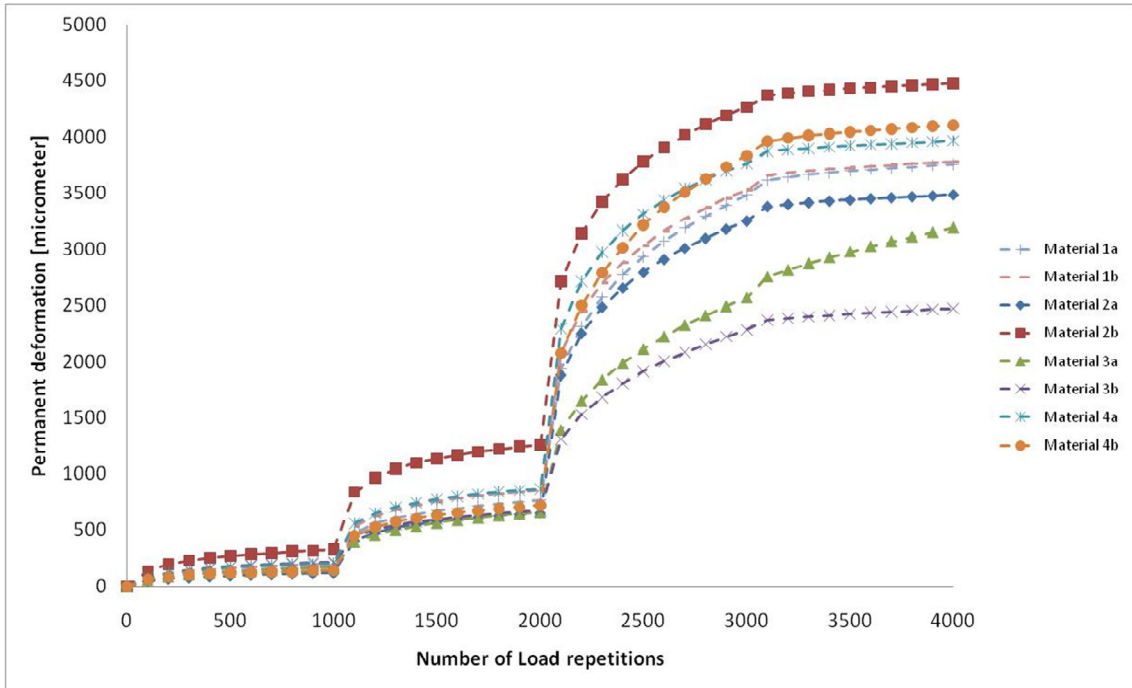


Figure B1. Permanent deformation the first 4000 load repetitions for material 1 to 4 and water content 80% of optimum.

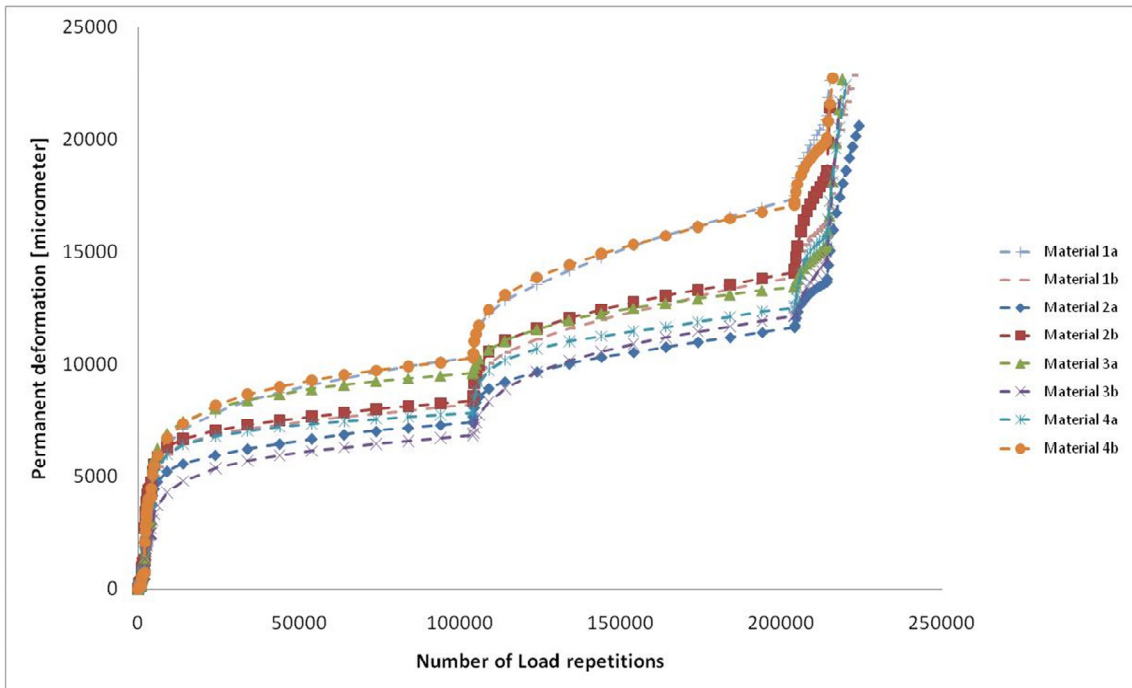


Figure B2. Permanent deformation all load repetitions for material 1 to 4 and water content 80% of optimum.

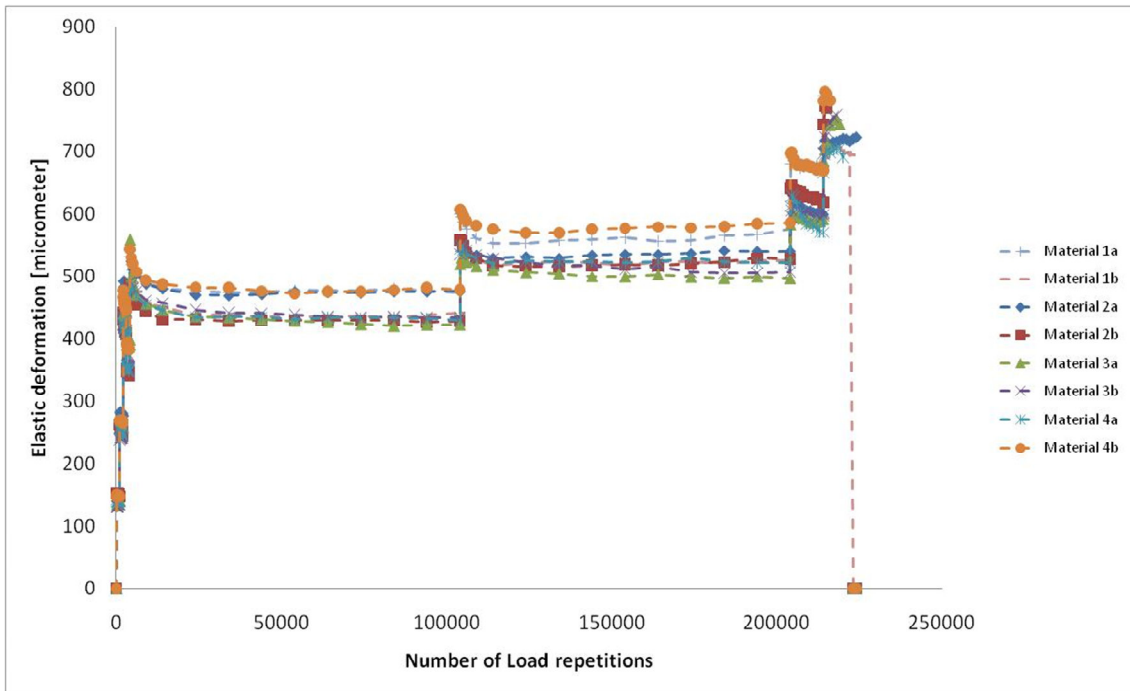
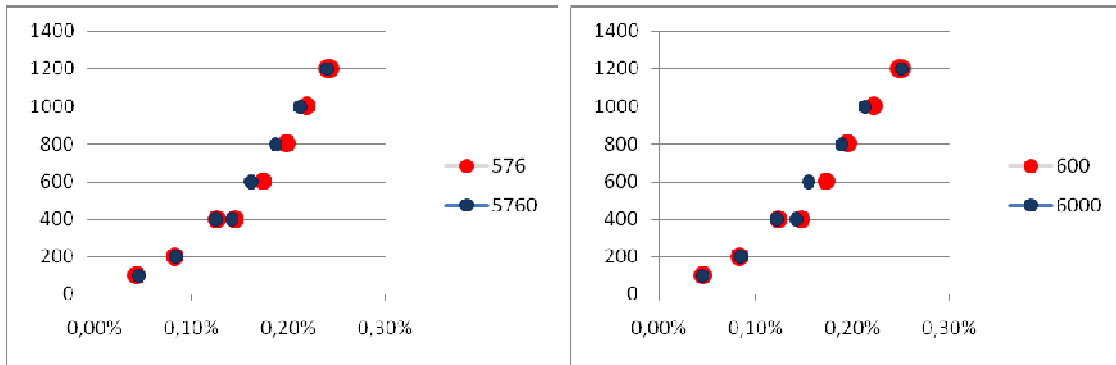
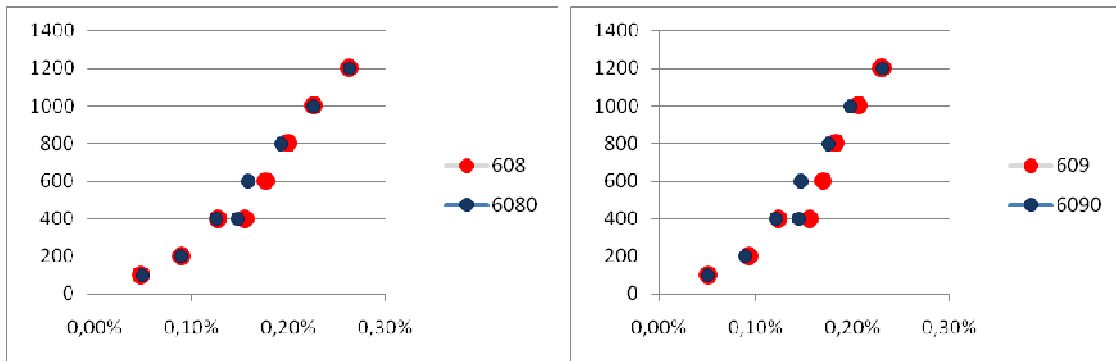


Figure B3. Elastic deformation during the triaxial test of all materials for all load repetitions

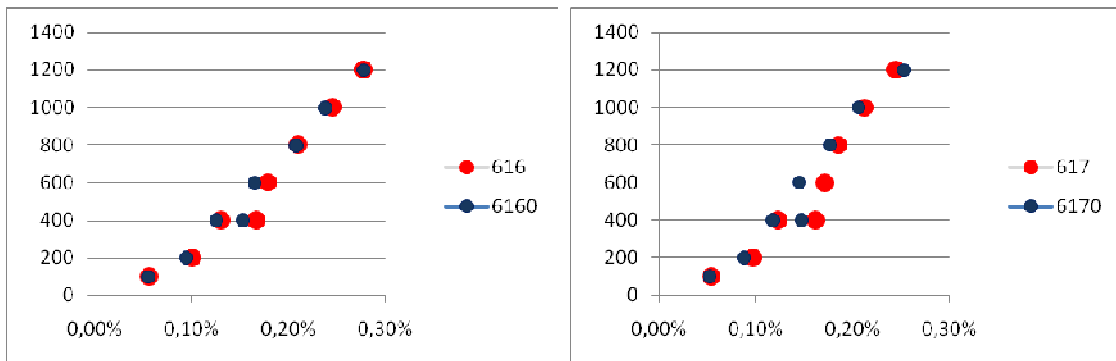
Appendix



60%



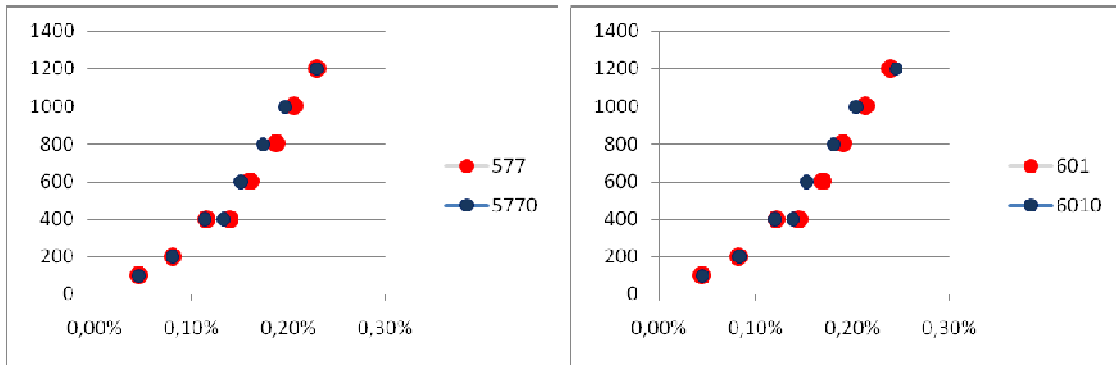
80%



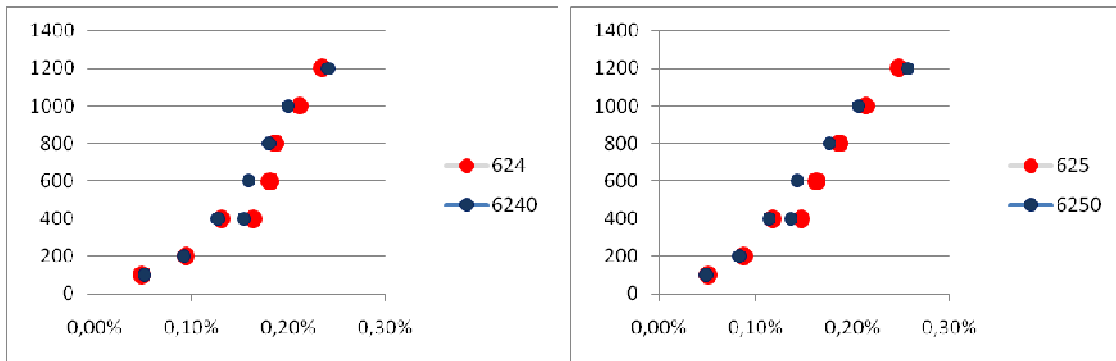
100%

Figure B4. The stress-strain relationship for all eight load steps in the triaxial test at the 100th and the last load repetition for Material 1 and at a water content of 60% to 100% of optimum.

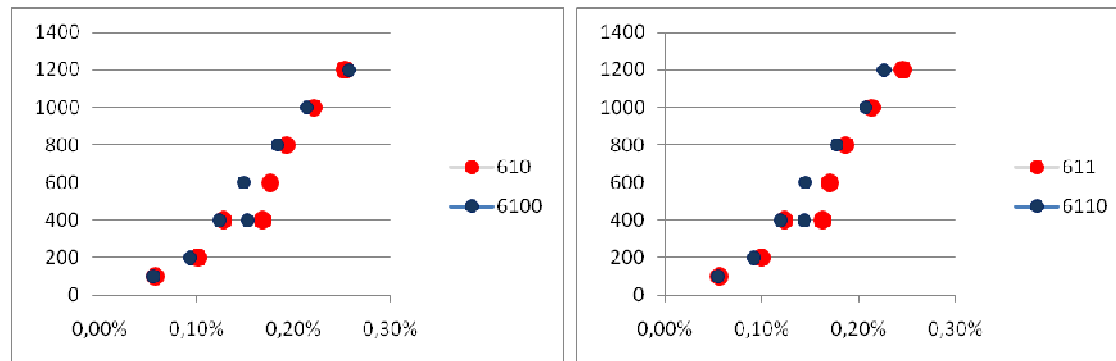
Appendix



60%



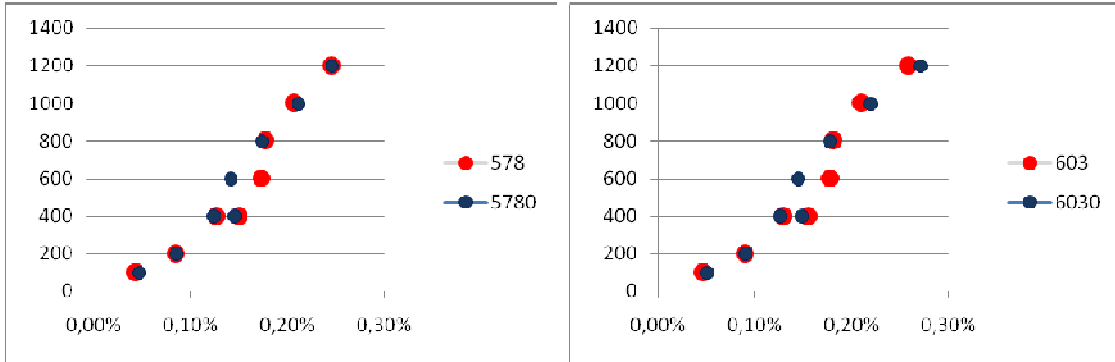
80%



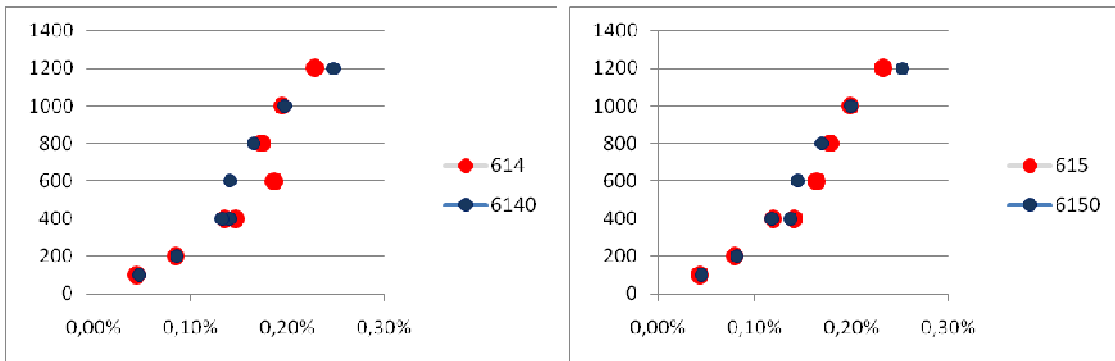
100%

Figure B5. The stress-strain relationship for all eight load steps in the triaxial test at the 100th and the last load repetition for Material 2 and at a water content of 60% to 100% of optimum.

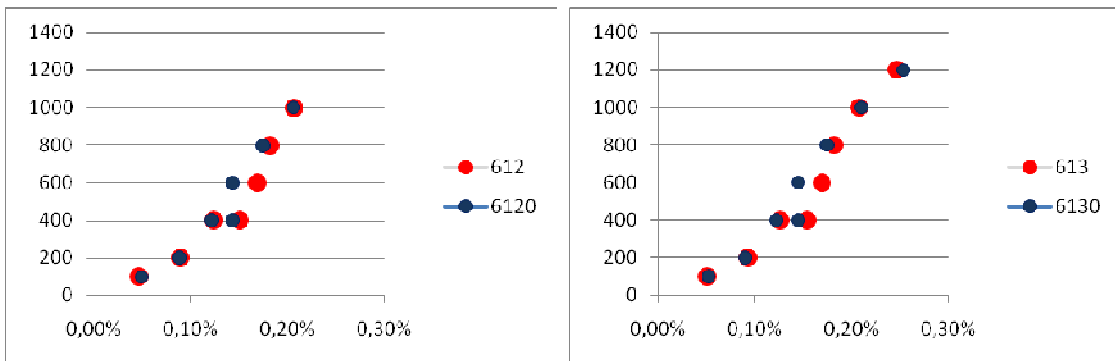
Appendix



60%



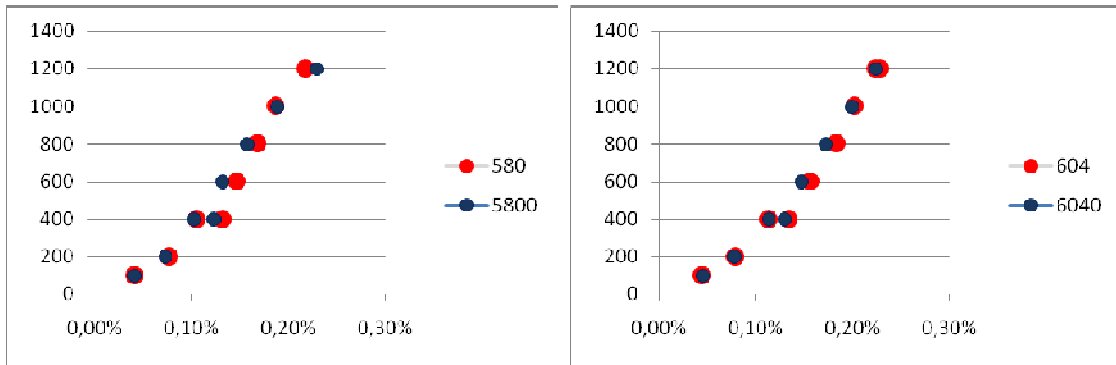
80%



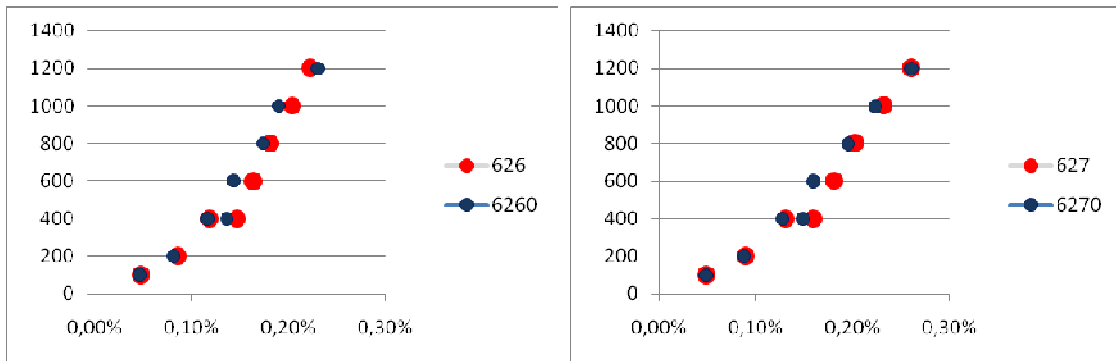
100%

Figure B6. The stress-strain relationship for all eight load steps in the triaxial test at the 100th and the last load repetition for Material 3 and at a water content of 60% to 100% of optimum.

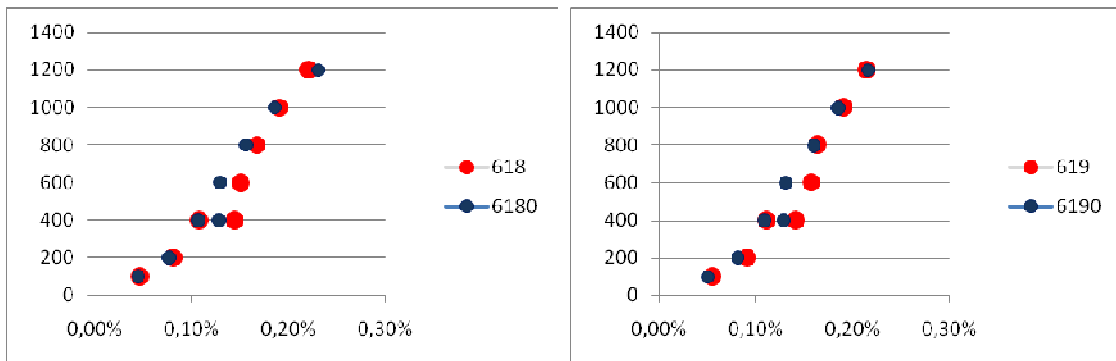
Appendix



60%



80%



100%

Figure B7. The stress-strain relationship for all eight load steps in the triaxial test at the 100th and the last load repetition for Material 4 and at a water content of 60% to 100% of optimum.

Appendix C

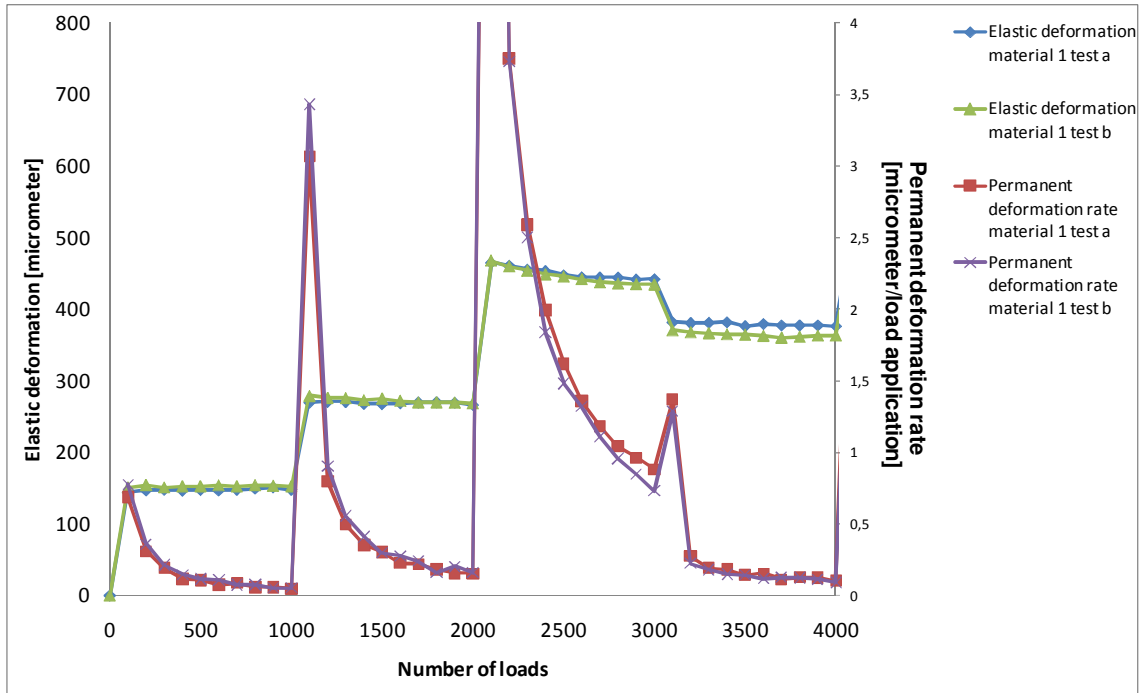


Figure C1. Comparison of elastic deformation and permanent deformation rate for load cycle 0 to 4000 of Material 1, water content 80% (test a and b).

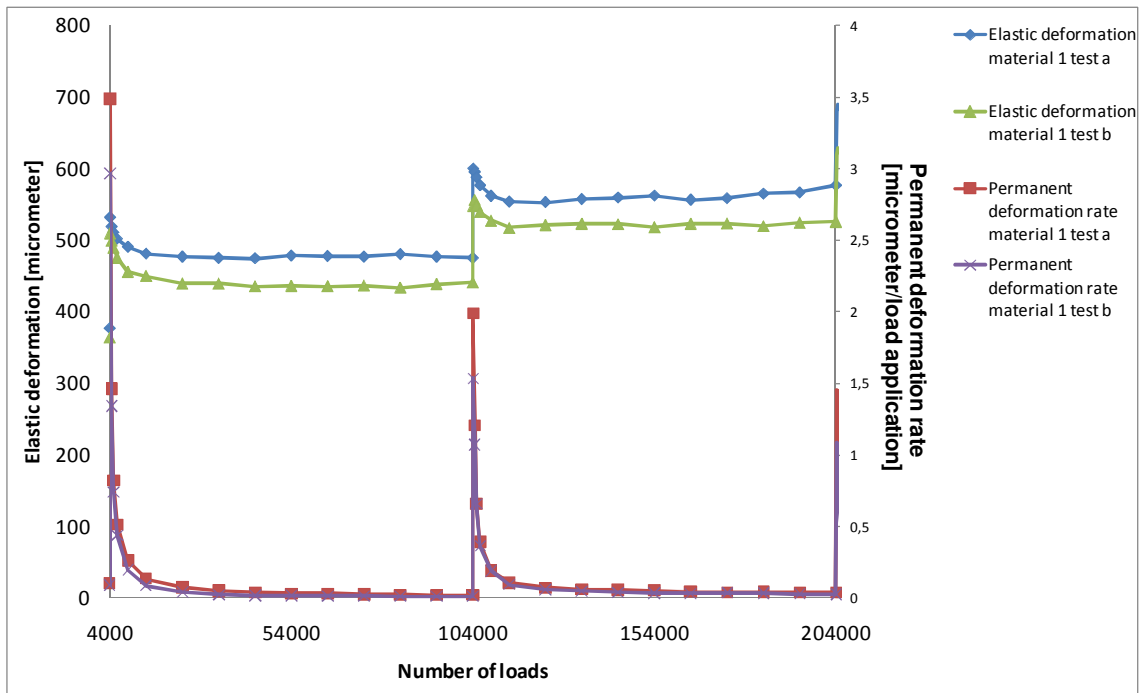


Figure C2. Comparison of elastic deformation and permanent deformation rate for load cycle 4000 to 204000 of Material 1, water content 80% (test a and b).

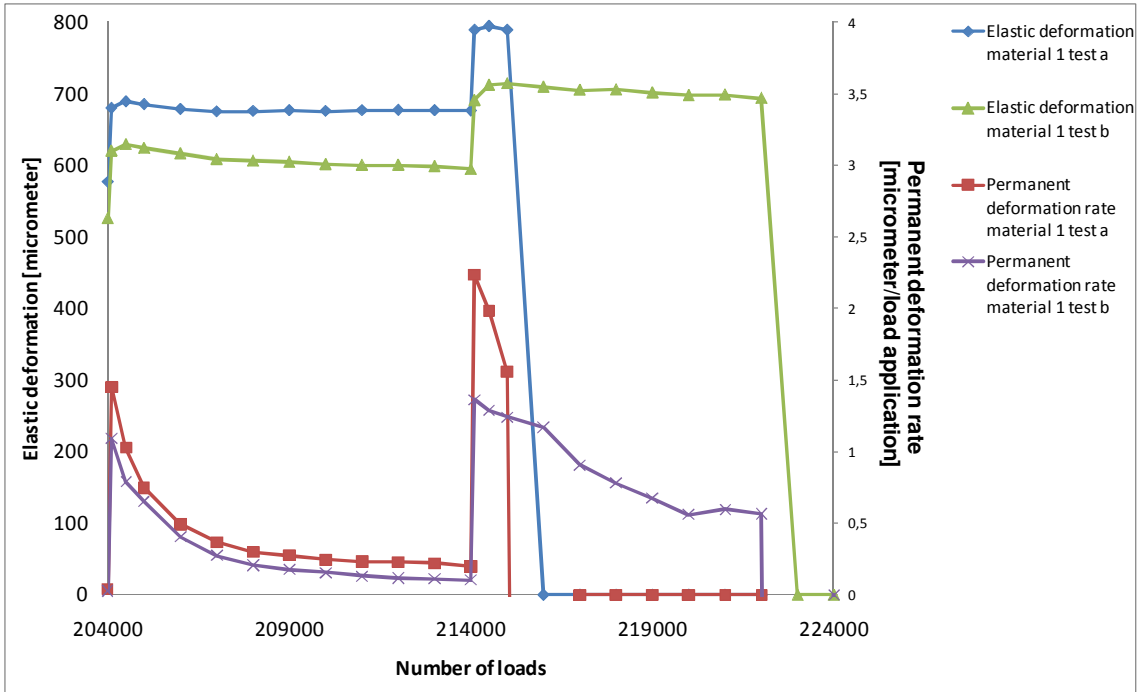


Figure C3. Comparison of elastic deformation and permanent deformation rate for load cycle 204000 to 224000 of Material 1, water content 80% (test a and b).

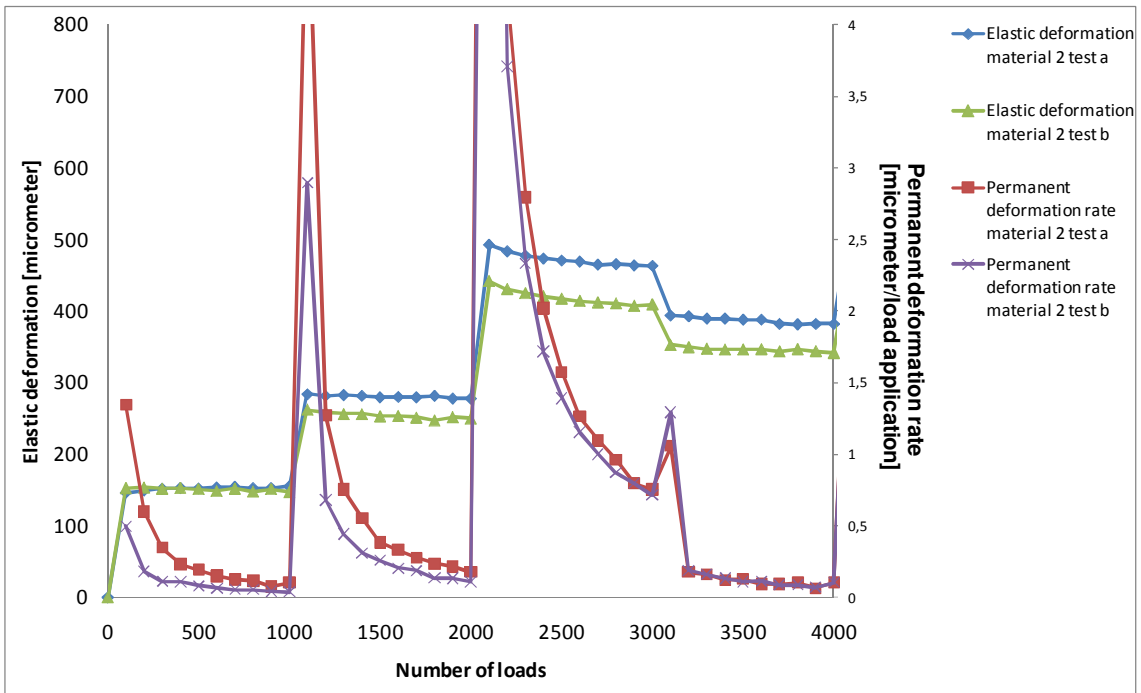


Figure C4. Comparison of elastic deformation and permanent deformation rate for load cycle 0 to 4000 of Material 2, water content 80% (test a and b).

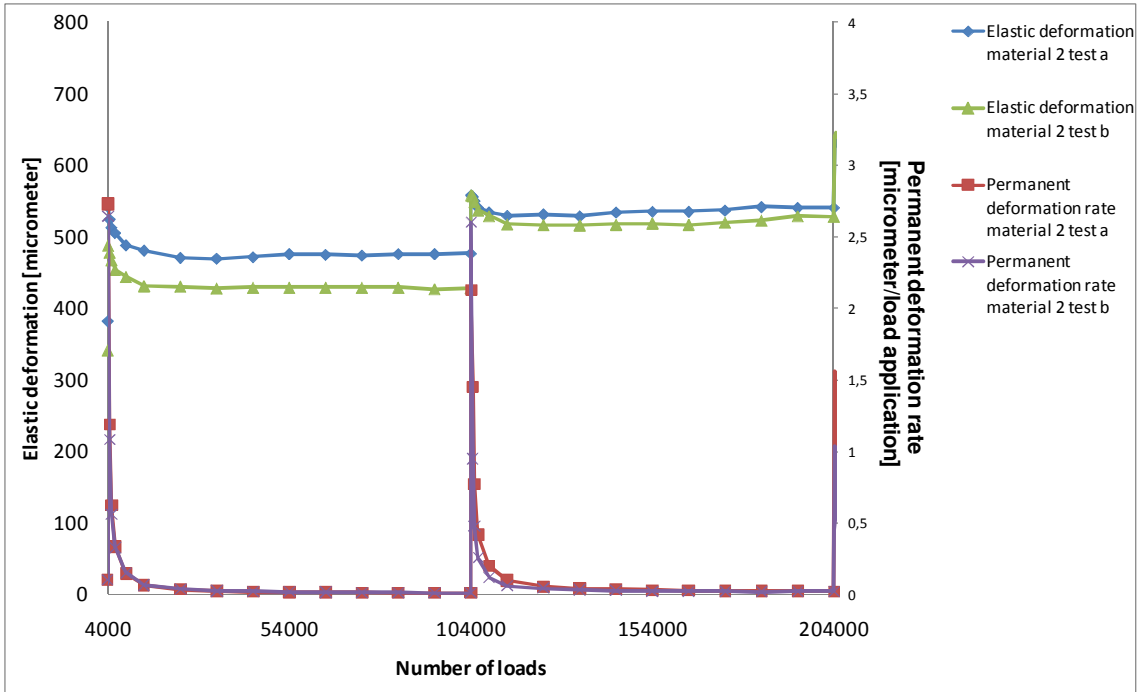


Figure C5. Comparison of elastic deformation and permanent deformation rate for load cycle 4000 to 204000 of Material 2, water content 80% (test a and b).

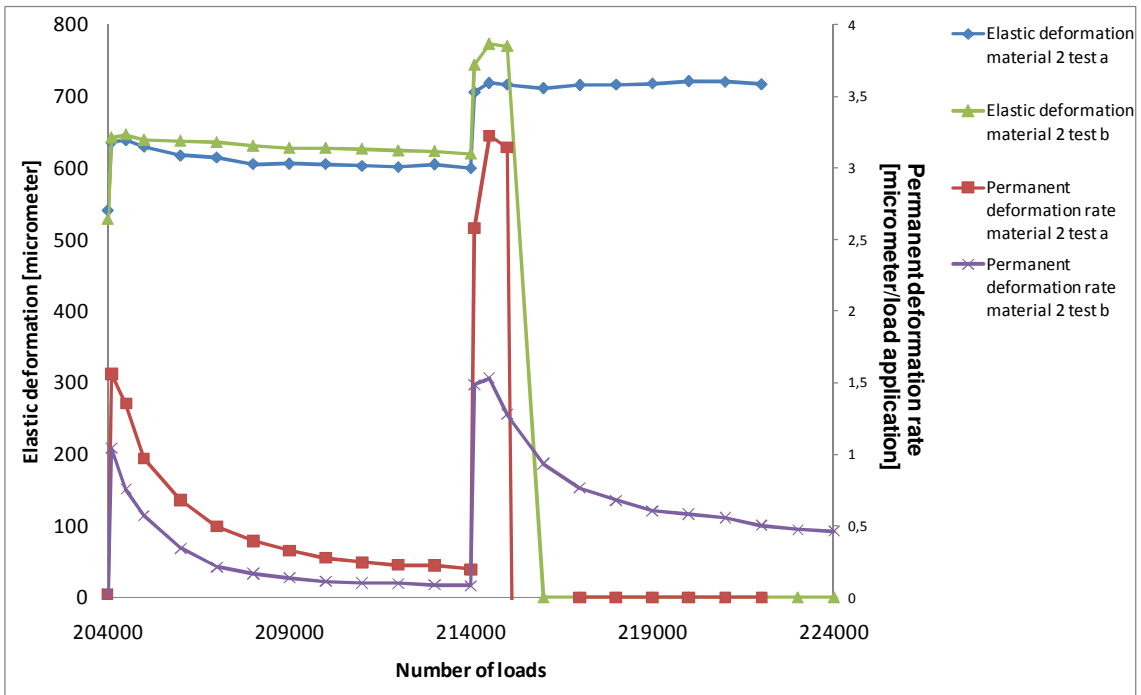


Figure C6. Comparison of elastic deformation and permanent deformation rate for load cycle 204000 to 224000 of Material 2, water content 80% (test a and b).

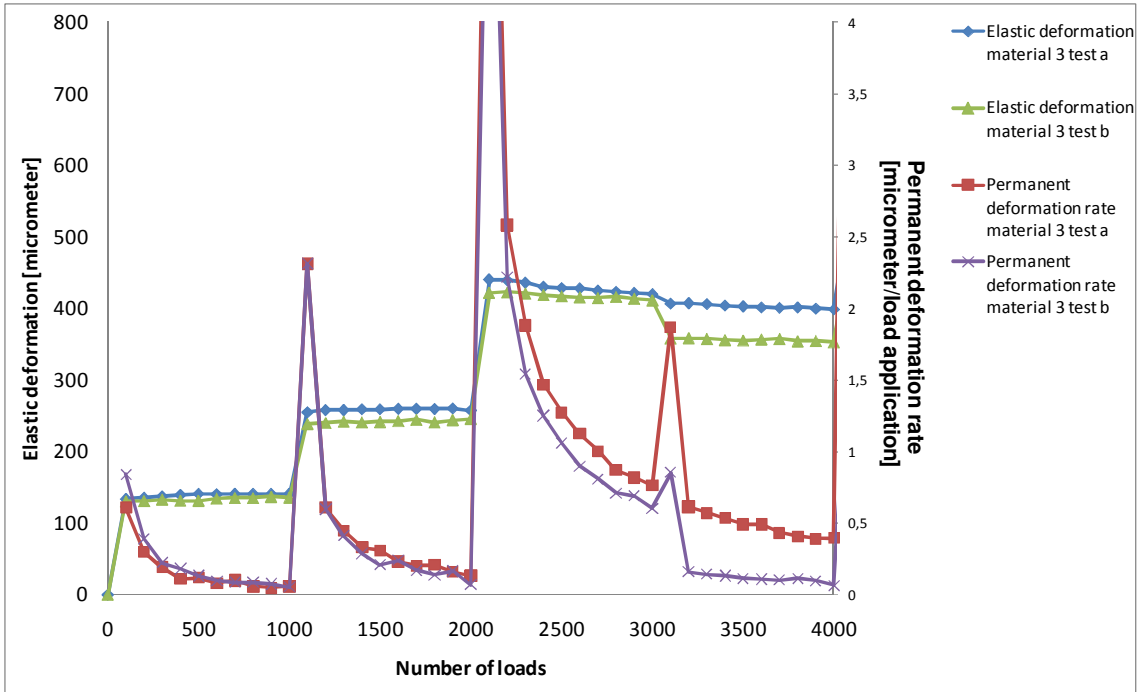


Figure C7. Comparison of elastic deformation and permanent deformation rate for load cycle 0 to 4000 of Material 3, water content 80% (test a and b).

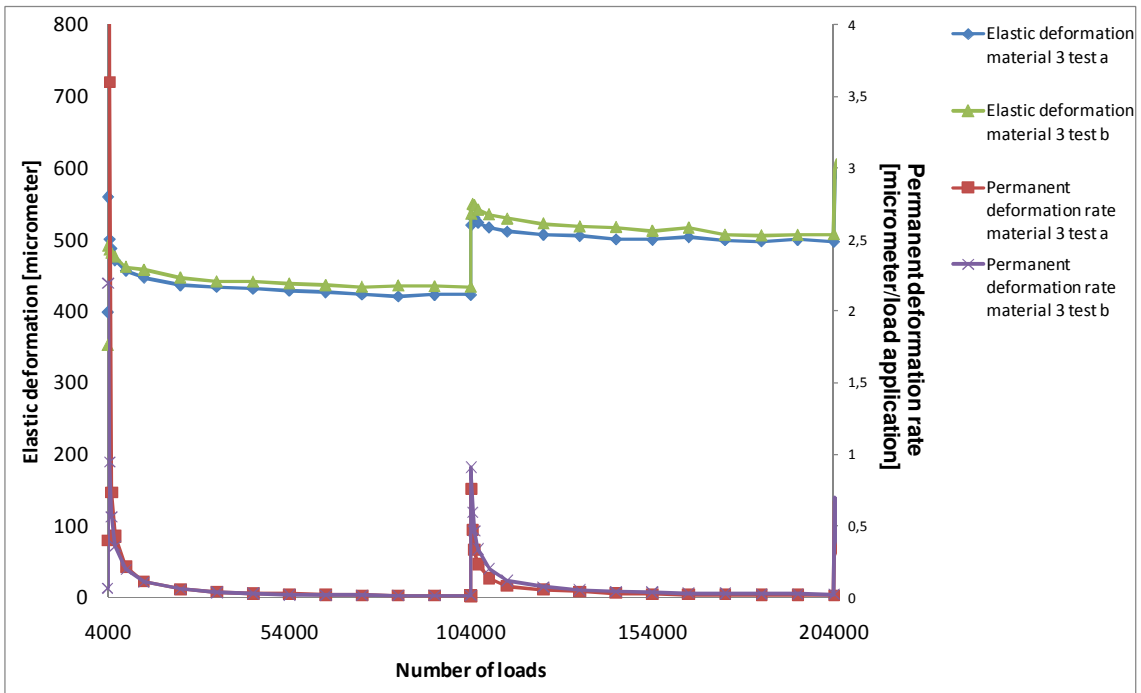


Figure C8. Comparison of elastic deformation and permanent deformation rate for load cycle 4000 to 204000 of Material 3, water content 80% (test a and b).

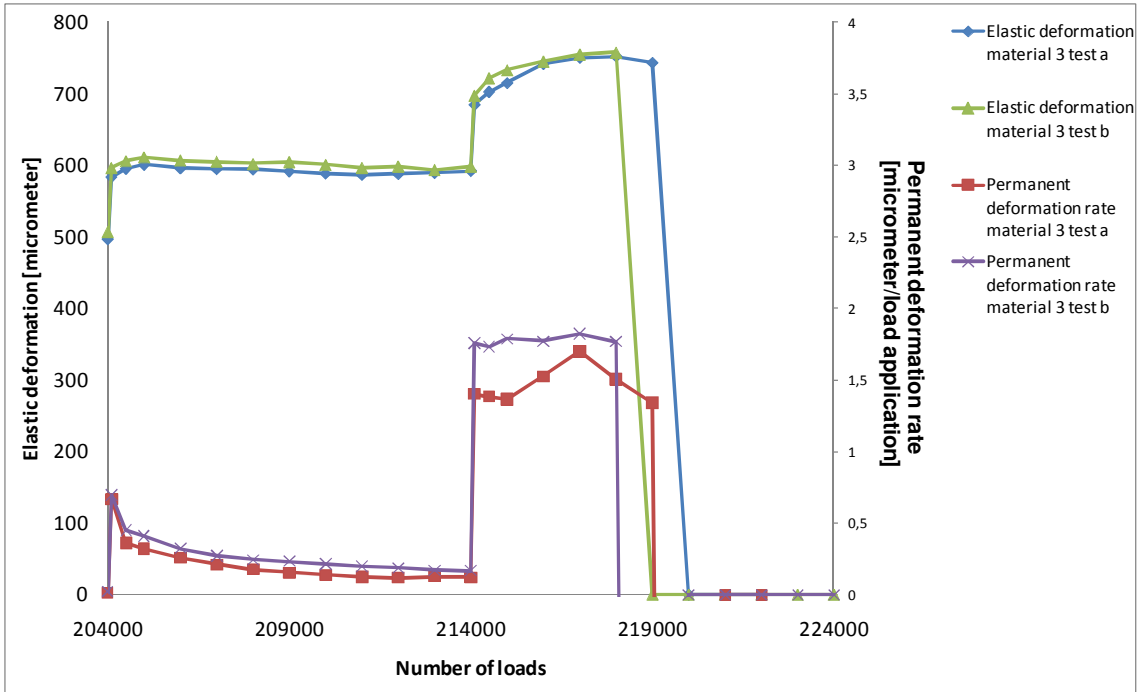


Figure C9. Comparison of elastic deformation and permanent deformation rate for load cycle 204000 to 224000 of Material 3, water content 80% (test a and b).

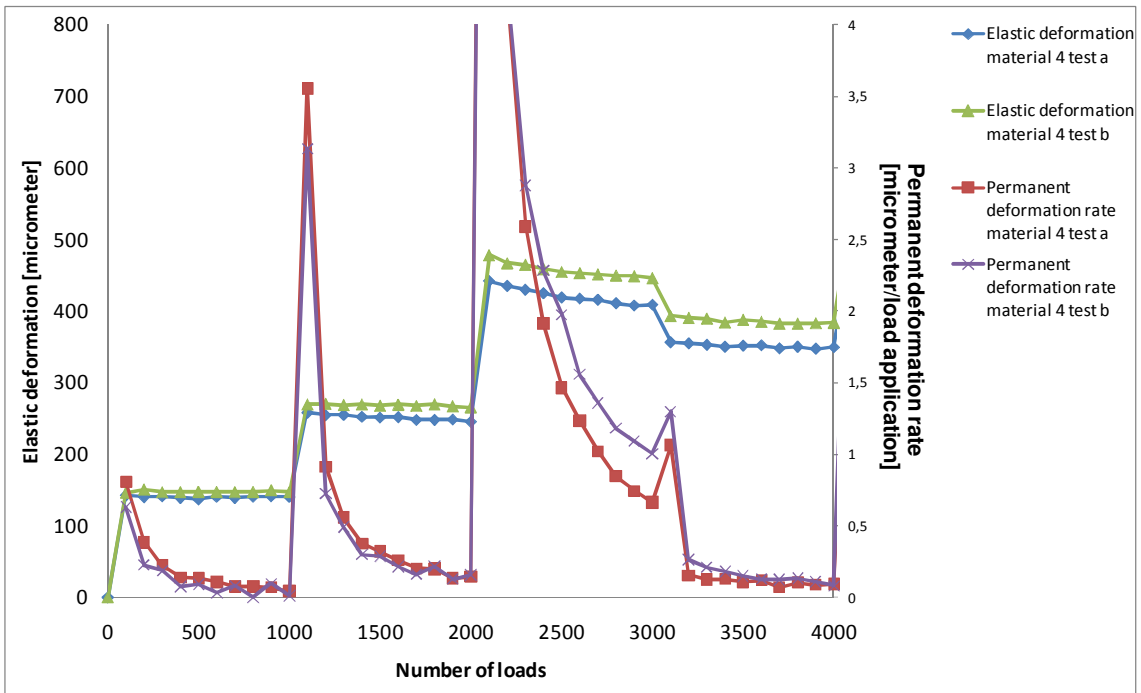


Figure C10. Comparison of elastic deformation and permanent deformation rate for load cycle 0 to 4000 of Material 4, water content 80% (test a and b).

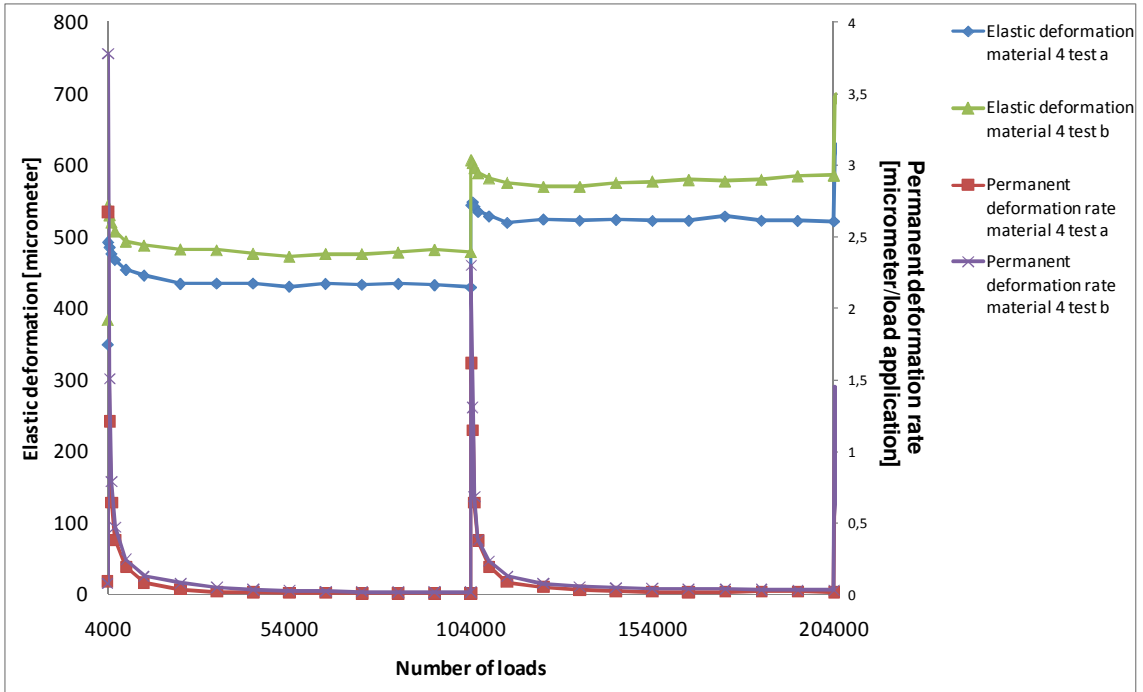


Figure C11. Comparison of elastic deformation and permanent deformation rate for load cycle 4000 to 204000 of Material 4, water content 80% (test a and b).

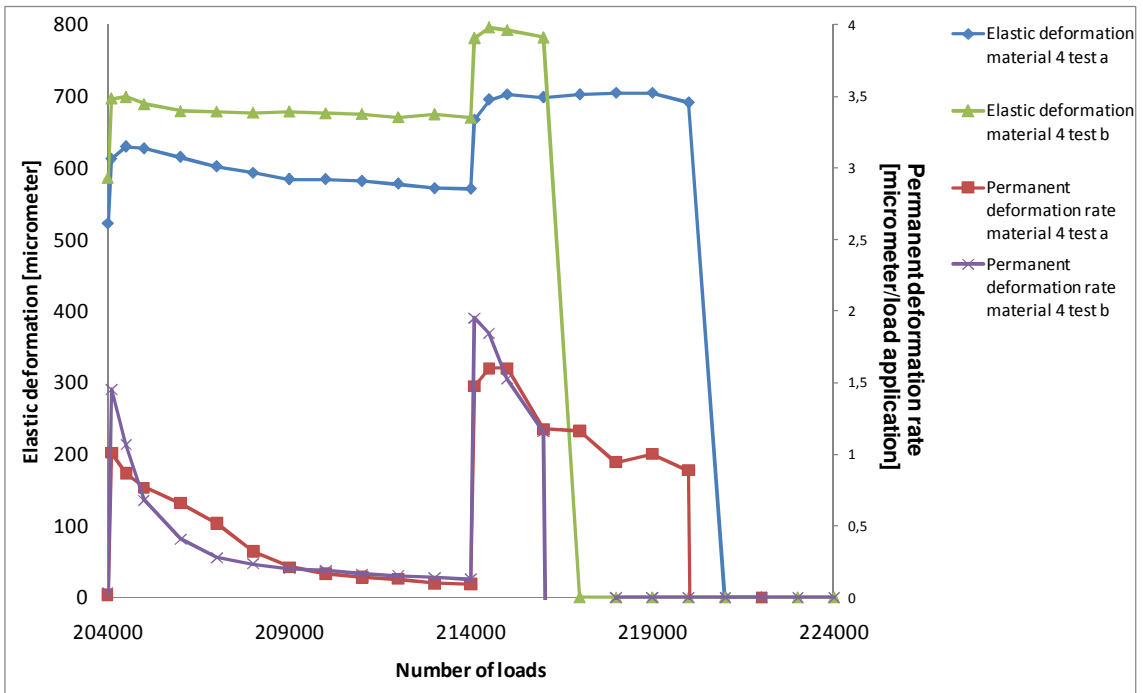


Figure C12. Comparison of elastic deformation and permanent deformation rate for load cycle 204000 to 224000 of Material 4, water content 80% (test a and b).

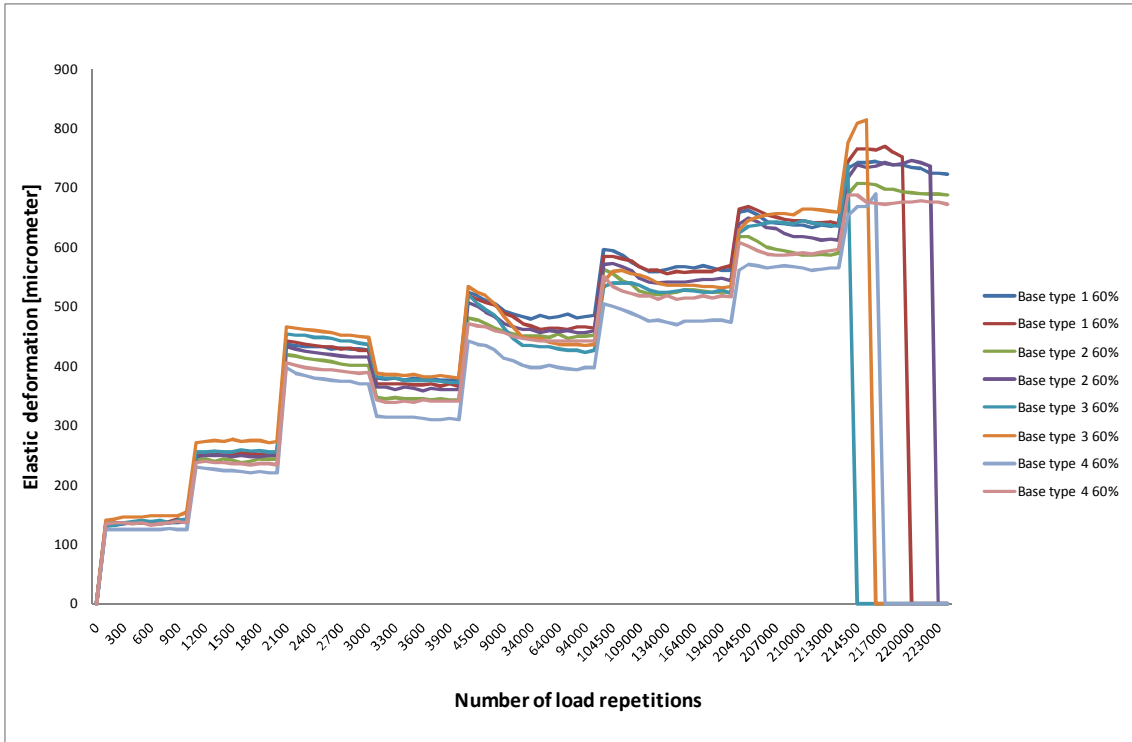


Figure C13. Elastic deformation for all load cycles and all material with water content 60% of optimum.

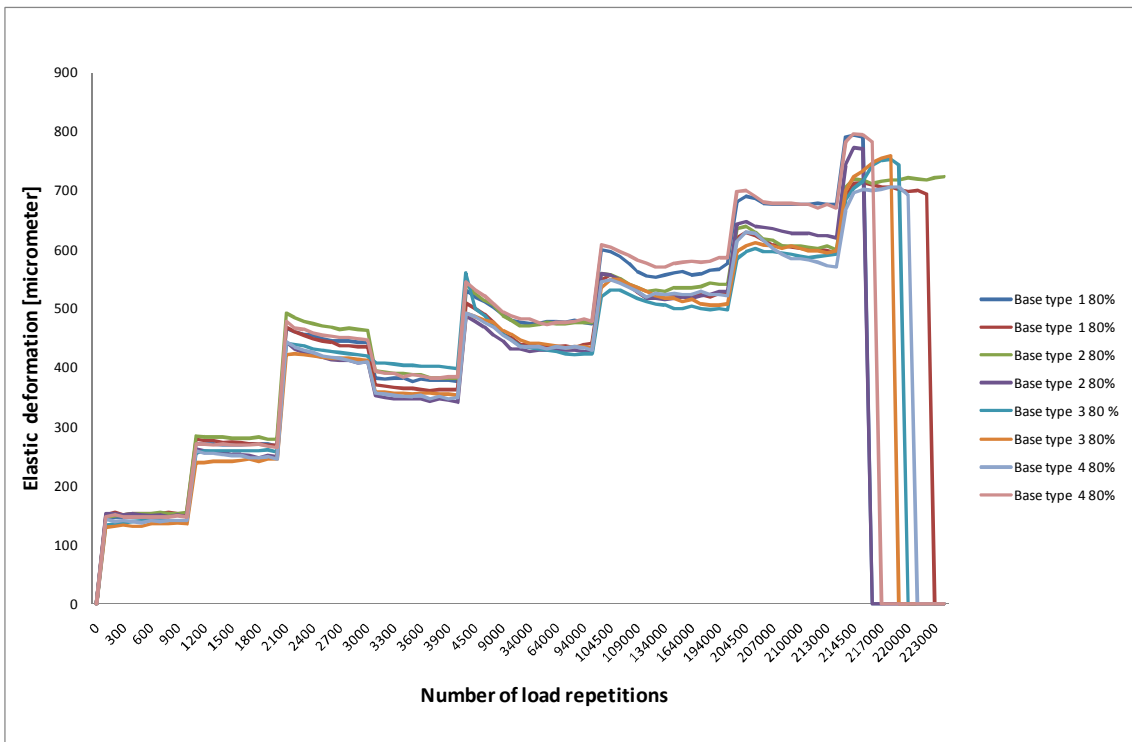


Figure C14. Elastic deformation for all load cycles and all material with water content 80% of optimum.

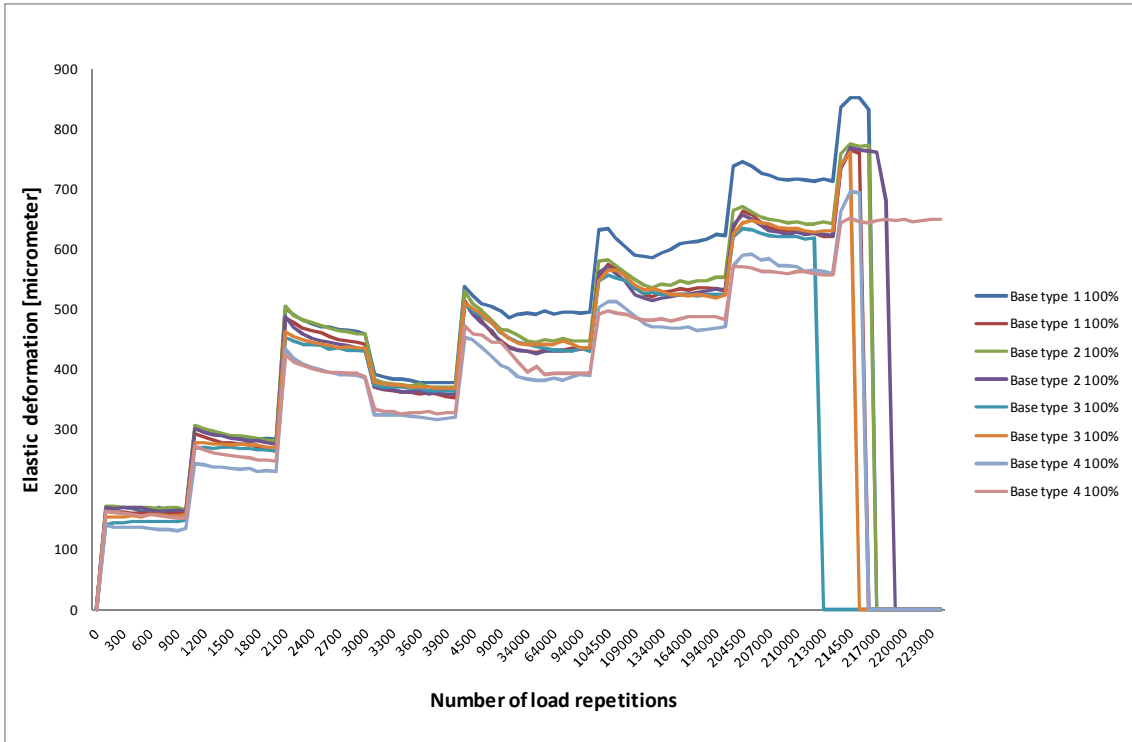


Figure C15. Elastic deformation for all load cycles and all material with water content 100% of optimum.

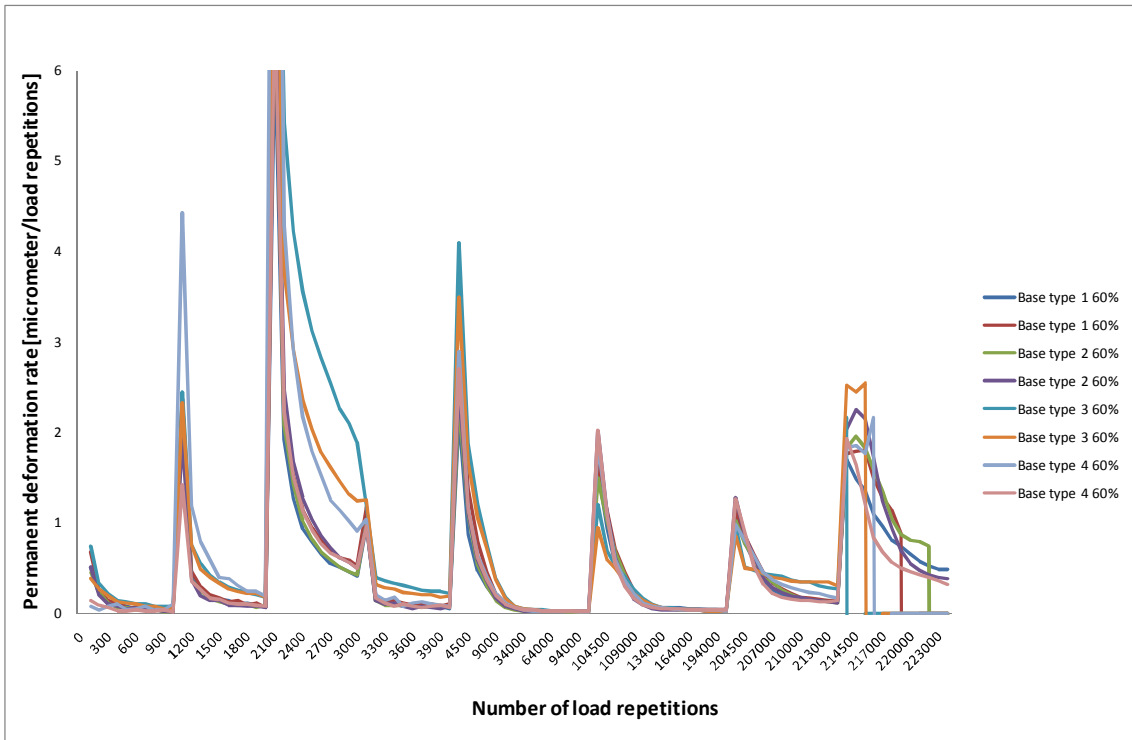


Figure C16. Permanent deformation rate for all load cycles and all material with water content 60% of optimum.

Appendix

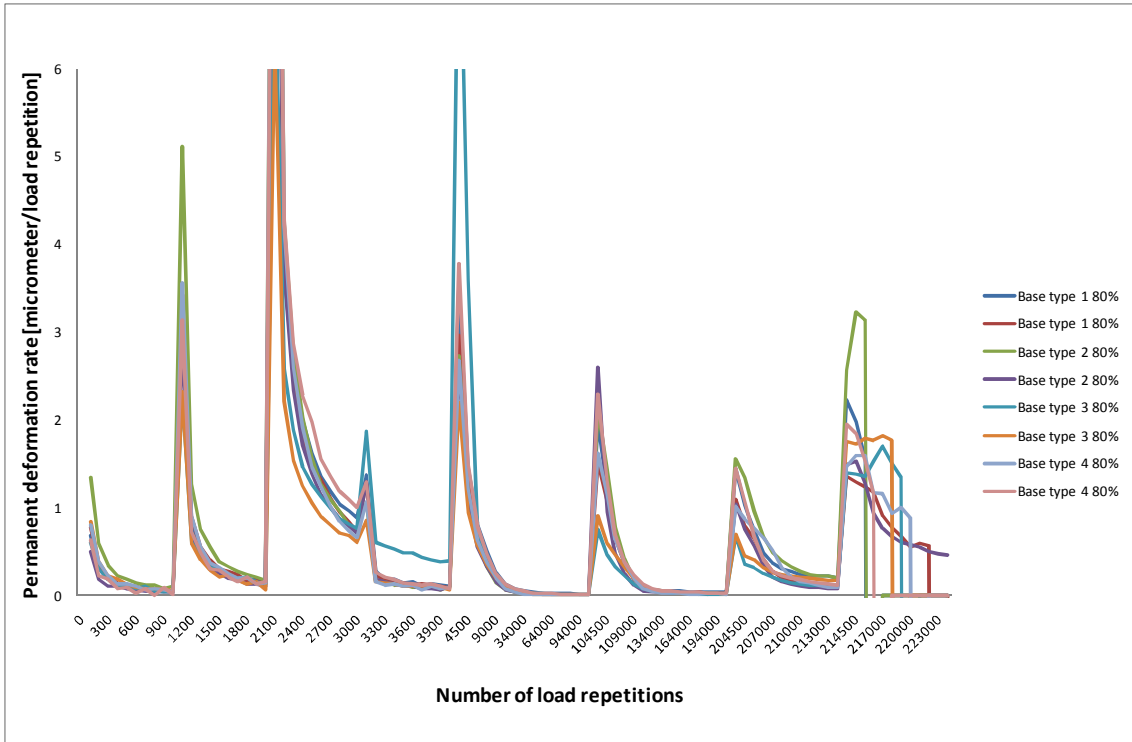


Figure C17. Permanent deformation rate for all load cycles and all material with water content 80% of optimum.

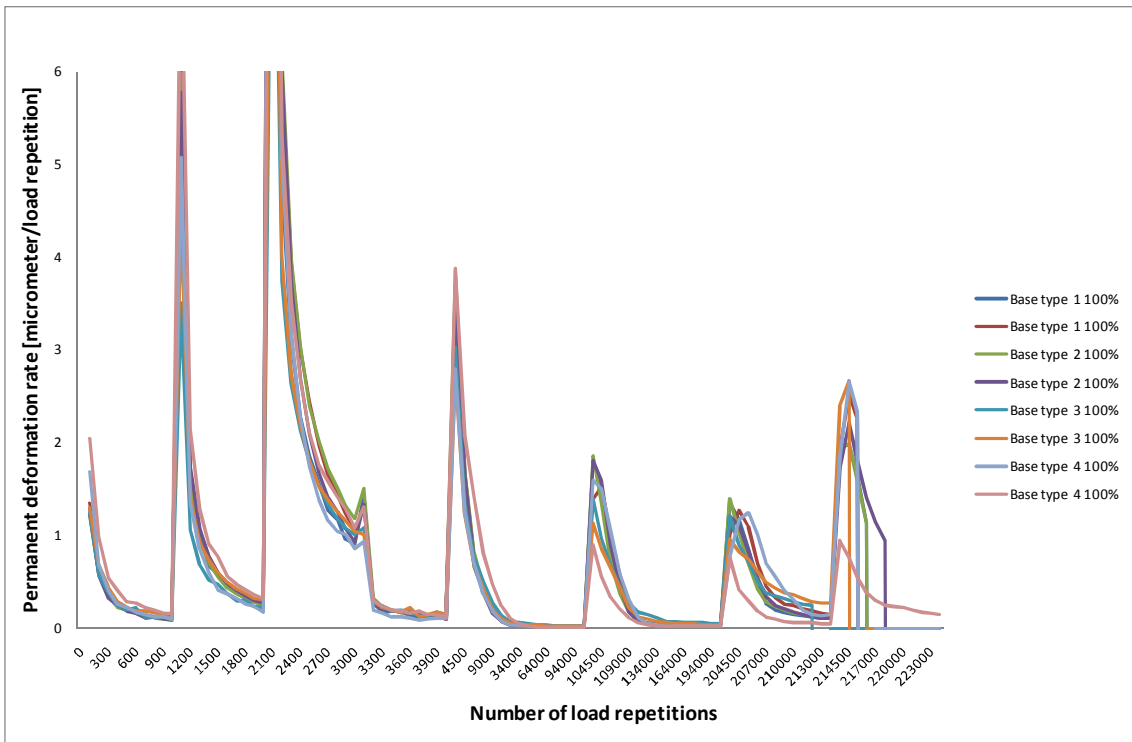


Figure C18. Permanent deformation rate for all load cycles and all material with water content 100% of optimum.

Appendix

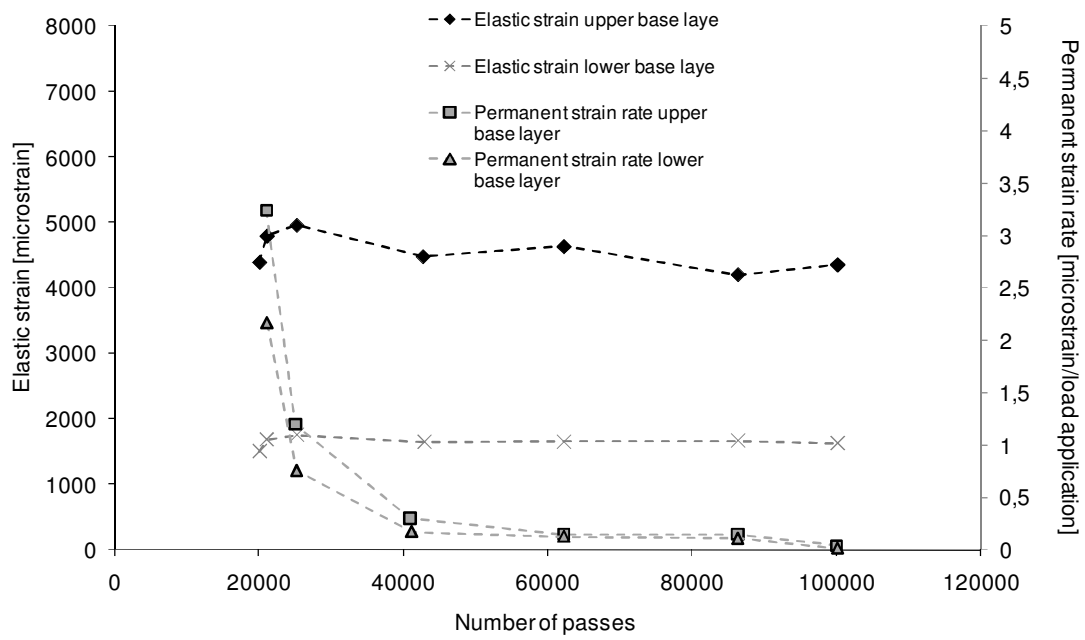


Figure C19. The relationship between elastic deformation and permanent deformation rate in the unbound base layer of Test Cell #2.

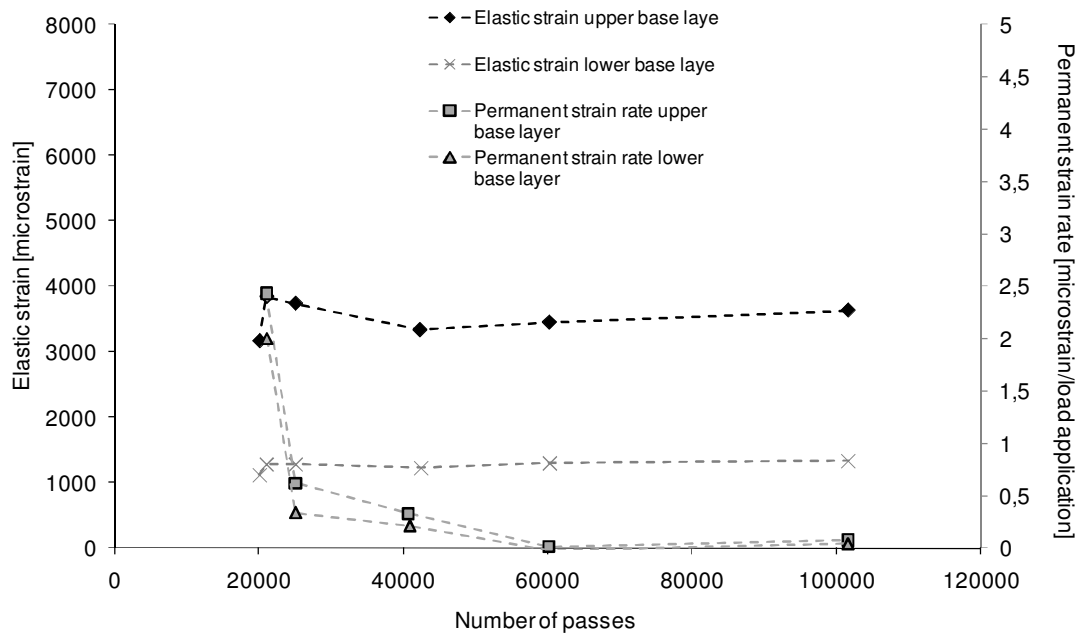


Figure C20. The relationship between elastic deformation and permanent deformation rate in the unbound base layer of Test Cell #3.

Appendix

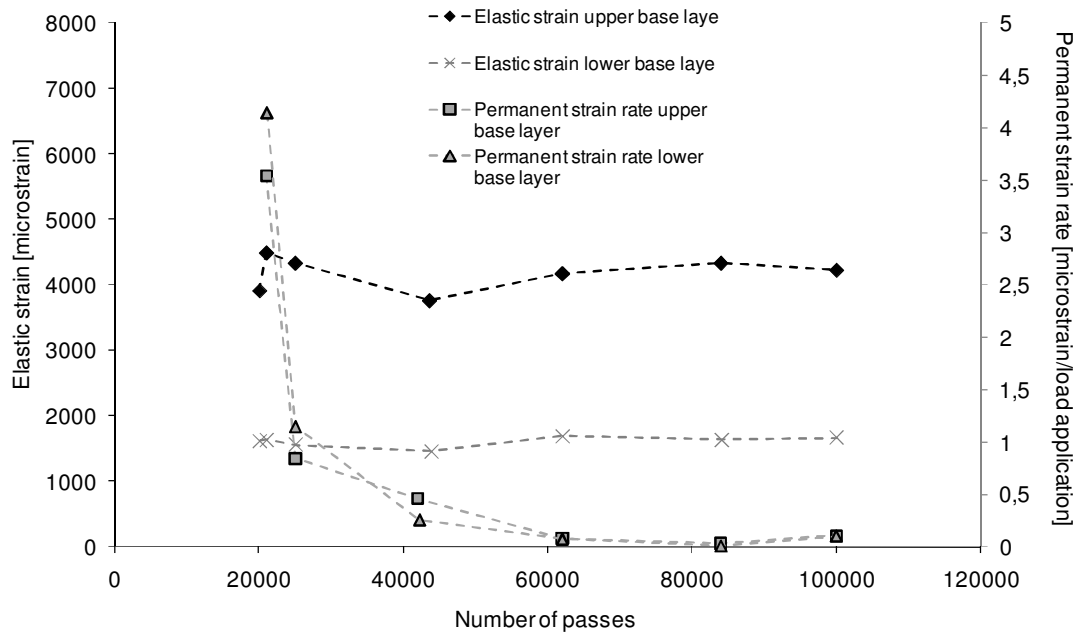


Figure C21. The relationship between elastic deformation and permanent deformation rate in the unbound base layer of Test Cell #4.

Appendix D

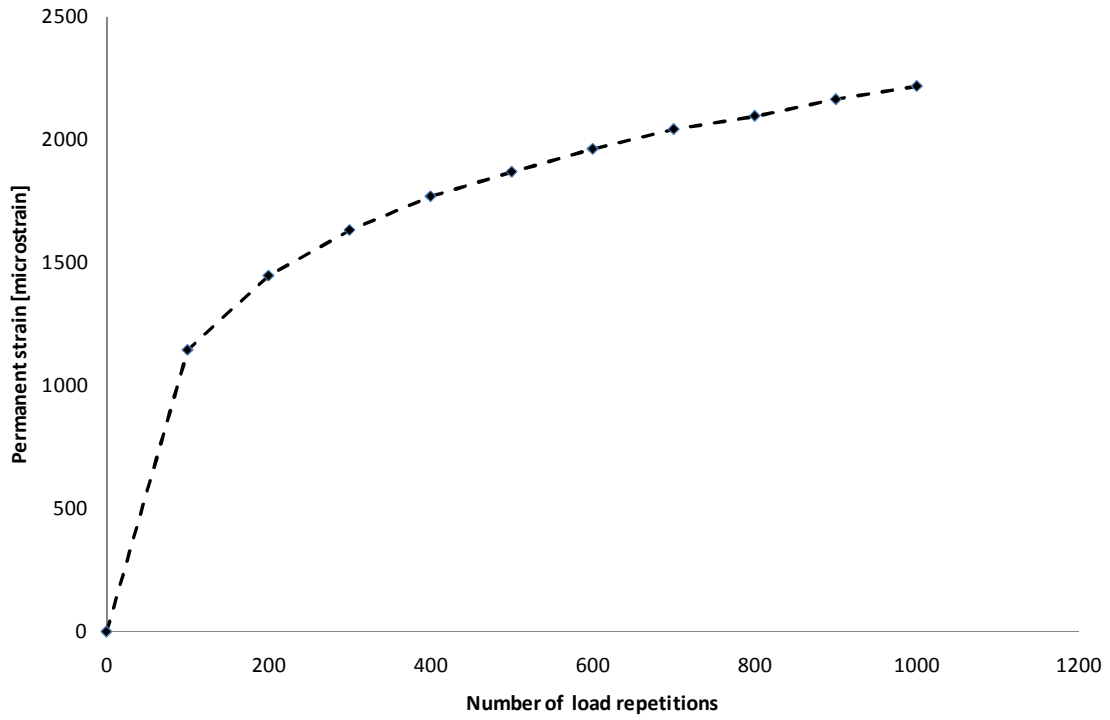


Figure D1. Material 1 80% water content of optimum load step 2 (load repetition 1000 - 2000), lin – lin relationship.

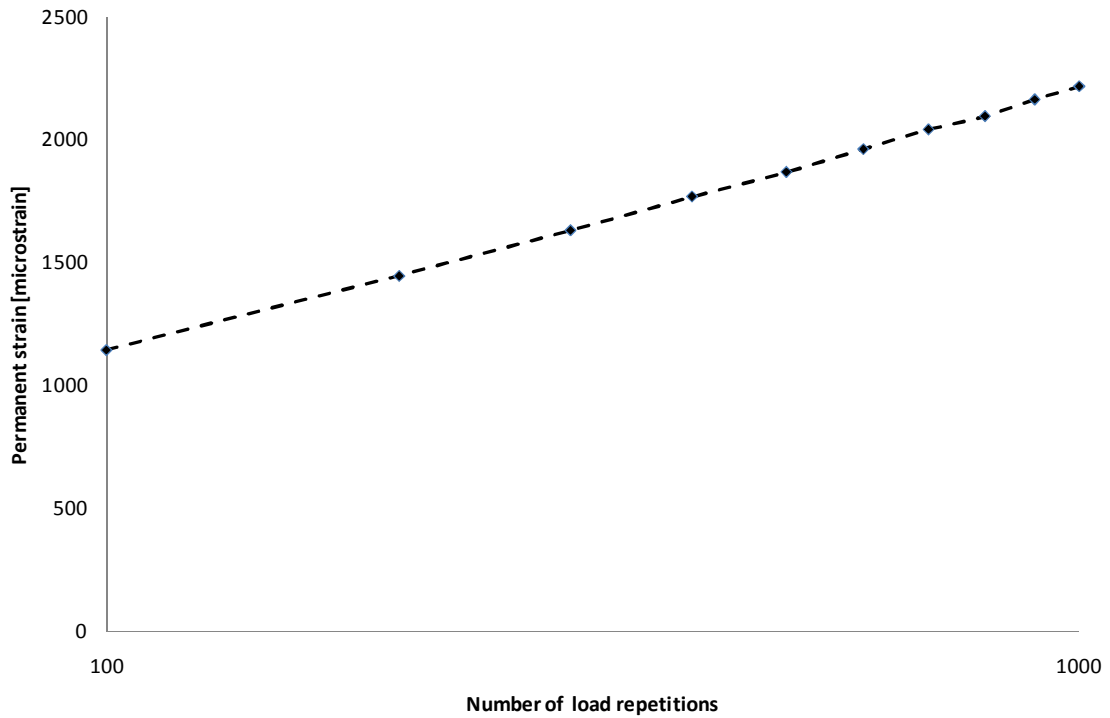


Figure D2. Material 1 80% water content of optimum load step 2 (load repetition 1000 - 2000), lin – log relationship.

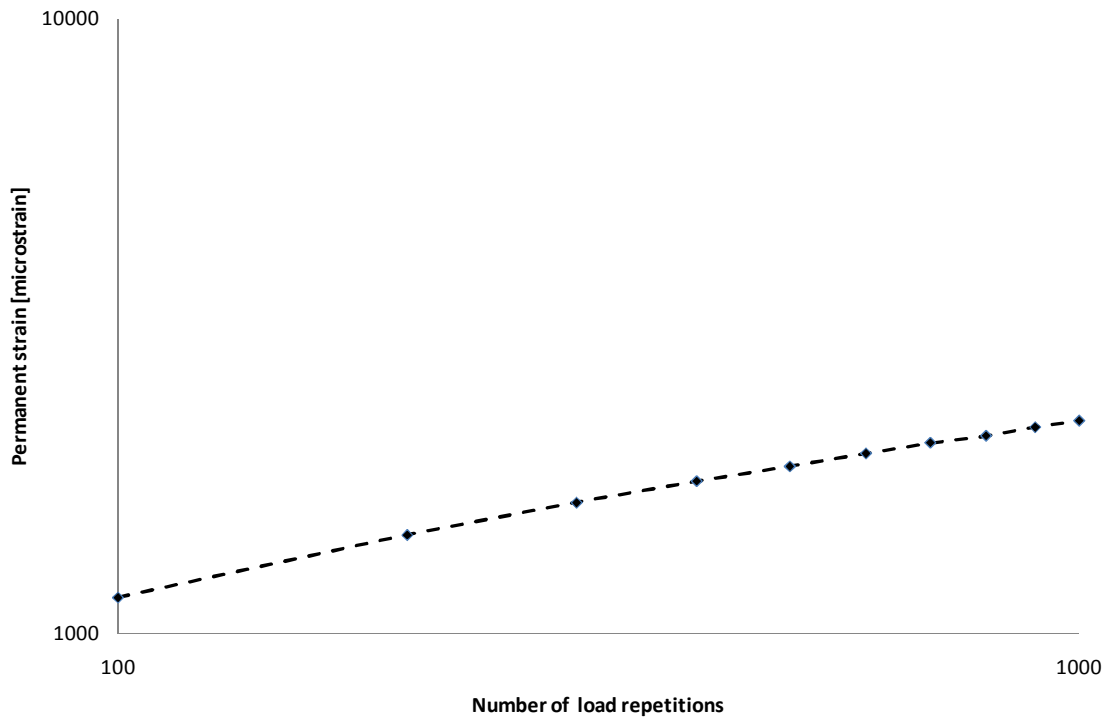


Figure D3. Material 1 80% water content of optimum load step 2 (load repetition 1000 - 2000), log - log relationship.

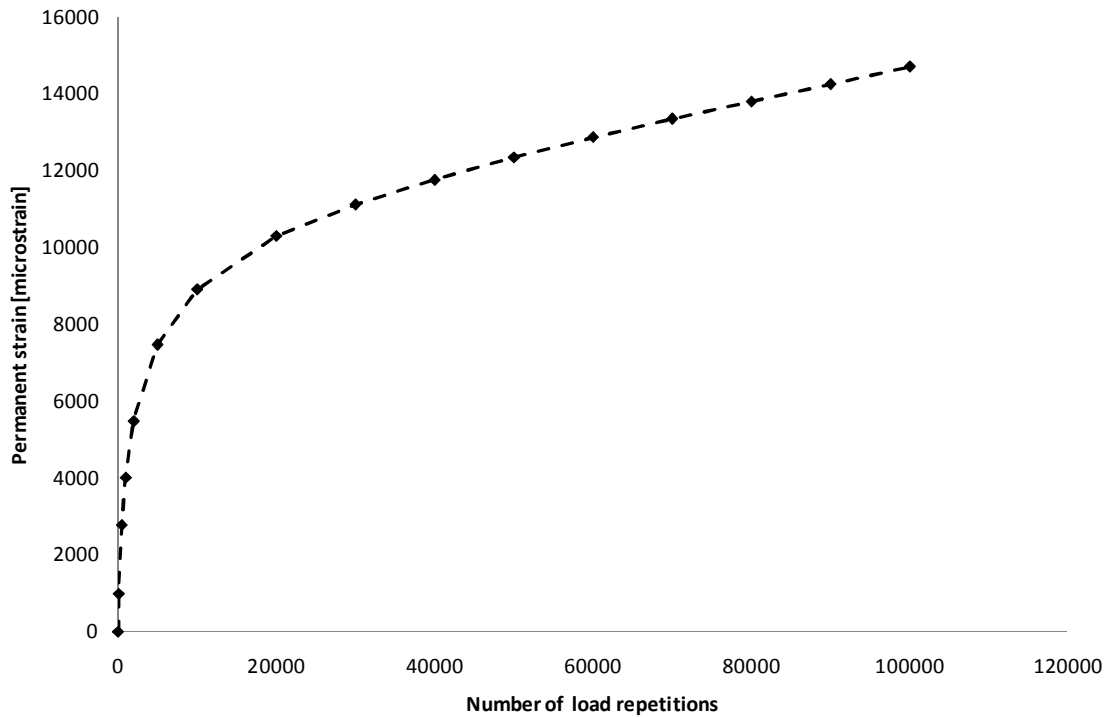


Figure D4. Material 1 80% water content of optimum load step 5 (load repetition 4000 - 104000), lin - lin relationship.

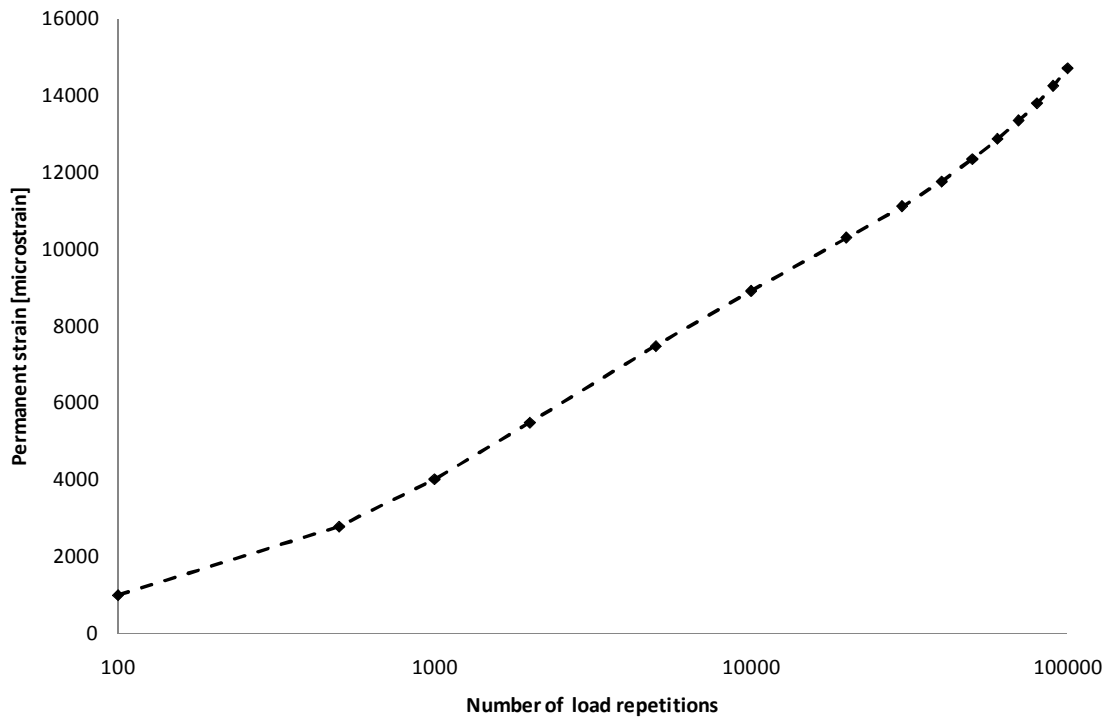


Figure D5. Material 1 80% water content of optimum load step 5 (load repetition 4000 - 104000), lin - log relationship.

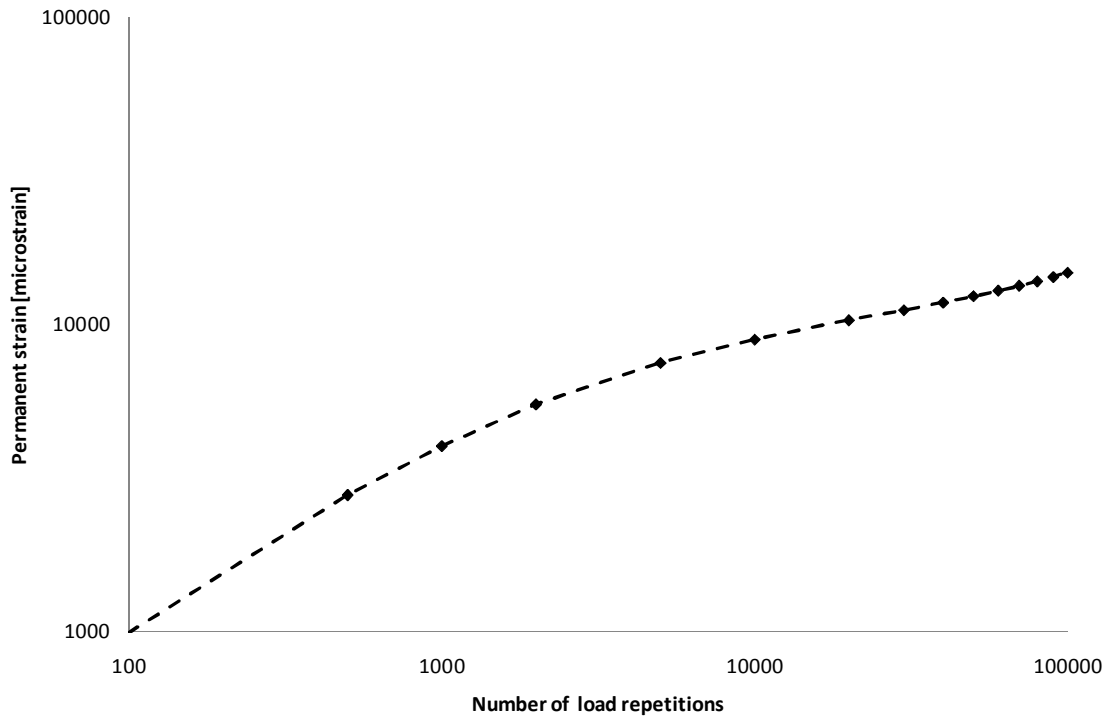


Figure D6. Material 1 80% water content of optimum load step 5 (load repetition 4000 - 104000), log - log relationship.

Appendix

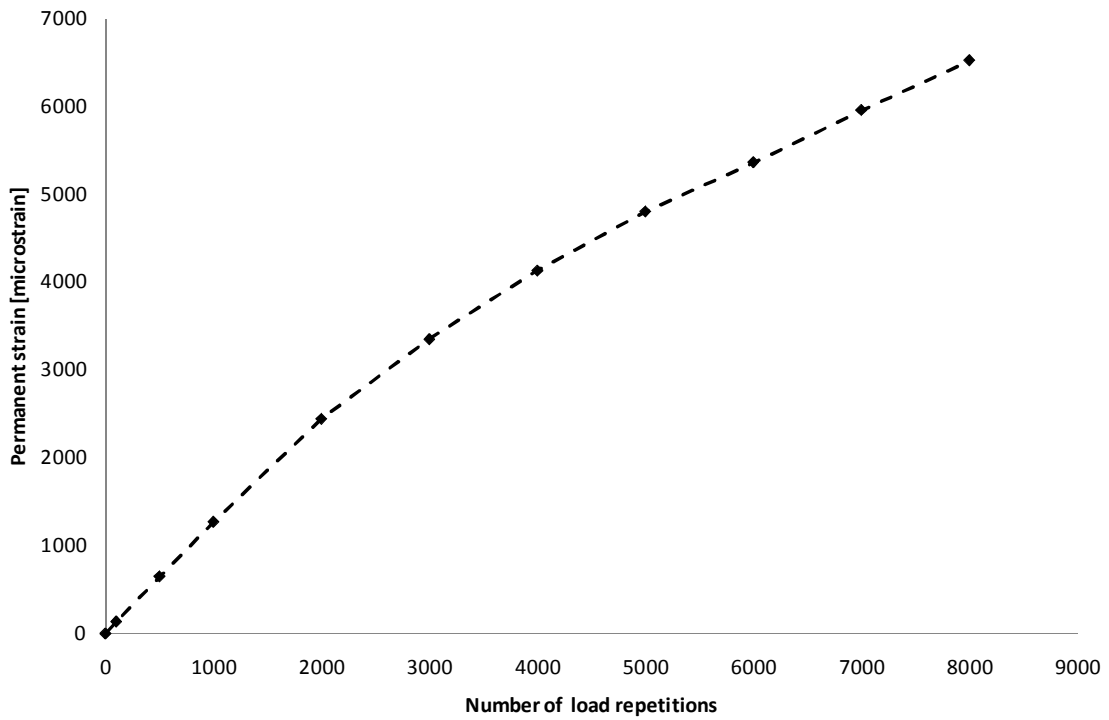


Figure D7. Material 1 80% water content of optimum load step 8 (load repetition 214000 - 224000), lin - lin relationship.

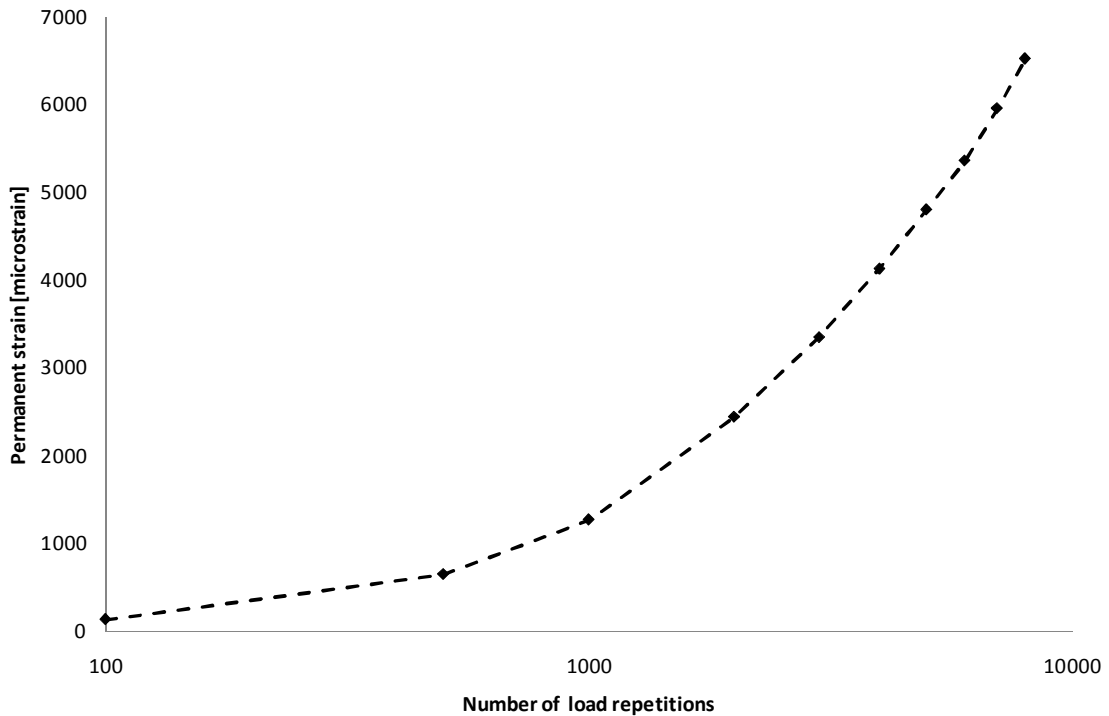


Figure D8. Material 1 80% water content of optimum load step 8 (load repetition 214000 - 224000), lin - log relationship.

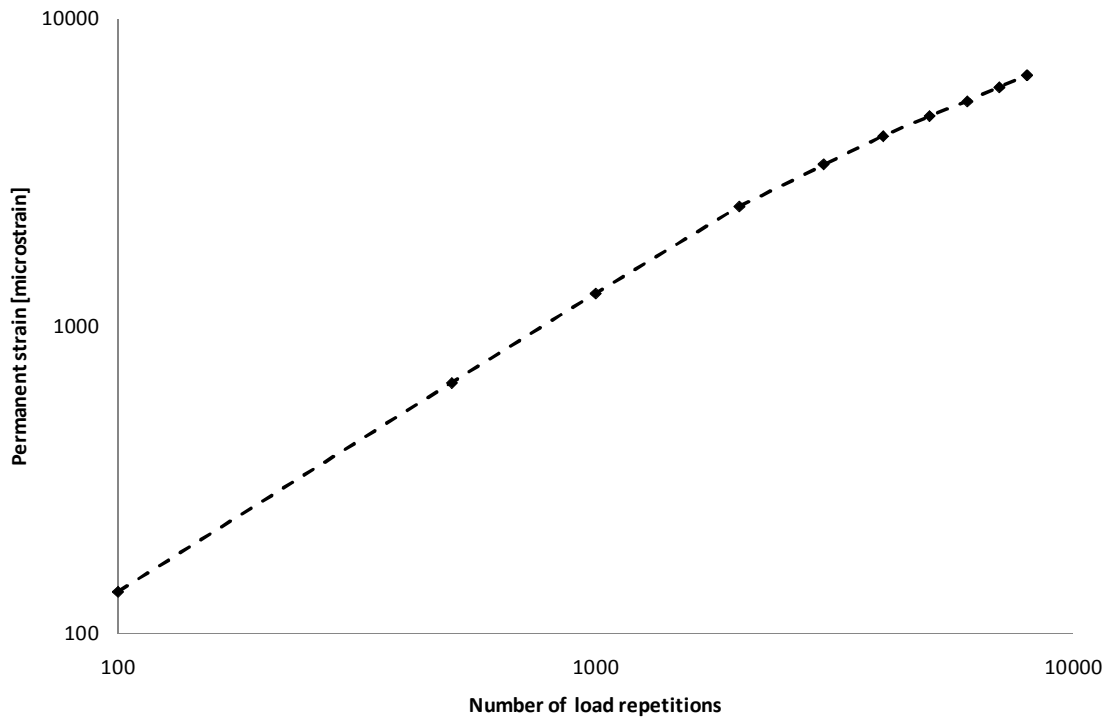


Figure D9. Material 1 80% water content of optimum load step 8 (load repetition 214000 - 224000), log – log relationship.

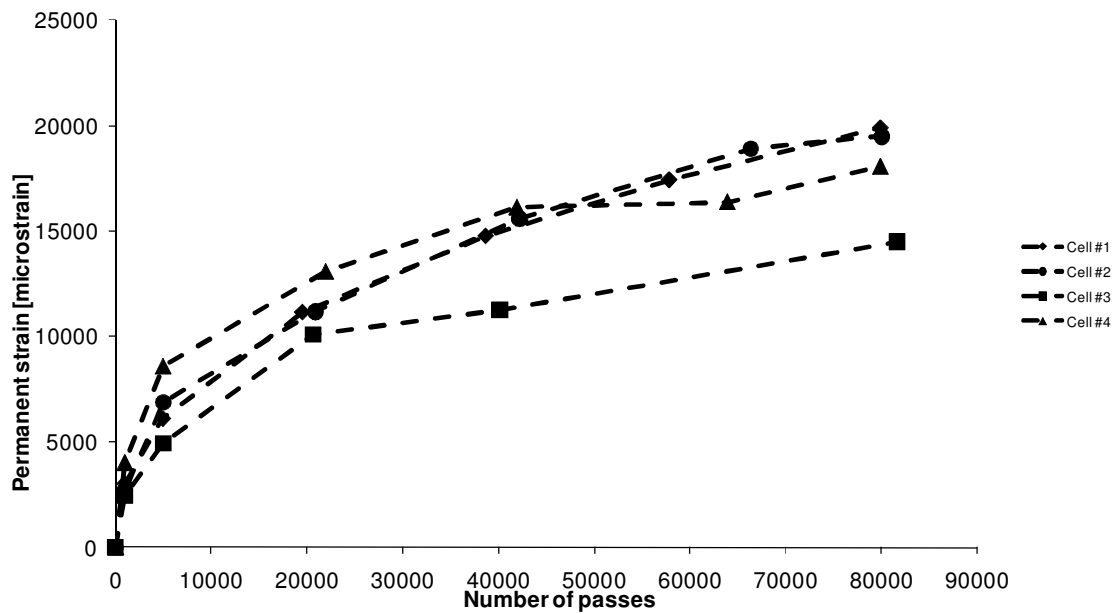


Figure D10. HVS test upper base layer passing 20000 – 100000, lin – lin relationship.

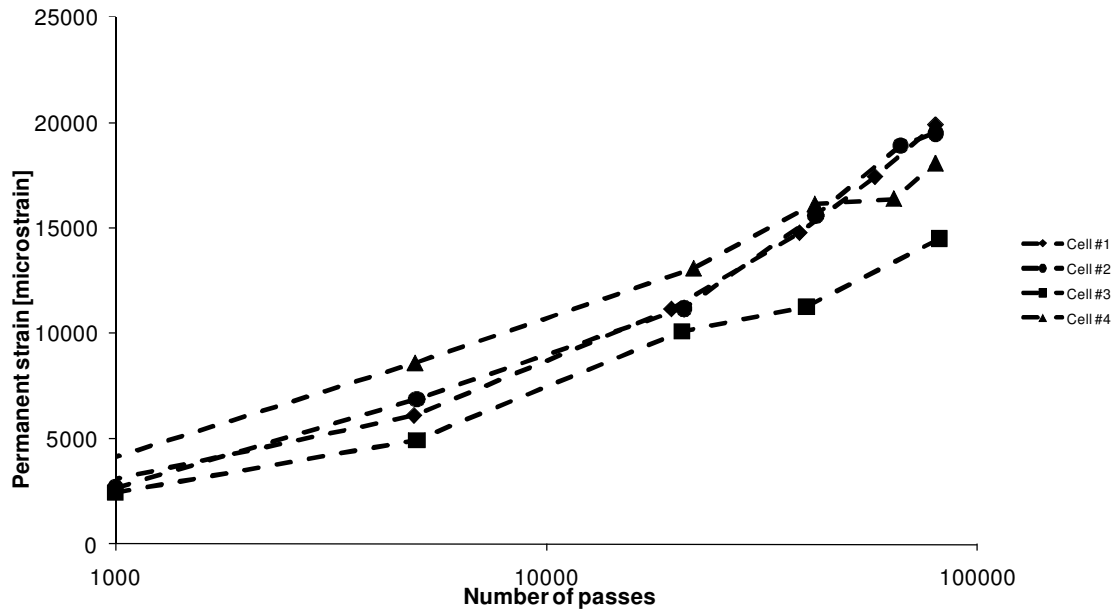


Figure D11. HVS test upper base layer passing 20000 – 100000, lin – log relationship.

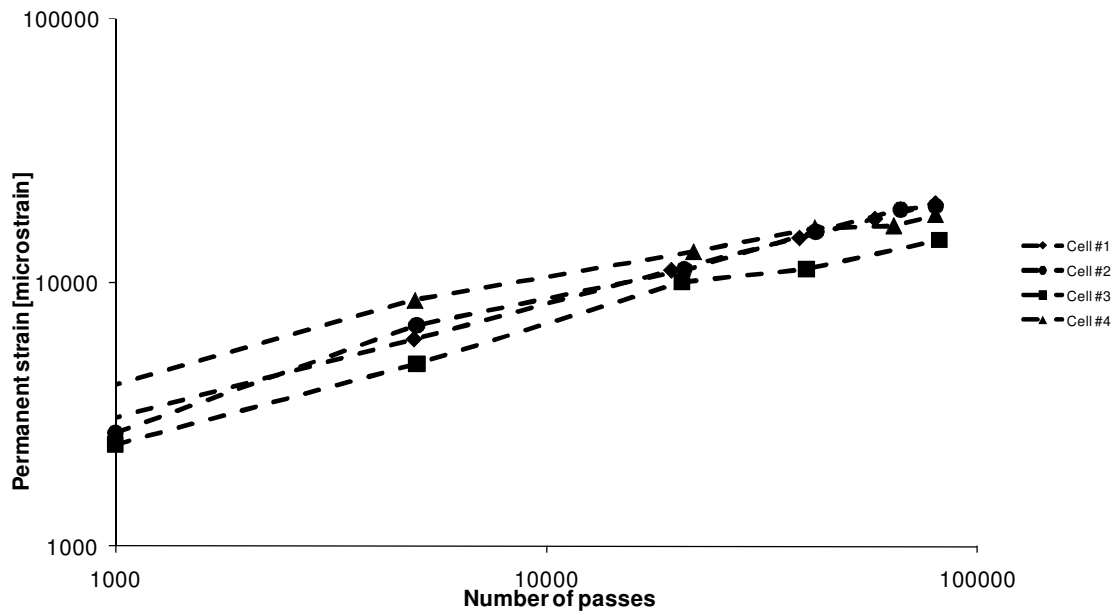


Figure D12. HVS test upper base layer passing 20000 – 100000, log – log relationship.

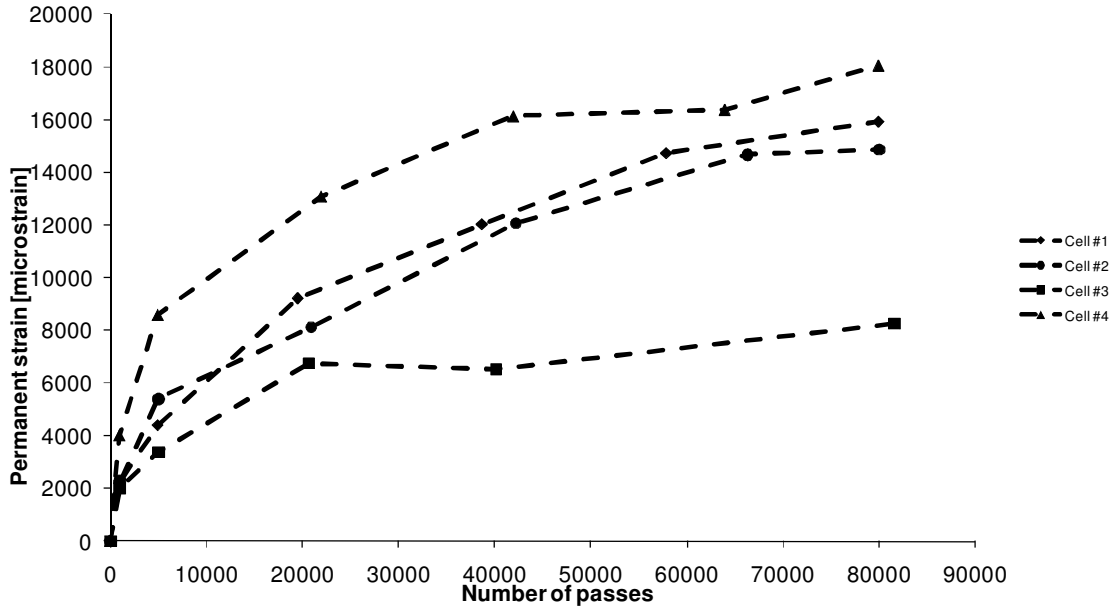


Figure D13. HVS test lower base layer passing 20000 – 100000, lin – lin relationship.

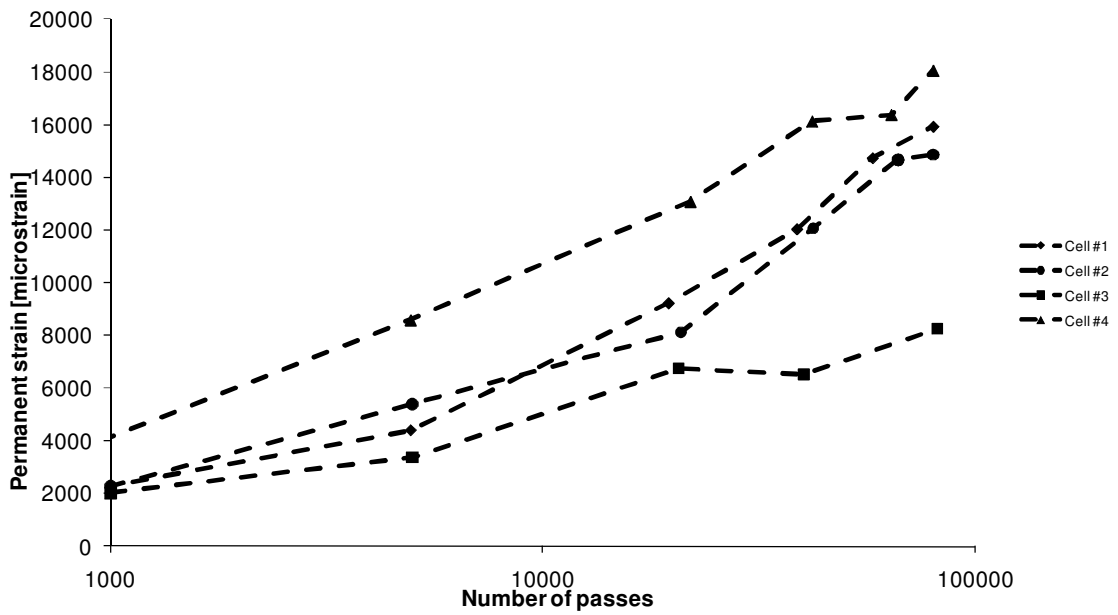


Figure D14. HVS test lower base layer passing 20000 – 100000, lin – log relationship.

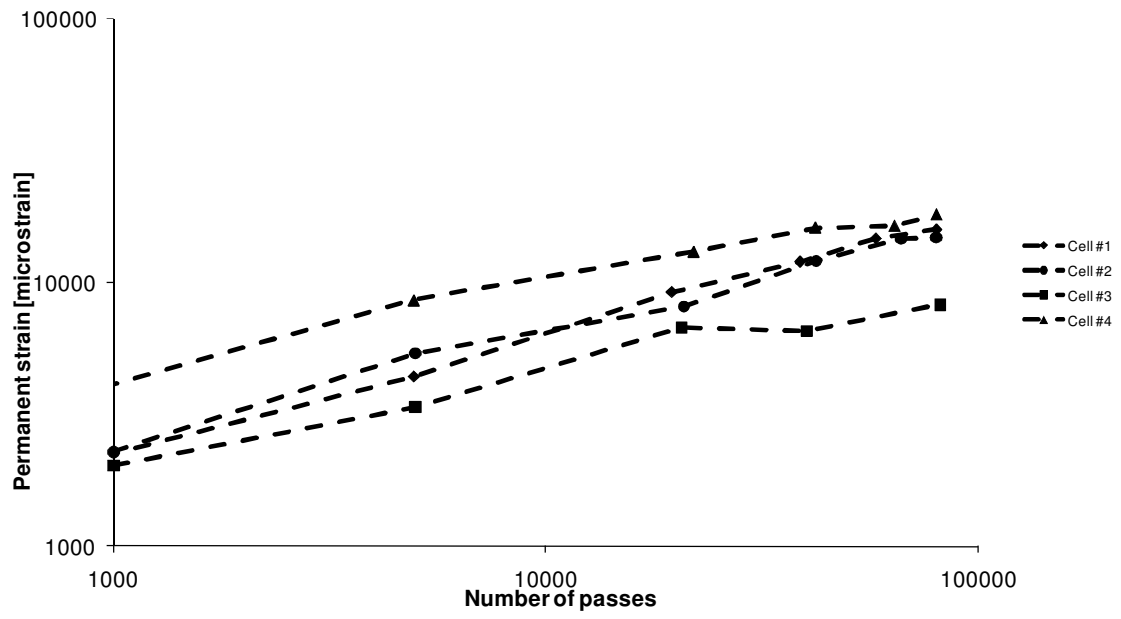


Figure D15. HVS test lower base layer passing 20000 – 100000, log – log relationship.

Appendix E

The relationship between S and M in the $q - p$ space and k and $\sqrt{\gamma}$ in $\sqrt{J_2} - I_1$ space can be described by studying Figure E1 and Figure E2 and Equation 2.2 and Equation 2.3.

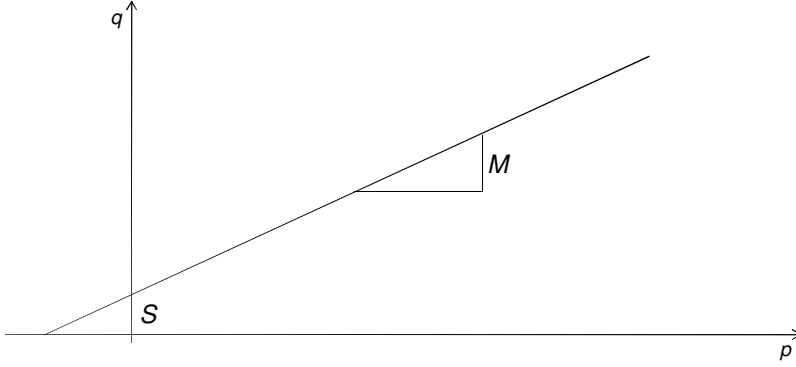


Figure E1. Failure envelope in $q - p$ space.

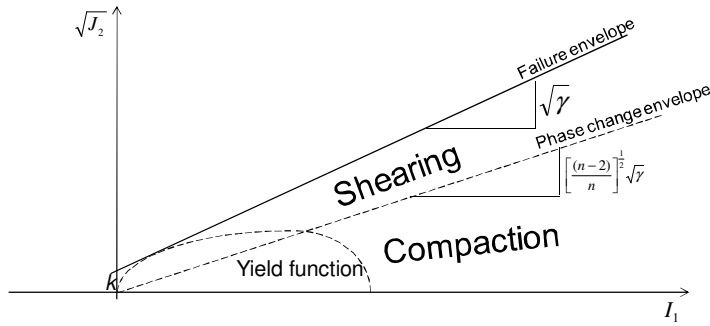


Figure E2. Failure envelope in $\sqrt{J_2} - I_1$ space.

If it is assumed that $\sigma_2 = \sigma_3$ (as is normal for laboratory triaxial tests) Equation 2.2 can be described as in Equation E1.

$$J_2 = \frac{1}{6}[(\sigma_1 - \sigma_2)^2 + (\sigma_1 - \sigma_2)^2 + (\sigma_2 - \sigma_3)^2] = \frac{1}{6}[2(\sigma_1 - \sigma_3)^2] = \frac{(\sigma_1 - \sigma_3)^2}{3} \quad (E1)$$

By using Equation 2.3 $\sqrt{J_2}$ can be described as in Equation E2.

$$\sqrt{J_2} = \sqrt{\frac{(\sigma_1 - \sigma_3)^2}{3}} = \sqrt{\frac{q^2}{3}} = \frac{q}{\sqrt{3}} \quad (\text{E2})$$

S and k can be related by relate the q and $\sqrt{J_2}$ axis as in Equation E3.

$$\frac{S}{k} = \frac{q}{\sqrt{J_2}} = \frac{q}{\frac{q}{\sqrt{3}}} = \sqrt{3} \Rightarrow S = \sqrt{3}k \quad (\text{E3})$$

M and $\sqrt{\gamma}$ can be related by relate the quotes between $\sqrt{J_2}/I_1$ and q/p as in Equation E4.

$$\frac{\sqrt{\gamma}}{M} = \frac{\frac{\sqrt{J_2}}{I_1}}{\frac{q}{p}} = \frac{\frac{\frac{q}{\sqrt{3}}}{3p}}{\frac{q}{p}} = \frac{\frac{q}{3\sqrt{3}p}}{\frac{q}{p}} = \frac{1}{3\sqrt{3}} \Rightarrow \sqrt{\gamma} = \frac{M}{3\sqrt{3}} \quad (\text{E4})$$

The relationship between S and M in the $q - p$ space and ϕ and c in the $\tau - \sigma_n$ space could be described by studying Figure E3 and Hansbo (1975).

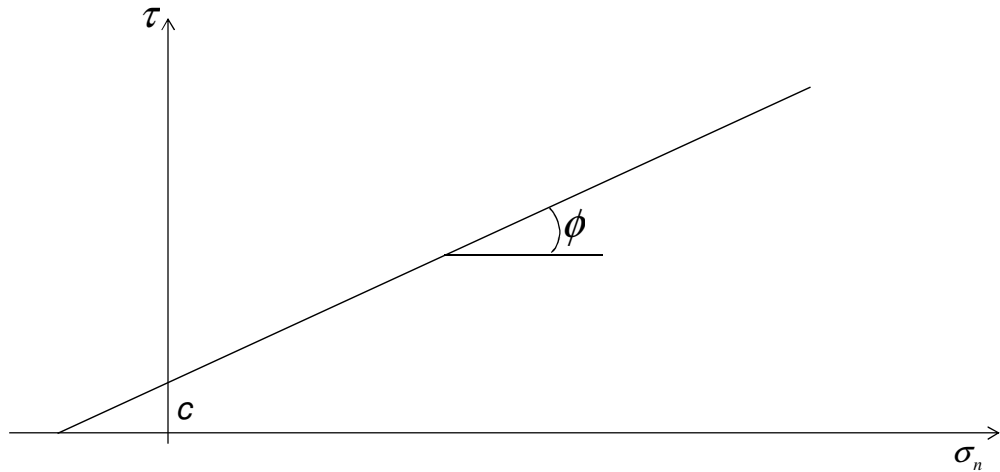


Figure E3. Mohr-Coulomb

According to Hansbo (1975) the failure envelope could be described as in Equation E5.

$$\frac{1}{2}(\sigma_1 - \sigma_3) = \frac{3 \sin \phi}{3 - \sin \phi} \left[\frac{1}{3}(\sigma_1 + 2\sigma_3) + \frac{c}{\tan \phi} \right] \quad (\text{E5})$$

Comparison between Figure E1 and Figure E3 gives the relationship between M and ϕ as described in Equation E6.

$$M = \frac{6 \sin \phi}{3 - \sin \phi} \quad (\text{E6})$$

From Equation E6 ϕ can be derived from M by Equation E7.

$$M = \frac{6 \sin \phi}{3 - \sin \phi} \Rightarrow 3M = (6 + M) \sin \phi \Rightarrow \sin \phi = \frac{3M}{6 + M} \Rightarrow \phi = \arcsin \frac{3M}{6 + M} \quad (\text{E7})$$

For compression the relationship between S and c can be described by Equation E8.

$$S = \frac{c(6 \sin \phi)}{\tan \phi(3 - \sin \phi)} \Rightarrow c = \frac{S \tan \phi(3 - \sin \phi)}{6 \sin \phi} \quad (\text{E8})$$

Appendix F

The grain size distribution determines the strength of the unbound material.

The grain size distribution of the four material evaluated in the present thesis is presented in Table F1.

Table F1. Grain sizes distribution of the four materials analyzed in the present thesis.

Grain size distribution:

Sieve size:	0,063	0,125	0,25	0,5	1	2	4	5,6	8	11,2	16	22,4	31,5	45
Passing Weight-% material 1	1,850	3	5,5	8	12	16,8	25,8	32,5	42,25	53,8	67,5	83,5	99	100
Passing Weight-% material 2	3,000	5	7,75	11,8	17,6	24	33,5	40,3	48,25	58	70,3	83,5	97,8	100
Passing Weight-% material 3	0,900	2	4,25	8	13,2	20	28	33,5	42	52,8	67	82	97,5	100
Passing Weight-% material 4	2,1	5,5	8,0	12,3	15,6	20,3	29,0	35,3	45,0	57,8	69,0	81,0	94,5	100,0

An empirical expression for determining internal friction angle can be found in “Handboken Bygg, Geoteknik” 04:5e page 99 (in Swedish) (Equation F1). This expression is described by Hansbo (1975) (Brinch-Hansen).

$$\phi = 26 + 10I_D + 0.4C_u + 1.6 \log d_m \quad (F1)$$

$$I_D = 0.8 \text{ (from table G04:22d in “Handboken Bygg, Geoteknik”)}$$

$$C_u = \frac{11.2}{0.5}$$

$$d_{50} = 5.6 \text{ mm}$$

This gives $\phi = 44^\circ$

Appendix G

The relationship between k_1 and k_2 is described by Equation G1 (Equation 6.12)

$$k_2 = -D_1 \ln k_1 + D_2 \quad (\text{G1})$$

D_1 describes the slope of the $k_1 - k_2$ relationship and D_2 the k_2 value for $k_1 = 1$. Which parameters that controls D_1 and D_2 can be explained by study the derivate of the $k - \theta$ model (rewritten as in Equation G2).

$$M_r = k_1 \left(\frac{\theta}{\theta_0} \right)^{k_2} = \exp \left(\ln[k_1] + k_2 \ln \left[\frac{\theta}{\theta_0} \right] \right) \quad (\text{G2})$$

The derivate regarding k_1 is written as in Equation G3.

$$\frac{dM_r}{dk_1} = \left(\frac{\theta}{\theta_0} \right)^{k_2} \quad (\text{G3})$$

The derivate regarding k_2 is written as in Equation G4.

$$\frac{dM_r}{dk_2} = \exp \left(\ln[k_1] + k_2 \ln \left[\frac{\theta}{\theta_0} \right] \right) \cdot \ln \left[\frac{\theta}{\theta_0} \right] = k_1 \left(\frac{\theta}{\theta_0} \right)^{k_2} \cdot \ln \left[\frac{\theta}{\theta_0} \right] \quad (\text{G4})$$

A change of M_r as a result of changes of both k_1 and k_2 can be written as in Equation G5.

$$\partial M = \frac{\partial M}{\partial k_1} \partial k_1 + \frac{\partial M}{\partial k_2} \partial k_2 = \theta^{k_2} \partial k_1 + k_1 \theta^{k_2} \cdot \ln[\theta] \partial k_2 \quad (\text{G5})$$

If M_r is constant, the relationship between k_1 and k_2 can be written as in Equation G6.

$$\partial M = 0 \Rightarrow \theta^{k_2} \partial k_1 = -k_1 \theta^{k_2} \ln[\theta] \partial k_2 \Rightarrow \frac{\partial k_2}{\partial k_1} = -\frac{1}{k_1 \ln[\theta]} \quad (\text{G6})$$

Compared to Equation G1, D_1 can be related to θ as in Equation G7.

$$D_1 \approx \frac{1}{\ln[\theta]} \tag{G7}$$

Appendix H

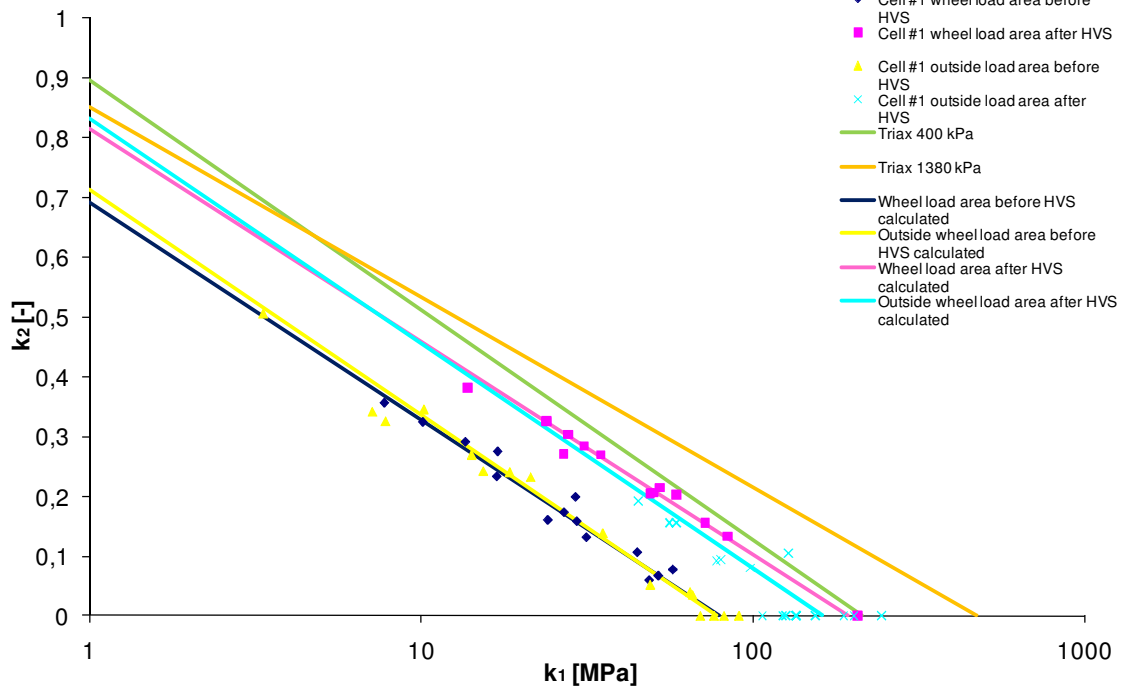


Figure H1. Relationship between k_1 and k_2 for the FWD test results of Test Cell #1. The green line represent the calculated one for bulk stress 400 kPa and 1380 kPa of the triaxial test as shown in Figure 6.25.

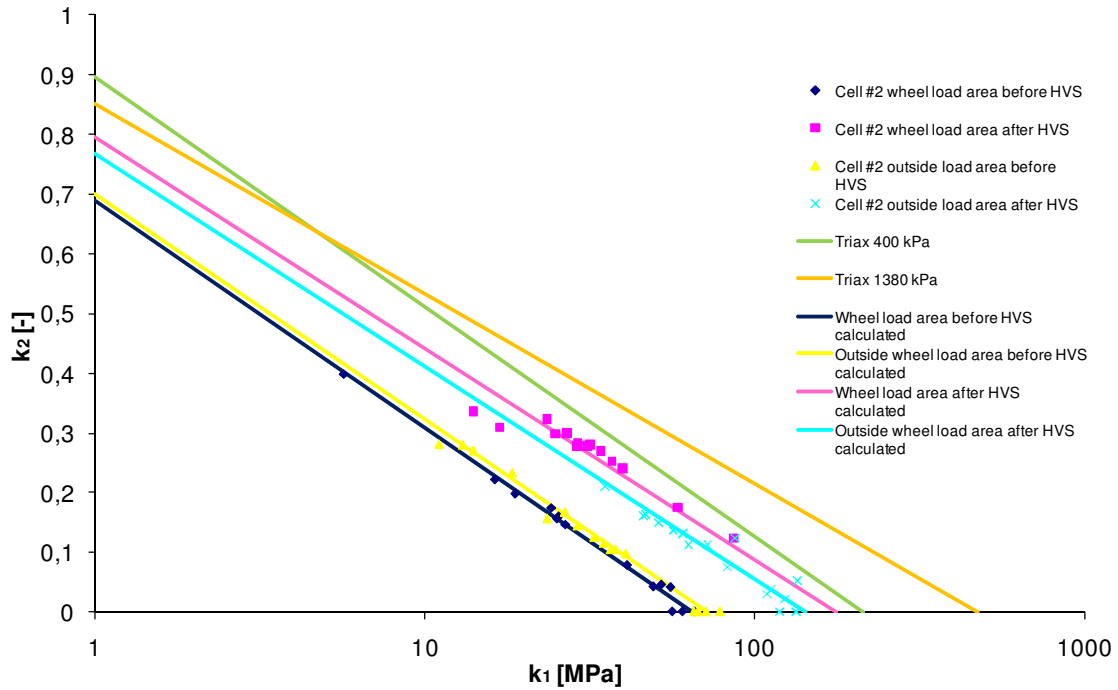


Figure H2. Relationship between k_1 and k_2 for the FWD test results of Test Cell #2. The green line represent the calculated one for bulk stress 400 kPa and 1380 kPa of the triaxial test as shown in Figure 6.25.

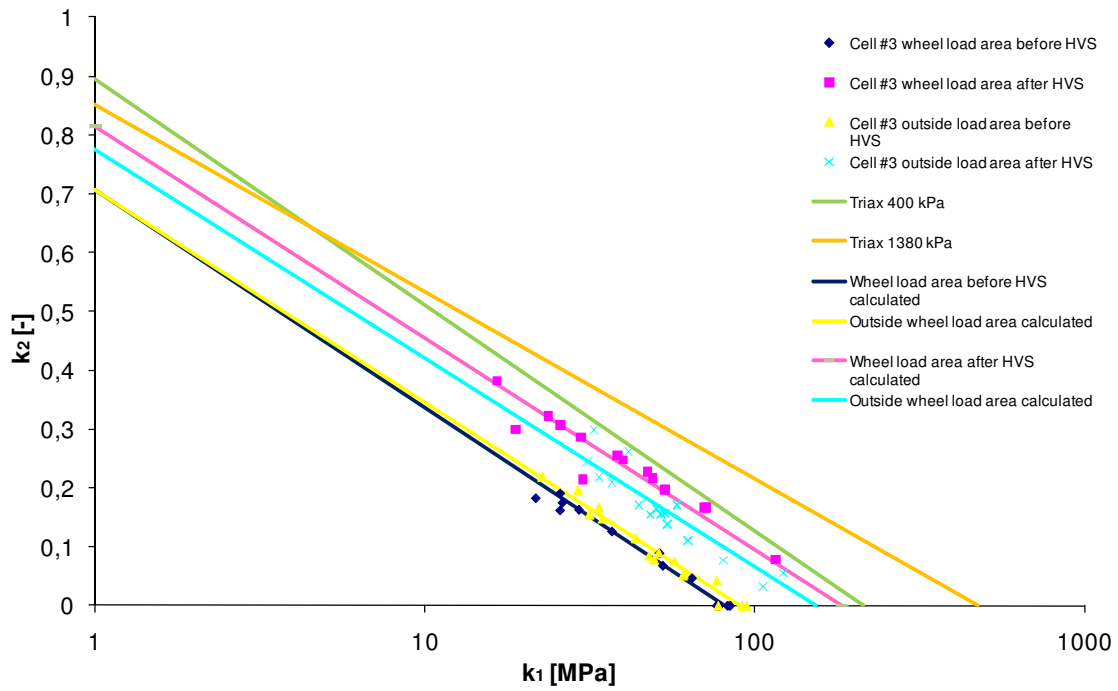


Figure H3. Relationship between k_1 and k_2 for the FWD test results of Test Cell #3. The green line represent the calculated one for bulk stress 400 kPa and 1380 kPa of the triaxial test as shown in Figure 6.25.

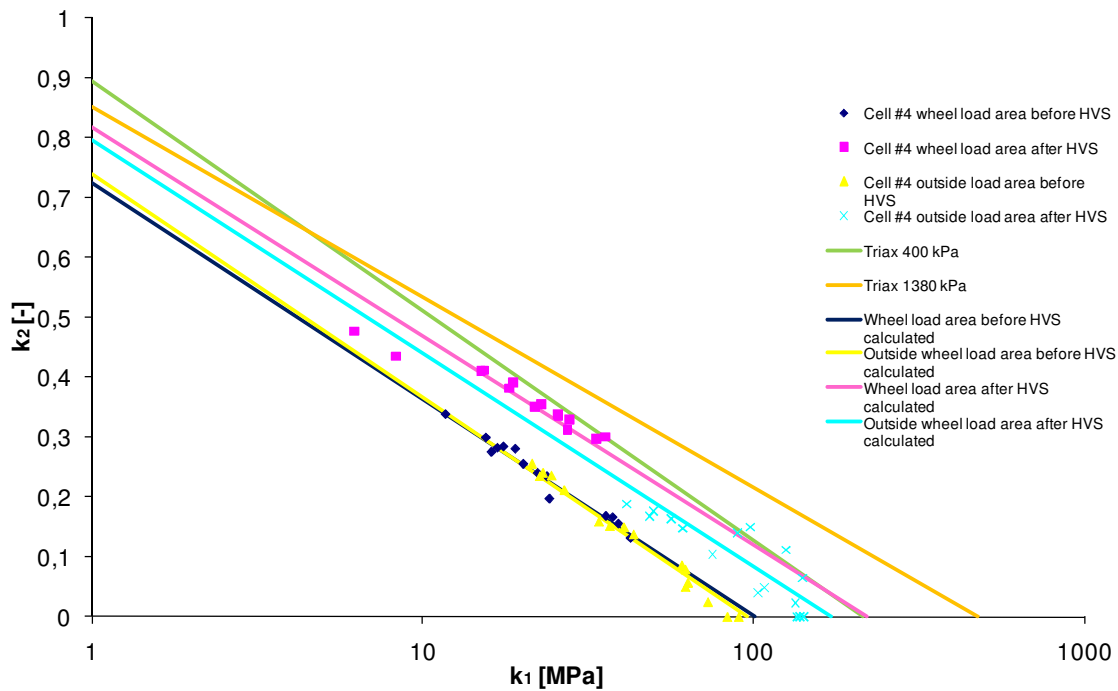


Figure H4. Relationship between k_1 and k_2 for the FWD test results of Test Cell #4. The green line represent the calculated one for bulk stress 400 kPa and 1380 kPa of the triaxial test as shown in Figure 6.25.